New Explorations in Visible-Light Mediated Energy and Single Electron Transfer for Nitrogen Heterocycle Synthesis

by

Meghan Jessica Oddy

Thesis presented for the degree of

Doctor of Philosophy

Department of Chemistry

University of Cape Town

Supervisor: Dr Wade F. Petersen

February 2024

Declaration

I, **Meghan Jessica Oddy**, declare the following:

1. That the work on which this thesis is based is my original work, both in concept and execution, except where acknowledgements indicate otherwise.

2. That in cases where others' work has been cited, this has been acknowledged and referenced accordingly.

3. That no part of this work has been, is being, or is to be submitted for another degree at this or any other university.

4. That I authorize the University of Cape Town to reproduce this work, in whole or in part, for the purpose of research.

Signed: **Meghan Jessica Oddy** Date: **February 2024**

Signed by candidate

Abstract

With the recent push toward green chemistry, photocatalysis has emerged as a powerful alternative for reactions that might otherwise need high temperatures, poor atom economy or harsh reactants to proceed. This thesis explores the use of visible-light mediated photocatalysis for the synthesis of biologically important nitrogen containing heterocycles, investigating both single electron transfer and energy transfer methods.

The results section of this thesis is presented in three chapters, each focusing on a different ring size, namely 4, 5 and 6 membered nitrogen heterocycles. Chapter two explores the use of photocatalysis to enable stereoselective access to 3,3-disubstitued oxindoles via newly developed *N*-acyl chiral auxiliaries, serving as chiral C1 radical synthons. These acyl radicals are generated under visible-light mediated single electron transfer to *N*-hydroxyphthalimido esters, which then undergo a radical addition–cyclisation sequence with *N*-phenyl acrylamides. A model 3,3-disubstitued oxindole is isolated as separable diastereomers in 81% yield with 2.2:1 dr. This advanced intermediate could be telescoped toward the formal synthesis of the natural cyclotryptamine alkaloid, physovenine.

Chapter three describes an efficient thioxanthone-catalysed triplet energy transfer process for the synthesis of 3,4-dihydroquinolin-2-ones from *N*-acrylamides. This work features a rare example of a metal-free formal C(sp^2)–H/C(sp^3)–H arylation mediated by visible-light. Using 450 nm light with 2-chlorothioxanthone in 2,2,2-TFE:$CHCl_3$, a selection of 23 substituted 3,4-dihydroquinolin-2-ones are isolated in moderate to excellent yields (16–97%). The reaction is amenable to gram-scale synthesis, and the 3,4-dihydroquinolin-2-ones obtained are easily oxidized to the corresponding quinolin-2-ones, ultimately producing facile access to two privileged bioactive scaffolds. The reaction mechanisms presented are supported by Stern-Volmer plots as well as deuterium labelling studies.

Finally, chapter four explores the synthesis of 2-azetidinones (β-lactams) from simple acrylamide starting materials by visible-light-mediated energy transfer catalysis. The reaction features a C(sp^3)−H functionalisation via a variation of the Norrish–Yang photocyclisation involving a rare carbon-to-carbon 1,5-hydrogen atom transfer. The proposed mechanism is supported by deuterium labelling and DFT calculations. The optimised reaction conditions use 2-chlorothioxanthone under irradiation with 405 nm light which enables the synthesis of 30 substrates in moderate to excellent yields (40–98%), mostly as 2 separable diastereomers (generally 1.5:1 dr).

Publication and Presentation of Work

Publications

Späth, J.; **Oddy, M. J**.; Hunter, R.; Petersen, W. F. Chiral Acyl Radicals Generated by Visible Light Enable Stereoselective Access to 3,3-Disubstituted Oxindoles: Application toward the Synthesis of (–)- and (+)-Physovenine. *Synthesis* **2023**, *55*, 1736–1743. https://doi.org/10.1055/a-1959-1930.

Oddy, M. J.; Kusza, D. A.; Petersen, W. F. Visible-Light Mediated Metal-Free 6π-Photocyclisation of N-Acrylamides: Thioxanthone Triplet Energy Transfer Enables the Synthesis of 3,4-Dihydroquinolin-2-Ones. *Org. Lett.* **2021**, *23*, 8963–8967. https://doi.org/10.1021/acs.orglett.1c03487.

Oddy, M. J.; Kusza, D. A.; Epton, R. G.; Lynam, J. M.; Unsworth, W. P.; Petersen, W. F. Visible-Light-Mediated Energy Transfer Enables the Synthesis of B-Lactams via Intramolecular Hydrogen Atom Transfer. *Angew. Chem. Int. Ed.* **2022**, *61*, e202213086. https://doi.org/10.1002/anie.202213086.

Book Chapter

Oddy, M. J.; Petersen, W. F. Visible-Light Mediated Strategies for the Synthesis of Nitrogen-Based Heterocycles. In *Photochemistry*; Royal Society of Chemistry, 2023; pp 410–435. https://doi.org/10.1039/BK9781837672301-00410.

Conferences

44th SACI National Convention, South Africa, 2023 – *Invited Lecture*.

Acknowledgements

To my supervisor, Dr Wade F. Petersen, I am immensely grateful for your guidance, support and mentorship throughout this journey. Your energetic and passionate approach to research has been a constant source of inspiration. Thank you for pushing me to achieve more in my research than I ever thought possible.

To the Petersen research group, thank you for the hours of companionship during the long lab days. I am so grateful for the collaborative and supportive environment we shared in our group. A special thanks to my 7A lab mates; to Josef Späth, thank you for the many interesting discussions. To Dr Daniel Kusza, thank you for sharing your passion for chemistry with me. I am honoured to have collaborated so closely with you during my PhD.

I would like to thank the Hunter research group as well as everyone in the Department of Chemistry at UCT who helped me on this journey. Additionally, I would like to thank my colleagues and supervisor, Prof. Andrew Orr-Ewing, at the University of Bristol. Thank you for making me feel so welcome and answering my many questions with patience and enthusiasm.

Thank you to my friends and house mates, for your encouragement and support during this time. And to my dog, Gino, for the evening walks and comforting cuddles.

To my love, Claude, thank you for everything you have done for me. Thank you for being my greatest support. You have made the challenges more bearable and the successes more joyful.

Finally, to my mom, dad, brother and sister, thank you for shaping me into the person I am today. I struggle to find the words to express how important you each are to me. I love you.

Abbreviations

ACN	acetonitrile
Ar	aromatic
AT	atom transfer
BDE	bond dissociation energy
Bn	benzyl
BNAH	1-benzyl-1,4-dihydronicotinamide
BPin	bis(pinacolato)diboron
bs	broad singlet
C	celsius
CFL	compact fluorescent light
CTX	2-chlorothioxanthone
$Cu(acac)_2$	copper(II) acetylacetonate
CzIPN	1,2,3,5-tetrakis(carbazol-9-yl)-4,6-dicyanobenzene
d	doublet
DBU	1,8-diazabicyclo[5.4.0]undec-7-ene
DCA	dichloroacetic acid
DCE	1,2-dichloroethane
DCM	dichloromethane
dd	doublet of doublets
diff	diffusion
DMA	dimethylacetamide
DMDC	dimethyl dicarbonate
DMF	dimethylformamide
DMSO	dimethyl sulfoxide
dr	diastereomic ratio
ee	enantiomeric excess
EnT	energy transfer
eq	equivalence
EWG	electron withdrawing group
FDA	Food and Drug Administration
FG	functional group
FRET	Förster resonance energy transfer
g	gram

HAS	homolytic aromatic substitution
HAT	hydrogen atom transfer
HOMO	highest occupied molecular orbital
HPLC	high performance liquid chromatography
hrs	hours
IR	infrared
$Ir(ppy)_3$	tris(2-phenylpyridine)iridium
ISC	intersystem crossing
ITX	2-iodothioxanthone
IUPAC	International Union of Pure and Applied Chemistry
J	coupling constant
KIE	kinetic isotope effect
LEDs	Light-emitting diode
LG	leaving group
LUMO	lowest unoccupied molecular orbital
M	molar
m	meter
Me	methyl
MeCN	acetonitrile
MECP	minimum energy crossing point
mg	milligram
mins	minutes
mL	millilitres
mM	millimolar
MS	mass spectrometry
NCS	*N*-chlorosuccinimide
NFSI	*N*-fluorobenzenesulfonimide
nm	nanometer
NMR	nuclear magnetic resonance
NOE	nuclear Overhauser effect
Ox	oxidative
p-	para
PC	photocatalyst
PET	photoinduced energy transfer

Ph	phenyl
Phth	phthalimide
q	quartet
Red	reductive
rt	room temperature
$Ru(bpy)_3$	tris(bipyridine)ruthenium(II) chloride
s	singlet
SET	single electron transfer
SOMO	singly occupied molecular orbital
Sub	substrate
T	triplet state
t	triplet
TAS	transient absorption spectroscopy
TBHP	tert-butyl hydroperoxide
TEMPO	2,2,6,6-tetramethylpiperidin-1-yl)oxyl
TFA	trifluoroacetic acid
TFE	trifluoroethanol
THF	tetrahydrofuran
TLC	thin layer chromatography
tm	transition metal
TS	transition state
TX	thioxanthone

Table of Contents

1. Chapter 1 - Introduction

When chemists design new reaction methods, one the greatest teachers to learn from is Mother Nature herself. The idea of photocatalysis is inspired by nature's own photosynthesis — the ability to utilise light energy as a driver for chemical synthesis.

The broad definition by IUPAC of photocatalysis is defined as "*The change in the rate of a chemical reaction or its initiation under the action of ultraviolet, visible or infrared radiation in the presence of a substance—the photocatalyst—that absorbs light and is involved in the chemical transformation of the reaction partners"*.[1] Photocatalysis represents a unique and powerful tool in organic synthesis. By utilising the energy delivered by a light source, we are able perform reactions that are difficult, sometimes even impossible, to carry out under normal conditions.

Classical photochemistry,[2,3] which typically uses high-powered ultraviolet light for the *direct* excitation of organic compounds, is a highly developed field of chemistry. However, many organic chemists regard this as a challenging technique, as it is not always straightforward to apply and typically suffers from competitive and uncontrollable side reactions. The field of photocatalysis, which involves the use of a light absording catalyst, has changed this perception around photochemistry and promoted photocatalysis as a simple yet powerful tool to drive organic transformations. Recently, the increased use of visible-light for the excitation of these catalysts is causing photocatalysis to be a front runner in the movement toward green chemistry.[4]

Nitrogen-containing heterocycles are essential to human life. These molecular scaffolds serve as the basis for many biologically important substances, most notably DNA nucleobases, which hold the information needed for all life on earth, as well as vitamins, hormones, dyes, antibiotics, herbicides and pharmaceuticals (Figure 1.1).[5–12] Their importance in the pharmaceutical industry cannot be overstated. Approximately 60% of FDA approved drugs feature a nitrogen heterocycle.[13,14] Considering these significant profiles in chemical biology, these fragments continue to serve as the synthetic chemist's 'targeting platform' to benchmark innovations in chemical synthesis.[15–19]

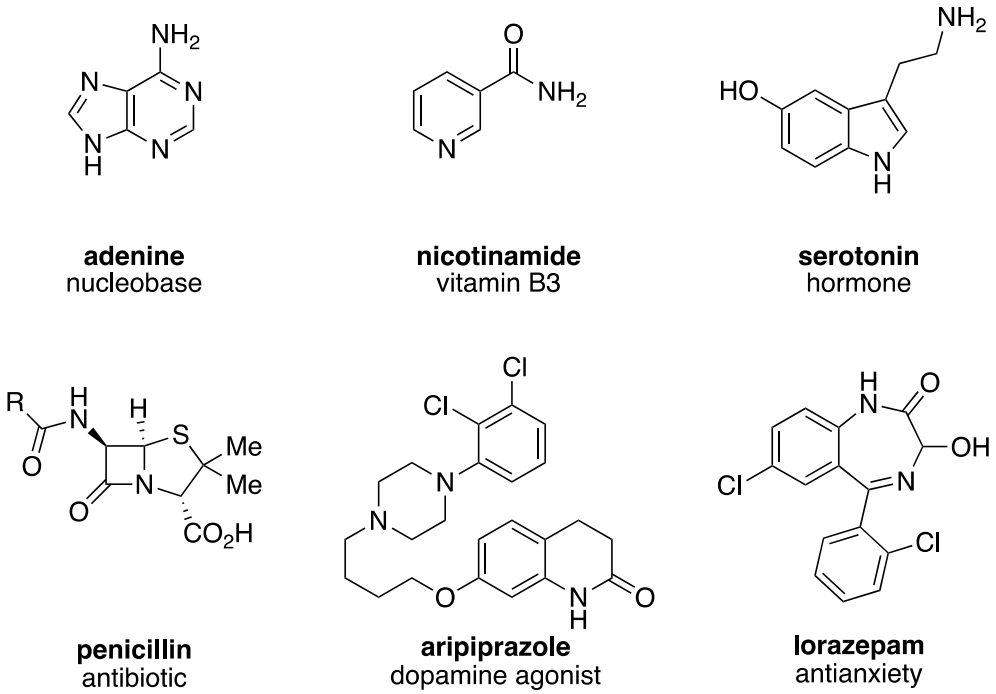

Figure 1.1: A selection of biologically important nitrogen containing heterocycles.

The purpose of this thesis is to explore powerful yet environmentally friendly approaches for the synthesis of biologically important molecules. In this way, the class of nitrogen containing heterocycles represents an ideal target to investigate new photocatalytic methods. Furthermore, a heavy emphasis is placed on optimizing reactions which meet the requirements of sustainable chemistry, namely mild reaction conditions, cheap and renewable resources, optimal atom economy and less hazardous materials.

1.1 Photocatalysis

Visible-light mediated photocatalysis has gained immense popularity in recent years. There are several factors that have come together to make this possible. The most notable of which is the increased awareness for the use of renewable energy sources (solar, wind, hydro, tidal etc.) over fossil fuels in an attempt to curb greenhouse gas emissions. The push for chemists to develop more environmentally friendly reaction conditions has identified photocatalysis as a powerful alternative for reactions that might otherwise need high temperatures, poor atom economy or harsh reactants to proceed. Another factor that has contributed to an increase in popularity of photocatalysis is the broad commercial availability of light-emitting diodes that are able to provide high-intensity, visible-light in a narrow wavelength range for all

colours/wavelengths.[20] Additionally, advances in flow chemistry[21] and the use of flow reactors have improved the reproducibility and upscaling of photochemical reactions.

1.1.1 Early Work

The idea of using visible-light to promote organic transformations is far from a novel concept. The first use of this technique can be traced back more than 100 years, when Italian chemist Giacomo Ciamician and his colleague Paul Silber of the Chemical Institute of the University of Bologna, Italy, developed photochemical reactions using visible-light.[22] In an eloquent publication in 1912, Professor Ciamician describes the vast amount of energy delivered to the earth by the sun and the potential to harness this energy for a variety of transformations. Ciamician and Silber attempted to utilize this solar energy by placing their reactions outside on the balcony to be irradiated by sunlight.

Despite this revolutionary concept, the field of photochemistry remained somewhat stagnant in the following years. It wasn't until the 1970's, with the exploration into light absorbing catalysts, that the field of photocatalysis began to develop. One of the first photocatalysts to be studied was the tris(2,2'-bipyridine)ruthenium complex ($Ru(bpy)_3^{2+}$). In 1978, Kellogg and co-workers [23,24] from University of Groningen, Netherlands, demonstrated that the photo mediated reduction of sulfonium ions to the corresponding alkanes and thioethers could be accelerated by addition of a catalytic amount of $[Ru(bpy)_3]Cl_2$ and the use of Hantzsch esters as the terminal reductant (Scheme 1.1).

Kellogg (1978): Reductive Desulfuration

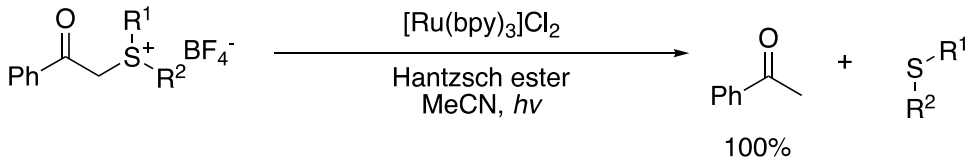

Scheme 1.1: Early report of photocatalysis by Kellogg and co-workers for the reduction of sulfonium ions using $[Ru(bpy)_3]Cl_2$.

In 1984, Cano-Yelo and Deronzier [25] of from the Université de Grenoble in France published the first visible-light mediated Pschorr cyclisation, producing phenanthrene in quantitative yields (Scheme 1.2). Their work demonstrated the importance of utilizing a photocatalyst

($Ru[bpy]_3Cl_2$), as direct irradiation with wavelengths >360 nm of their stilbenediazonium ion starting material resulted in only 10-20% of the desired product and 80% of an unwanted side product.

Deronzier and Cano-Yelo (1984): Photocatalytic Pschorr Reaction

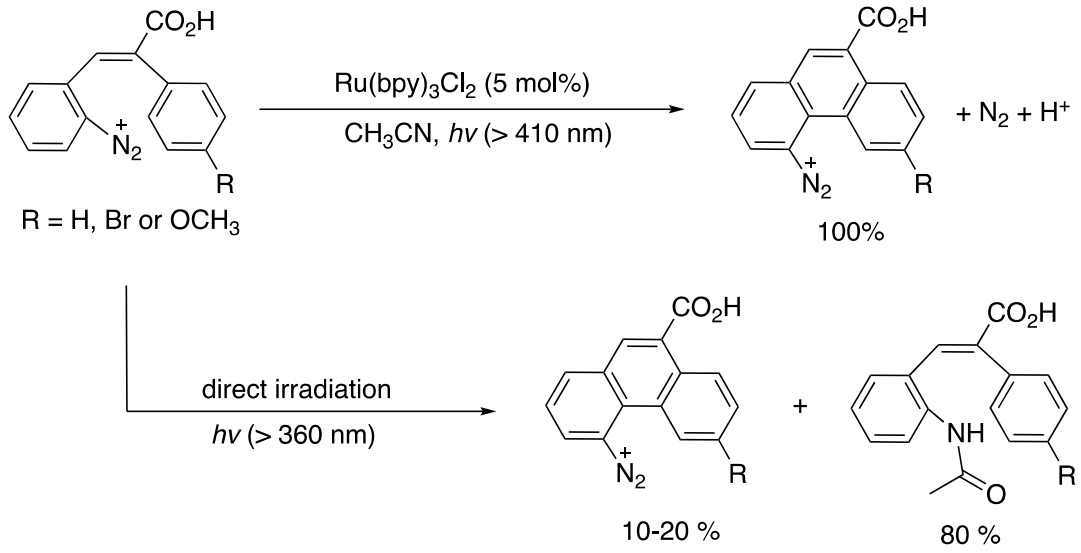

Scheme 1.2: Photoredox-catalysed Pschorr reaction for the synthesis of substituted phenanthrenes and undesired products resulting from direct irradiation.

Seminal work by Okada and co-workers[26] in 1991 demonstrated that decarboxylation of *N*-(acyloxy)phthalimide could be used as a convenient source of alkyl radicals (Scheme 1.3). Visible-light mediated fragmentation using $[Ru(bpy)_3]Cl_2$ and 1-benzyl-1,4-dihydro-nicotinamide (BNAH) generated C-centred radicals that could engage in Giese additions[27] with Michael acceptors (Scheme 1.3a). Delighted with this success, the authors further expanded the scope of the reaction to include hydro-decarboxylation (Scheme 1.3b)[28] and phenyl-selenylation (Scheme 1.3c)[29].

Okada (1991): Photoredox Mediated Decarboxylation

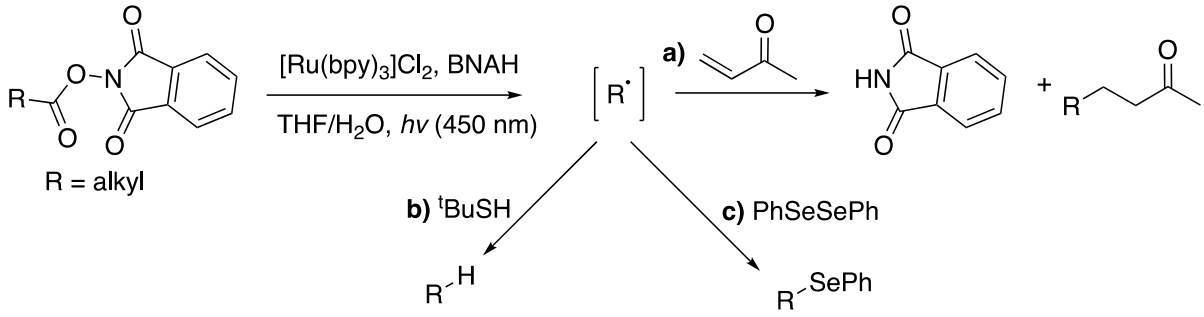

Scheme 1.3: Reductive decarboxylation of redox-active esters for the use in conjugate additions (a), hydrogen atom abstraction (b) and phenylselenenylation (c).

In 1997, Pandey and co-workers from India developed a sequential electron transfer process using 9,10-dicyanoanthracene (DCA) as a visible-light harvesting electron acceptor and Ph_3P as a sacrificial electron donor to drive one electron reductive β-activation of α,β-unsaturated ketones (Scheme 1.4). [30]

Pandey(1997): Photocatalytic Cyclisation

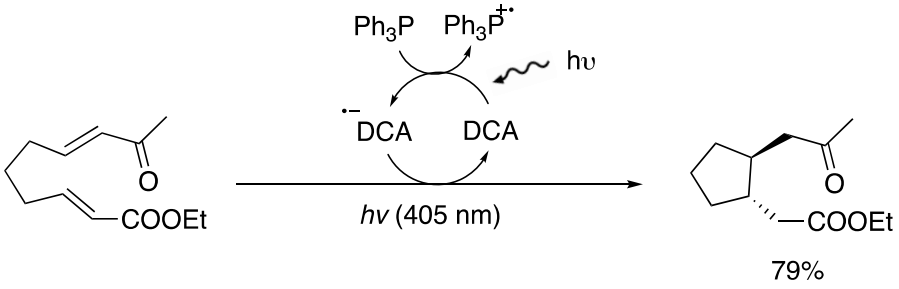

Scheme 1.4: Photocatalytic cycloadditions from sequential electron transfer.

A milestone in popularizing photocatalytic methods came in 2008 with a revolutionary publication by MacMillan and Nicewicz, who described the merging of photoredox catalysis with organocatalysis.[31] This reaction exploited the unique properties of photoredox catalysis to generate electron-deficient radicals that can combine with catalytically generated enamines to produce enantioenriched α-alkylated aldehydes in excellent yields (Scheme 1.5).

MacMillan (2008): Asymmetric α-Alkylation

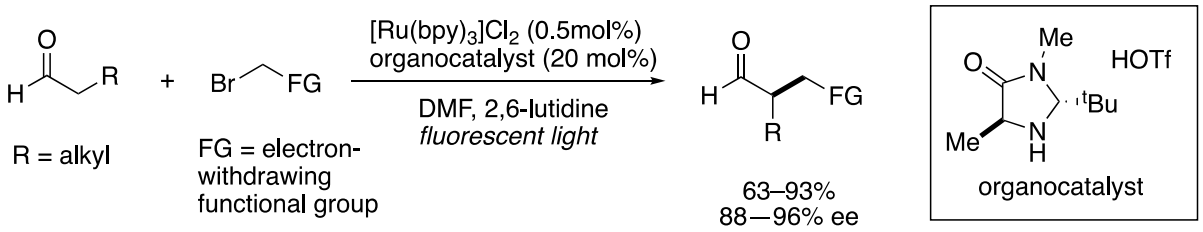

Scheme 1.5: Dual photoredox organocatalytic method for the asymmetric α-alkylation of aldehydes.

The above reactions highlight a few key examples of influential work into the field of photocatalysis in the past half-century.

1.1.2 Photodynamics of Excitation

In order to design efficient photocatalytic methods, it is important to understand the photophysics of a photoreaction. Jablonski diagrams can be used to describe the position and energy of an excited electron. Upon irradiation with a relevant light source, a photocatalyst is able to absorb a photon, leading to the excitation of an electron from the singlet ground state S_0 to an excited singlet state S_n (Figure 1.2).[32]

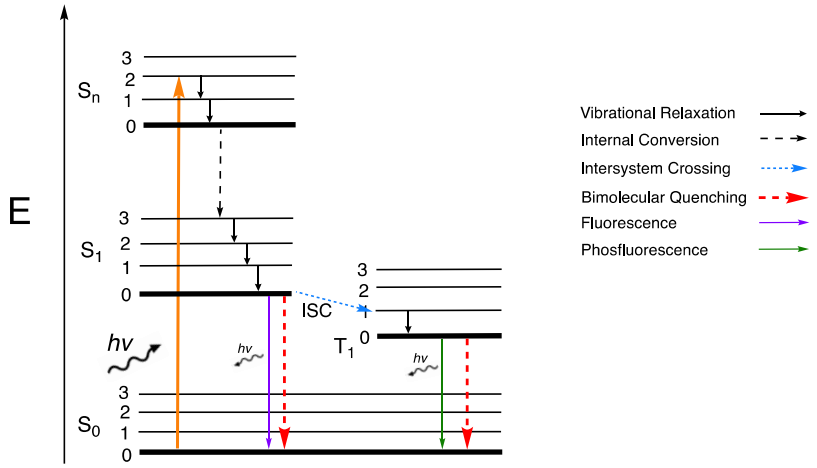

Figure 1.2: Simplified Jablonski diagram of photoexcitation from the singlet ground state (S_0) to an excited state (S_n) and various modes of decay (radiative and non-radiative) as well as intersystem crossing to the long-lived triplet state (T_1).

The singlet excited state is short lived and rapidly decays back to the ground state via radiative decay (fluorescence)[33] and non-radiative decay (vibrational relaxation or internal conversion). The S_1 excited state is also able to participate in bimolecular quenching (i.e. reactions with a substrate), but the possibility of this is dependent on the lifetime of the fluorescence (τ_f).

Generally, fluorophores with τ_f < 1 ns will not readily participate in bimolecular quenching[34] and therefore this decay route is highly unlikely. Once the electron has fallen to the lowest energy S_1 state, however, it is possible for it to undergo intersystem crossing (ISC) to the long-lived triplet excited state (T_1), as this state is energetically more favourable than S_1. ISC is associated with an electron spin reversal and is described as "spin forbidden". However, it is not completely impossible due a phenomenon called "spin-orbit coupling", a relativistic effect which occurs whenever a particle with non-zero spin moves around a region with a finite electric field.[35] This triplet state possesses a lifetime of > 100 ns[36] in solution and emission from the lowest energy level of T_1 to S_0 (phosphorescence) is slow due to it being spin-forbidden. This allows non-radiative decay in the form of bimolecular quenching to take place.[34,36–39]

1.1.3 Modes of Activation

A photocatalyst in its ground state consists of a HOMO (highest occupied molecular orbital) and LUMO (lowest unoccupied molecular orbital) (Figure 1.3). When excited by light, an electron in the HOMO absords energy and is able to "jump" to the LUMO. In this excited state, both frontier orbitals become singly occupied molecular orbits (SOMO), creating what's known as an electron-hole pair.[32] Intersystem crossing (ISC) can then occur which creates a long-lived triplet excited state, as discussed above.

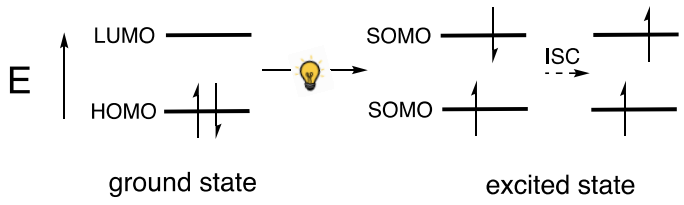

Figure 1.3: Light mediated excitation of an electron from HOMO to LUMO resulting in two SOMOs.

The interaction between an electronically excited photocatalyst and an organic molecule is possible through three different modes of activation, namely photoinduced electron transfer (PET) (Figure 1.4A), atom transfer (AT) (Figure 1.4B) and energy transfer (EnT) (Figure 1.4C).[37,39,40]

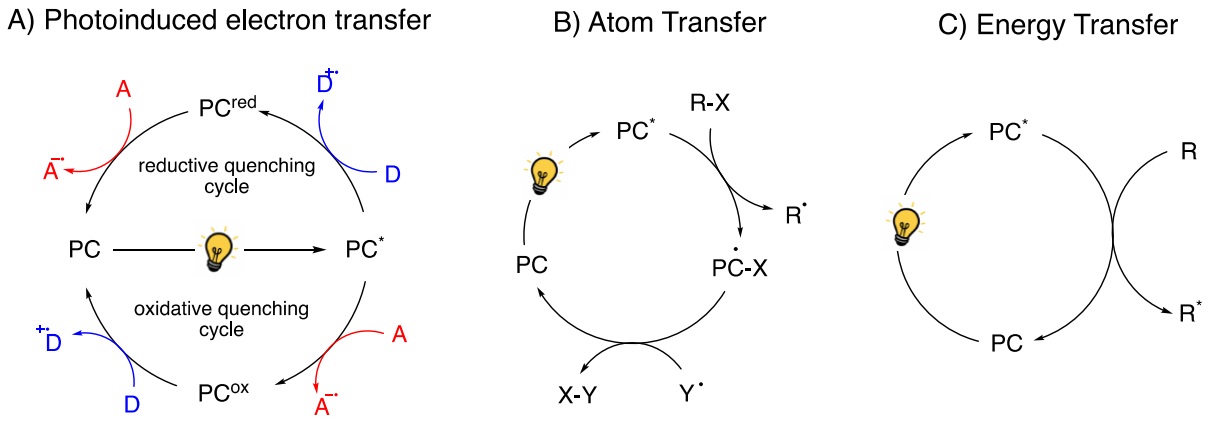

Figure 1.4: Various modes of activation between excited state photocatalysts and organic substrates.

(A) Photoinduced Electron Transfer (PET) – This class of reactions is known as photoredox catalysis and is the most studied of all the photocatalytic methods. Absorption of a photon by the photocatalyst (PC) leads to the electronically excited state (PC*). The excited photocatalyst (PC*) is then able to accept or donate a single electron, enabling reductive or oxidative quenching cycles, respectively. During a reductive quenching cycle, the PC* oxidizes a donor (D), resulting in a reduced photocatalyst (PC^{red}) and oxidized donor ($D^{+\bullet}$). PC^{red} can then donate an electron to a suitable acceptor (A) to close the catalytic cycle. Similarly, the inverse events can occur during an oxidative quenching cycle.

(B) Atom Transfer – A second important mode of photocatalytic activation involves production of radical intermediates via the transfer of an atom (X) from an organic substrate (R) directly to a photoexcited catalyst (PC*). The catalytic cycle is closed by a subsequent atom transfer (X-Y) to regenerate the ground state PC. The most popular of these reactions is hydrogen atom transfer (HAT), where X = H. HAT proceeds through a homolytic cleavage of a C-H bond, to produce substrate radical $R^{\bullet}$.

(C) Energy Transfer – Photocatalysts that undergo EnT are generally referred to as photosensitisers. A suitable photosensitiser is able to absord a photon to reach its excited state (PC*). This excited photosensitiser is able to transfer its energy to a ground state substrate (R), which is raised to a higher energy state (R*) and thereby able to undergo chemical transformations which were previously unattainable.

This review will focus exclusively on PET and EnT as these two areas of photocatalytic methods were investigated in my research.

1.2 Electron Transfer Catalysis

1.2.1 Definition

Electron transfer photocatalysis, commonly known as photoredox catalysis, involves a single electron transfer (SET) from an excited state photocatalyst. This process utilizes the high redox potential of various catalysts to either accept or donate an electron to a corresponding substrate, as a result of either an oxidative or reductive quenching cycle. The interaction between an electronically excited photocatalyst and an organic molecule can result in a diverse array of reactive intermediates for the formation of synthetically useful bond constructions.

1.2.2 Mode of action

As described in Figure 1.3 above, photoinduced promotion of an electron from the molecule's HOMO to its LUMO results in the formation of a charge-separated electron-hole pair. Electron transfer can occur from the energetically higher HOMO of a donor molecule to the lower lying SOMO of the excited PC* (reductive quenching cycle; Figure 1.5A) or from the higher SOMO of PC* to the lower LUMO of an acceptor molecule (oxidative quenching cycle; Figure 1.5B).

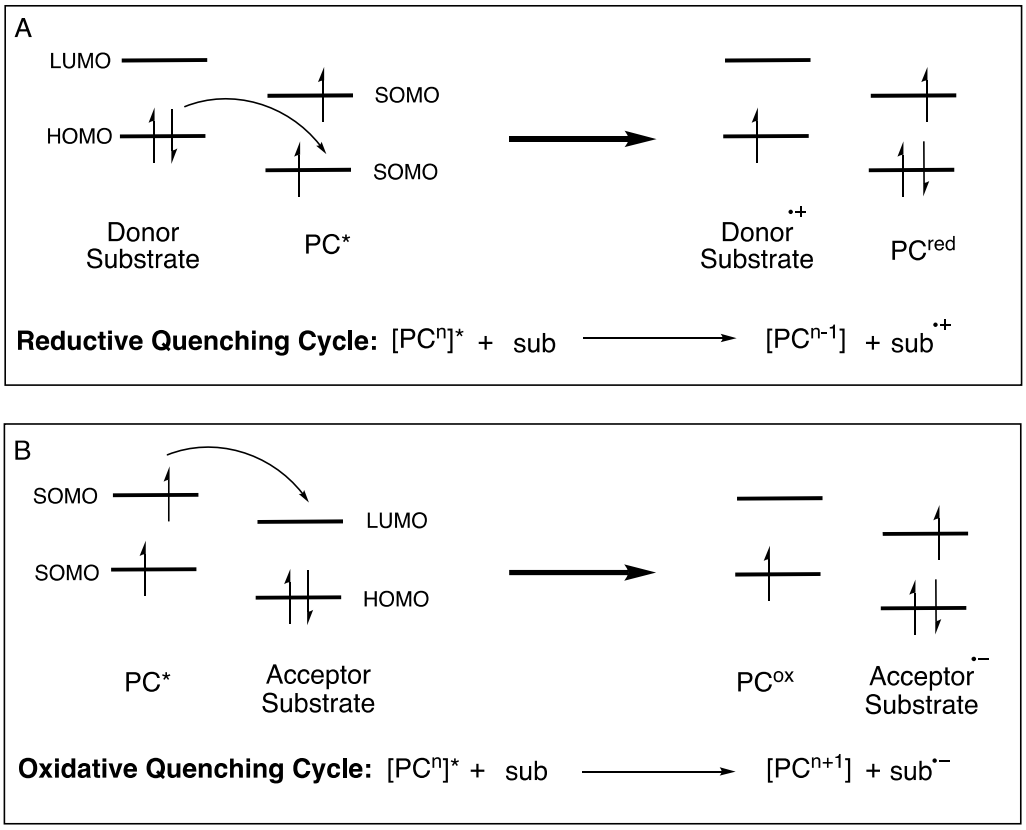

Figure 1.5: Energy scheme of orbitals involved in photochemical electron transfer and the general equation associated with each one.

An excited photocatalyst is typically both a stronger reductant and a stronger oxidant than its ground-state counterpart.

1.2.3 Thermodynamic Parameters

When designing a photoredox reaction, it is necessary to consider thermodynamic properties in order to determine whether an electron transfer between a photocatalyst and substrate will occur. Photoinduced electron transfer, like all redox reactions, can be envisioned as two half-reactions, an oxidation process and a reduction process. The free energy of a PET can be determined using redox potentials, as seen in equation (1) below.

$$\Delta G_{PET} = -F[(E_{ox}(D^{\bullet+}/D) - (E_{red}(A/A^{\bullet-})] - E_{0,0} - w \quad (1)$$

Where F is Faraday's constant, which describes the amount of charge carried by one mole of electrons.

In the above equation $E_{ox}(D^{\bullet+}/D)$ is the "oxidation potential of a donor D" and is defined by the half reaction:

$$E_{ox}: \quad D \xrightarrow{-e^-} D^{\bullet+} \tag{2}$$

Similarly, $E_{red}(A/A^{\bullet-})$ is the "reduction potential of an acceptor A" and is defined by the half reaction:

$$E_{red}: \quad A \xrightarrow{+e^-} A^{\bullet-} \tag{3}$$

Redox potentials of photocatalyst are determined using cyclic voltammetry and are well documented in the literature.[34,41,42]

A photocatalyst can act as either the electron acceptor (A) or electron donor (D) as discussed previously. However, since we are considering the free energy of a PET, the PC must first be excited to PC* (either A $\rightarrow$ A* or D $\rightarrow$ D* above). To account for the energy required to excite an electron from the ground state to an excited state, the term $E_{0,0}$ is used. $E_{0,0}$ can be approximated by the maximum emission of the catalyst.[38]

Additionally, equation 1 includes an electrostatic work term *w*, which accounts for the solvent-dependent energy difference due to the Coulombic impact of charge separation. Generally, the *w* term is frequently omitted on the basis that the correction it applies to ΔG_{PET} is relatively small.[34] $\Delta G_{PET} < 0$ represents an exergonic reaction, where energy is released, and $\Delta G_{PET} > 0$ is an endergonic reaction in which energy is absorbed by the reaction.

1.2.4 Kinetic Parameters

In addition to favourable thermodynamics, successful reaction design requires consideration of proper kinetics for the various steps associated with an electron transfer process. For any photoredox catalytic cycle there are at least two outer-sphere electron transfer processes that must occur: (1) an electron transfer to quench the excited state PC* and (2) a subsequent electron transfer to regenerate the ground-state catalyst. In both cases, a number of steps are required to generate the relevant products. For example, let us consider the oxidative quenching of a PC* (Figure 1.6). The excited photocatalyst, PC*, must first engage in a

diffusional encounter, k_d, with a quencher, Q, to form a precursor complex, **A**. This is a reversible process, k_{-d}, that can result in the starting reactants. Complex **A** can then undergo an electron transfer reaction, k_r, to form successor complex, **B**. At this point, there is the potential for the complex to experience the reverse electron transfer, known as charge recombination, k_{-r}, to regenerate the quencher and PC*. Alternatively, the radical ion pair of **B** may escape the solvent cage, k_s, to give the desired products of the oxidative quenching process **C**.

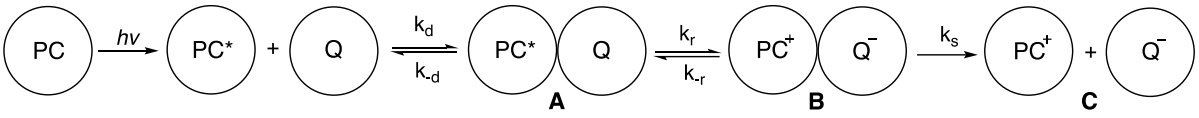

Figure 1.6: Outer sphere electron transfer process showing oxidative quenching of PC*

The rate constant of quenching k_q can be determined by the following equation.[38,43]

$$k_q = \frac{k_d}{1 + \frac{k_d}{k_r} + \frac{k_d}{k_s}.\frac{1}{K_r}} \qquad (4)$$

Where $K_r = \frac{k_r}{k_{-r}}$

Marcus Theory

The Marcus theory allows for the relation of rate of the electron transfer reaction, k_r, to several thermodynamic parameters.[44] Outer sphere electron transfer does not involve the making or breaking of bonds, however, it changes the electronic configuration of the reaction partners as well as causes a reorganization of the solvent cage. Consequently, an activation barrier, $\Delta G^{\ddagger}$, must be overcome in order for electron transfer to take place. According to the Marcus Theory, this $\Delta G^{\ddagger}$ can be represented by the intersection of the energy surface parabolas of the precursor complex, Figure 1.7 parabola A, and successor complex, Figure 1.7 parabola B. These parabolas are shifted vertically by ΔG° (ΔG_{PET} for the case of photoinduced electron transfer).

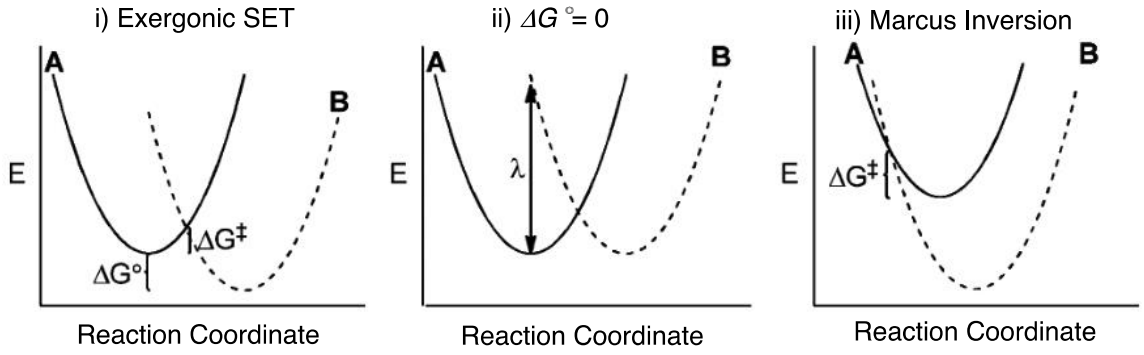

Figure 1.7: Marcus-Parabolas for different outer-sphere electron transfer.

Figure 1.7(i) depicts the reaction coordinate of an exergonic electron transfer. The intersection of these curves represents the activation barrier $\Delta G^{\ddagger}$. Figure 1.7(ii) represents a self-exchange reaction with $\Delta G^{\circ} = 0$. The reorganization energy, λ, represents the energy required for the reorganization of the precursor complex to the same nuclear configuration of the successor complex without letting the electron transfer occur. It is dependent on both the differences in the molecular configuration of the reactants and products as well as the reorganization of the solvent cage. The Gibbs free energy of activation can be expressed in terms of λ and ΔG° as in equation 5 below.[45]

$$\Delta G^{\ddagger} = \frac{(\lambda + \Delta G^{\circ})^2}{4\lambda} \qquad (5)$$

For the case of 1.7(ii) above with $\Delta G^{\circ} = 0$, $\Delta G^{\ddagger} = \lambda/4$. Figure 1.7(iii) depicts the Marcus inverted region, which occurs after a certain point with an increasingly exergonic reaction, in which $\Delta G^{\ddagger} > 0$. This represents a decrease in reaction rate.

The overall Marcus theory states that as ΔG° approaches -λ, the reaction rate *increases*. When $\Delta G^{\circ} =$ -λ, the reaction becomes barrierless, i.e. $\Delta G^{\ddagger} = 0$ (as per equation 5). As ΔG° becomes even more negative the rate of the reaction *decreases* ($\Delta G^{\ddagger} > 0$). This counterintuitive prediction was under debate for decades until its experimental validation in the 1980s by Miller and co-workers.[46–48] Qualitatively, this inverted Marcus region means that if the potential energy of the products is significantly lower than that of the reactants, the rate of the reaction can decrease.

1.2.5 Redox Cycles

Photoredox catalytic reactions are classified by two mechanistic cycles: (i) oxidative quenching cycle, where the excited state PC* is quenched by donating an electron; (ii) reductive quenching cycle where PC* is quenched by accepting an electron (Figure 1.8). After an electron transfer, it is necessary to regenerate the ground state catalyst. This involves reduction of the oxidized $PC^{\bullet+}$ in the oxidative cycle and oxidation of the reduced $PC^{\bullet-}$ in the reductive cycle. The substrate can therefore undergo electron transfer in the PET step or in the turnover step, and an external redox-active reagent is required for the alternative step. A net oxidative reaction produces an oxidized substrate and requires an external oxidant to accept an electron. Likewise, a net reductive reaction involves an external reductant and results in a reduced substrate.

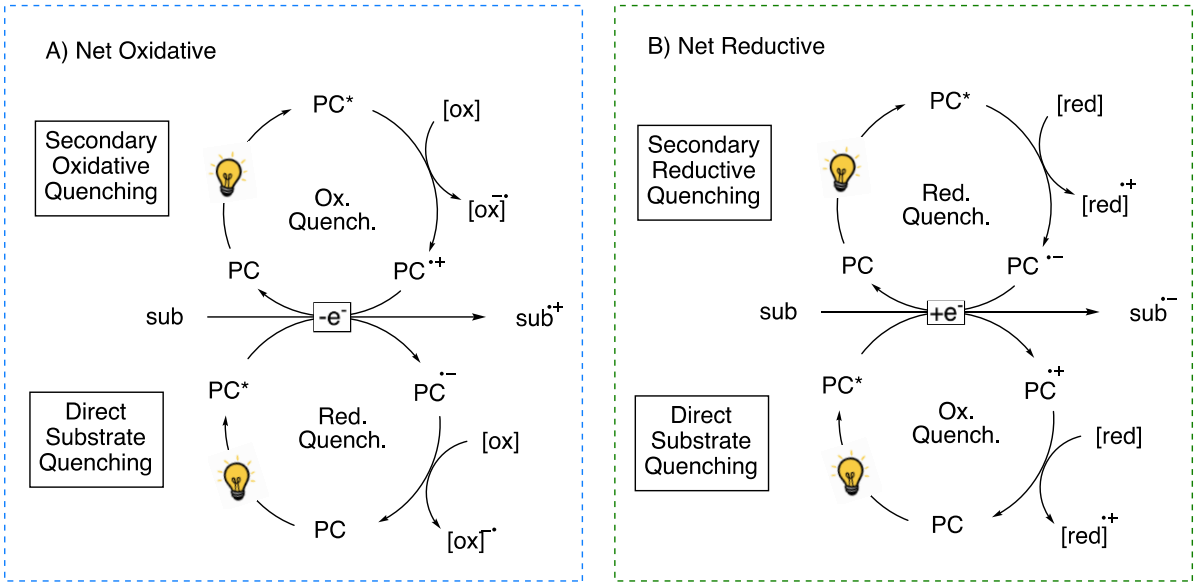

Figure 1.8: Net redox cycles for photoredox transformations

If the substrate first directly quenches the excited state of the photocatalyst and a balancing redox reagent then turns over the catalyst it is known as direct substrate quenching.

Finally, there is the potential for the substrates to be both oxidized and reduced by the photocatalyst, negating the use of a terminal stoichiometric redox reagent. These processes are called net redox-neutral and are sometimes mediated by a redox-active co-catalyst.

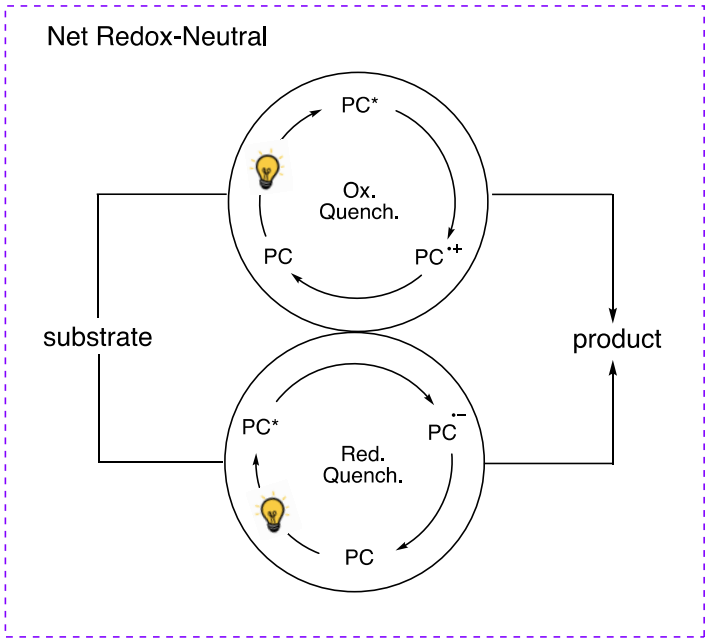

Figure 1.9: Net redox-neutral photoredox catalytic cycle

The first examples of redox neutral photocatalytic reactions were published by Deronzier. [25] (Scheme 1.2 above). In 2011, MacMillan and co-workers[49] developed a redox neutral transformation for α-amino C-H arylations using $Ir(ppy)_3$. The authors proposed an oxidative quenching cycle in which the excited photocatalyst is first oxidized by the cyanoarene coupling partner to produce a radical anion and the Ir(IV) state of the photocatalyst. The ground state catalyst is then regenerated by oxidizing the relevant *N*-arylamines. Radical-radical coupling followed by elimination of cyanide generates the benzylic amine products (Scheme 1.6).

Macmillan (2011): Redox Neutral C-H Arylation

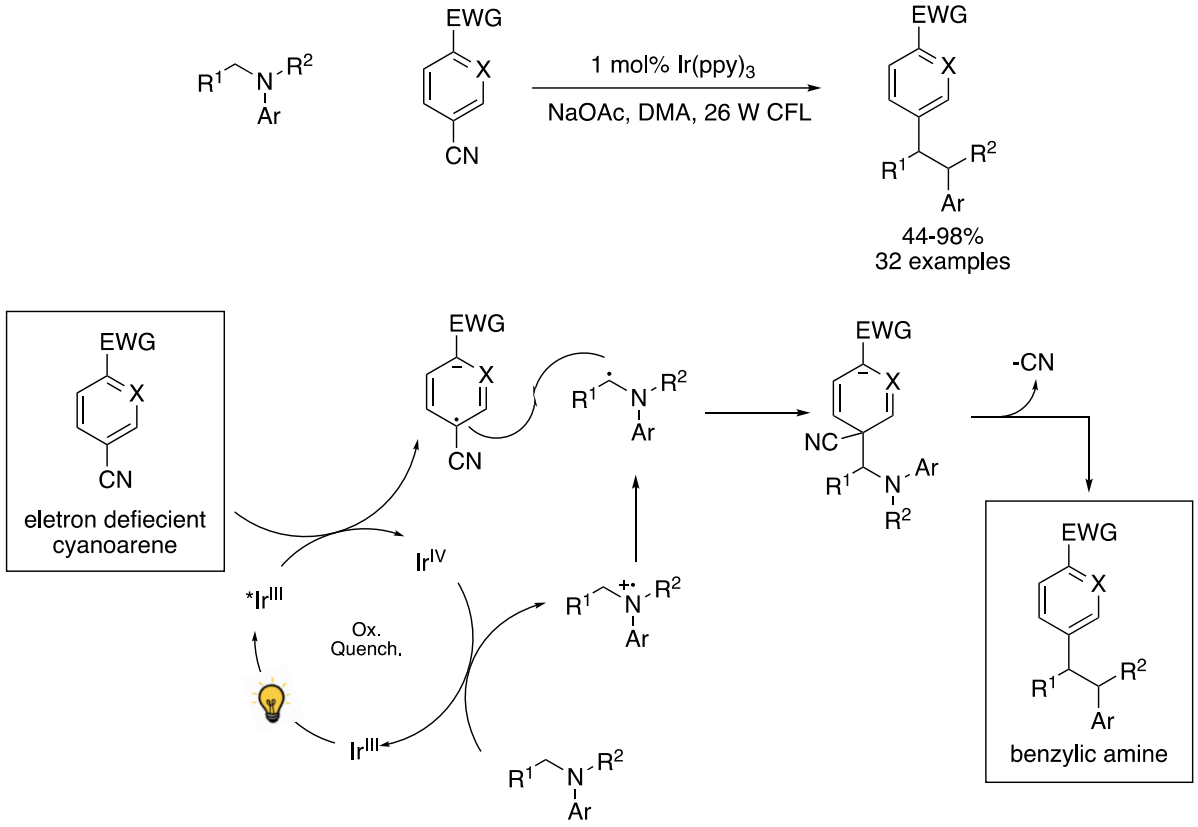

Scheme 1.6: A redox-neutral approach to α-Amino C-H arylation of electron deficient cyanoarenes and the proposed mechanistic pathway.

1.2.6 Photocatalysts

An important benefit of photoredox catalysis is the availability of a diverse range of photocatalyst structures that span a broad range of triplet energies and redox potentials. In general, photocatalysts comprise either redox-active transition metal complexes, organic dyes or inorganic clusters. Several typical photoredox catalysts with their respective absorption maxima and estimated excited-state reduction and oxidation potentials[50,51] are shown in Figure 1.10. As one might expect from molecules designed to interact with light, this class of catalysts is dominated by highly conjugated systems. Transition metal photocatalysts consist of mostly Ru- and Ir- based complexes whose properties can be easily tuned by ligand modification. In a quest for cheaper, more environmentally sustainable photocatalysts, a collection of organic dyes have been identified as powerful alternatives to metal photocatalysts.

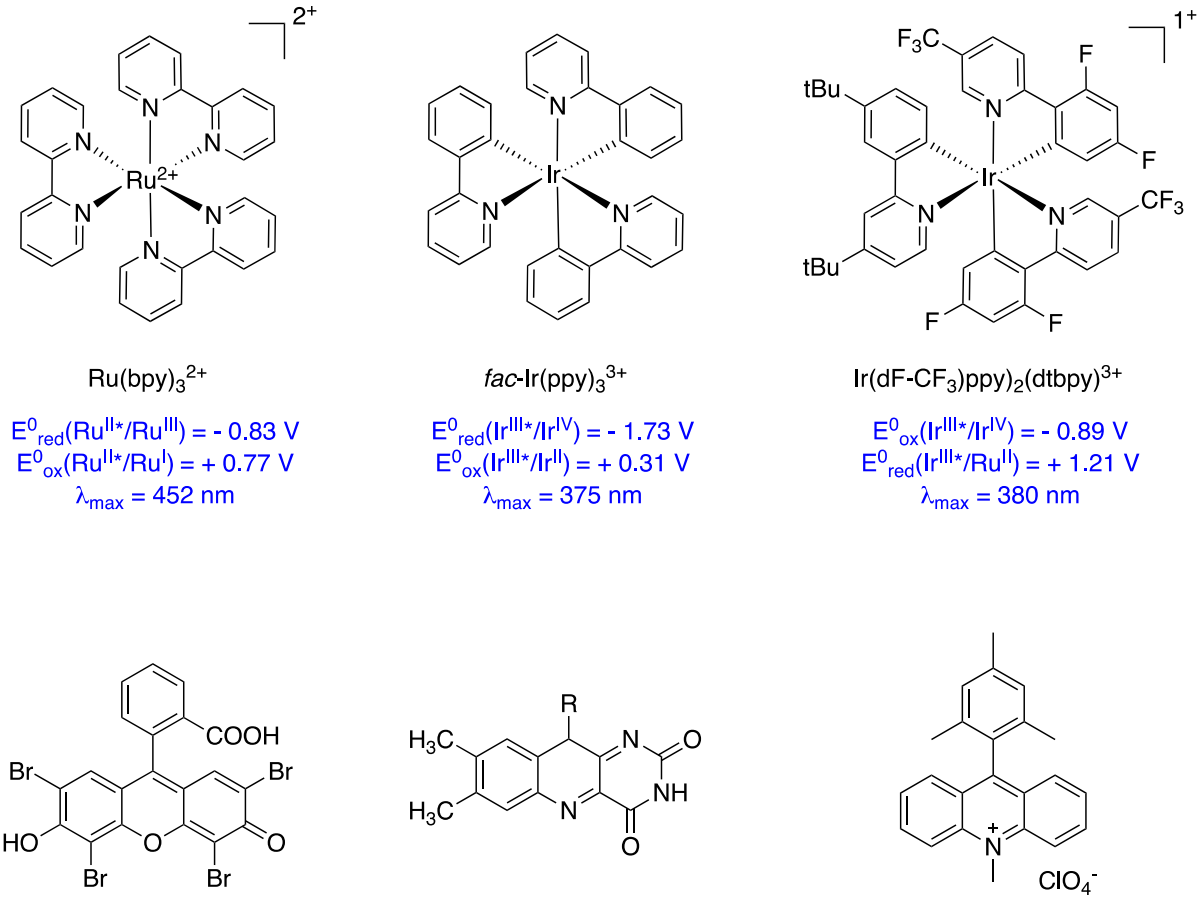

Figure 1.10: A selection of common photoredox catalysts with associated reduction and oxidation potentials and absorption maxima.

1.2.7 Dual Catalytic Methods

It is sometimes necessary to combine photocatalysis with conventional catalytic methods. Co-catalysts can be used to influence photoredox transformations by mediating the electron transfer, by independently generating an intermediate species that undergoes photocatalytic activation *in situ*, or by controlling a reactive intermediate downstream of the photoinduced electron-transfer process itself. The most well developed dual catalytic methods with photoredox catalysis are (i) organocatalysis, (ii) transition metal catalysis and (ii) Lewis acid catalysis.

(i) Organocatalysis

The majority of the dual organocatalytic activation modes involve the use of the

organocatalyst directly in the activation step; either by inducing an electron transfer or by generating an intermediate species that participates directly in the PET step. As discussed earlier, pioneering work by Nicewicz and MacMillan.[31] in 2008 described the first dual photoredox organocatalysis method for the enantioselective α-alkylation of aldehydes. A chiral secondary amine is used as the organocatalyst, which undergoes condensation with the aldehyde starting material. The photoexcited $Ru(bpy)_3^{2+}$ is reduced by the organocatalytic cycle, forming $Ru(bpy)_3^{+}$. This reduces an alkyl halide which then undergoes dehalogenation to afford electron-deficient α-ketoradical. Radical addition of this species in the organocatalytic cycle, followed by oxidation by the photocatalytic cycle and hydrolysis results in the α-alkylated product (Scheme 1.7).

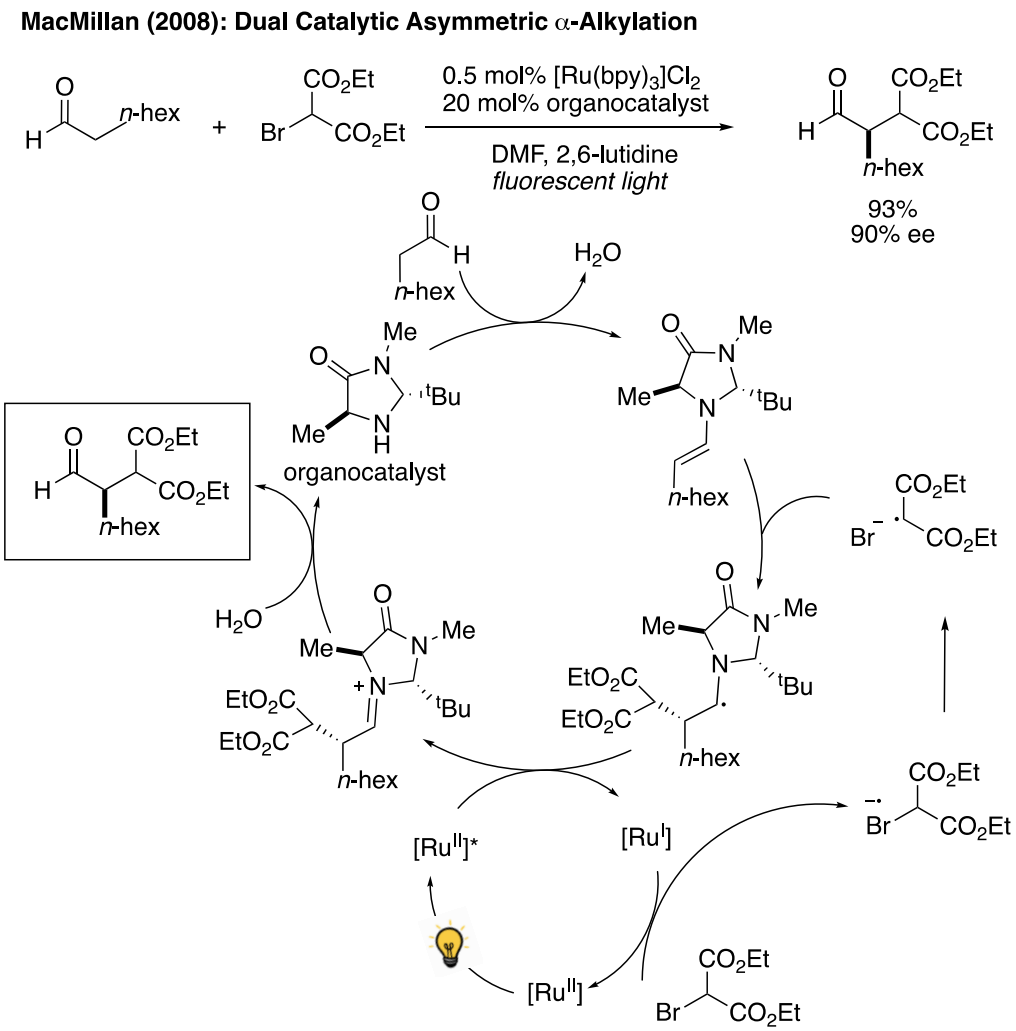

Scheme 1.7: Dual photoredox and organocatalytic method for the direct asymmetric alkylation of aldehydes and proposed mechanistic pathway.

(ii) Transition Metal Catalysis

Similarly to dual organocatalytic reactions, transition metal-catalysed reactions can aid in photocatalysis, either by direct electron transfer between the organometallic complex and the photocatalyst or mediated by a photogenerated reactive intermediate. Rueping and co workers[52] developed an indole synthesis based upon the intramolecular oxidative C-H arylation of enamides. In their proposed mechanism, the Ir photocatalyst is used to reoxidize Pd^0 to Pd^{II} (Scheme 1.8).

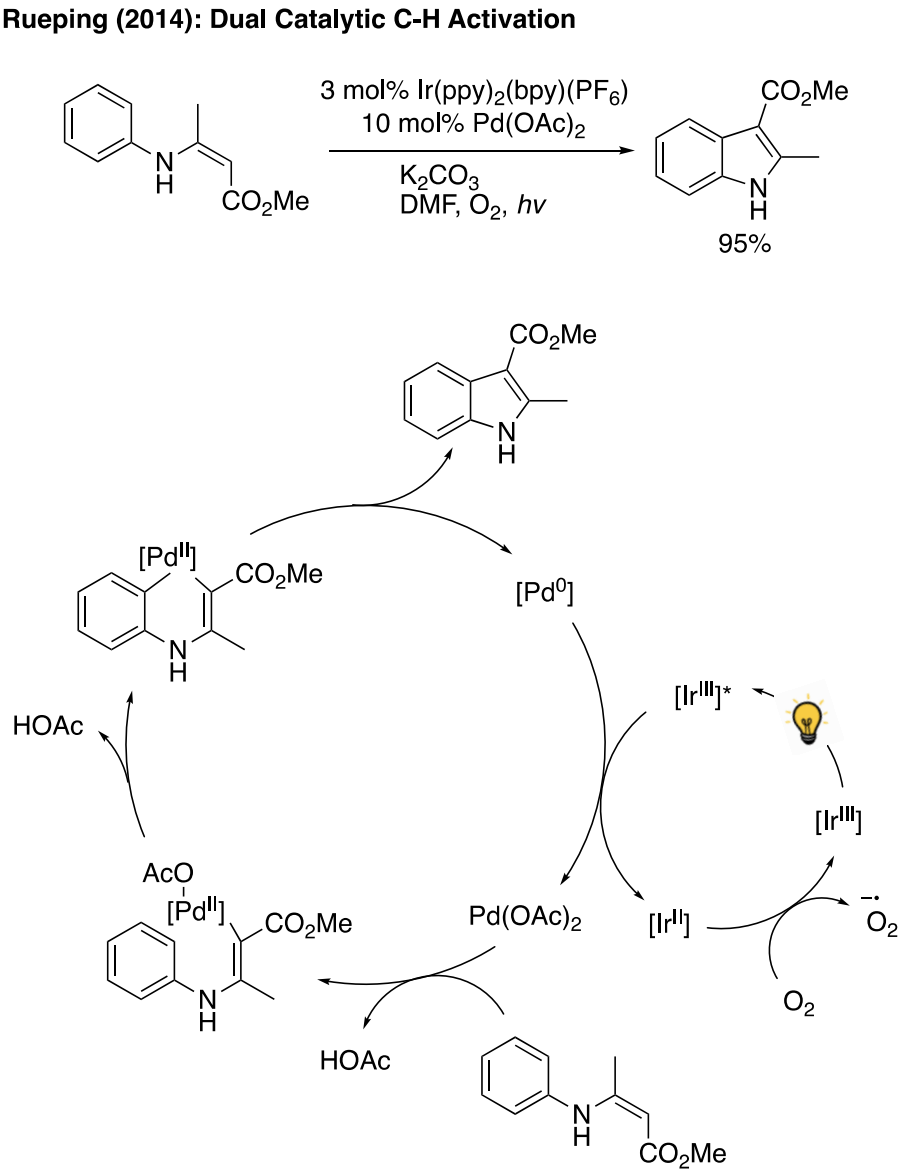

Scheme 1.8: Dual photoredox and transition metal catalysis for the synthesis of indoles via C-H activation and proposed mechanistic pathway.

(iii) Lewis Acid Catalysis

Coordination of a Lewis acid with a heteroatom containing substrate can withdraw electron density, activating the substrate towards nucleophilic attack. The strong prevalence of ketone and enone functional groups in photochemistry make Lewis acids a powerful co-catalyst. They can also impact the rate of a reaction by stabilizing a ketyl radical or other photoreduced anionic intermediates. Shortly after MacMillan's dual organocatalytic publication, Yoon and co-workers[53] disclosed a $Ru(bpy)_3^{2+}$ catalysed diastereoselective intramolecular [2+2] enone cycloaddition reaction with the use of a Lewis acid additive ($LiBF_4$) to control the reactivity of the enone substrate (Scheme 1.9).

Yoon (2008): Dual Catalytic [2+2] Enone Cycloaddition

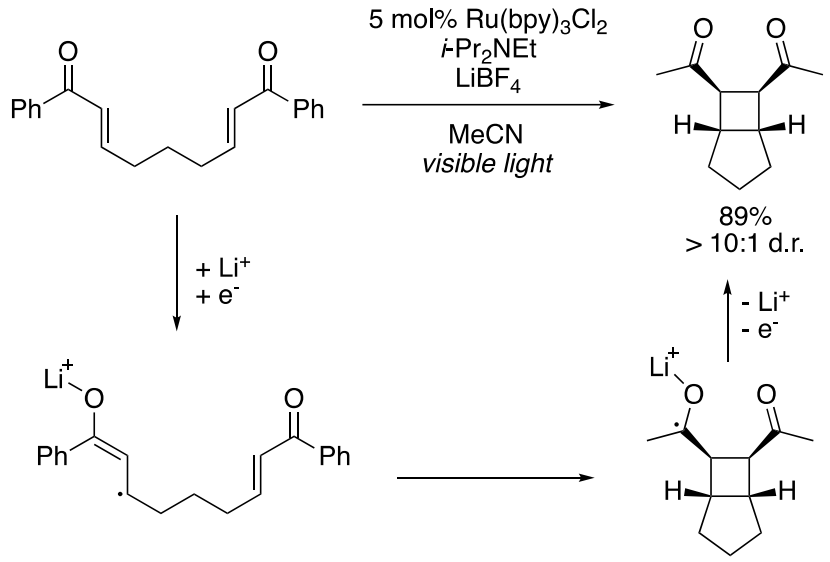

Scheme 1.9: Dual photoredox and Lewis acid catalysed approach for a diastereoselective intramolecular [2+2] enone cycloaddition and proposed mechanistic pathway.

1.3 Energy Transfer Catalysis

1.3.1 Definition

Energy transfer (EnT) is formally defined as ''*The photophysical process in which an excited state of one molecular entity (the donor D) is deactivated to a lower-lying state by transferring energy to a second molecular entity (the acceptor A), which is thereby raised to a higher energy state.*''[54] In energy transfer catalysis, the donor represents the catalyst (photosensitiser) that can be excited by direct absorption of visible-light. This is followed by an energy transfer to a substrate (the acceptor) which is "sensitised" or indirectly excited. Unlike photoredox catalysis, which has received great interest within the last two decades, EnT catalysis has remained relatively underdeveloped.

1.3.2 Mode of Action

Once an electron has reached its excited state, it is able to decay back to its ground state via bimolecular quenching with a suitable acceptor. There are two different mechanisms proposed for this non-radiative EnT, namely coulombic interactions and exchange interactions.

(i) Förster (Resonance) Energy Transfer (FRET)[55,56]

The first mechanism proceeds via a dipole-dipole (coulombic) interaction (Figure 1.11). After absorption of a photon, the excited electron relaxes back to the ground state, releasing energy. If the acceptor is sufficiently close by, this excess energy may simultaneously excite the acceptor. The efficiency of FRET is dependent on (1) the distance between the donor and acceptor (typically in the range of 1-10 nm), (2) the spectral overlap of the donor emission spectrum and the acceptor absorption spectrum and (3) the relative orientation of the donor emission dipole moment and the acceptor absorption dipole moment.

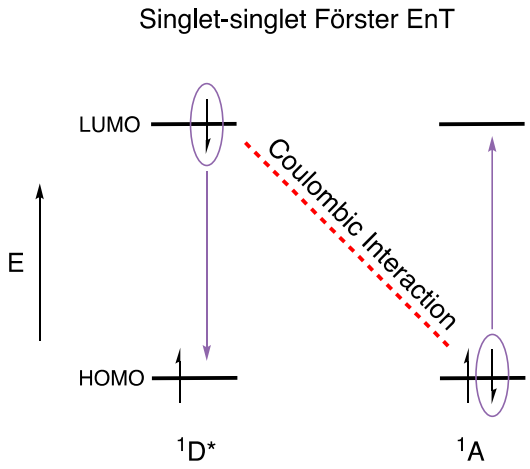

Figure 1.11: Schematic diagram of coulombic interaction.

FRET has many applications, mainly in biotechnology and biological studies and the pharmaceutical industry. However, EnT by a photocatalyst to an organic substrate cannot be described by FRET. This is because the relaxation from a photocatalyst in its triplet excited state to its singlet ground state represents a spin reversal process. Similarly, the simultaneous excitation of the acceptor from its ground state to triplet excited state also represents a forbidden process. These 2 spin reversal processes violate Wigner's spin conservation rules.[1]

(ii) Dexter Energy Transfer[57]

Dexter energy transfer describes the simultaneous intermolecular exchange of ground state and excited-state electrons respectively (Figure 1.12). The reaction rate of a Dexter energy transfer decays exponentially as the distance between the molecules increases, dropping to negligibly small values if the distance increases to the order of 2 or more molecular diameters. For this reason it is also referred to as short-range energy transfer. This exchange mechanism gives access to the triplet excited state of the acceptor while preserving the Wigner spin conservation rules.

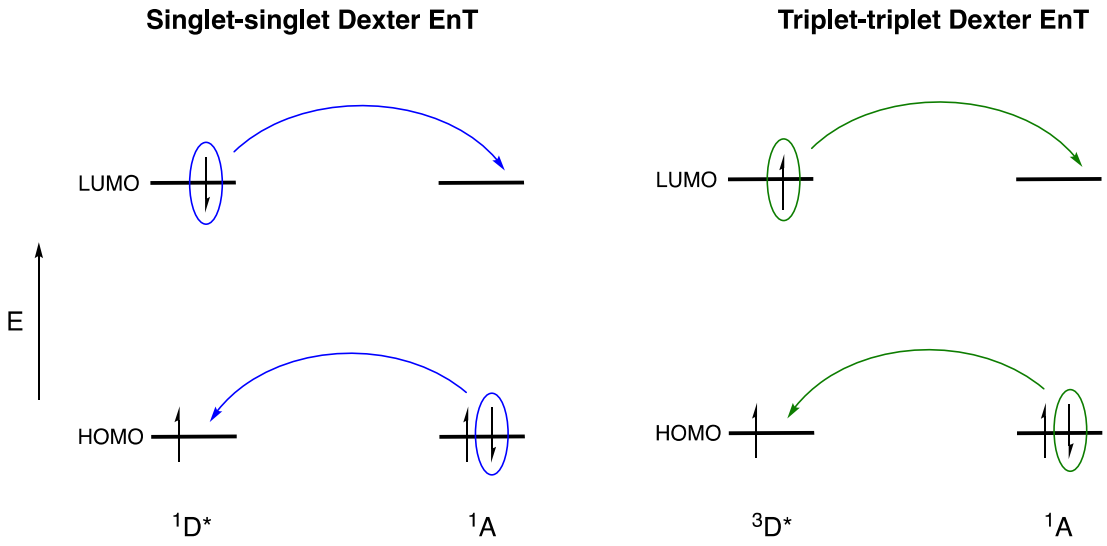

Figure 1.12: Schematic diagram of singlet-singlet and triplet-triplet exchange interactions.

Similarly to FRET, an overlap between the emission spectra of D and the absorption spectra of A is needed. In addition, for an exchange energy transfer, there needs to be an overlap of the wavefunctions, otherwise described as the electron cloud.

The rate constant of exchange energy transfer is given by:

$$k_{EnT} = K \cdot J \cdot e^{\frac{2R_{DA}}{L}} \quad (6)$$

Where *J* is the normalized spectral overlap integral, K is an experimental parameter related to orbital interactions, R_{DA} is the distance between the donor and acceptor and L is the sum of the van der Waal's radii. The Dexter energy transfer can be represented as a concerted electron-hole exchange interaction. It involves a double electron transfer to and from the donor and acceptor molecules.

1.3.3 Triplet Energy Transfer

Dexter energy transfer can be used to describe a triplet EnT process from a photocatalyst's excited triplet state to a substrate. The general scheme of a triplet energy transfer is shown below:

$$D^* (T_1) + A (S_0) \longrightarrow D (S_0) + A^* (T_1) \quad (7)$$

The donor in its triplet excited state transfers its energy to the ground state acceptor, which is excited to its triplet state. As the overall spin multiplicity of the donor and acceptor on the reactant side is the same as on the product side, this energy transfer is spin-allowed.

EnT can be represented using a simplified Jablonski energy diagram. As with photoredox catalysis, an electron in the photocatalyst (donor) is excited to its singlet ground state S_1. Intersystem crossing can then occur, resulting in the triplet excited state of the donor. This is followed by a coupled non-radiative transition in which the deexcitation of T_1 to S_0 in the donor induces a coupled S_0 to T_1 transition of the same energy in the ground state acceptor molecule (Figure 1.13).[36]

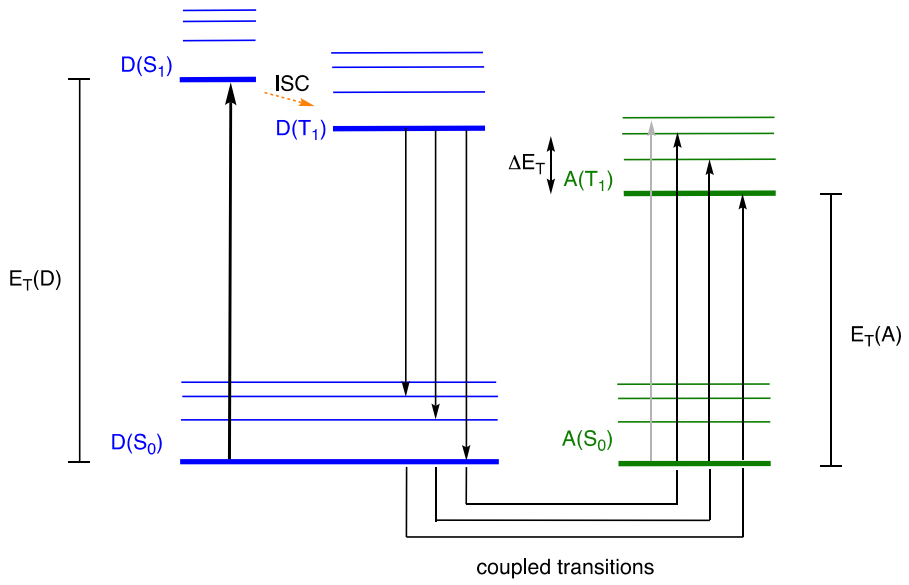

Figure 1.13: Simplified Jablonski scheme of coupled transitions for Dexter energy transfer.

The mechanism by which an EnT reaction in solution occurs is described by the potential energy diagram below (Figure 1.14). First, the excited photosensitiser (donor D) and substrate (acceptor A) approach each other through diffusion to form a solvent-shared encounter complex. As D* and A approach each other, the excitation energy becomes delocalized resulting in a lowering of energy. Collision within this encounter complex leads to an exciplex,[58] which, due to the greater polarizability of excited state molecules, is stabilized though London dispersion interactions. The point where the potential energy surfaces cross

is referred to as r_c, and it becomes favourable for the excitation energy to shift from D to A. Another exciplex is reached, where the energy mostly resides on A, followed by the dissociation of the collision complex and diffusion out of the solvent cage to give the products D and A*. It is also possible for phosphorescence to occur at any point, causing the molecules to fall to their ground states.

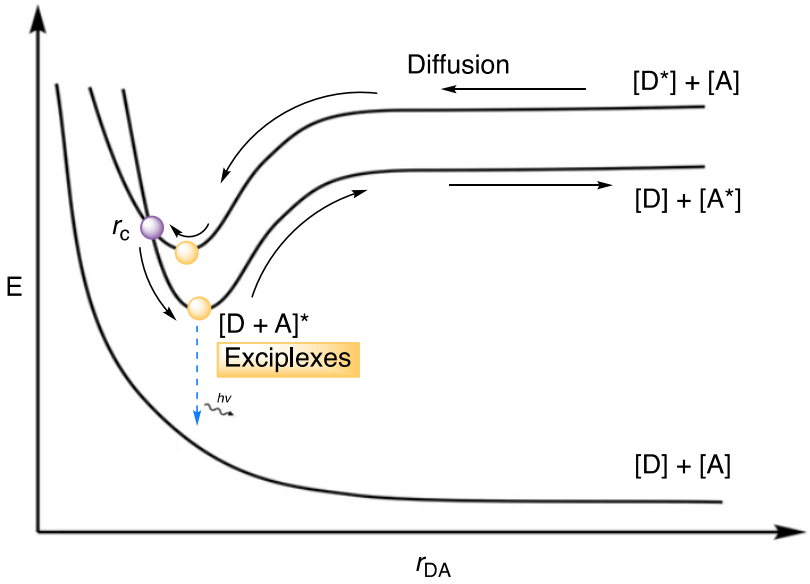

Figure 1.14: Potential energy diagram for an EnT between D and A in solution.

1.3.4 Kinetic Parameters

The overall rate of quenching of an EnT reaction depends on the rate of diffusion, k_{diff}, and the probability that an energy transfer occurs during the lifetime of the encounter complex, k_{EnT} (Figure 1.15).[59]

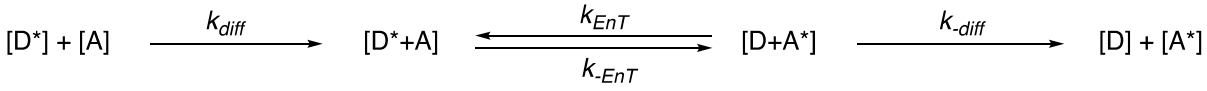

Figure 1.15: Simplified overview of the molecular process of triplet-triplet EnT in solution.

From the Stern-Volmer equation it can be determined that the rate of the quenching process, k_q, is given by equation 8.

$$k_q = \left[\frac{k_{EnT}}{k_{-diff} + k_{EnT}}\right] k_{diff} \qquad (8)$$

We can thus distinguish two limiting cases:

(i) If the EnT is sufficiently faster than the rate of backwards diffusion ($k_{EnT} >> k_{-diff}$) then $k_q = k_{diff}$ and the quenching process is **diffusion controlled**,[60] meaning that every time D* encounters A, quenching occurs.

(ii) If the reverse is true ($k_{EnT} << k_{-diff}$), then $k_q = k_{EnT}(k_{diff}/k_{-diff})$ and the EnT event itself becomes the rate-limiting step.

As described above in equation 6, the rate of a Dexter EnT, k_{EnT}, is governed by the normalized spectral overlap integral *J*. 'Normalized' means that the absorption spectra and emission spectra are adjusted to the same scale and have the same highest level. For Dexter EnT, *J* is defined by:[57]

$$J = \int_0^\infty f_D(v) \cdot \varepsilon_A(v) dv \tag{9}$$

Where f_D is the normalized donor emission spectrum (phosphorescence spectrum) and ε_A is the normalized acceptor (singlet-to-triplet) absorption spectrum.

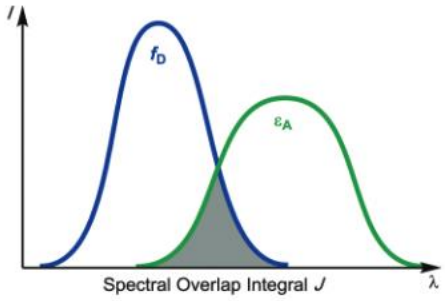

Figure 1.16: Normalized spectral overlap integral, *J*, for Dexter EnT.

In a Jablonski diagram (Figure 1.13), *J* represents the number of coupled transitions between D and A.[61]

1.3.5 Thermodynamic Parameters

The difference in the triplet excited state energies of the donor and acceptor, $\Delta E_T = E_T(A) - E_T(D)$, determines the efficiency of the EnT.

For an exothermic EnT ($\Delta E_T < 0$), there are a large number of coupled transitions, resulting in a fast rate of energy transfer. In this case, the reaction is usually diffusion controlled. Endothermic energy transfer ($\Delta E_T > 0$) is not forbidden by the laws of thermodynamics, however it is (typically) negligibly slow.

1.3.6 Determining Triplet Energies

The triplet energies (E_T) of different molecules can be determined experimentally using three different techniques. The preferred method is with the use of short-wavelength phosphorescence spectra.[62] By measuring the phosphorescence excitation, one can make direct comparisons with the ground state to triplet excited state energy (E_T). Usually, the measurements are performed at cryogenic temperatures (< 100K), as this reduces the rate of non-radiative decay from the T_1 state and allows a better spectral resolution.

It is also possible to measure the singlet to triplet (S → T) absorption energy by direct absorption measurements, however there are a number of difficulties associated with this method, namely need to separate the S → T absorption from the tail of the singlet to singlet (S → S) absorption.

Finally, by measuring the energy transfer rate constant of a series of triplet donors being quenched by acceptors, the triplet energy of a donor can be estimated. As long as the donor's triplet energy is above that of the acceptor's, the quenching proceeds at a rate constant approaching that of diffusion controlled (see Kinetic Parameters). Once the donor's triplet energy falls below the acceptor's, the rate constant decreases rapidly.

In recent years, a theoretical method for determining triplet energies has gained widespread popularity. The use of density-functional theory (DFT) calculations has been implemented in estimating triplet energies of excited state molecules as well as any intermediates that occur during a particular reaction.[63]

1.3.7 Photosensitisers

There are a vast number of photosensitisers capable of performing a variety of organic transformations. In order for a photosensitiser to be a suitable EnT catalyst for organic reactions, it needs to possess four general properties[64]: (1) high absorption abilities at the desired wavelength, (2) efficient intersystem crossing to its triplet state, (3) significantly long excited triplet state lifetimes and (4) higher triplet excited-state energy than the substrate acceptor. The photophysical properties of many photosensitisers have been extensively studied and are well documented.[61,65] Figure 1.17 below shows some common transition metal and organic photosensitisers and their corresponding triplet energies (E_T), longest absorption wavelength (λ_{max}), triplet lifetimes (τ_T) and intersystem crossing yields (Φ_T).

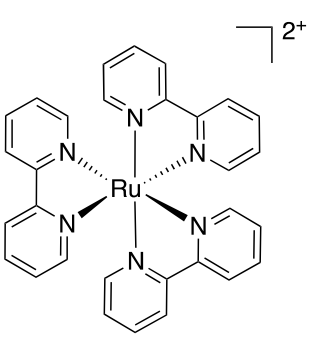

$Ru(bpy)_3^{2+}$
E_T = 49.0 kcal.mol^{-1}
λ_{max} = 570 nm
τ_T = 1 µs
Φ_T > 0.95

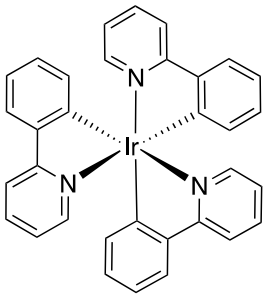

***fac*-Ir(ppy)$_3$**
E_T = 58.1 kcal.mol^{-1}
λ_{max} = 450 nm
τ_T = 2 µs
Φ_T > 0.95

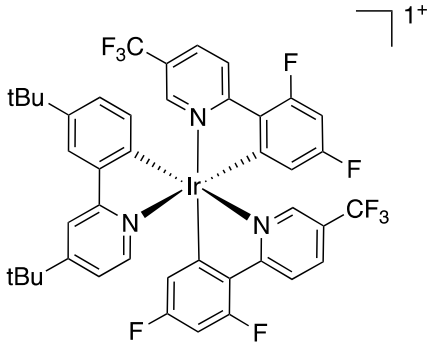

$Ir(dF(CF_3)ppy)_2(dtbpy)^+$
E_T = 61.8 kcal mol^{-1}
λ_{max} = 450 nm
τ_T = 3 µs
Φ_T > 0.95

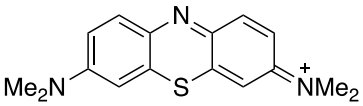

Methylene Blue
E_T = 32.0 kcal mol^{-1}
λ_{max} = 665 nm
τ_T = 450 µs
ΦT = 0.52

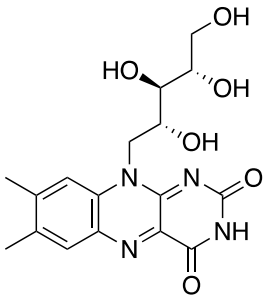

Riboflavine
E_T = 50.0 kcal mol^{-1}
λ_{max} = 450 nm
τ_T = 19 µs
Φ_T = 0.40

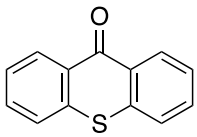

Thioxanthone
E_T = 63.4 kcal mol^{-1}
λ_{max} = 380 nm
τ_T = 73 µs
Φ_T = 0.6

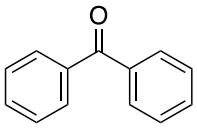

Benzophenone
E_T = 69.1 kcal mol^{-1}
λ_{max} = 380 nm
τ_T = 50 µs
Φ_T > 0.95

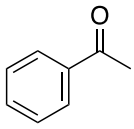

Acetophenone
E_T = 74.0 kcal mol^{-1}
λ_{max} = 350 nm
τ_T = 0.14 µs
Φ_T > 0.95

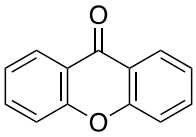

Xanthone
E_T = 74.0 kcal mol^{-1}
λ_{max} = 340 nm
τ_T = 17.9 µs
Φ_T > 0.95

Figure 1.17: A selection of common photosensitisers with associated photophysical properties.

It should be noted that the corelation between triplet energies and molecular structures of photosensitisers are not well understood. Usually, an enlargement of the conjugated π-system corresponds to a decreasing of triplet energies. However, not much is known about a correlation between substituents and triplet energies.

1.3.8 Identification of Triplet Energy Transfer

It is necessary to be able to identify and analyse EnT processes in order differentiate from competitive SET pathways, especially since many photocatalysts can act as both photoredox catalysts and triplet energy sensitizers. The most efficient way to determine whether an EnT process has occurred is with the use of transient absorption spectroscopy (TAS), a pump-probe spectroscopic technique utilised to measure the excited state absorption energies and associated lifetimes of molecules.[62,66] First, the molecule is excited by a light source (pump pulse), next, a second light source (probe pulse) measures the change in the excited-state absorption. This process is repeated for different delay times between the pump and probe pulses to measure the change in transmitted energy (Figure 1.18).

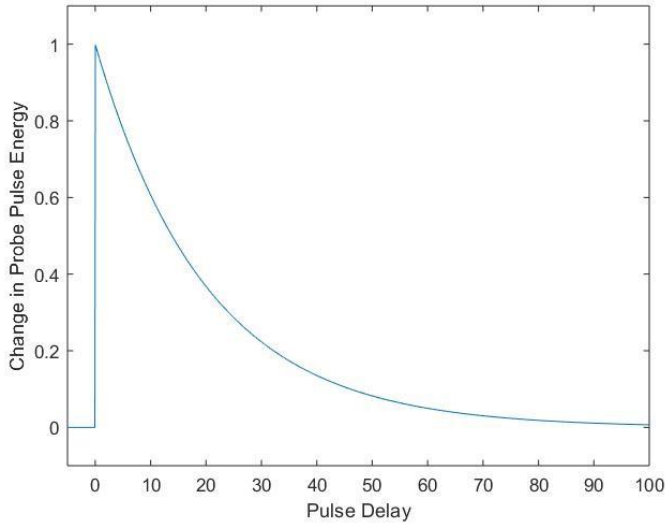

Figure 1.18: Simulated pump-probe TAS kinetic decay data taken from https://www.avantes.com/applications/cases/introduction-to-transient-absorption-spectroscopy/

Proof of an EnT event can then be obtained by monitoring whether the transient absorption spectra of the excited donor is quenched with addition of an acceptor, and the transient absorption spectra of an excited acceptor arises.

Transient absorption spectroscopy requires an expensive, specialist instrument which is not widely available. As such, it is beneficial to identify alternative strategic studies to confirm an EnT pathway is occurring. Stern-Volmer luminescence quenching studies can be used to reveal information about the rate of the reaction.[67] As the rate of an EnT is highly dependent

on the sensitizers E_T, experimental correlation between various known energy sensitizers and Stern-Volmer constant, K_{SV}, can be used to confirm an EnT pathway is occurring.

1.3.9 Applications in Organic Synthesis

Although the field of energy transfer catalysis is highly underdeveloped compared to the more popular photoredox catalysis, there have been a number of powerful synthetic applications using EnT, especially in the last decade.[64] These applications can be organized into four main categories: cyclisation reactions, isomerisations, bond dissociations and excitation of transition metal complexes.

Cyclisation Reactions

The formation of new carbon-carbon (C-C) bonds is one of the most explored areas of organic chemistry. Visible-light mediated photochemical cycloadditions are powerful tools towards the formation of new C-C bonds under mild and environmentally friendly conditions. One of the most explored of these cyclisation reactions is the [2+2] cycloaddition. The construction of cyclobutane scaffolds from two olefins in a [2+2] cycloaddition is of utmost importance. However, the mechanism by which this occurs differs from traditional pericyclic reactions. First, excitation to the triplet state generates a biradical; olefin addition then generates a 1,4-biradical intermediate which is followed by intersystem crossing and radical recombination (Scheme 1.10).

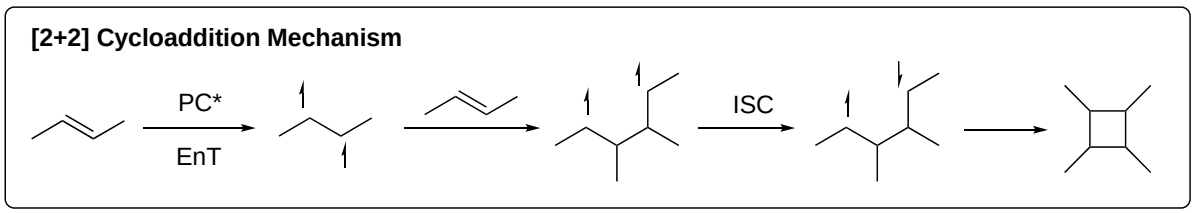

Scheme 1.10: General mechanism of photosensitised pericyclic reaction for the formation of cyclobutane.

Pioneering work by Yoon and co-workers[68] in 2012 describes the intramolecular [2+2] photocycloaddition of styrenes for the formation of cyclobutane in excellent yields (Scheme 1.11). An iridium catalyst was used as the photosensitiser and a compact fluorescence light (CFL) was used to irradiated the reaction.

Yoon (2012): Intramolecular [2+2] cycloaddition

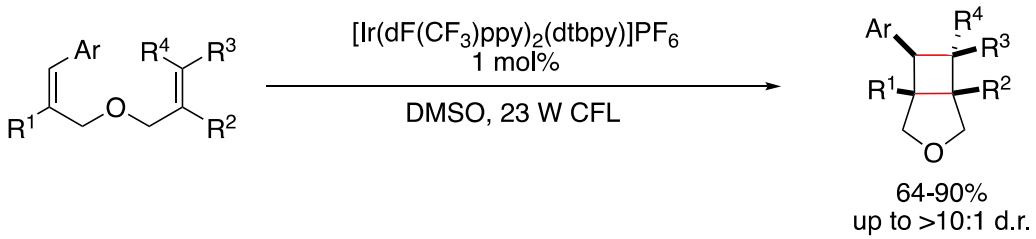

Scheme 1.11: EnT catalysis for the [2+2] photocycloaddition of styrenes

Another significant challenge that has been overcome with EnT photocatalysis, is an enantioselective approach to [2+2] cycloadditions. Bach and co-workers[69] developed an elegant chiral thioxanthone catalyst that is able to coordinate to a quinolone substrate through hydrogen bonding in order to direct the cycloaddition with excellent enantioselectivities. Enantioface differentiation is provided by the planar thioxanthone so that attack at the quinolone double bond occurs with high selectivity (Scheme 1.12).

Bach (2014): Enantioselective [2+2] Cycloaddition

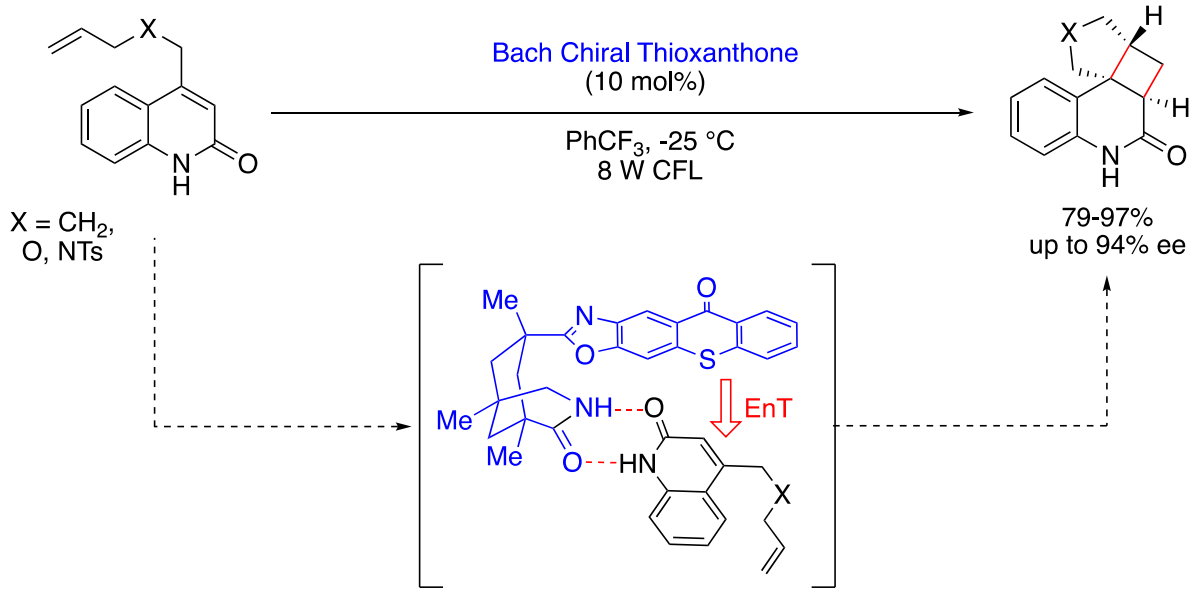

Scheme 1.12: EnT catalysis for enantioselective [2+2] photocycloaddition using a chiral thioxanthone photosensitiser.

Yoon and co-workers[70] made another significant advancement in enantioselective EnT with the use of a chiral Lewis acid co-catalyst for the asymmetric [2+2] photocyclisation of 2'-hydroxychalcones using tris(bipyridyl) ruthenium(II) as a sensitizer. In addition to the Lewis acid directing the stereochemistry via a coordination complex, it also became evident that

the coordination dramatically lowered the triplet energy of the chalcone substrate from E_T = 54 kcal.mol^{-1} to E_T = 33 kcal.mol^{-1}. This difference in triplet energy was sufficient to allow the Ru photosensitiser (E_T = 49 kcal.mol^{-1}) to sensitize the substrate in a fast exergonic EnT (Scheme 1.13).

Yoon (2016): Asymmetric intermolecular [2+2] Cycloaddition

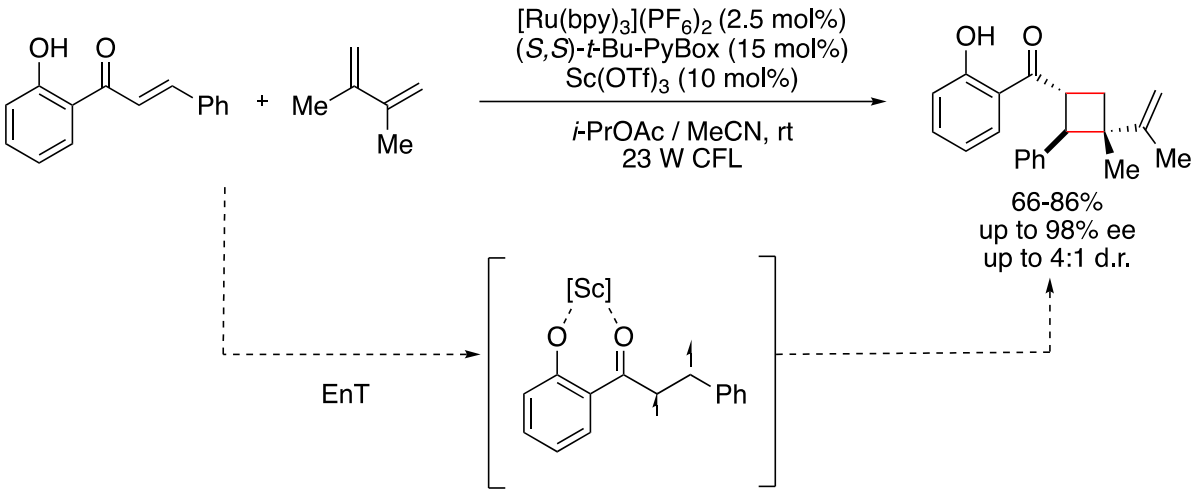

Scheme 1.13: Enantioselective [2+2] photocycloaddition enabled by dual Lewis acid and EnT catalysis.

In addition to [2+2] cycloadditions, there have been a number of efficient pericyclic reactions powered by EnT catalysis. Smith and co-workers[71] developed a visible-light mediated EnT enabled 6π heterocyclisation of cyclic enones with *N*-aryl or *O*-aryl substituents with excellent diastereomeric ratios. Excitation of cyclic 2-aryloxyketones to the triplet state via Ir(dF-ppy)$_3$ with blue LEDs leads to the diradical which undergoes heterocyclisation. After ISC back to the singlet state, a [1,4]-H shift affords the *trans*-cyclisation product which rapidly epimerizes to the more stable *cis*-isomer (Scheme 1.14).

Smith (2017): 6π Heterocyclisation

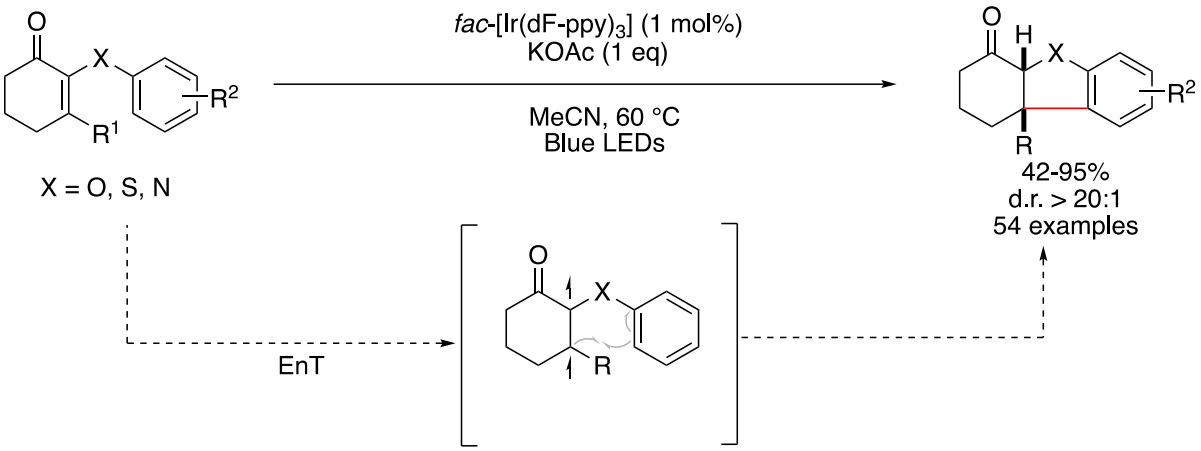

Scheme 1.14: EnT catalysis for a 6π heterocyclisation of cyclic enones.

Photoisomerisation

E/Z stereocontrol of alkenes has been a central issue in olefin chemistry. The thermodynamically less stable *Z*-alkenes are abundant in nature, despite the difficulty of synthesizing them under laboratory conditions. Geometrical *E* → *Z* isomerisation has been identified as a powerful tool to access *Z*-isomers and photosensitisation via selective EnT has emerged as an effective tool to achieve this goal.[72] In their excited states, alkenes undergo geometrical rotation around the C-C bond in order to minimize overlap between two unpaired electrons. This lowered energy, reactive triplet state then relaxes back to the ground state via either the *Z*- or *E*- configuration. The *Z*-isomer has a higher triplet state energy due to non-bonding interactions and steric effects disrupting conjugation. Therefore, if a photosensitiser is used that has an E_T lower than that of the *Z*-isomer but higher than the *E*-isomer, selective sensitisation can occur resulting in a gradual *E* → *Z* isomerisation (Figure 1.19).

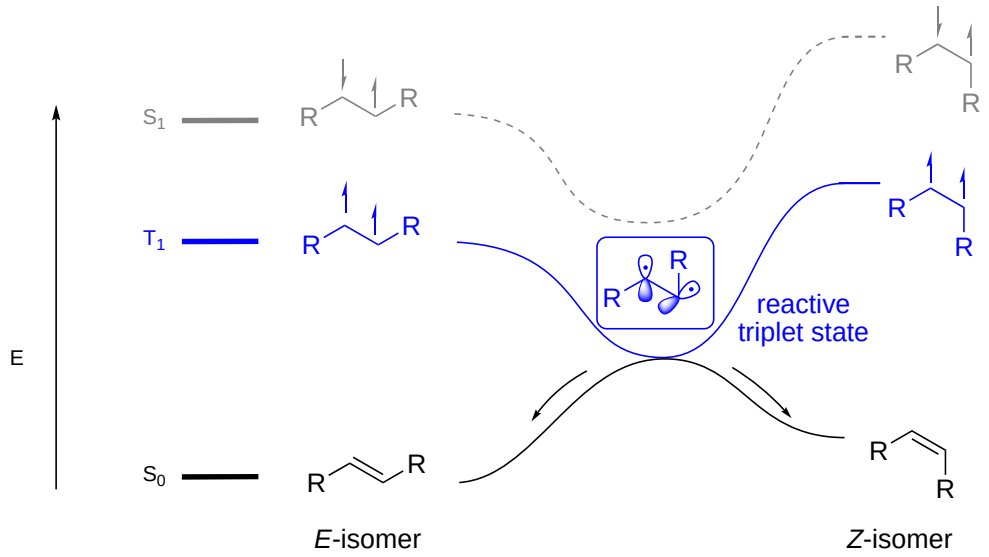

Figure 1.19: Simplified energy diagram explaining the energy transfer mediated geometrical isomerisation process.

In 2014 Weaver and co-workers[73] described the triplet sensitised isomerisation of styrenyl substrates with excellent selectivity. They utilized *fac*-[Ir(ppy)$_3$] and visible-light to generate the *Z*-isomer under kinetic control (Scheme 1.15).

Weaver (2014): E/Z Isomerisation of Styrenyl Alkenes

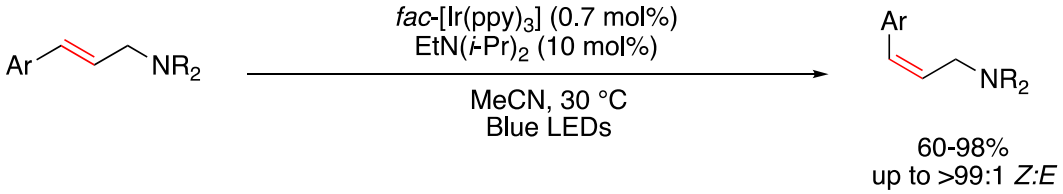

Scheme 1.15: EnT catalysis enabled selective *E* → *Z* isomerisation of styrenyl alkenes.

Drawing inspiration from nature, Metternich and Gilmour[74] developed a strategy for the selective *E* → *Z* isomerisation of cinnamyl derivatives using (–)-riboflavin as a sensitizer. They found that methyl and ethyl β-substituted derivatives yielded excellent selectivities (up to 99:1 *Z:E*), which they proposed was due to the twisted π-system and minimized non-bonding interactions (Scheme 1.16).

Gilmour (2015): Bio-Inspired E/Z Isomerisation of Styrenyl Alkenes

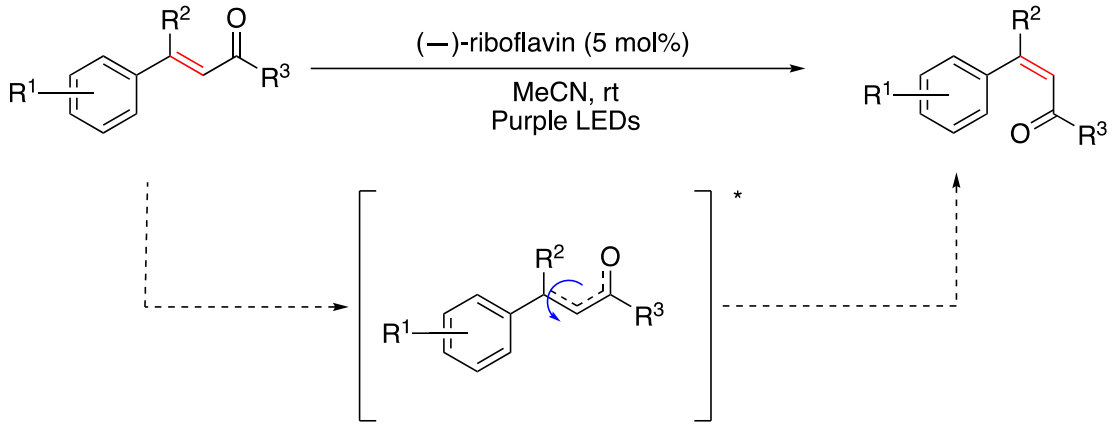

Scheme 1.16: EnT catalysis enabled selective *E* → *Z* isomerisation of styrenyl alkenes.

Finally, Bach and co-workers [75] published an alternative type of photoisomerisation reaction by performing a deracemization of chiral allenes by sensitised excitation with visible-light. They utilized their previously developed chiral thioxanthone catalyst (Scheme 1.12 above) to convert 17 chiral racemic allenes into single enantiomers with ee's up to 97%. Since triplet energy transfer is strongly distance dependent, the increased distance between enantiomer B and the thioxanthone (510 pm) results in a slower sensitisation rate (Scheme 1.17).

Bach (2018): Deracemization of Chiral Allenes

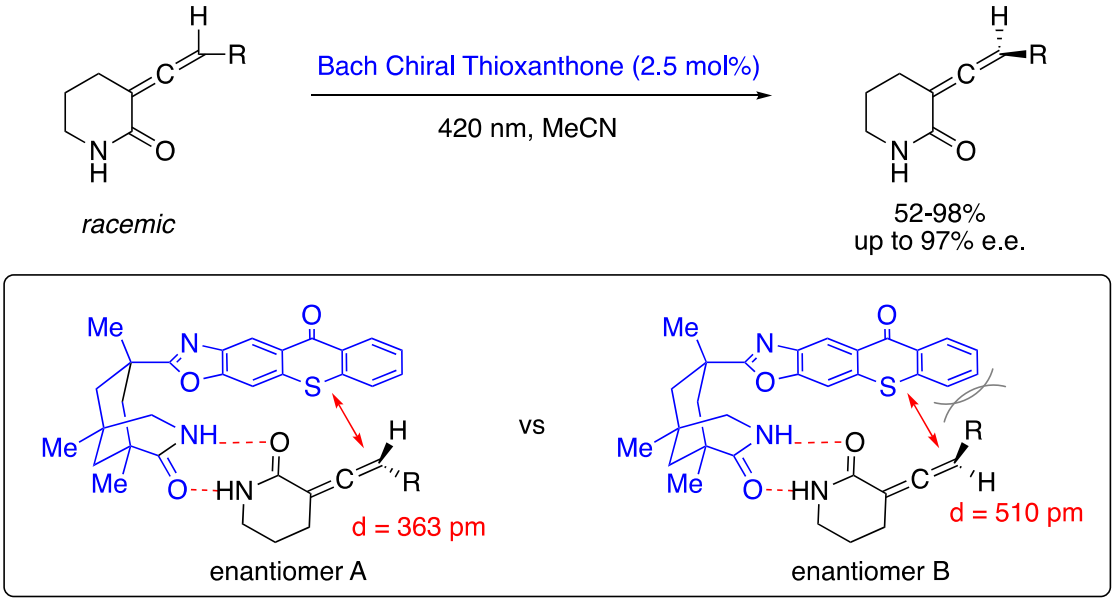

Scheme 1.17: EnT catalysis enabled deracemization of chiral allenes with a chiral thioxanthone photosensitiser.

Bond Dissociation

So far, we have only discussed the sensitisation of π-systems in aromatics or alkenes. Conversely, bond dissociation involves the direct cleavage of a σ-bond via the EnT population of σ* orbital. The first reports of this involved symmetrical σ-bond cleavage of N-N bonds which proceeded via a heterolytic bond dissociation to form a triplet nitrene after release of N_2 gas. Yoon and co-workers[76] described the formation of pyrroles from these nitrene intermediates generated from triplet sensitisation of azides using $Ru(dtbpy)_3^{2+}$ as a sensitizer (Scheme 1.18).

Yoon (2014): Heterolytic Bond Cleavage of Azides

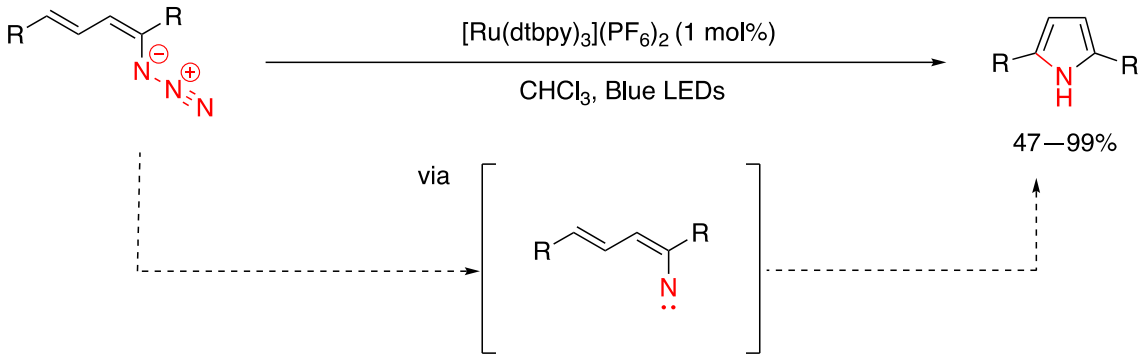

Scheme 1.18: Triplet excited state induced bond dissociation of dienyl azides for the formation of pyrroles.

Similarly, König and co-workers[77] utilized $Ru(pby)_3^{2+}$ and visible-light to generate triplet nitrene intermediates from benzoyl azides, which underwent C-H amidation of electron rich heteroarenes. Phosphoric acid was necessary for the reaction to proceed and the authors hypothesised that the benzoyl nitrene is protonated, giving electrophilic nitrenium ions, which react with electron rich heteroarenes (Scheme 1.19).

König (2015): Heterolytic Bond Cleavage of Azides

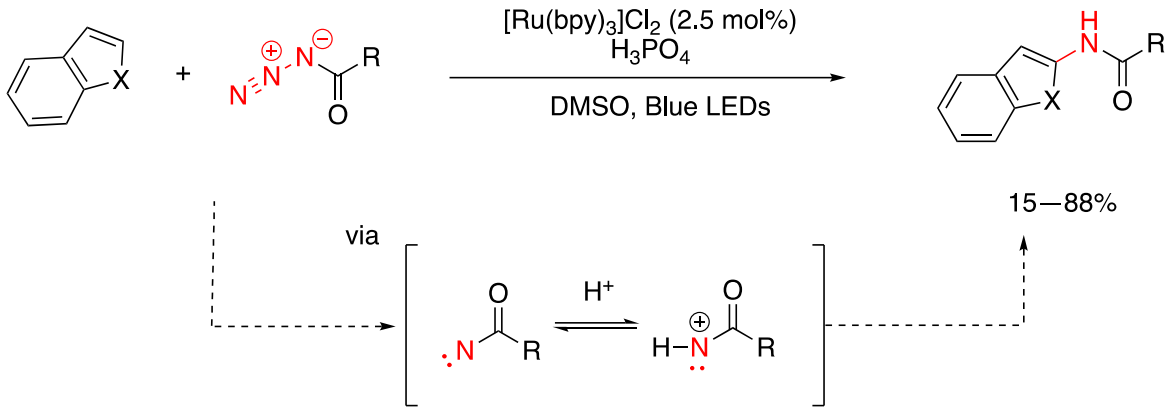

Scheme 1.19: Triplet sensitisation of benzoyl azides leading to reactive nitrene intermediates used for the C–H amidation of electron-rich heteroarenes.

In contrast to the above heterolytic bond cleavage reactions, there have also been reports of homolytic bond dissociation from EnT reactions. Glorius and co-workers[78] described the EnT enabled fragmentation of disulphide triplets to form thiyl radicals, which can be utilized to enable chemoselective anti-Markovnikov hydrofunctionalisation of olefins (Scheme 1.20).

Glorius (2018): Homolytic Bond Cleavage for Disulfide-Ene Reaction

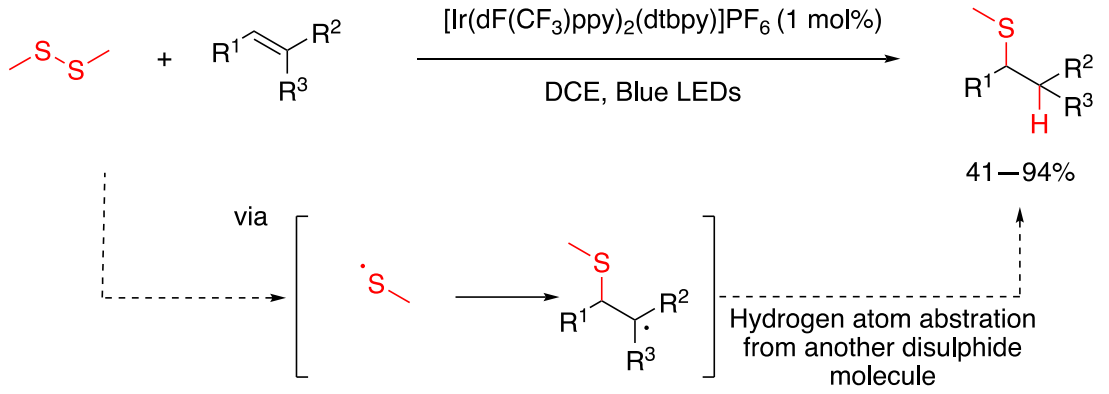

Scheme 1.20: EnT enabled disulfide-ene reaction via homolytic bond cleavage.

More recently, Glorius and co-workers[79] described the EnT mediated homolysis of unsymmetrical N-O σ-bonds for a concerted fragmentation/decarboxylation process. Both carbon-centred and nitrogen-centred radicals were generated from N-O cleavage-decarboxylation of benzophenone-derived oxime esters. This radical decarboxylation process is applicable to both aromatic and aliphatic carboxylic acids and the generated radical can be used in both C-C and C-X bond-forming reactions. Additionally, they reported the use of both

radicals in a carboimination of alkenes.[80] Addition of the alkyl radical to an alkene generates a transient radical for selective radical-radical cross coupling with the iminyl radical (Scheme 1.21).

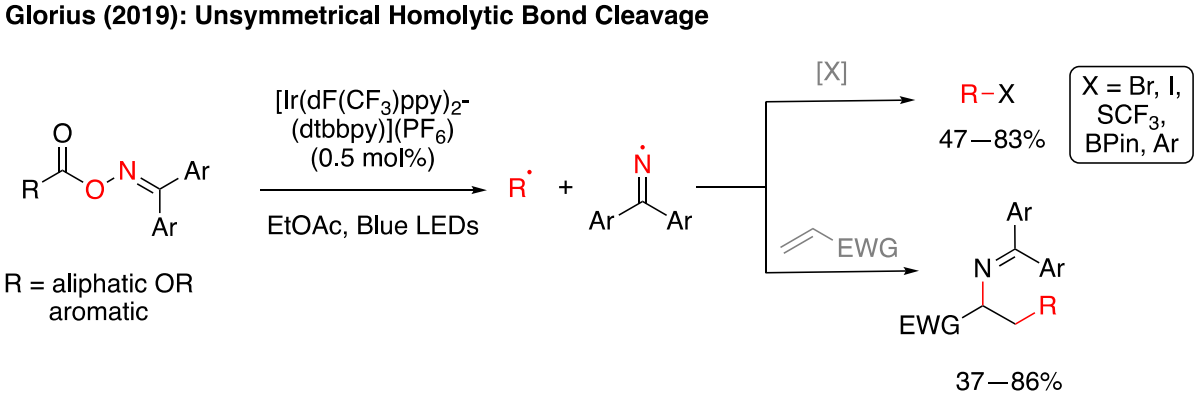

Scheme 1.21: Decarboxylative homolytic cleavage of oxime esters for the formation of new C-C and C-X bonds and carboimination of alkenes.

Sensitisation of Transition Metal Catalysts

Early studies have shown that excited state transition metal (TM) complexes enable valuable transformations that are not accessible via traditional ground state TM catalysis. Excited-state TM complexes are most commonly accessed via direct excitation in cases where the ligands possess large π-systems. Triplet-triplet EnT represents a potentially more general and ligand independent approach for the formation of excited-state TM complexes. One of the earliest examples of this approach was reported by Molander and co-workers[81] who described an EnT-enabled homolytic cleavage of Ni-Br bonds to facilitate a direct Ni-catalysed C(sp^3)-H cross coupling. EnT from the Ir^{III} photosensitiser to the Ni^{II} complex generates an excited state nickel complex, which is thought to populate the antibonding type orbitals, liberating a bromine radical. Following C-H abstraction from activated α-heterosubstituted or benzylic C(sp^3)-H bonds, the resultant reactive alkyl radical can engage in Ni-catalysed arylations (Scheme 1.22).

Molander (2016): Formal Transmetalation

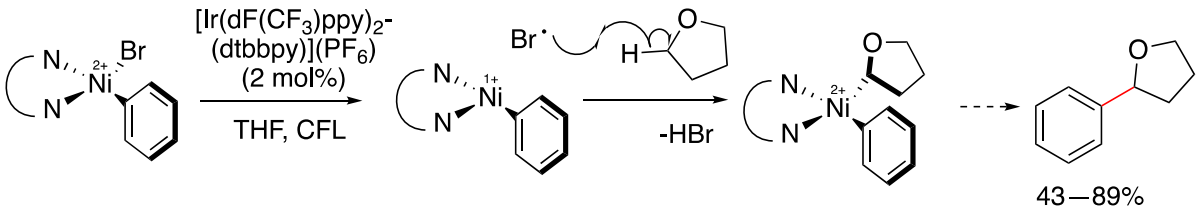

Scheme 1.22: EnT enabled Ni-catalysed C(sp^3)-H arylation.

In 2017, MacMillan and co-workers[82] showed how triplet energy sensitisation of ground state TM complexes could be used to access challenging reductive eliminations. Triplet-triplet energy transfer enabled the reductive elimination from an aryl Ni^{II} acetate complex, resulting in a new C-O bonds. They later reported how this concept was applied to a C-N bond forming reductive elimination (Scheme 1.23).[83]

MacMillan (2017): Reductive Elimination

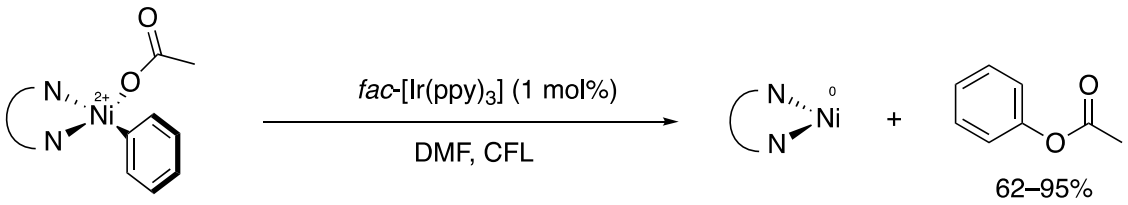

Scheme 1.23: EnT enabled reductive elimination via sensitisation of a Ni^{II} complex.

2. Chapter 2 - Stereoselective Access to Oxindoles

This work was published in Synthesis (*Synthesis,* **2023**, 55, 1736–1746) titled, "Chiral Acyl Radicals Generated by Visible Light Enable Stereoselective Access to 3,3-Disubstituted Oxindoles: Application toward the Synthesis of (–)- and (+)-Physovenine"[84]

2.1 Background

Indoline alkaloids are a prominent class of natural products owing to their wide range of biological profiles.[85–89] Some noteworthy natural products featuring the indoline moiety include (-)-physostigmine[86–88] used in the treatment of glaucoma, and (-)-physovenine,[89] shown to exhibit nearly equipotent activity in vitro (Figure 2.1). Both of these alkaloids are isolated from African *Physostigma venenosum* (Calabar bean).

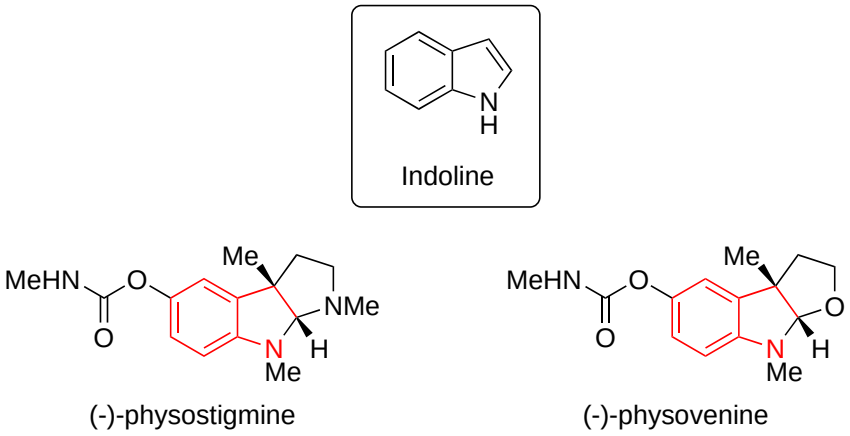

Figure 2.1: Representative indoline alkaloid natural products.

Approaches to the synthesis of these indoline motifs typically involve modifications of advanced 3,3-disubstituted oxindole intermediates (Scheme 2.1).[90–97]

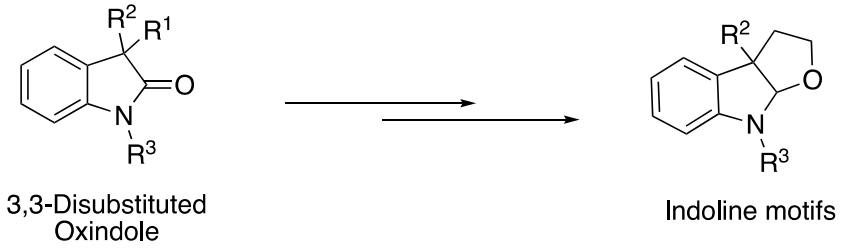

Scheme 2.1: Indoline synthesis from 3,3-disubstituted oxindoles.

Oxindoles themselves are also pharmacologically advantageous compounds that are highly valuable substructures in medicinal chemistry (Figure 2.2).[90] They exhibit an extensive range of biological activities such as anti-cancer, anti-diabetic, anti-HIV, anti-tumor and anti-Alzheimer's amongst others. [98,99] The oxindole moiety and its derivatives are also found in many natural products.[100]

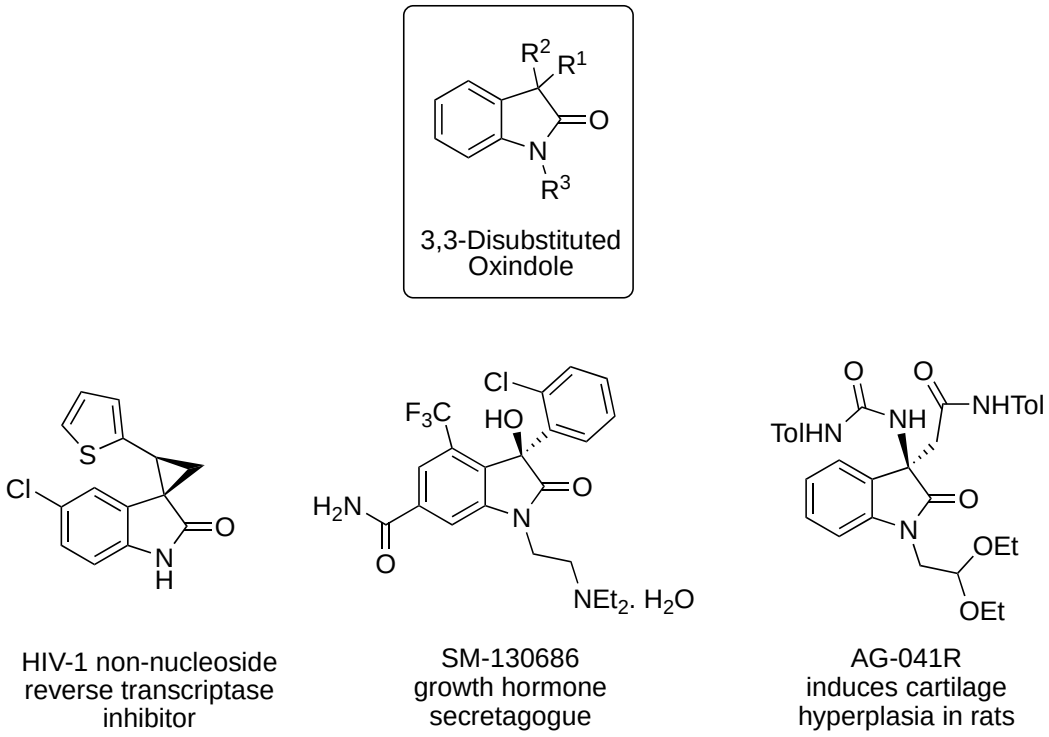

Figure 2.2: Representative indoline alkaloid natural products.

To this end, methods for accessing enantiopure, disubstituted oxindoles from simple and acyclic precursors, in a low-cost and energy-efficient manner are highly desirable.[91,92] There have been many approaches reported for the preparation of oxindoles. These methods typically involve cyclisation at different positions on the indoline ring. Many oxindole

syntheses utilise a $C_3 - C_{3a}$ cyclisation, which is most commonly achieved via transition metal-mediated reactions[91,101,102] or homolytic aromatic substitution (HAS) reactions.[103–112]

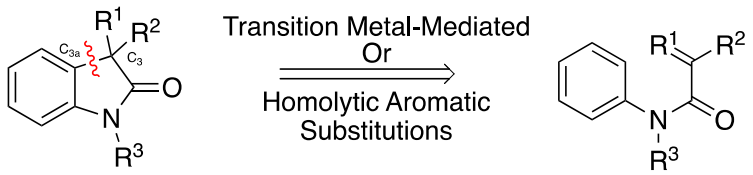

Scheme 2.2: Retrosynthetic approach to oxindole synthesis via C_3 - C_{3a} cyclisation.

Focusing on the latter group, homolytic aromatic substitution (HAS) reactions represent a popular approach to the synthesis of oxindoles, which proceed via cyclisation of α-carbonyl radicals generated by either, (i) radical addition to *N*-arylacrylamides,[103,104] (ii) reduction of α-haloarylamides [105] or (iii) oxidation of the corresponding enolates[106–112] (Scheme 2.3)

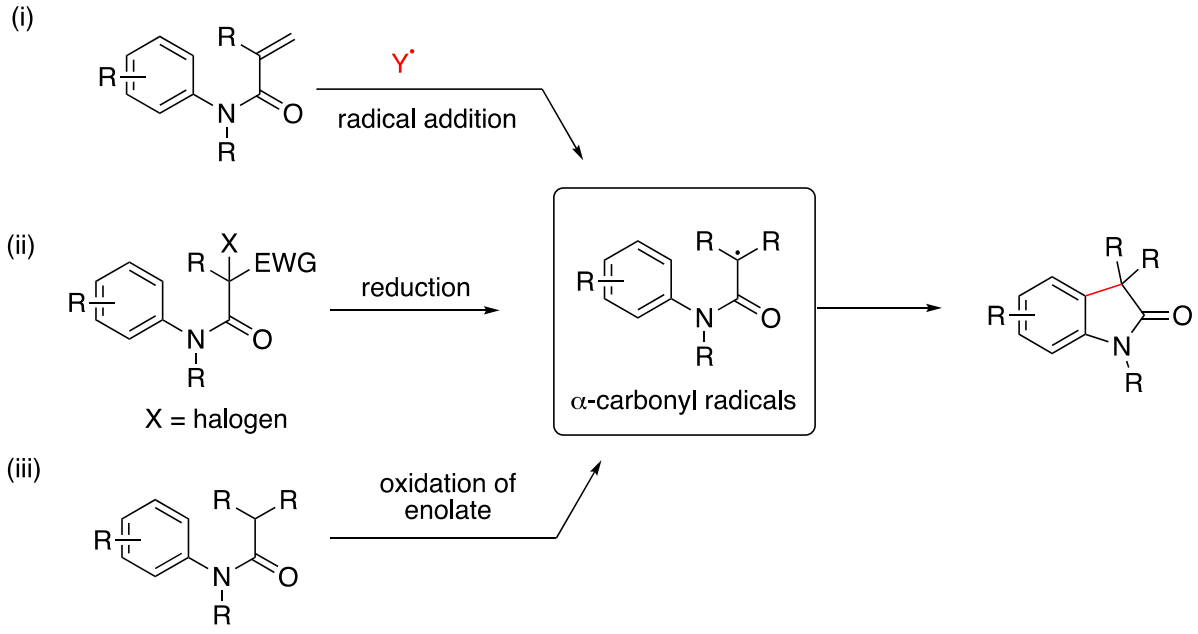

Scheme 2.3: Different approaches to α-carbonyl radicals for the synthesis of oxindoles.

In many cases, these strategies are also associated with drawbacks such as the requirement of expensive metals (Pd, Rh, Ru) and ligands, high temperatures and toxic radical initiators.

On the other hand, visible-light mediated photoredox approaches offers unique solutions to this; enabling environmentally friendly alternatives. In recent years, there have been many

reports for the application of visible-light mediated strategies for the synthesis of oxindoles.[93] The most convenient of these extends from route (i) above, which harnesses the power of photoredox catalysis to generate to the key Y· radical. Applied in this way, both carbon and heteroatoms radicals can be utilised, broadening the utility of this classical Giese-type addition-cyclisation sequence.[30]

Some common radicals generated from photoredox catalysis for the synthesis of oxindoles includes (i) aminium radicals, (ii) sulfonyl radicals, (iii) alkyl radicals or (iv) acyl radicals. Scheme 2.4 below shows some previous reports utilising these radical types for radical addition-cyclisation reactions all using visible-light mediated photoredox approaches. [113–116]

(i) Liu (2020): Amination/Cyclisation of Arylacrylamides[113]

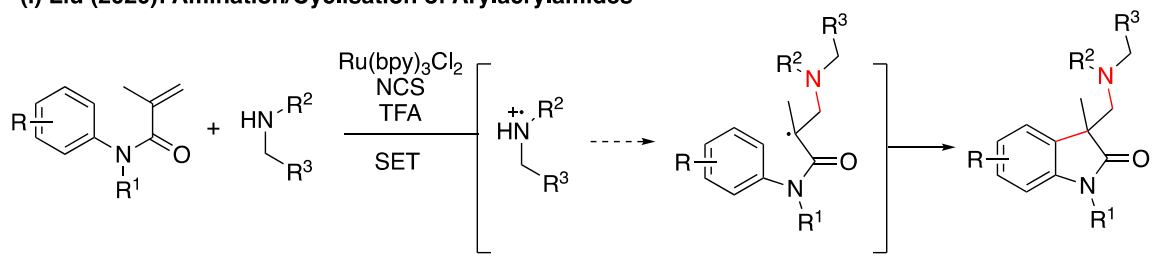

(ii) Wang (2020): Sulfonation/Cyclisation of Arylacrylamides[114]

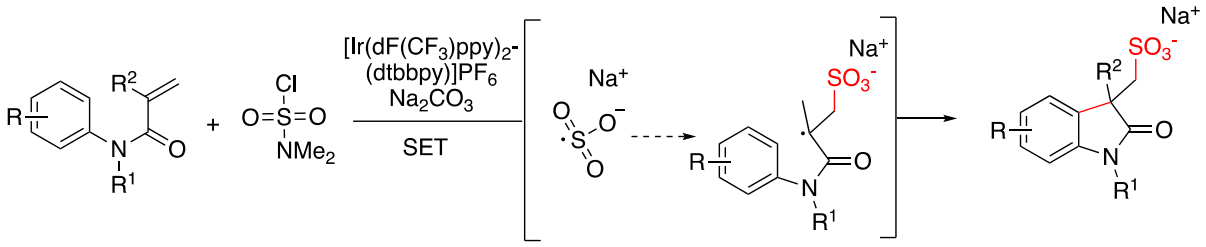

(iii) Wang (2019): Deboronative Alkylarylation of Acrylamides[115]

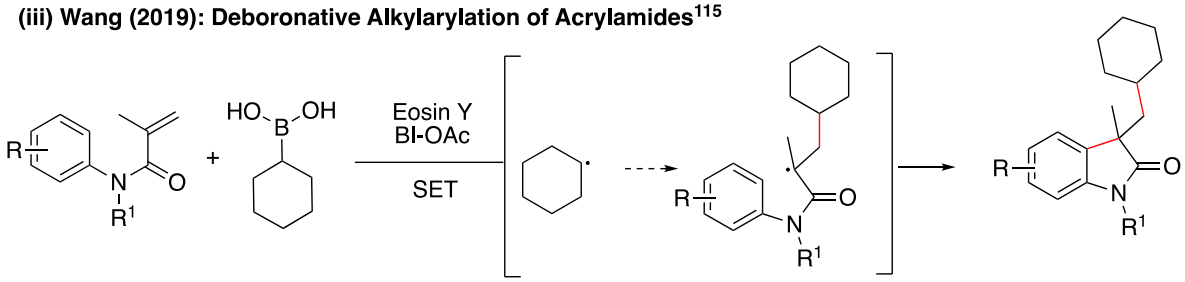

(iv) Wallentin (2015): Acyl Radical Generation from Aromatic Carboxylic Acids[116]

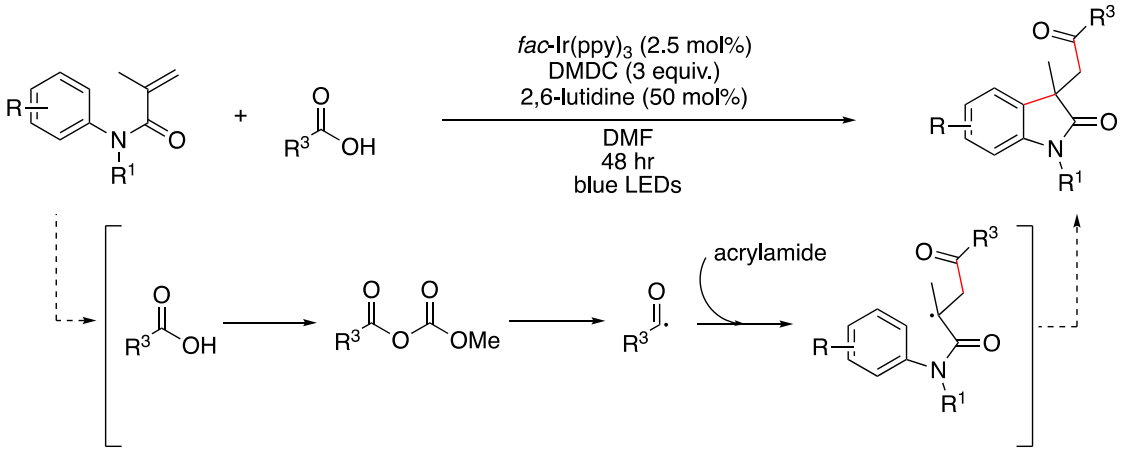

Scheme 2.4: Visible-light mediated photoredox approaches for the synthesis of 3,3-disubstituted oxindoles via radical addition-cyclisation utilising different carbon and heteroatom radicals.

Looking further than acyl radicals just for the synthesis of 3,3-disubstituted oxindoles, visible-light mediated photoredox catalysis has enabled easy access to acyl radicals that can undergo a diverse range of synthetically useful transformations.[117–120]

2.2 Aims and Objectives: Stereoselective Radical Addition-Cyclisation Approach

A major drawback of all the above mentioned radical addition-cyclisation applications toward 3,3-disubstituted oxindoles is the generation of racemic products. This is due to the inherent challenges of achieving enantioselectivity in radical reactions. Chiral auxiliary-controlled chemical synthesis is a cornerstone strategy for enabling stereoselective access to important biomolecules.[121,122] There are a range of efficient chiral auxiliaries that are frequently used in carbon-carbon bond formations with high stereoselectivity. Some examples of common chiral auxiliaries include Corey's auxiliary, Evan's auxiliary and Enders chiral auxiliary (Figure 2.3).

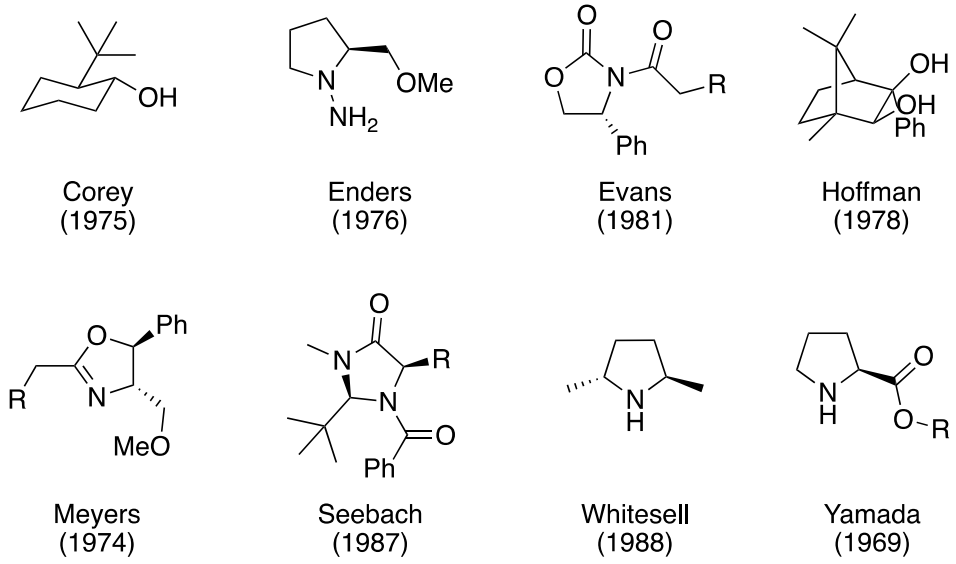

Figure 2.3: Representative examples of common chiral auxiliaries.

When considering approaches for stereoselective catalysis, there are many methods to consider, owing to the impressive advances in modern enantioselective synthesis. Diastereoselective chiral auxiliary approaches are often easily dismissed as viable methods because of the need to install and remove a requisite chiral director for each reaction/application, as well as the stoichiometric by-product this produces. However, auxiliary-controlled processes are generally more robust and do not require intense substrate-specific optimisations.[123] Furthermore, diastereomeric products obtained from such processes, even when perfect selectivity is not obtained, are often easily separated by

using standard chromatography techniques, ultimately leading to perfect enantiopurity following the removal of the chiral auxiliary. This is particularly useful at the initial stages of drug discovery programmes.[124] It is important to mention that the subsequent recovery and reuse of the chiral auxiliary (in most cases) significantly increases their attractiveness in enabling circular and sustainable chemistry.[125,126]

To this end, we set out to develop a chiral-auxiliary-controlled stereoselective approach for the synthesis of 3,3-disubstitued oxindoles using photoredox catalysis.

2.3 Results and Discussion

Given the success of the chiral acyl auxiliaries, our investigation began with identifying a suitable *N*-acyl chiral auxiliary starting material which could be converted to a chiral C1 acyl-radical synthon under photoredox catalysis. The Petersen research group has previously been interested in imidazolidinone derived chiral auxiliaries, so we commenced our studies with investigating oxamic acid precursor **2.2** (Scheme 2.5). We hypothesized that in the presence of a suitable base, this oxamic acid could be deprotonated to the anion, which, following SET from an excited photocatalyst, could undergo decarboxylation to the acyl radical. This acyl radical could then undergo radical addition and cyclisation to the acrylamide to produce the required 3,3-disubtitued oxindole; with oxygen envisaged to be the terminal oxidant catalyst turnover.

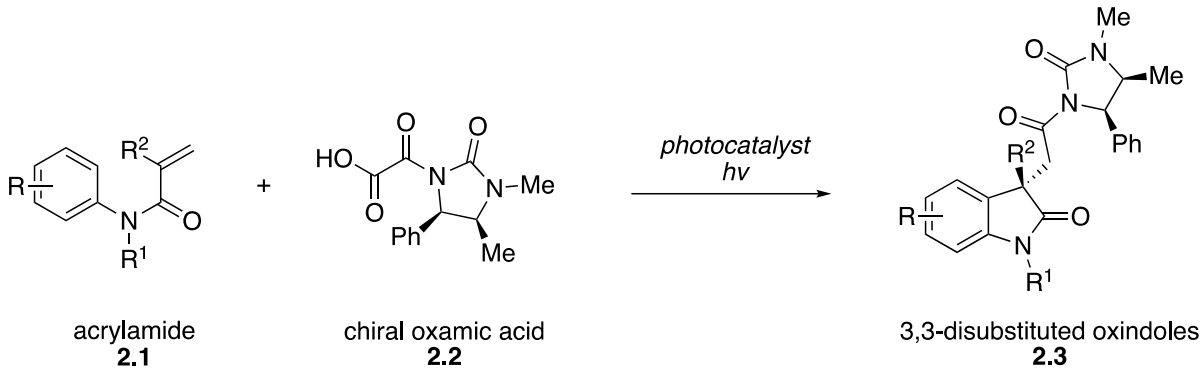

Proposed Mechanism

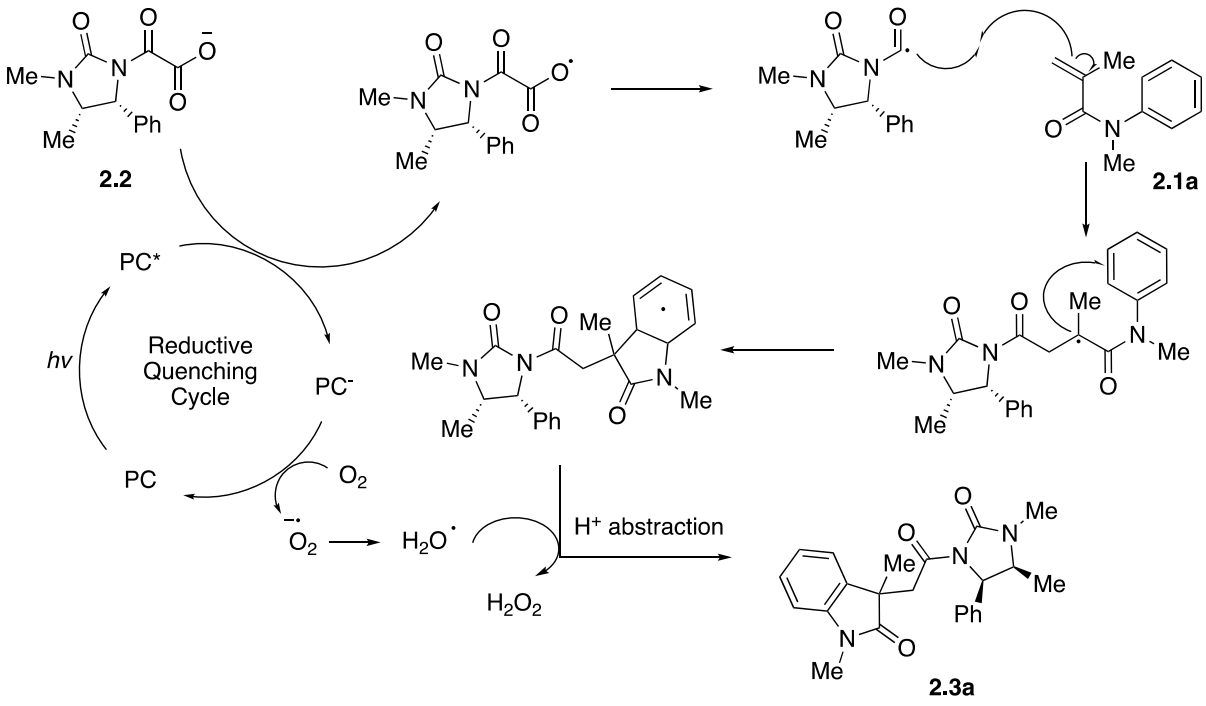

Scheme 2.5: Proposed diastereoselective route to 3,3-disubsitued oxindoles via visible light mediated photoredox catalysis and proposed mechanism.

The model acrylamide **2.1** was easily accessed via a standard Mukaiyama peptide coupling.

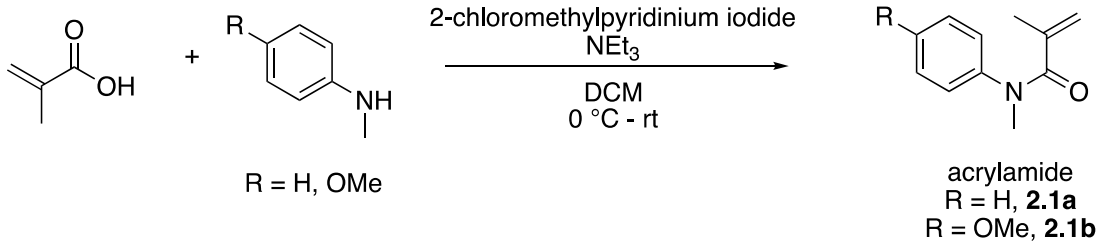

Scheme 2.6: Mukaiyama peptide coupling for the preparation of model acrylamide starting materials.

For the synthesis of chiral oxamic acid precursor **2.2**, we initially envisaged treating the auxiliary, (4*R*,5*S*)-1,5-dimethyl-4-phenylimidazolidin-2-one, with methyl 2-chloro-2-oxoacetate under reflux conditions to produce the methyl ester **2.4**, followed by hydrolysis in the presence of a strong base to yield the desired chiral oxamic acid (Scheme 2.7).

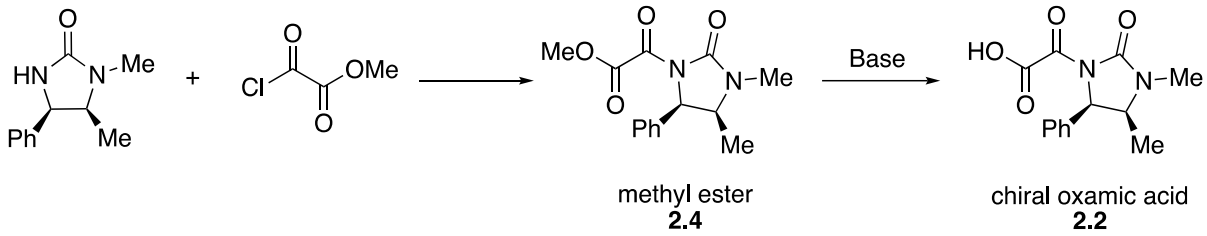

Scheme 2.7: Initial approach for synthesis of key chiral oxamic acid precursor **2.2**.

^{1}H NMR spectroscopy confirmed we had isolated the correct ester **2.4**. However, upon treatment with KOH in the presence of THF and water, ^{1}H NMR and ^{13}C NMR revealed we had instead regenerated the starting auxiliary (Scheme 2.8). This was not too surprising since the auxiliary anion is a superior conjugate base than methoxide.

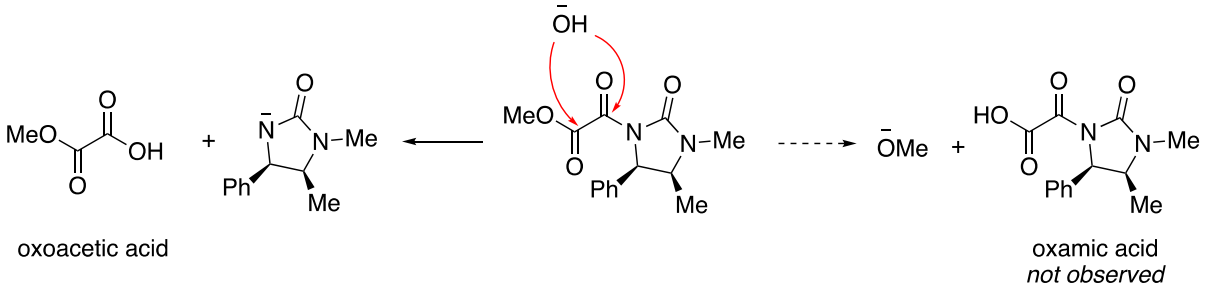

Scheme 2.8: Regioselective attack of hydroxyl group.

We then turned to a two-step, one-pot strategy involving treating our auxiliary directly with oxalyl chloride in anhydrous THF at low temperature, and then quenching with NaOH to form oxamic acid **2.2** (Scheme 2.9). Gratifyingly, this approach produced our desired chiral oxamic acid **2.2** in 81% yield.

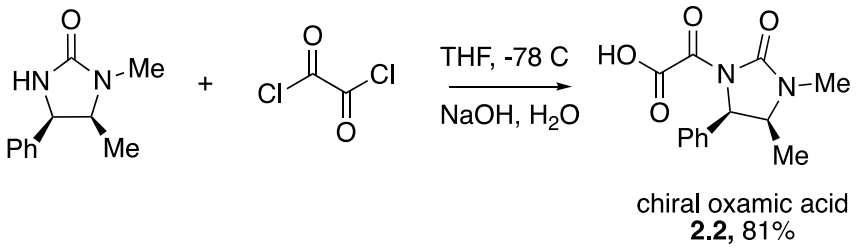

Scheme 2.9: Synthesis of chiral oxamic acid **2.2** via oxalyl chloride.

With our desired starting material in hand we began investigating the key photocatalytic step. The different reaction conditions are shown in Table 2.1 below.

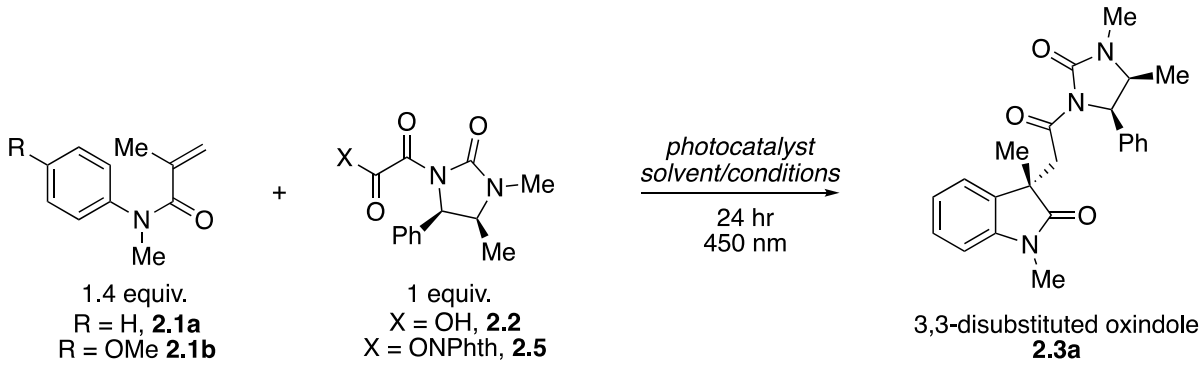

Entry	Acrylamide (**R**)	Chiral precursor (**X**)	Photocatalyst	Solvent	Yield (%)[a]
1[b]	H	OH	$[Ru(bpz)_3](PF_6)_2$	toluene	0
2[b]	H	OH	$[Ir\{dF(CF_3)ppy\}_2(dtbpy)]PF_6$	toluene	0
3[b]	H	OH	Mes-Acrydinium	toluene	0
4[c]	OMe	OH	4-CzIPN (2 mol%)	ACN:H_2O (1:1)	35
5	OMe	ONPhth	$Ir(ppy)_3$ (2 mol%)	ACN	72
6	OMe	ONPhth	$Ir(ppy)_3$ (2 mol%)	THF	82
7	OMe	ONPhth	$Ir(ppy)_3$ (2 mol%)	EtOAc	83
8	OMe	ONPhth	$Ir(ppy)_3$ (2 mol%)	toluene	88
9	OMe	ONPhth	$[Cu(dap)_2]Cl$ (2 mol%)	toluene	0[d]
10	OMe	ONPhth	$Ir(ppy)_3$ (2 mol%)	toluene	0[d,e]
11	OMe	ONPhth	none	toluene	0[e]

Table 2.1: Optimisation table for photocyclisation reaction of acrylamides using chiral auxiliary precursors. [a] Yields determined by ^1H NMR with 1,3,5-trimethoxybenzene as an internal standard; [b] Conditions: PC (1 mol%), K_2CO_3 (1.1 equiv.), 48 h; [c] Conditions: 4-CzIPN (2 mol%), $AgNO_3$(50 mol%), $K_2S_2O_8$ (3 equiv.), 48 h; [d] Starting material recovered; [e] No light

Our initial studies investigated three commonly used photocatalysts with strong oxidizing abilities in their photoexcited states, namely $[Ru(bpz)_3](PF_6)_2$, $[Ir\{dF(CF_3)ppy\}_2(dtbpy)]PF_6$, and Mes-Acridinium. We performed the reaction in toluene using potassium carbonate as a weak base. Disappointingly, after 24hrs of irradiating with blue LEDs, TLC analysis showed no product forming (Table 2.1, entries 1-3).

We acknowledged that atmospheric oxygen may not be a suitable oxidizing agent. The use of $AgNO_3/K_2S_2O_8$ is a well-known system for net oxidative transformations, particularly in the context of decarboxylation chemistry.[127–130] In fact, the Petersen research group recently reported a silver-catalysed double decarboxylative strategy[131] for the synthesis of quinolin-2-ones from α-keto acids in which the decarboxylation to the acyl radical was performed using 4-CzIPN irradiated with 450 nm light in ACN/H_2O in the presence of a $AgNO_3$ co-catalyst and $K_2S_2O_8$ (Scheme 2.10).

Petersen (2022): Silver-Catalysed Double Decarboxylative Strategy

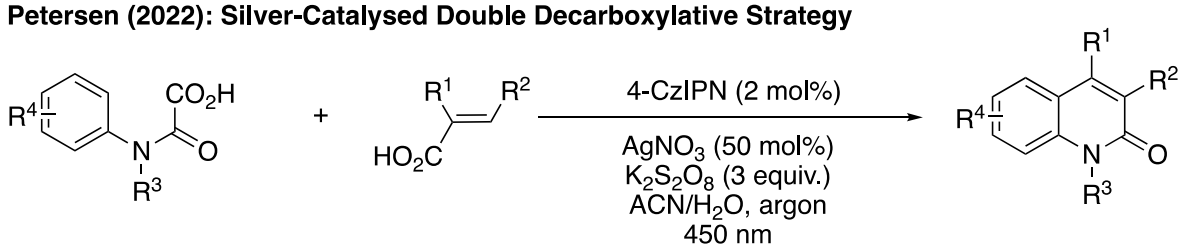

Scheme 2.10: Synthesis of quinolinones via a silver-catalysed double decarboxylative addition–cyclisation–elimination cascade sequence.

Applying this protocol, the desired oxindole **2.3a** was gratifyingly (albeit modestly) obtained 35% yield (Table 2.1, entry 4).

Taking into account stability issues of the auxiliary acid as well as the low yields and net oxidative photocatalytic conditions, we considered an alternative auxiliary starting material. In accordance with work published in 2017 by Petersen *et. al.* we considered switching to *N*-hydroxyphthalimido esters in the presence of $Ir(ppy)_3$ as a photocatalyst.[132] These *N*-hydroxyphthalimido esters could be easily accessed using a similar acid chloride formation as described in Scheme 2.9 above. Oxalyl chloride was added to *N*-hydroxyphthalimide followed by the addition of the chiral auxiliary, (4*R*,5*S*)-1,5-dimethyl-4-phenylimidazolidin-2-one.

At this point, the project was slowly handed over to an MSc. student in the group, Josef Späth, for the purposes of research training. Josef was thus responsible for carrying out the balance of the work. For completeness of this section however, the main findings will be summarised next, but full details are reported in the published work.[84] A detailed optimisation was completed which revealed the best conditions to involve the use of $Ir(ppy)_3$ in toluene; providing **2.3a** in 88% yield and an isolated diastereomeric ratio of 2.2:1 (Table 2.1, entry 8). The diastereomeric ratio of the crude product could not be determined by either ^1H NMR spectroscopy or HPLC analysis owing to significant signal overlap of diastereomers.

The proposed mechanism for this redox neutral catalytic approach is shown in Scheme 2.11 below. Upon excitation with visible-light, the excited-state Ir^{III*} species is oxidatively quenched with chiral *N*-hydroxyphthalimido ester **2.5** to produce a highly oxidising Ir^{IV} species together with the radical anion, which subsequently loses CO_2 and the phthalimide anion to afford the key chiral acyl radical. Michael addition to the acrylamide affords conjugate radical, which after homolytic aromatic substitution affords a cyclohexadienyl radical. Oxidation of this radical species by Ir^{IV} and loss of a proton affords the desired oxindole **2.3b** with the concomitant return of the photocatalyst to its ground state.

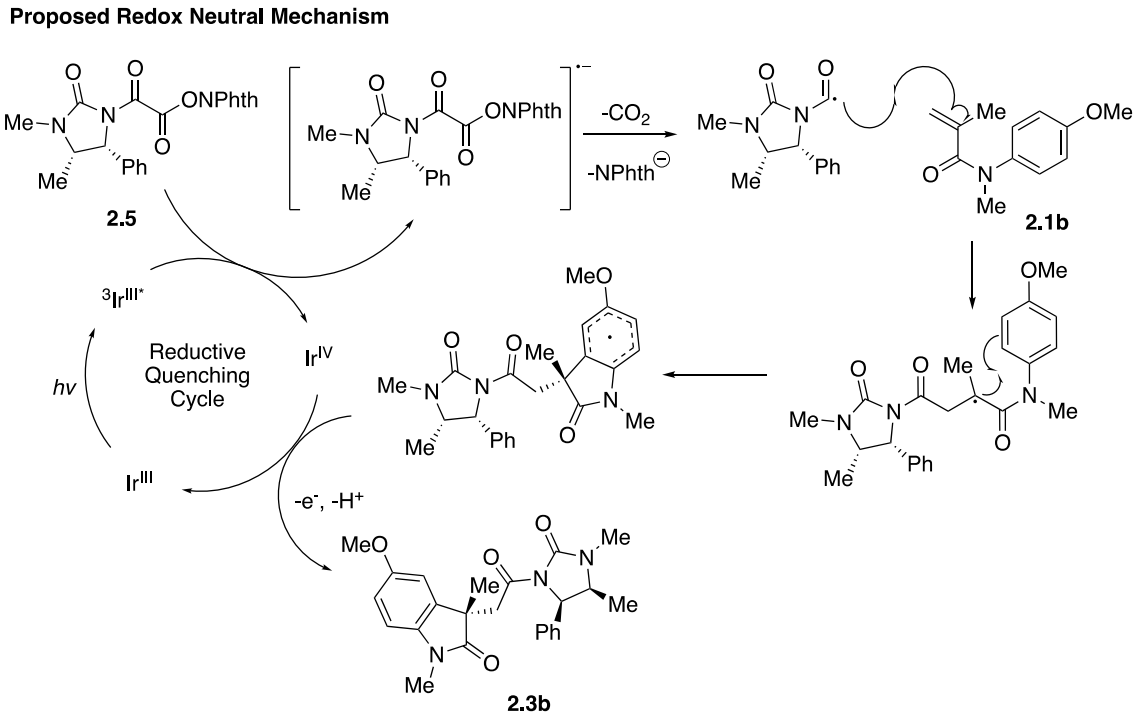

Scheme 2.11: Proposed mechanism for photoredox approach to 3,3-disubstitued oxindoles from chiral *N*-hydroxyphthalimido esters via a redox neutral reductive quenching cycle.

Mechanistic evidence to provide support for the existence of the acyl radical, was obtained by virtue of a TEMPO radical trapping experiment, which afforded TEMPO adduct **2.6** in 40% yield (Scheme 2.12). Adding 1.4 equivalents of TEMPO to the standard conditions yielded the TEMPO-oxamide (**2.6**) in 49%.

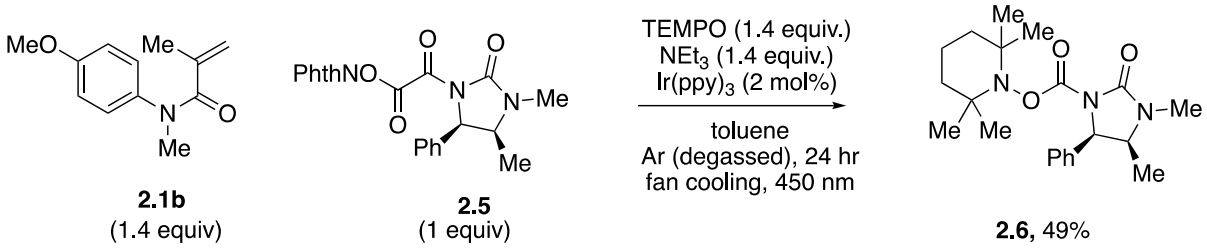

Scheme 2.12: Radical trapping experiment using TEMPO.

It is worth mentioning that the method extended to the use of the Evans-derived auxiliary, which afforded oxindole **2.8** in 69% yield, however with no diastereoselectivity (Scheme 2.13).

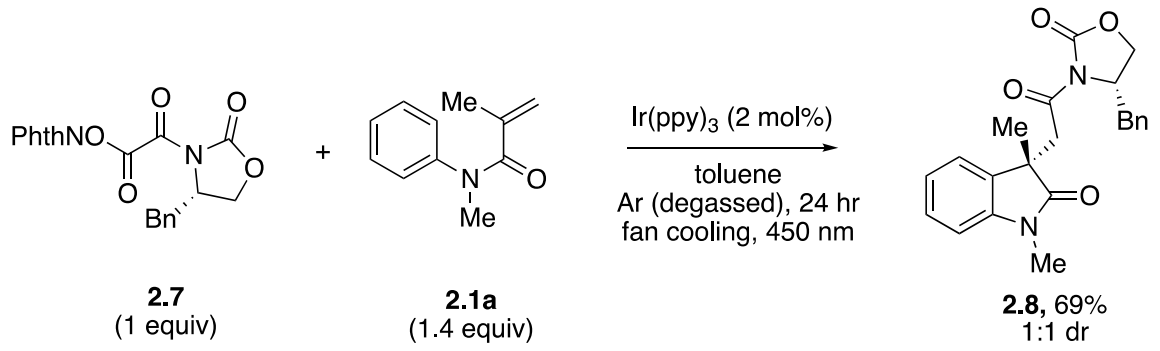

Scheme 2.13: Photocatalytic approach to 3,3-disubstitued oxindoles using Evans chiral auxiliary ester.

Ultimately, Josef demonstrated that the methodology was applicable to a small substrate scope, varying the substituent on the aromatic ring of the acrylamide, and that oxindole **2.3b** could be successfully telescoped to produce intermediate **(*S*)-2.9** — the advanced intermediate to complete the formal synthesis to (–)-physovenine (Scheme 2.14) as described by Overman and co-workers.[133] X-ray analysis on the isolated diastereomers (**2.3**) gratifyingly revealed the major diastereomer to possess the correct *(S)* stereochemistry consistent with the natural product (–)-physovenine.

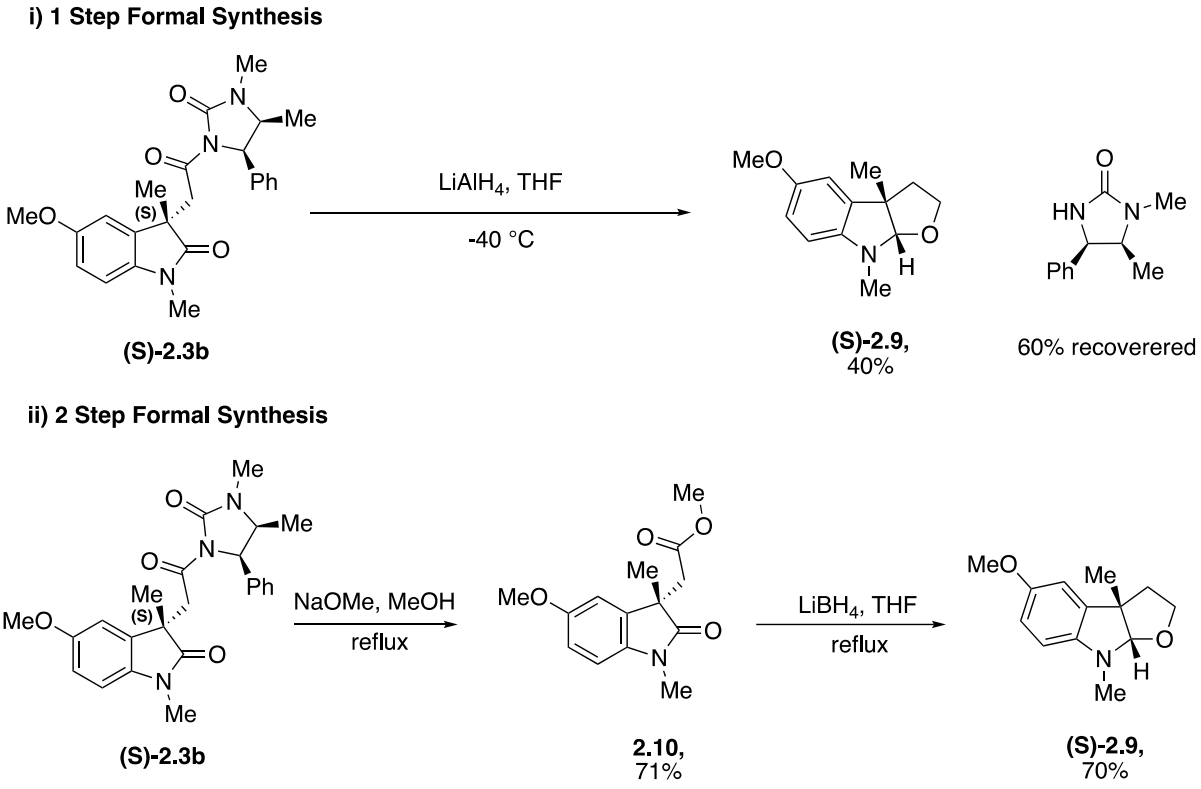

Scheme 2.14: Proposed formal synthesis of (-)-physovenine.

2.4 Conclusion and Future Work

In conclusion, this work describes the repurposing of *N*-acyl chiral auxiliaries as C1 radical synthons and their application to accessing enantiopure indoline alkaloids via a diastereoselective addition–cyclisation sequence of simple acrylamides. Despite only modest diastereocontrol in the cyclisation step, the ease of separation of the diastereomeric products has enabled access to both enantiomeric products in perfect enantiopurity (after auxiliary removal) and in sufficient quantities for further analysis and use in drug discovery and chemical biology programmes.

3. Chapter 3 - Thioxanthone Catalysed Triplet Energy Transfer for the Synthesis of 3,4-Dihydroquinolin-2-ones

This work was published in Organic Letters (*Org. Lett.* **2021**, *23*, 8963–8967) titled, "Visible-Light Mediated Metal-Free 6π-Photocyclization of *N*-Acrylamides: Thioxanthone Triplet Energy Transfer Enables the Synthesis of 3,4-Dihydroquinolin-2-ones."[134]

3.1 Background and Reaction Design

3,4-Dihydroquinolinones are important molecular scaffolds in many bioactive compounds and pharmaceuticals (Figure 3.1).[135–138] The dihydroquinolinone moiety (Figure 3.1, red) is found in drugs such as aripiprazole, an approved agent for the treatment of schizophrenia;[139] CYP11B2 inhibitors, a treatment for breast cancer and cardiovascular diseases;[140] and Yaequinolones, a fungal insecticidal antibiotic.[141] This privileged scaffold is also present in a number of important natural product families, e.g. *Melodinus* alkaloids[142] such as (+)-meloscine and (+)-scandine; as well as indole alkaloids such as trigolutesin A.[143]

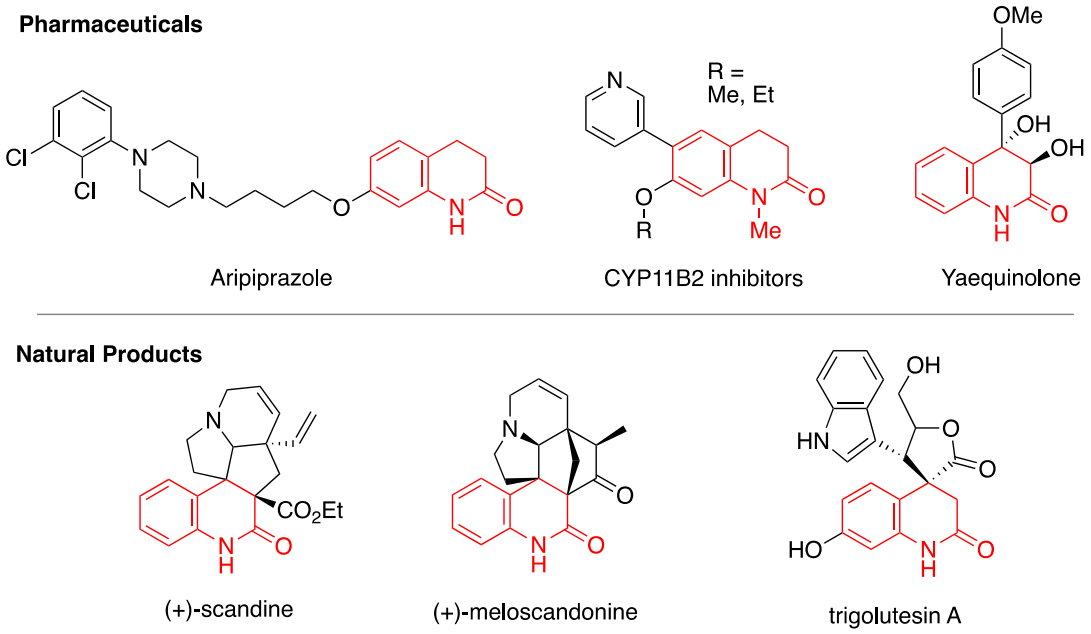

Figure 3.1: Representative pharmaceuticals and natural products containing the 3,4-dihdroquinolin-2-one scaffold.

In previous years there have been a multitude of strategies reported for the synthesis of 3,4-dihydroquinolin-2-ones, including Friedel-Crafts cyclisations,[144,145] C-H activations/cyclisations,[146–149] radical cyclisations[150–155] and others (Figure 3.2).[156–158]

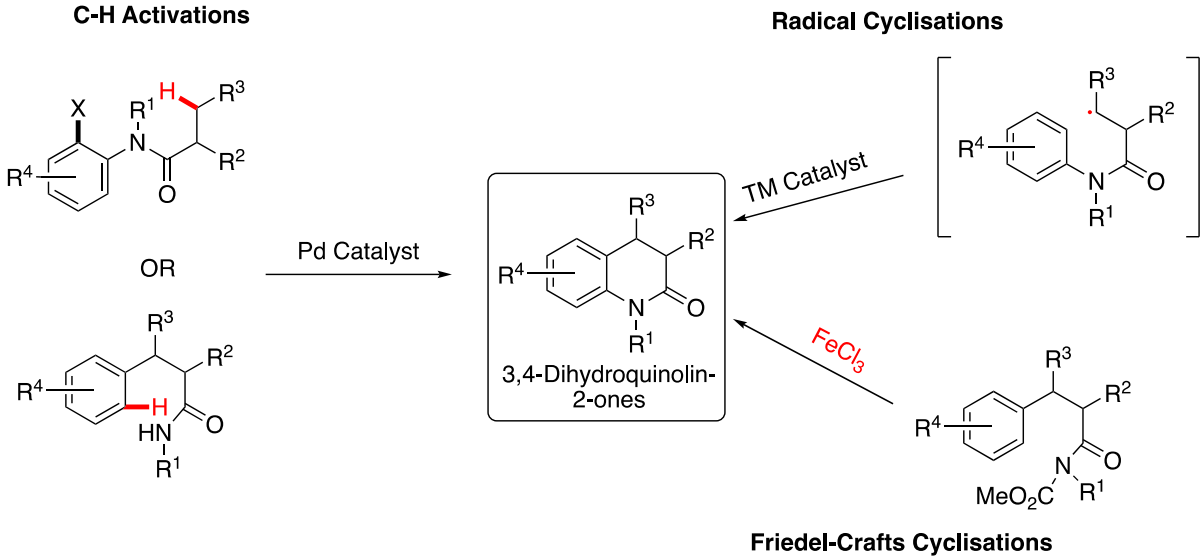

Figure 3.2: Examples of 3,4-dihydroquinolin-2-one formation.

A more recent example of 3,4-dihydroquinolin-2-one synthesis was reported by Yang *et. al.*[159] in 2020 who described the redox-triggered switchable synthesis of 3,4-dihydroquinolin-2-one derivatives via a cascade hydride transfer/*N*-dealkylation/*N*-acylation process (Scheme 3.1). Using morpholine as a catalyst, the authors were able to access 3-unsubstituted and 3-mono substituted 3,4-dihydroquinolin-2-ones with the application of Meldrum's acid and 4-hydroxycoumarins, respectively. Additionally, the released formaldehyde could be used *in situ* by the unreacted 4-hydroxycoumarins, which, upon Michael addition with the 3-monosubstituted 3,4-dihydroquinolin-2-ones, leads to the formation of 3,3'-disubstituted 3,4-dihydroquinolin-2-ones. A major drawback of this method is the necessity of high reaction temperatures (80 °C) and relatively low yields (~50-60%). The substrate scope is also limited due the fact that strongly electron-withdrawing functional groups on the *o*-aminobenzaldehyde starting materials inhibit the reaction and prevent product from forming.

Li (2020): Hydride Transfer/*N*-Dealkylation/*N*-Acylation

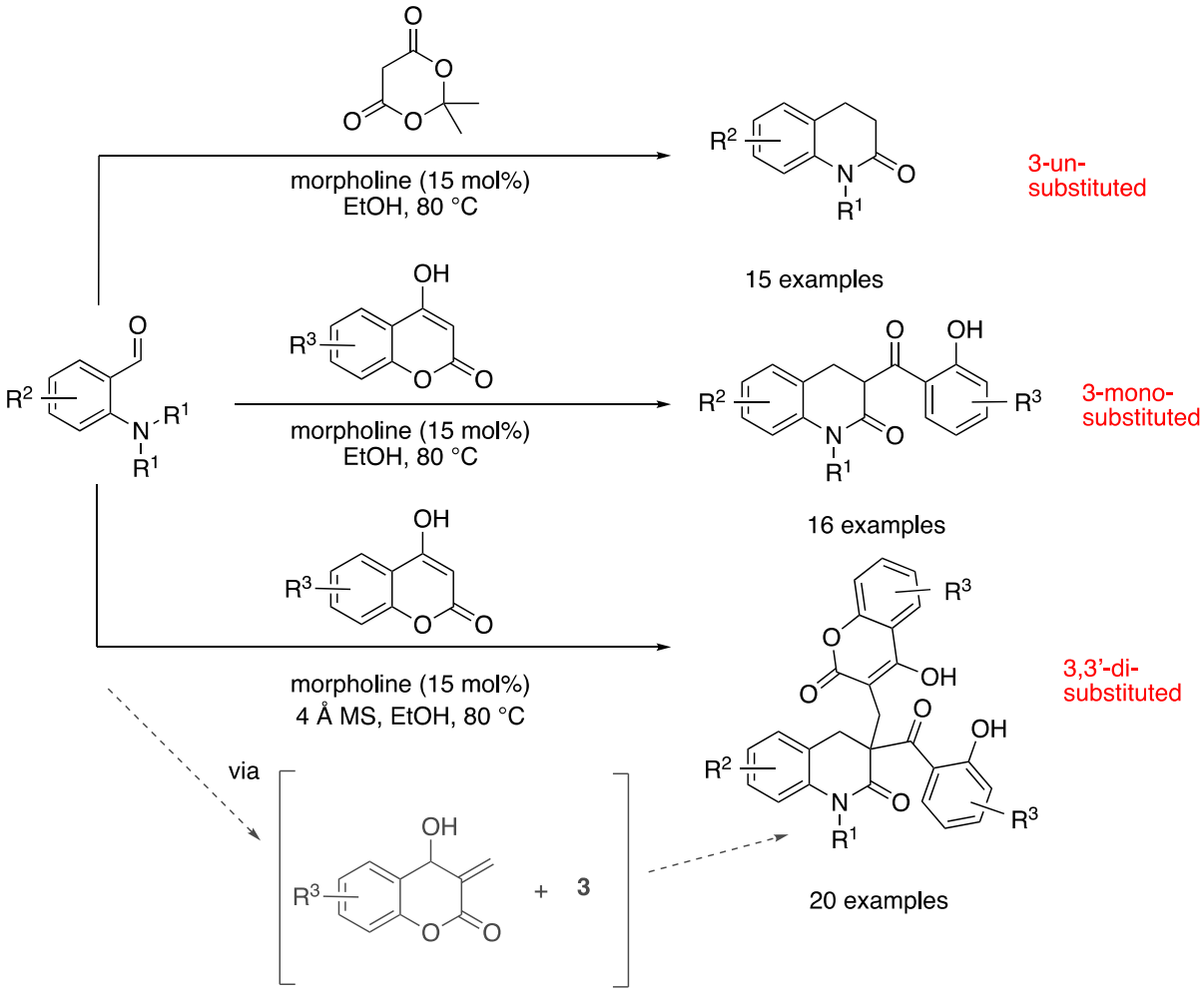

Scheme 3.1: Redox-triggered switchable synthesis of 3-non, 3-mono and 3,3'disubstituted 3,4-dihydroquinolin-2-ones.

In 2021, Yu and co-workers[160] reported a ruthenium-catalysed cyclisation of 1,4,2-dioxazol-5-ones to form 3,4-dihydroquinolin-2-ones via a formal intramolecular arene C(sp^2)-H amidation (Scheme 3.2). The reaction proceeds regioselectively by a tandem electrophilic spirocyclisation and C-C migration. The need for a highly specialised ruthenium catalyst, a silver hexafluoroantimonate additive and elevated temperatures (50 °C) results in this method being less than ideal for the current push to more sustainable chemistry methods.

Yu (2021): Arene C(sp^2)-H Amidation

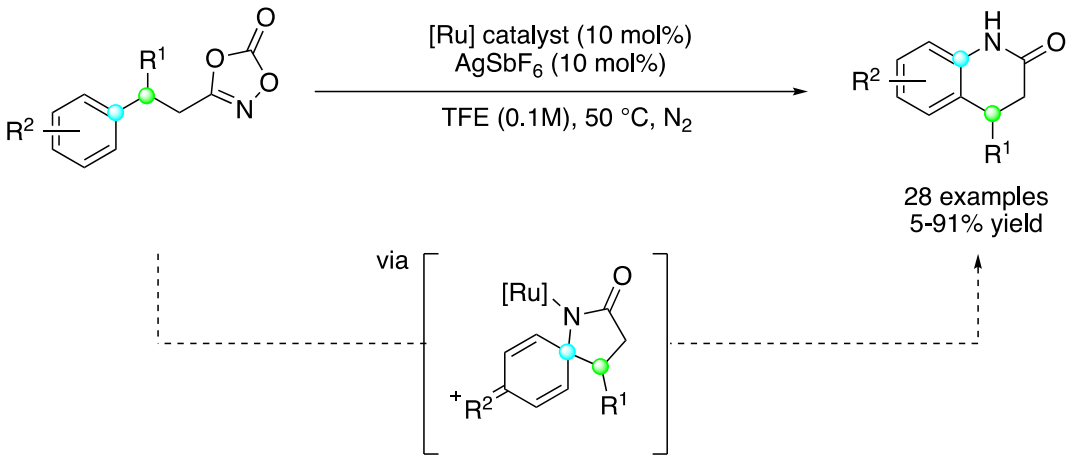

Scheme 3.2: Ruthenium-catalysed intramolecular arene C(sp^2)-H amidation via an electrophilic spirocyclisation.

As described in Chapter 1, photocatalysis can be a highly sustainable and desirable area of organic synthesis. To date, there have only been a handful of visible-light mediated photocatalytic methods for the formation of 3,4-dihydroquinolin-2-ones reported.

Notably, Donald and co-workers[132] described a redox-neutral intermolecular addition-cyclisation approach for the formation of 3,4-dihydroquinolin-2-ones (Scheme 3.3). Carbamoyl radicals were generated from reductive single-electron fragmentation of *N*-hydroxyphthalimido esters using an iridium photocatalyst, which could then undergo addition-cyclisation to electron-deficient alkenes.

Donald (2017): Photoredox Addition-Cyclisation

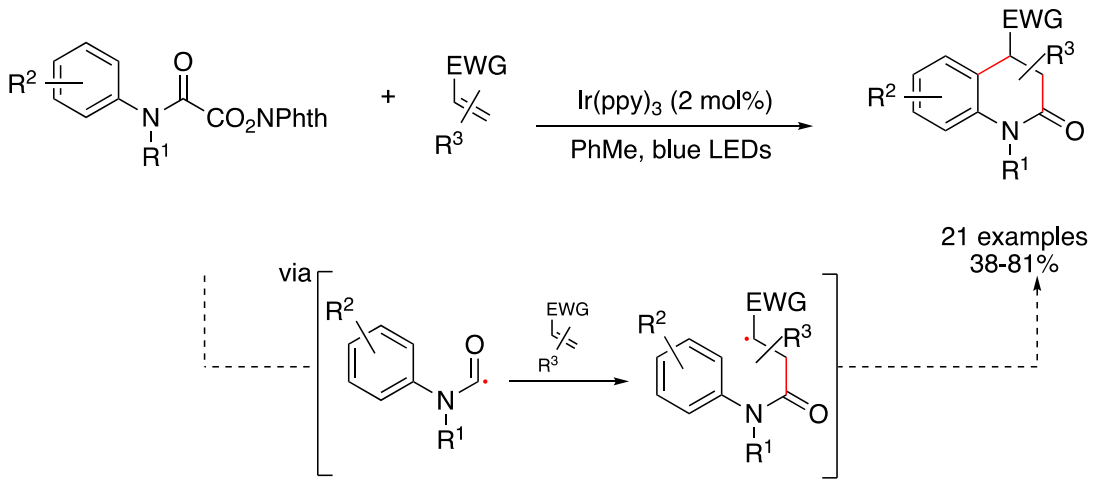

Scheme 3.3: Redox-neutral intermolecular addition-cyclisation reaction via a carbamoyl radical.

Based on the work by Smith and co-workers,[71] who reported a visible-light mediated Ir-catalysed 6π heterocyclisation for the formation of fused heterocyclic systems via an energy transfer (EnT) reaction as described in Chapter 1 (Scheme 1.14), we hypothesized that 3,4,-dihydroquinolinones could similarly be accessed through cyclisation of diradical triplet $\mathbf{2}^{3*}$, generated through visible-light mediated EnT to acrylamide precursor **2**, overall encompassing a formal C(sp^2)-H/C(sp^3)-H hydroarylation (Scheme 3.4). There have been a number of UV-light mediated hydroarylations in past years,[161–163] but within the visible-light manifold, only few examples have been described, and none relating to the visible-light mediated synthesis of 3,4,-dihydroquinolinones (at the time of reaction optimisation).

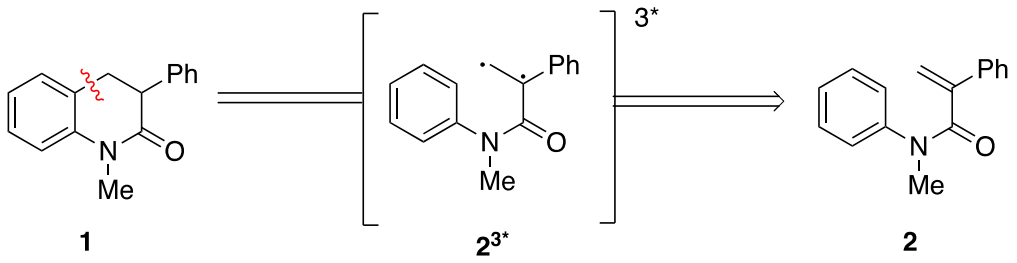

Scheme 3.4: Our proposed retrosynthetic approach to 3,4-dihydroquinoinones via a visible-light mediated EnT.

We were aware that in the aforementioned EnT hydroarylation strategies, the need to utilize expensive transition metal catalysts was apparent. Aligned with the theme of my research project, we questioned whether this requirement was due to a fundamental reactivity barrier and if it was possible to instead use organic small molecule photosensitisers that would facilitate a more sustainable and cost-effective alternative. Thus we were also determined to develop a metal-free variation of this reaction. Thioxanthone photosensitisers represent a powerful class of small molecule, metal-free photosensitisers and we envisaged using them as metal replacement catalyst for EnT reactions.

Thioxanthone Photosensitisers

Thioxanthone (**TX**) (Figure 3.3) and its derivatives are well-studied photoactive compounds capable of performing a variety of chemical transformations.[164] In comparison with other aromatic ketones, **TX** has a high triplet energy (63.4 kcal mol^{-1}; higher than the iridium photosensitisers used in related processes) and a relatively long triplet lifetime (73 μs),[61,65,165] thus making it an ideal EnT photosensitiser. Despite these promising photodynamic and cost

attributes, the study of this class of molecules has featured largely in the physical chemistry and polymerisation literature and their utility toward small molecule synthesis — especially given the resurgence of interest in photocatalysis — has been surprisingly unexplored. Furthermore, **TX** is considerably cheaper than most other organic photosensitisers (approximately $2/g), and certainly than metal photocatalysts.

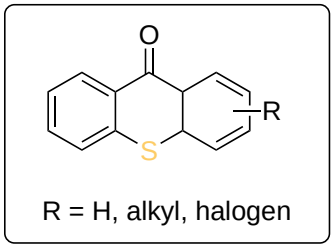

Figure 3.3: Thioxanthone (**TX**: R^1,R^2 = H) and potential derivatives as organic alternatives to metal photocatalysts.

The pioneering work in the studies of **TX** in synthetic chemistry came by the work of Bach. Most significantly, his contribution toward the design of a chiral **TX** sensitiser (Scheme 3.5) to facilitate enantioselective [2+2] photocyclisations.[69,166]

Bach: Enantioselective [2+2] Cycloaddition

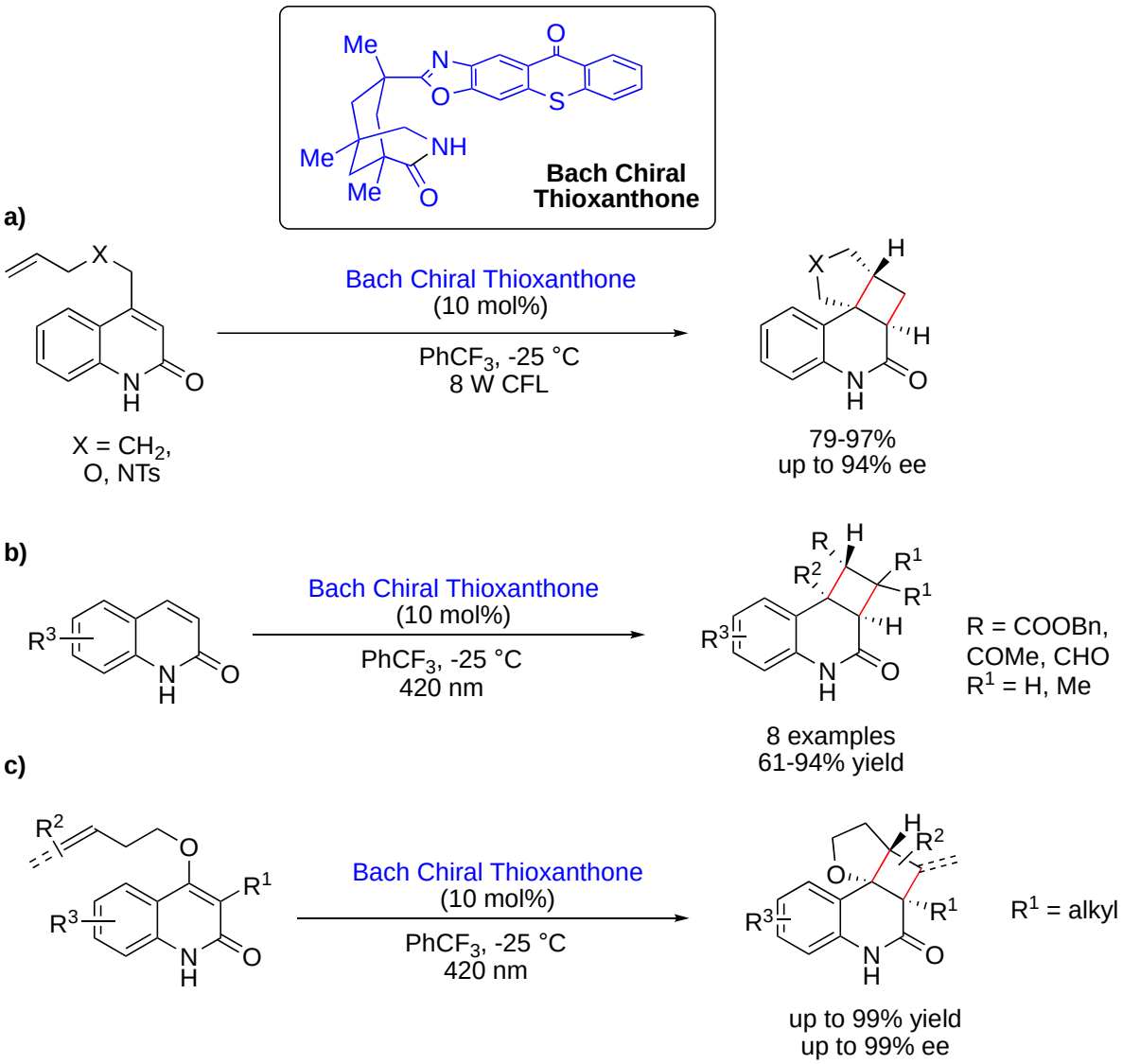

Scheme 3.5: [2+2] photocyclisations mediated by Bach's chiral thioxanthone catalyst: a) enantioselective intramolecular photocycloaddition of quinolone derivative; b) enantioselective intermolecular photocycloaddition of quinolones with electron-deficient alkenes; c) enantioselective intramolecular photoaddition of hydroxyquinolones tethered with alkenes and allenes to form cyclobutene derivatives.

Other than [2+2]-cycloadditions, and at the time of commencing this research, there were only few other applications of **TX** photocatalysis. Notably, in 2019 Gilmour and co-workers[167] reported a one-pot synthesis of fused dihydrocoumarins from cinnamic acids which comprised a photosensitised *E*/*Z* isomerisation, followed by subsequent lactonisation and an intramolecular [2+2] cycloaddition via two energy transfer events (Scheme 3.6).

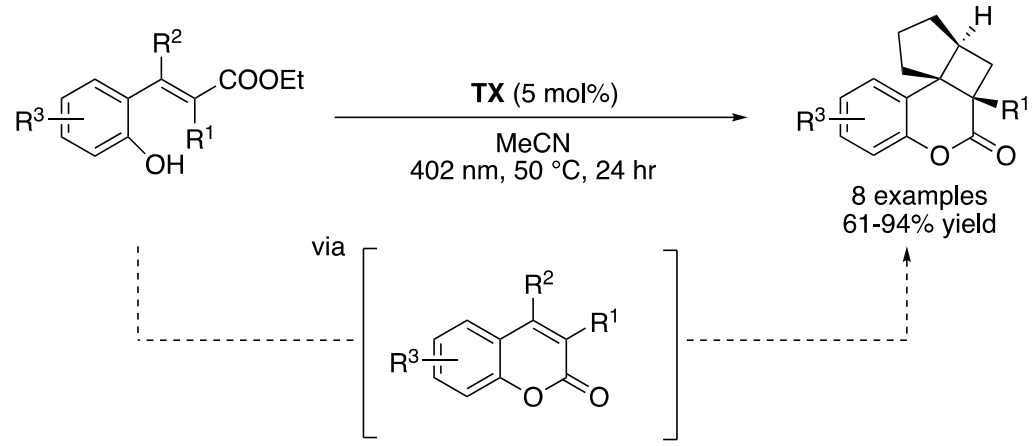

Scheme 3.6: **TX** catalysed one-pot synthesis of fused dihydrocoumarins.

To this end, we aimed to extended the reactivity profile of this class of photosensitisers to include our envisaged hydroarylation for the synthesis of 3,4-dihydroquinolin-2-ones.

3.2 Aims and Objectives

Our overall objective for this chapter was to develop a method for the synthesis of biologically important 3,4-dihydroquinolin-2-ones utilizing visible-light mediated photocatalysis. We wanted to identify metal-free photocatalyst alternatives for a triplet energy transfer to *N*-acrylamides. We aimed to develop a method with a broad reaction scope that was well tolerated with substituents on the acrylamide and perform mechanistic studies to correctly identify the mechanism of the reaction. We were also curious about the possibility of scaling-up the desired reaction for potential industry use in the future. Finally, we envisage demonstrating further synthetic utility by converting 3,4-dihydroquinolin-2-ones into the corresponding quinoline-2-ones via an oxidation process.

3.3 Results and Discussion

Based on the precedent that olefins can be sensitised to their triplet states and undergo cyclisation onto aromatics, we set out to identify a suitable *N*-aryl acrylamide starting material for our hydroarylation. Preliminary experiments revealed 1-methyl-3-phenyl-3,4-

dihydroquinolin-2(1*H*)-one **3.2a** to be the ideal model substrate, as the phenyl substituent provided suitable radical stabilising effects of the intermediate.

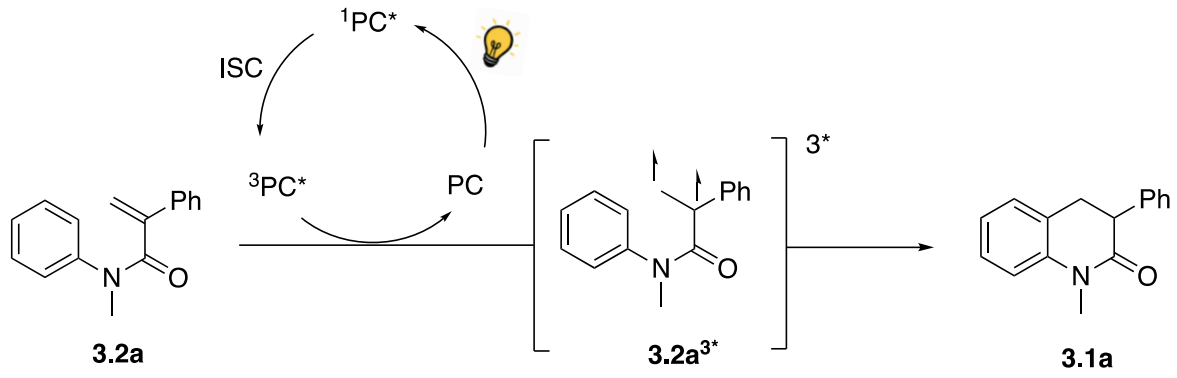

Scheme 3.7: Proposed photocyclisation to 1-methyl-3-phenyl-3,4-dihydroquinolin-2(1H)-one via a triplet energy transfer.

The model acrylamide **3.2a** was easily accessed with a standard peptide coupling between the requisite aniline and acrylic acid using Mukaiyama's reagent. ^{1}H NMR and ^{13}C NMR spectroscopy was used to analyse the acrylamide and confirm we had isolated the correct product (see supplementary information for details).

It is worth noting that as we began to expand the substrate scope it became evident that an alternative method for the synthesis of acrylamides would be necessary; when investigating substituents on the aniline, we found that highly electron withdrawing groups such as fluorine and trifluoromethyl reduced the nucleophilicity of the aniline and prevented the amidation from occurring under Mukaiyama's coupling conditions. For these substrates, the more reactive acid chlorides were required.

With a suitable method for the synthesis of acrylamides in hand, we turned our attention to the key photocyclisation step. Preliminary studies with 450 nm LEDs and ((Ir(dF(CF_3)ppy)$_2$dtbpy)PF_6) in toluene gratifyingly afforded the desired 3,4-dihydroquinolinones in excellent yield. We opted for an iridium catalyst at this early stage to test the viability of the chemistry itself. The isolated product was analysed by ^{1}H NMR and ^{13}C NMR. When comparing the ^{1}H NMR spectrum of the uncyclised acrylamide **2a** to the product **1a**, it can be seen that the aromatic region is reduced from 10 protons to 9 protons. The *N*-

methyl protons (H_d) are still present as a singlet at 3.43 ppm, however additional peaks in the form of a doublet and a triplet are present accounting for the newly saturated bond. H_b appears as a triplet at 3.87 ppm and H_a appears as a doublet at 3.23 ppm both with a coupling constant of 7.5 Hz as expected for protons on adjacent sp^3 carbons (Figure 3.4).

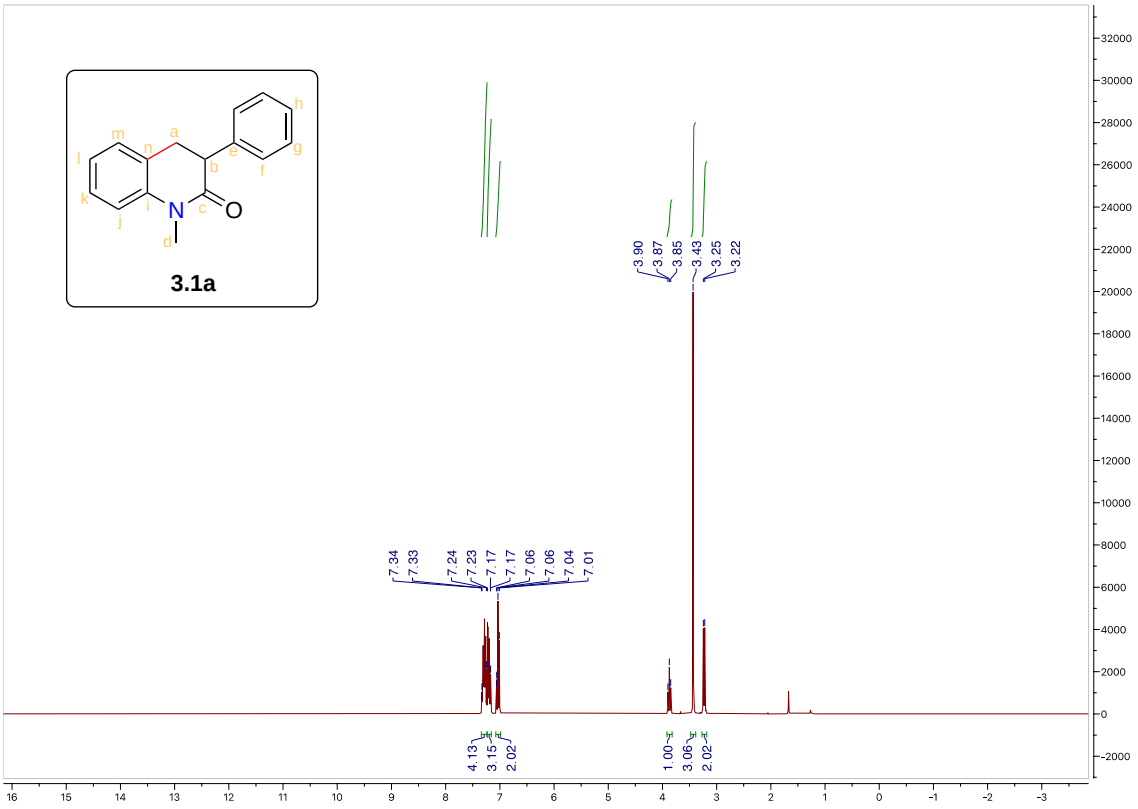

Figure 3.4: ^{1}H NMR spectrum of 3.**1a**

When analysing the ^{13}C NMR spectra for 3,4-dihydroquinolin-2-one **3.1a** (Figure 3.5) the main difference is the presence of 2 new peaks in the upfield alkyl region, namely C_a at 33.1 ppm and C_b at 47.0 ppm.

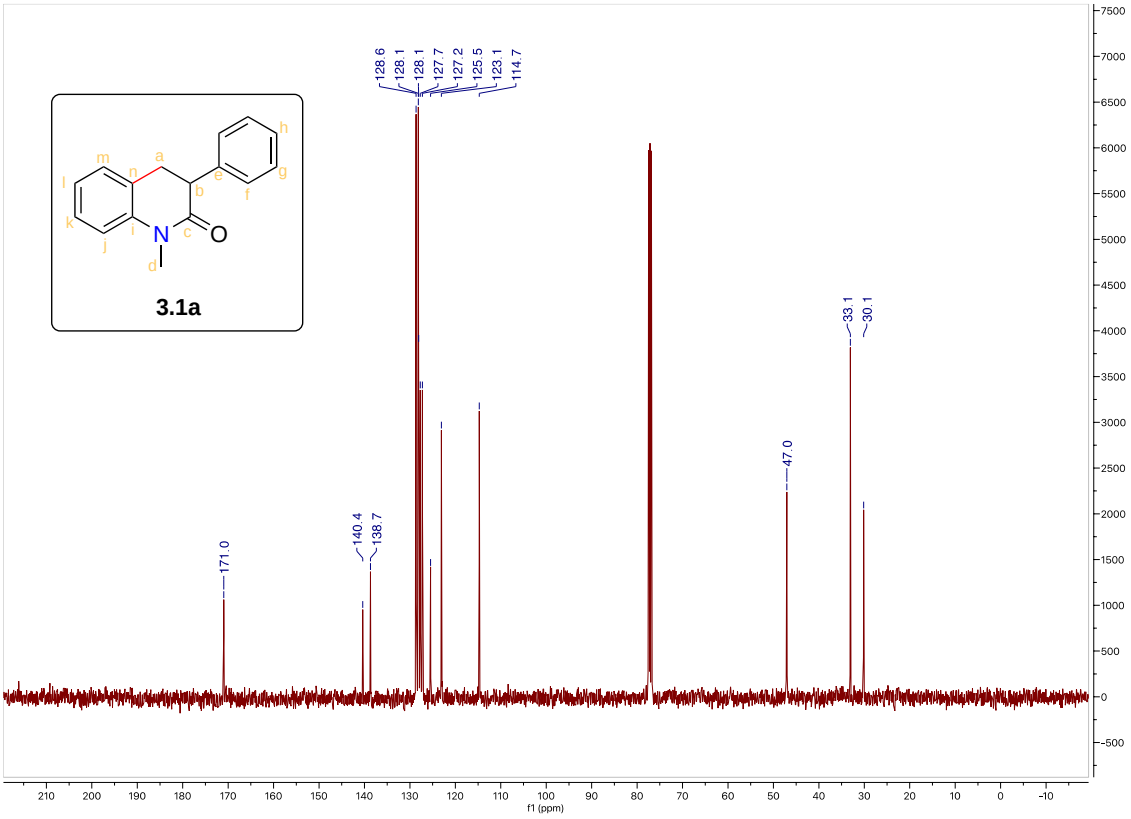

Figure 3.5: ^{13}C NMR spectrum of 3.**1a**

3.3.1 Optimisation Studies for Photocyclisation Step

Guided by the works of Smith[71] and Glorius[168] for iridium-catalysed photocyclisations we first screened a range of iridium photosensitisers and investigated the effects of catalyst loading and solvent.

Entry	Photocatalyst	Catalyst mol %	Solvent (M)	Yield (%)[a]
1	**Ir-1**	2%	PhMe (0.05)	99%
2	**Ir-2**	2%	PhMe (0.05)	79.5%
3	**Ir-3**	2%	PhMe (0.05)	92.5%
4	**Ir-1**	3%	DCM (0.05)	99%

5	**Ir-1**	3%	THF (0.05)	90%
6	**Ir-1**	3%	MeCN (0.05)	99%
7	**Ru(bpy)**	2%	PhMe (0.05)	No rxn

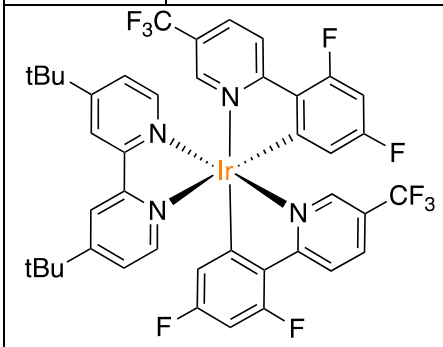

Ir-1
$(Ir(dF(CF_3)ppy)_2dtbpy)PF_6$

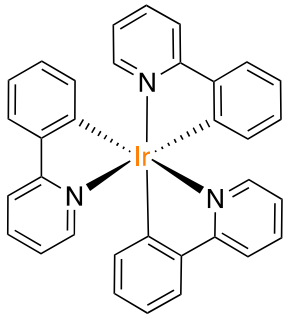

Ir-2
$Ir(dF(ppy)_3)$

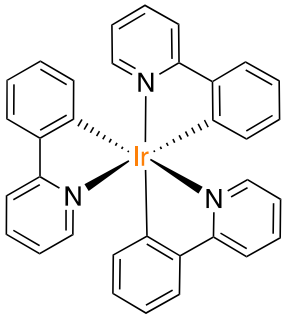

Ir-3
$Ir(ppy)_3$

Table 3.1.1: Optimisation table for photocyclisation reaction with transition-metal photosensitisers. [a]Determined by ^1H NMR against internal standard (1,3,5-trimethoxybezene).

To our delight, all 3 Ir-photocatalysts; **Ir-1** ($(Ir(dF(CF_3)ppy)_2dtbpy)PF_6$), **Ir-2** ($Ir(dFppy)_3$) and **Ir-3** ($Ir(ppy)_3$) produced the desired product **3.1a** in excellent yields (entries 1-3) in toluene. Most notably, **Ir-1** in toluene worked in near-perfect yields with 99% product formation according to ^1H NMR (entry 1). Expanding on the solvent effects, it was found that **Ir-1** works in excellent yields (>90%) for a variety of solvents, namely DCM, THF and acetonitrile at 0.05 M concentration (entries 4-6). Additionally we attempted the reaction with a ruthenium catalyst ($Ru(bpy)_3$), however no reaction was observed, and starting material was completely recovered (entry 7).

When considering whether a photocatalyst is able to promote a transformation there are a number of properties that need to be considered as described in Chapter 1. Apart from a suitable absorption wavelength, efficient intersystem crossing and a long-lived triplet excited state; it is important that the photosensitiser possesses a triplet excited-state energy that is higher than the substrate acceptor. When comparing the triplet excited states of the above photocatalysts, one can draw conclusions as to the effectiveness of the EnT. **Ir-1**, **Ir-2** and **Ir-3** have triplet state energies[65] of 61.8, 60.0 and 58.1 kcal mol^{-1} respectively, however $Ru(bpy)_3$ has a triplet state energy of only 49.0 kcal mol^{-1}, leading to the assumption that the triplet energy of the substrate **3.2a** is likely greater than 49 kcal mol^{-1} and as such $Ru(bpy)_3$ is unsuitable.

It is important to note that while we were working on this method, Che and co-workers.[169] disclosed a Pt-catalysed EnT process for the intramolecular photocyclisation of acrylanilides to give 3,4-dihydroquinolin-2-ones (Scheme 3.8). The authors proposed the reaction proceeded via an endergonic triplet-triplet EnT from a Pt-complex to access a triplet excited state acrylanilide, which then rapidly undergoes a radical ring closure and ISC back to the ground state. Intramolecular [1,5]-H shift results in the desired 3,4-dihydroquinolin-2-ones.

Che (2021): TET Photocyclisation

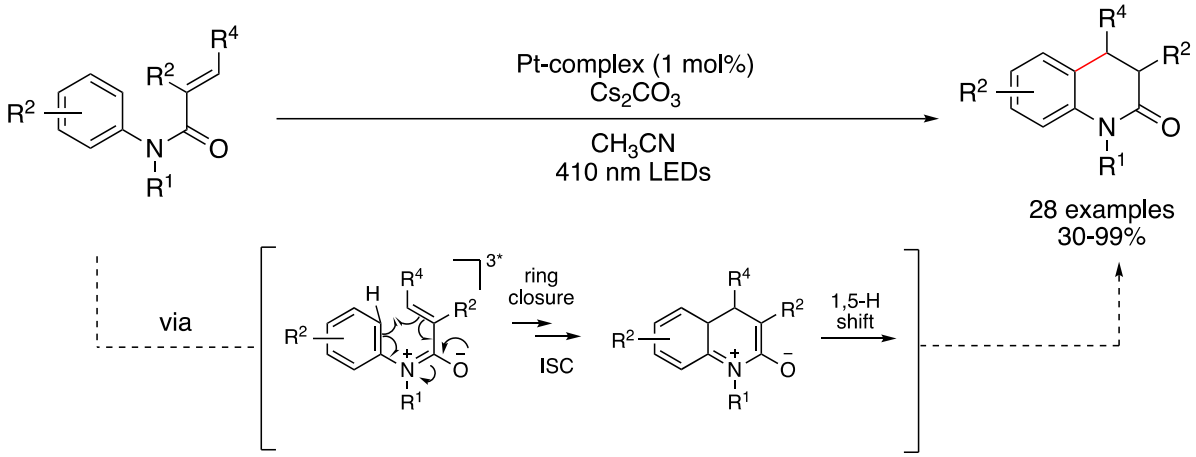

Scheme 3.8: Visible-light mediated triplet energy transfer for the formation of 3,4-dihydroquinolin-2-ones via a cyclisation and 1,5-H shift.

However this method still required the use of rare and expensive metals, which served as justification for our goal of developing a more sustainable and cost effective approach by identifying suitable metal replacement photosensitisers. Table 3.2.1 shows the continuation of the optimisation attempts, focusing on thioxanthone and thioxanthone derivatives as photosensitisers, as their triplet energies are known to be greater than that of the iridium catalysts tested above.

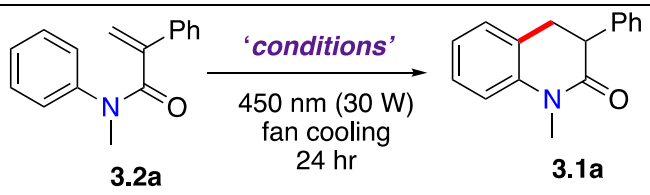

3.2a **3.1a**

Entry	Photocatalyst	Catalyst mol %	Solvent (M)	Yield (%)[a]
8	**xanthone**	10%	EtOH (0.05)	Trace
9	**TX**	10%	EtOH (0.05)	Trace

10	**2-CTX**	10%	EtOH (0.05)	37%
11[b]	**2-CTX**	20%	EtOH (0.05)	72.5%
12[b]	**2-IPrTX**	20%	EtOH (0.05)	68%
13[b]	**4-IPrTX**	20%	EtOH (0.05)	60.5%
14	**2-CTX**	10%	PhMe (0.05)	17%
15	**2-CTX**	10%	MeCN (0.05)	10%
16	**2-CTX**	20%	TFE (0.05)	100%
17	**2-CTX**	10%	TFE (0.05)	88%
18	**2-CTX**	5%	TFE (0.05)	52%
19	**2-ITX**	20%	TFE (0.05)	83%
20[c]	**2-CTX**	20%	TFE (0.05)	No rxn
21	none	-	TFE (0.05)	No rxn

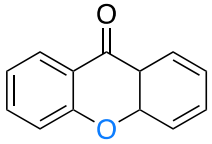

xanthone

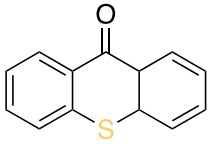

TX
thioxanthone

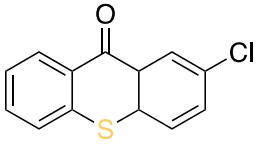

2-CTX
2-chlorothioxanthone

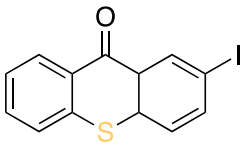

2-ITX
2-iodothioxanthone

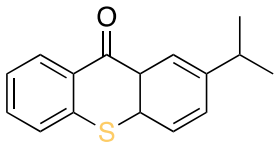

2-IPrTX
2-isopropylthioxanthone

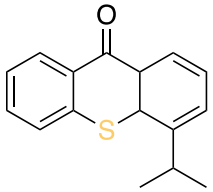

4-IPrTX
2-isopropylthioxanthone

Table 3.1.2: Continued optimisation table for photocyclisation reaction with organic photosensitisers. [a]Determined by ^{1}H NMR against internal standard (1,3,5-trimethoxybenzene). [b]Irradiated for 45 hrs. [c]No light.

Performing the reaction with a 450 nm LED and fan cooling with xanthone or thioxanthone as the photosensitiser produced only trace amounts of product **3.1a** in ethanol in 24 hrs (entries 8-9). Gratifyingly, we observed product formation when using 10 mol% **2-CTX**, albeit in poor yields with unreacted starting material accounting for the mass balance (entry 10). In an attempt to improve the yields we increased catalyst loading to 20 mol% and irradiation times to 48 hrs and noticed a significant increase in yield from 37% to 72.5% with **2-CTX** (entry 11). Further modifications on the thioxanthone substituent revealed 2- and 4-isopropylthioxanthones to be suitable photosensitisers which produced 3,4-dihydroquinolin-

2-one **3.1a** in moderate yields (entries 12-13). We ultimately decided **2-CTX** was our preferred catalyst as it produced the best yields and was the most accessible and inexpensive of the catalysts.

We next turned to optimising the solvent. Thioxanthone triplet sensitisers have been shown to be very solvent dependent in the literature. In 1974, Dalton *et. al.*[170] published a report investigating solvent effects on thioxanthone photocatalysts and determined that increasing the hydrogen bonding ability and polarity of the solvent leads to a red shift of the absorption maxima. This can be seen by analysing the difference between the UV-vis spectrum of **2-CTX** in ethanol and trifluoroethanol (TFE) (Figure 3.6(i)). The peak absorbance in ethanol occurs at 385 nm, while TFE has a maximum absorbance at 395 nm. We were aware that using a light source of lower wavelength that still falls within the visible range of (i.e. 405 nm) would likely improve the reaction yields over the timeframe, however at the time of this research, we did not have access to an LED with a wavelength lower than 450 nm (the impact of the Covid-19 pandemic played a significant role in this), and as such focussed on optimizing the conditions with 450 nm. The 450 nm LED was obtained from EvoluChem and the spectrum is shown in Figure 3.6(ii) below. As seen in the spectrum, the shorter wavelength tail of the emission overlaps with the absorbance spectra of **2-CTX** in TFE.

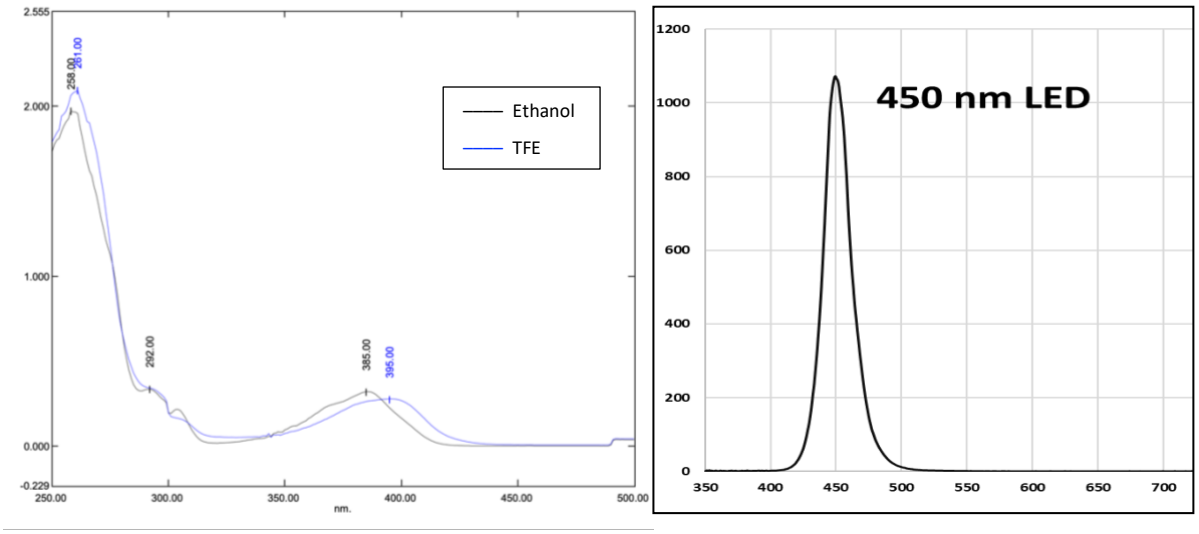

Figure 3.6: (i) UV-Vis spectrum of **2-CTX** in ethanol and TFE. (ii) EvoluChem 450nm LED emission spectra.

Therefore, as expected, carrying out the reaction in aprotic solvents generally gave poor yields (entries 14-15) and a significant increase in the rate of the reaction was observed when using

2,2,2-trifluoroethanol (2,2,2-TFE), which, gratifyingly, produced complete conversion at 100% yield in 24 hr (entry 16).

NOTE: Following publication, we were able to procure a 405 nm LED and performed the same cyclisation using acrylamide **3.2a**. Using **2-CTX** in methanol gave 90% ^{1}H NMR yield in 24 hrs. As expected, aprotic solvent toluene gave a significantly reduced yield of 41% after 24hrs (unpublished work).

It was found that yield decreased with decreasing **2-CTX** catalyst loading (entries 17-18), albeit over the standard 24 h time frame. The effect of the halosubstituent of the photosensitiser was also investigated. 2-Iodothioxanthone (**2-ITX**) also showed excellent yields with the ideal conditions, providing **3.1a** in a slightly lower 83% yield (entry 19).

Finally, control experiments were set up to confirm a light-mediated energy-transfer mechanism was occurring. No reaction was observed when there was no light (entry 20) or no catalyst (entry 21) present.

Satisfied with our ideal conditions of 20 mol% **2-CTX** in TFE for 24 hr with 450 nm LEDs and fan-cooling we began to expand upon the substrate scope. However, we encountered solubility issues that affected the efficiency of the transformation, presumably due to poor light penetration into the reaction mixture. Ultimately, a mixture of 2,2,2-TFE and $CHCl_3$ (4:1) — providing a more homogeneous reaction mixture — afforded the ideal conditions across the broad range of substrates (*vide infra*). Another advantage of this reaction is that it requires no work-up. Upon complete conversion of the starting material, confirmed by TLC, the solvent was removed under vacuo and the crude mixture purified directly by column chromatography. This further promotes this reaction as a 'greener' approach to 3,4-dihydroquinolin-2-ones as it requires less consumables and solvent in the purification steps.

3.3.2 Expanding the Substrate Scope

In exploring the substrate scope, we identified 4 areas of substrate variation (Figure 3.7): the substituents on the quinolinone aromatic ring (purple), the protecting group of the nitrogen

(blue), the substituents on phenyl ring (green), and altering the type and position of the dihydroquinolinone substituent (pink).

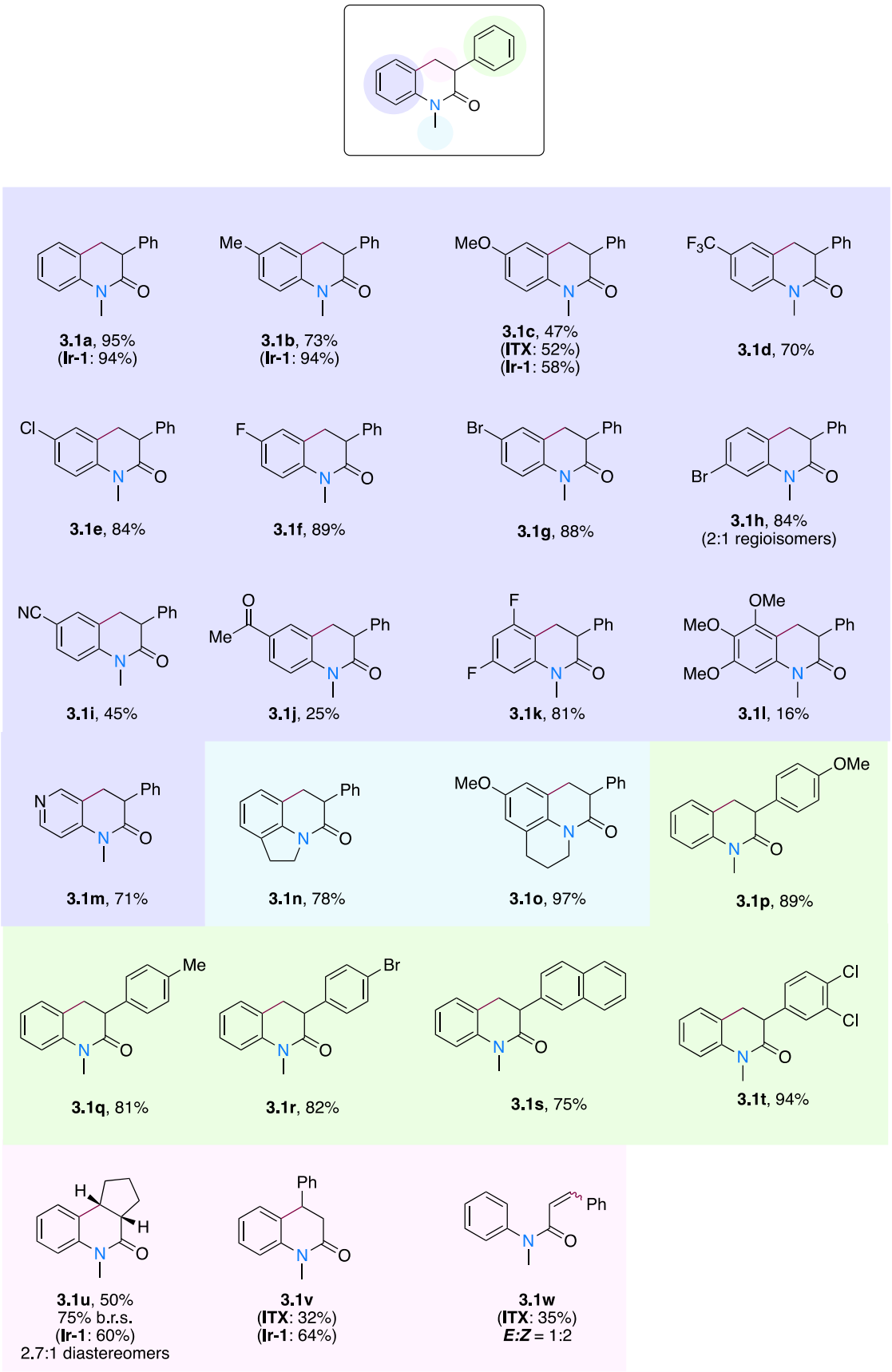

Figure 3.7: Expanding the substrate scope of 3,4-dihydroquinolin-2-ones.

The model substrate **3.1a** was produced in 95% isolated yield with **2-CTX**. When using **Ir-1**, a comparable isolated yield of 94% was obtained. Variations of the substituent on the aromatic group were well tolerated. Substrate **3.1b**, bearing a methyl substituent on the aniline, was obtained in 73% yield. Substrate **3.1c**, containing an electron-rich methoxy group, was produced in 47% yield, while carrying out the reaction using **2-ITX** instead gave an a slightly improved yield of 52%. When performing these two reactions using **Ir-1**, comparable yields of 73% (**3.1b**) and 58% (**3.1c**), respectively, were obtained. Electron-withdrawing CF_3 substituent was also tolerated affording **3.1d** in 70% yield. A number of halogen substituents were investigated and all afforded excellent yields: chlorine, fluorine and bromine were isolated in 84% (**3.1e**), 89% (**3.1f**) and 88% (**3.1g**) yield, respectively. Substrate **3.1h** was isolated in 84% with 2:1 ratio of the 5- and 7-bromo regioisomers. Electron-withdrawing nitrile (**3.1i**) and acetyl (**3.1j**) groups afforded 45% and 25% yield, respectively. Disubstituted quinolinone **3.1k** was efficiently produced in 81% yield, while the trisubstituted variant **3.1l** was obtained in a moderate 16% yield and modification of the aniline to a pyridine successfully produced **3.1m** in 71% yield.

When varying the protecting group of the nitrogen, we performed the reaction using indoline and quinoline base acrylamides. These modifications afforded tricyclic products **3.1n** in 78% and **3.1o** in 97% yields, respectively.

We next turned our attention to variations on the aromatic group of the 'acrylate' side of the molecule. Substituents at the 3-position were well tolerated, affording **3.1p-3.1r** in 81−89% yield. The naphthalene substituent produced **3.1s** in 75% yield and disubstituted chloro-quinolinone **3.1t** was isolated in 94%.

Finally, modifications of the vinyl group afforded tricyclic compound **3.1u** in 50% yield (75% yield based on recovered starting material). The iridium comparison, however, afforded **3.1u** in 60% isolated yield. Both reactions produced **3.1u** as a 2.7:1 ratio of diastereomers, according to HPLC analysis, with the major isomer corresponding to the cis-fused ring junction.[171] Switching the aromatic substitution to the 4- position afforded **3.1v** in 64% yield using **Ir-1**. Interestingly, however, **2-ITX** afforded compound **3.1v** in only 32% isolated yield, together with a 35% yield of recovered starting material. When this recovered starting material was analysed using ^{1}H NMR, it was determined that a *trans/cis* isomerisation had occurred in a 1:2 ratio (**3.1w**) (Scheme 3.9).

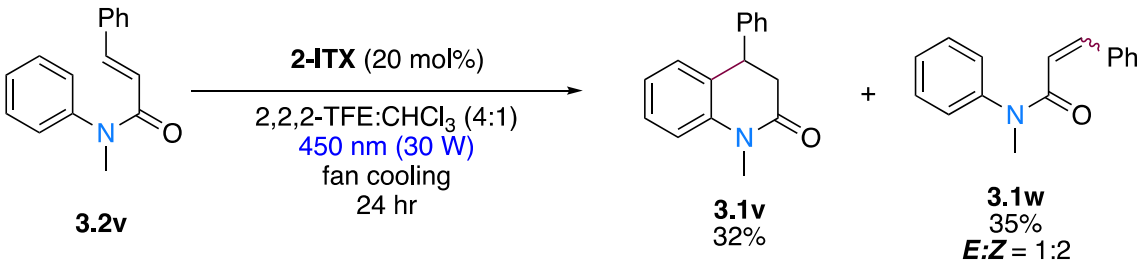

Scheme 3.9: *Trans/cis* photoisomerisation and photocyclisation of **2v**.

When comparing the ^{1}H NMR spectrum of the starting acrylamide **3.2v** (Figure 3.8), which is present as the *E* isomer, to the ^{1}H NMR of the recovered starting material (Figure 3.9) we see a doubling of signals. A characteristic peak at 3.41 for the *N*-methyl group in **3.2v** can still be seen but in addition, a second singlet is seen slightly upfield at 3.32 ppm, accounting for the *N*-methyl peak of the *Z* isomer. The relative integrations of these peaks determined that isomers were present in a 1:2 ratio of *E:Z*. This integration ratio is consistent throughout the spectrum. Considering that photoisomerisation is a well-known application of energy transfer catalysis, as described in Chapter 1, we were not too surprised by this result.

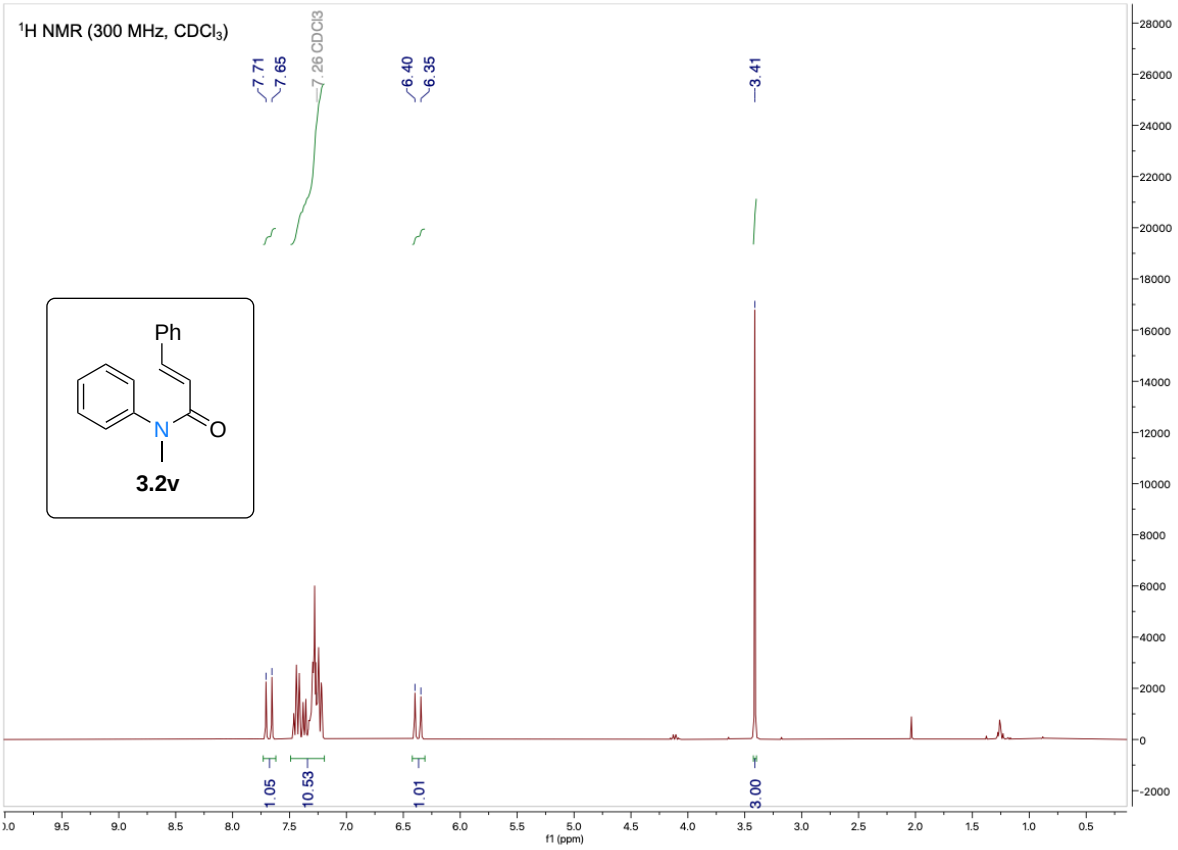

Figure 3.8: ^{1}H NMR spectrum of starting material **3.2v**.

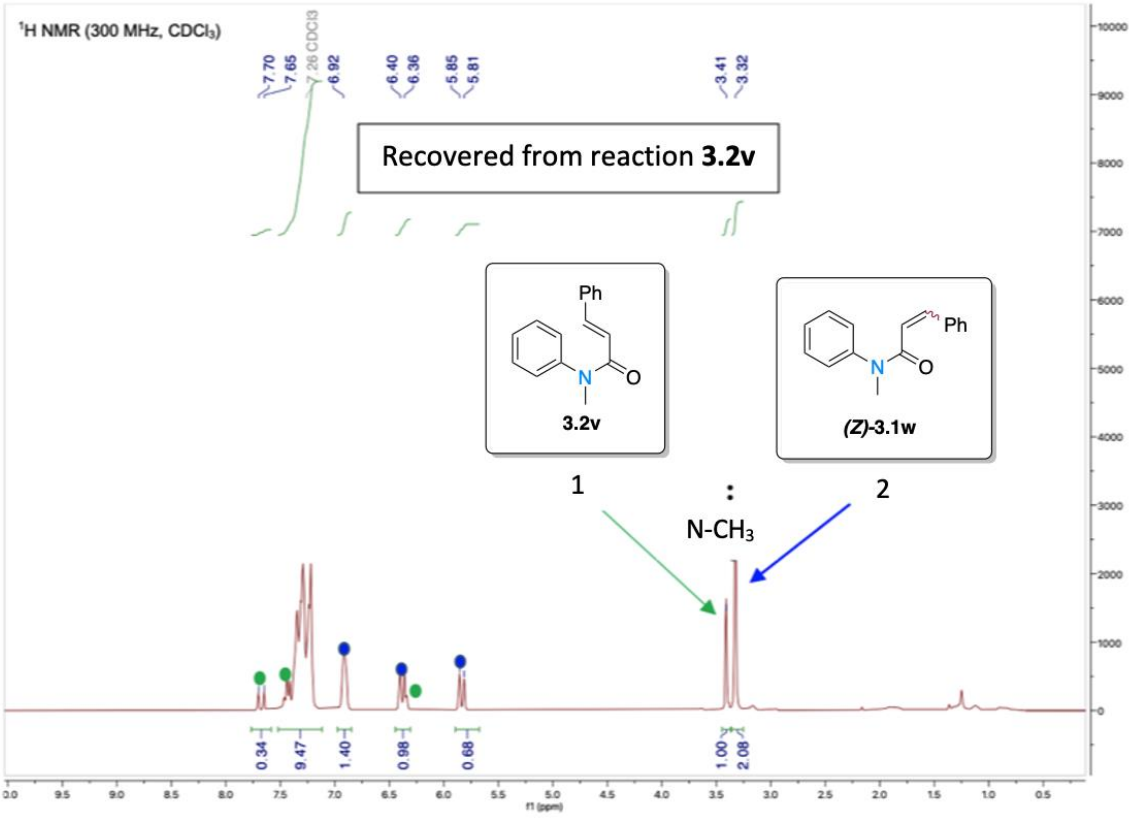

Figure 3.9: ^{1}H NMR spectrum of recovered starting material as a 1:2 ratio of *E:Z* isomer.

Although our reaction conditions were suitable for a wide range of substrates, we did encounter a number of unsuitable substrates. These are shown in Figure 3.10 below.

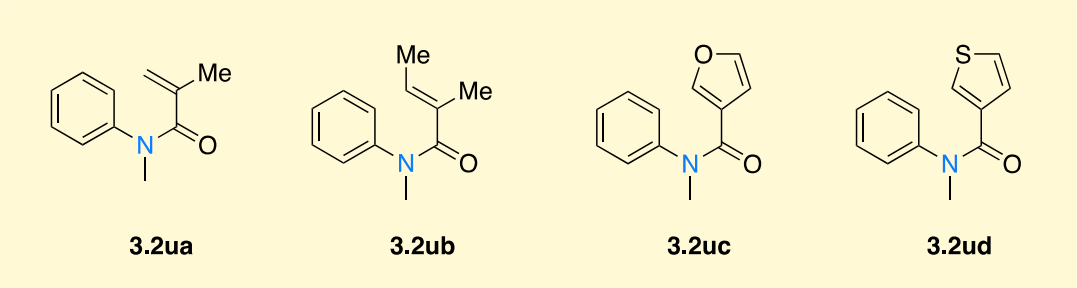

Figure 3.10: Unsuitable substrates

Acyclic acrylamides bearing nonaromatic substituents (**3.2ua** and **3.2ub**) were unsuitable for this transformations. Heterocyclic variants (**3.2uc** and **3.2ud**) also did not cyclise to produce the desired quinolinones. Notably, all 4 of the substrates were unsuitable using either the **2-TX** or **Ir-1** catalysts and starting material was recovered in all 4 cases. Tentatively, we speculate that these results relate to the triplet energy of these starting materials being

higher than that of the photosensitisers, though calculations to estimate these energies were not carried out and will be part of future investigations.

Shortly after our work, a related transformation by Liu *et. al.*[172] was published, which demonstrated that the organic cyanoarene photosensitiser, 4-CzIPN, could also facilitate this reaction. Additionally, their reaction conditions allowed for the cyclisation of substrates with a methyl group alpha to the olefin such as **3.1ua**, albeit in low yields and with 48 hr of irradiation.

3.3.3 Gram-Scale Synthesis and Catalyst Recyclability

As mentioned previously, the reaction is directly subjected to column chromatography. Due to the fact that **2-CTX** is fairly nonpolar (rf = 0.55; 1:4 EtOAc/Hexane), it can be completely recovered (very easily) from the column. In order to investigate the efficiency of the catalyst and the applicability toward large-scale synthesis, we performed a gram-scale reaction on the standard substrate (Scheme 3.10). As a result of the increased vial size and volume of solvent, the reaction was completed according to TLC in 7 days. Product **3.1a** was isolated in 90% yield starting with 1.10 g of acrylamide **3.2a**. Following recovery of the catalyst, we set up a second gram-scale reaction with substrate **3.2c** using the recovered catalyst. After 7 days, the desired product **3.1c** was isolated in 54% yield. Both these yields were consistent with that obtained on the small laboratory scale, confirming that this photocyclisation is tolerant of scale ups as well as confirming the catalyst can be recovered and reused.

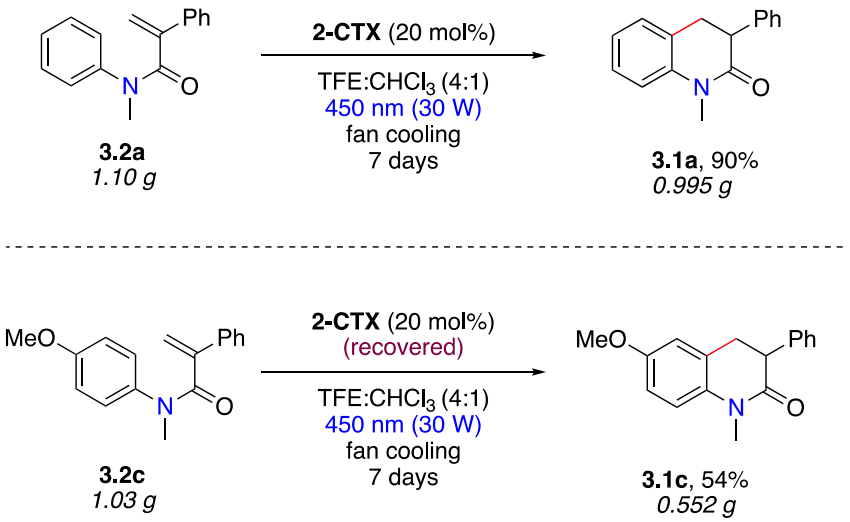

Scheme 3.10: Gram scale reaction of standard acrylamide **3.2a** and gram scale reaction of **3.2c** using the recovered **2-CTX**.

Although this scale up was performed in batch processes, we were aware that implementing an in-flow protocol could significantly reduce the overall reaction times and are currently in the process of acquiring the necessary equipment.

3.3.4 Reaction Mechanism and Mechanistic Studies

In order to understand the mechanism of this reaction, we performed a number of mechanistic studies. We proposed two mechanistic pathways; the first is an electrocyclisation via a closed-shell zwitterionic pathway and the second is via a diradical pathway.

Electrocyclisation Pathway

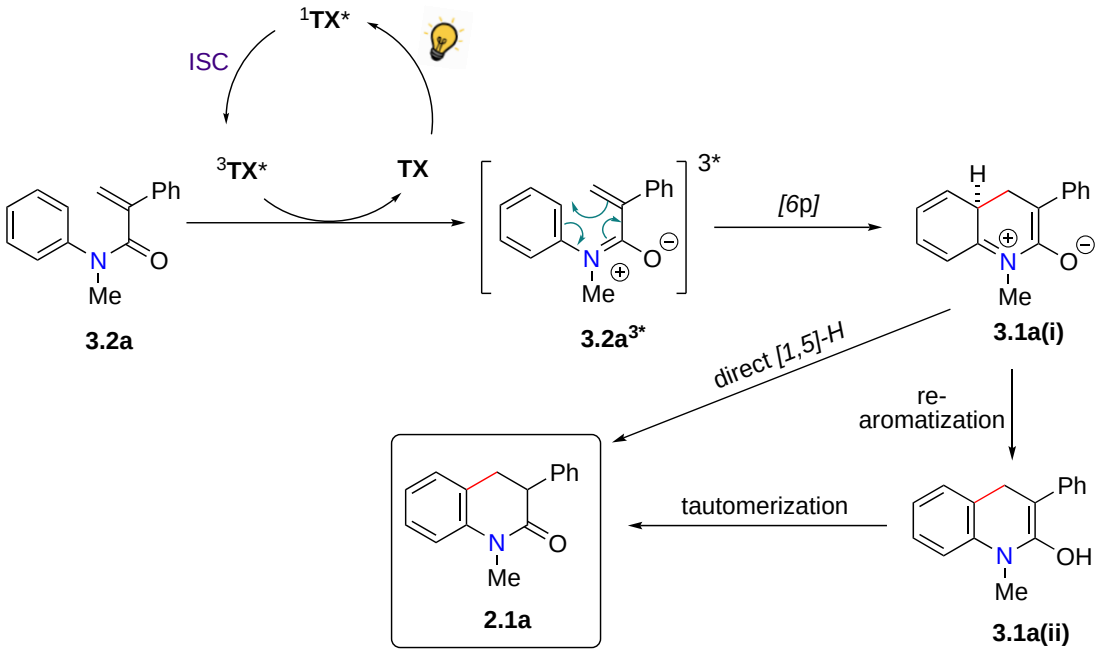

Scheme 3.11: Proposed mechanism for photocyclisation reaction following closed-shell zwitterionic pathway.

Diradical Pathway

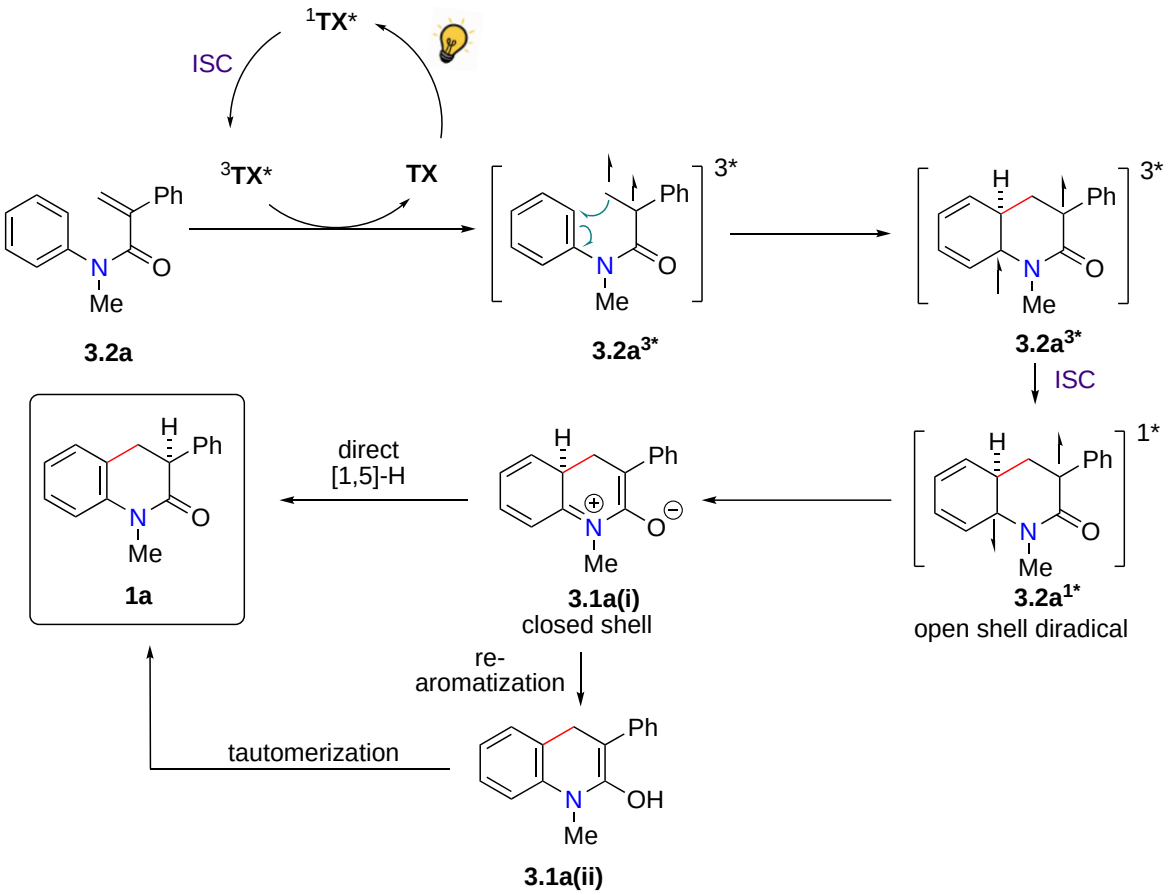

Scheme 3.12: Proposed mechanism for photocyclisation reaction following a diradical pathway.

As described in Chapter 1, both proposed mechanisms are initiated with the excitation of the catalyst from the ground state to the singlet excited state. Intersystem crossing then occurs to the triplet excited state of the catalyst. Triplet-triplet Dexter energy transfer between the catalyst and the acrylamide, results in the triplet excited intermediate **3.2a**^{3*} and regenerates the ground state catalyst. This triplet intermediate is stabilised by H-bonding with the protic solvent. From here, we proposed 2 alternative pathways. In the electrocyclisation pathway, **3.2a**^{3*} undergoes a 6π-electrocyclisation to produce intermediate **3.1a(i)**. Either a direct [1,5]-H shift or a two-step solvent-mediated rearomatization-tautomerization sequence subsequently produces product **3.1a.**

Alternatively, triplet diradical intermediate **3.2a**^{3*} can undergo a radical cyclisation to produce a second triplet intermediate **3.2a**^{3*}. ISC back to the singlet excited state results in singlet diradical **3.2a**^{1*}, which can be represented as the closed-shell zwitterionic intermediate

3.1a(i). From here, either a direct [1,5]-H migration or the same two-step rearomatization-tautomerization sequence as above can occur resulting in the desired product **3.1a**. In accordance with the reports by Smith and co-workers[71,173] we proposed the diradical pathway as the most probable mechanism for this reaction.

We performed deuterium labelling experiments using deuterated acrylamide ***d*$_5$-3.2a** in order to track the [1,5]-H migration (Scheme 3.13).

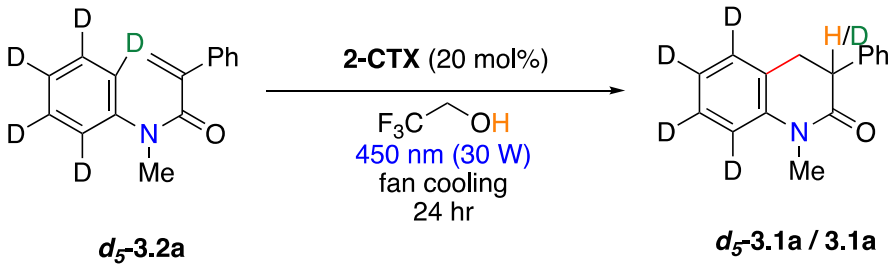

***d*$_5$-3.2a** ***d*$_5$-3.1a / 3.1a**

Scheme 3.13: Deuterium labelling experiments using deuterated acrylamide ***d*$_5$-3.2a** to track the [1,5]-H migration.

^{1}H NMR analysis of the crude reaction mixture (~25% complete) revealed a 45% deuterium incorporation accounting for a ratio of 1.2:1 of **3.1a;*d*$_5$-3.1a**, in which the proton was assumed to come from the protic solvent (Figure 3.11, orange). This supports the mechanism of both a direct [1,5]-H migration as well as at two-step rearomatization-tautomerization pathway to be in operation.

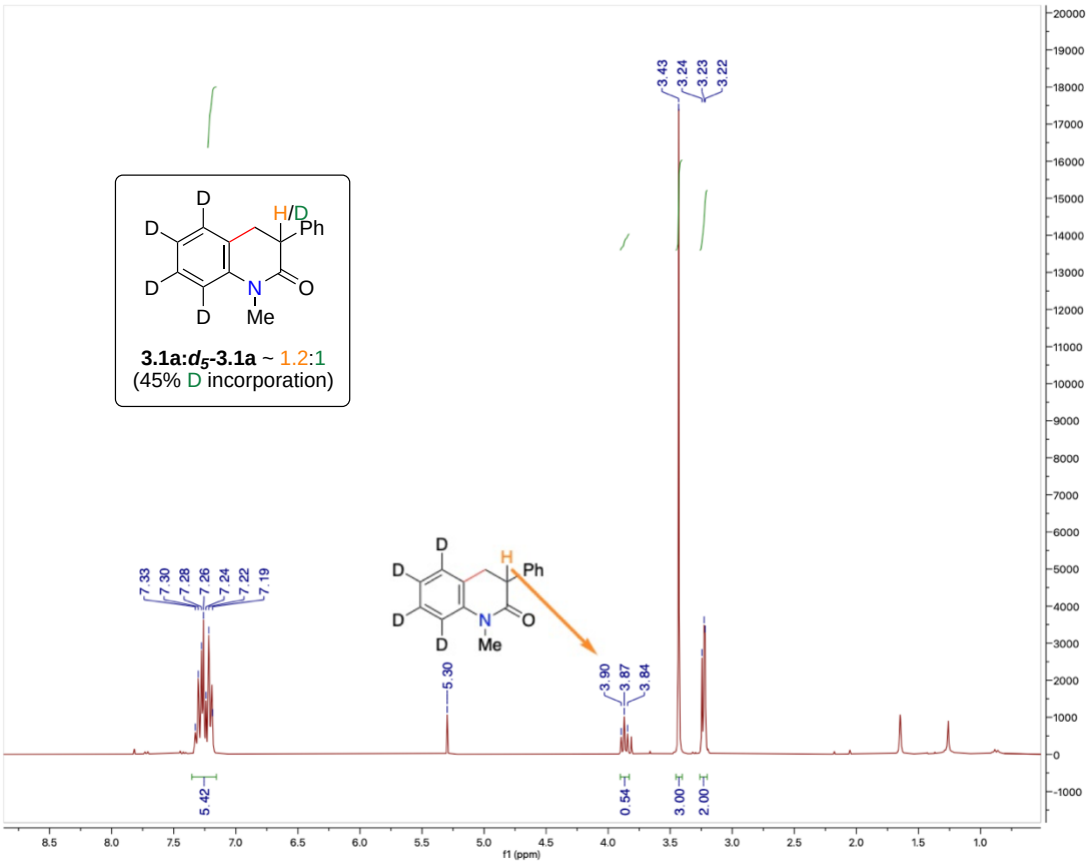

Figure 3.11: ^{1}H NMR spectrum of the crude reaction mixture of deuterium labeling experiment using **2-CTX**.

Interestingly however, when performing the photocyclisation on the deuterated acrylamide ***d*$_5$-3.2a** using the optimised iridium catalysed conditions (**Ir-1**) with DCM we see only a 27% deuterium incorporation (Figure 3.12). This result was unexpected as we assumed in the absence of a protic solvent the reaction would proceed completely via the [1,5]-H.

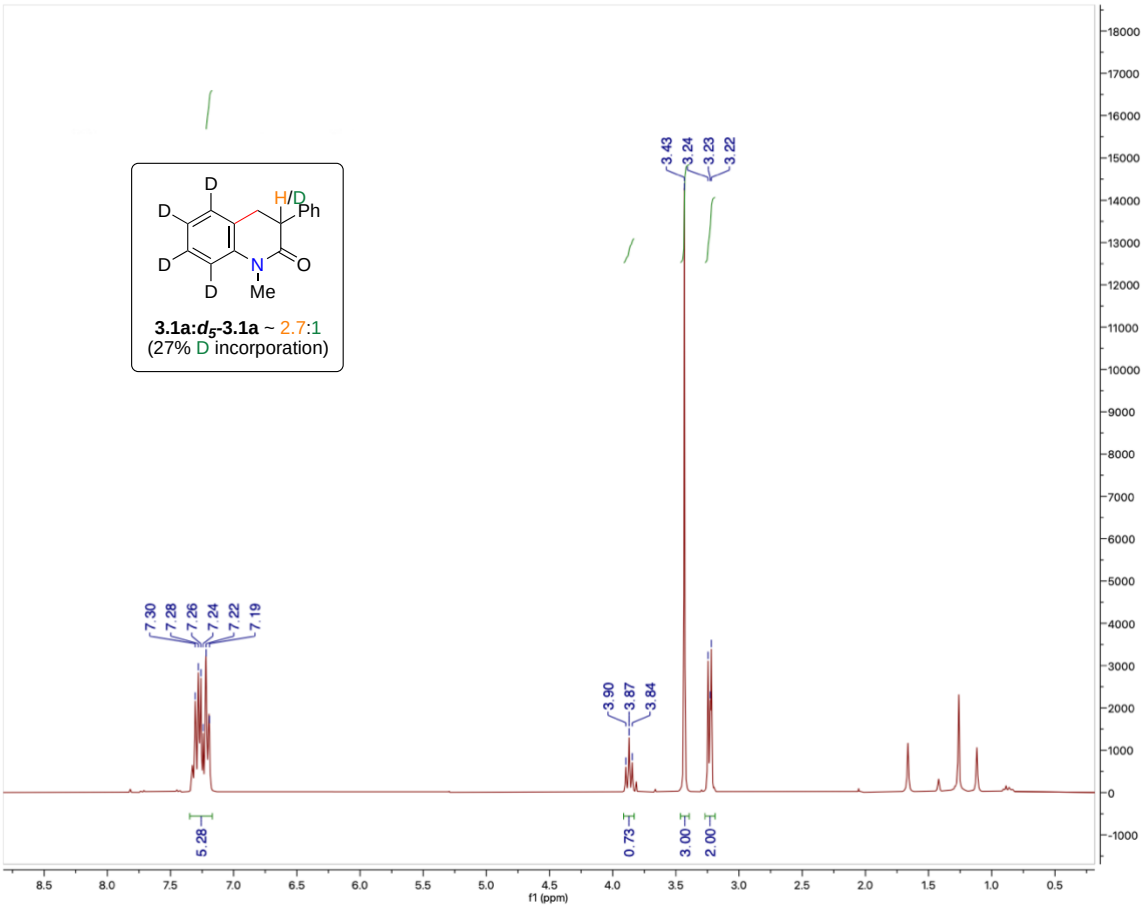

Figure 3.12: ^{1}H NMR spectrum of the crude reaction mixture of deuterium labeling experiment using Ir-photocatalyst.

When 2.2 equivalence of radical trapper TEMPO was added, no product was formed in both the **2-CTX** and **Ir-1** systems (Table 3.2). TEMPO is typically used as a radical scavenger to trap intermediate radicals and thus inhibit radical reactions. In the case of energy transfer, preferential quenching of the photosensitiser by a more efficient quencher (such as TEMPO), would similarly inhibit an EnT transformation. These results therefore support the proposed EnT.

Entry	Photocatalyst	Catalyst mol %	Solvent (M)	Yield (%)
23[a]	**2-CTX**	20%	TFE (0.05)	No rxn
24[a]	**Ir-1**	3%	TFE (0.05)	No rxn

Table 3.2: TEMPO radical trapping experiments. [a]With 2.2 equiv TEMPO.

Stern-Volmer quenching studies on both **2-TX** catalysts (**2-CTX** and **2-ITX**) as well as **Ir-1** using acrylamide **3.2a** as a quencher revealed a good linear relationship, consistent with efficient quenching of the photosensitisers, and supporting the energy transfer to the acrylamide (Figures 3.13–3.15).

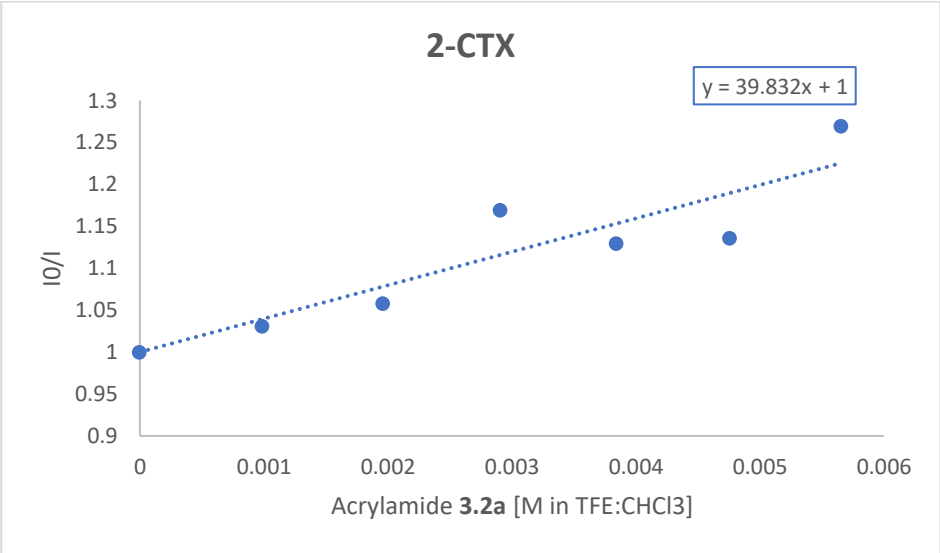

Figure 3.13: Stern-Volmer quenching studies using acrylamide **3.2a** as a quencher against **2-CTX.**

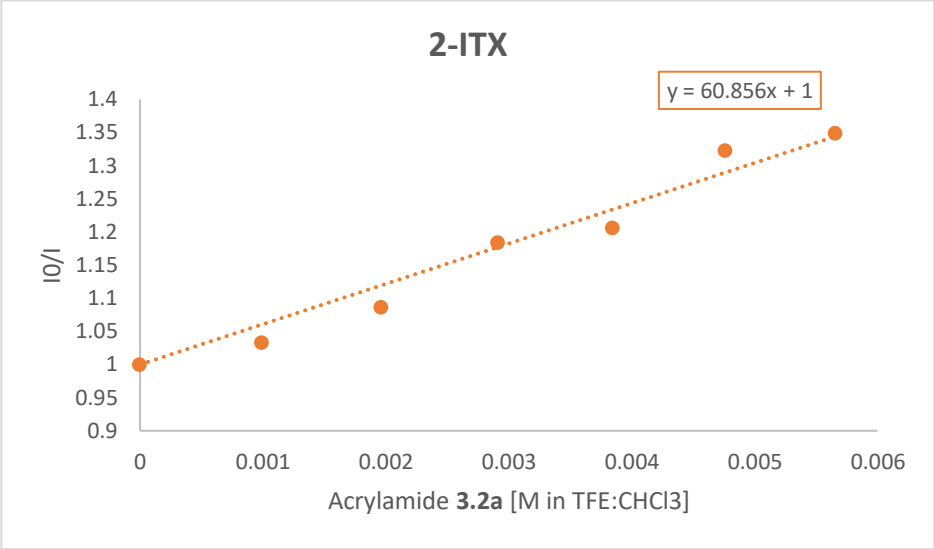

Figure 3.14: Stern-Volmer quenching studies using acrylamide **3.2a** as a quencher against **2-ITX**.

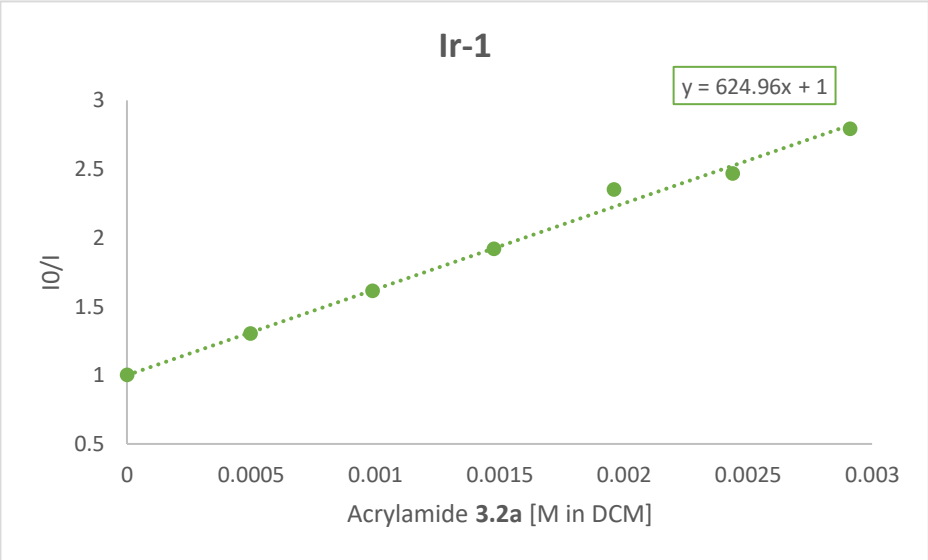

Figure 3.15: Stern-Volmer quenching studies using acrylamide **3.2a** as a quencher against **Ir-1**.

Similarly, TEMPO was also shown to be an effective quencher of the photosensitisers (Figures 3.16–3.17) and exhibited significantly faster quenching than the model acrylamide (**3.2a**) for both **2-CTX** (slope of 39.8x VS 108.09x) and **Ir-1** (slope 624.96x VS 5861.1x); consistent with our TEMPO experiments above.

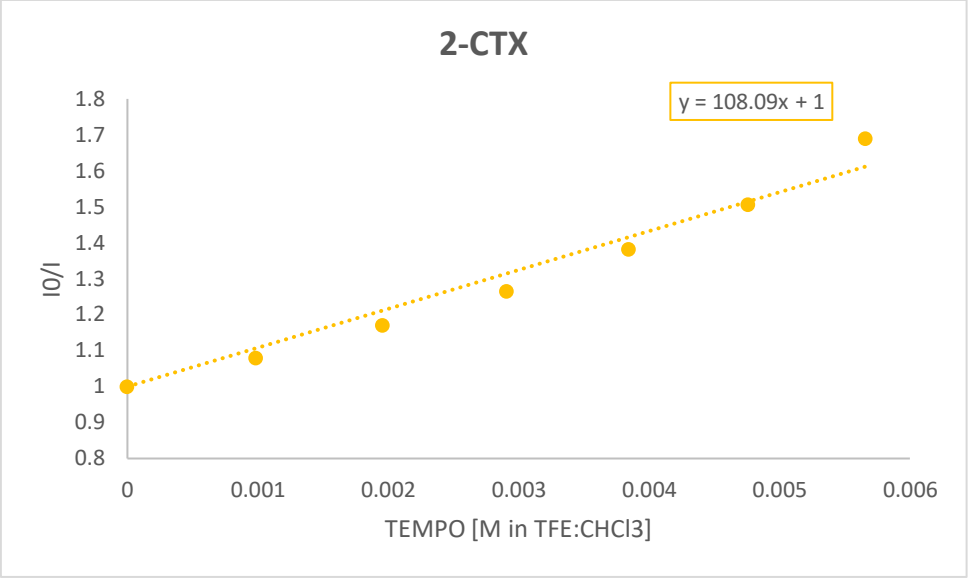

Figure 3.16: Stern-Volmer quenching studies using TEMPO as a quencher against **2-CTX**.

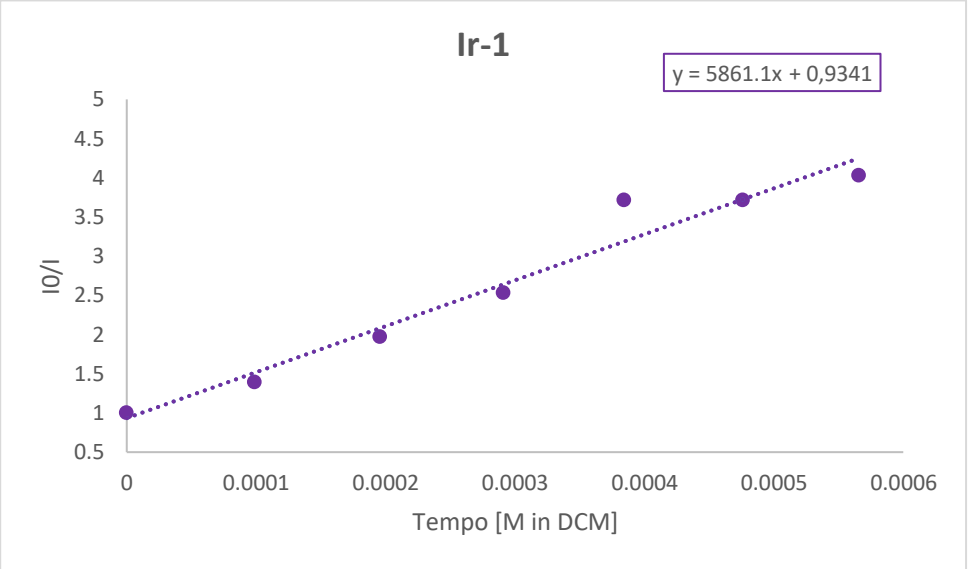

Figure 3.17: Stern-Volmer quenching studies using TEMPO as a quencher against **Ir-1**.

To gain further insight into the possible mechanistic pathway we performed DFT calculations on our model substrate **3.1a**. These calculations were performed by Dr William Unsworth, Ryan Epton and Jason Lynam from the University of York in the UK (unpublished at the time of thesis submission).

This data suggests that after triplet excitation of acrylamide **3.2a**, from the 2-substituted **TX** photocatalysts, cyclisation occurs via $\mathbf{TS_{AB}}$ (Figure 3.18). Intersystem crossing then occurs to the singlet surface, resulting in zwitterionic intermediate **D**. This latter intermediate might also provide insight to the observed non-perfect deuterium incorporation through a potential

step-wise keto/enol tautomerisation. The Gibbs energy of the minimum-energy crossing point (MECP) was calculated at −4 kJ mol^{-1} relative to **B**, suggesting that the MECP is barrierless. A 1,5-hydride migration can then occur through transition state **$TS_{D2'}$**, which would result in the final product. Experimentally, the reactions are typically performed over 24 hours, but the calculations don't account for the efficiency of the triplet excitation.

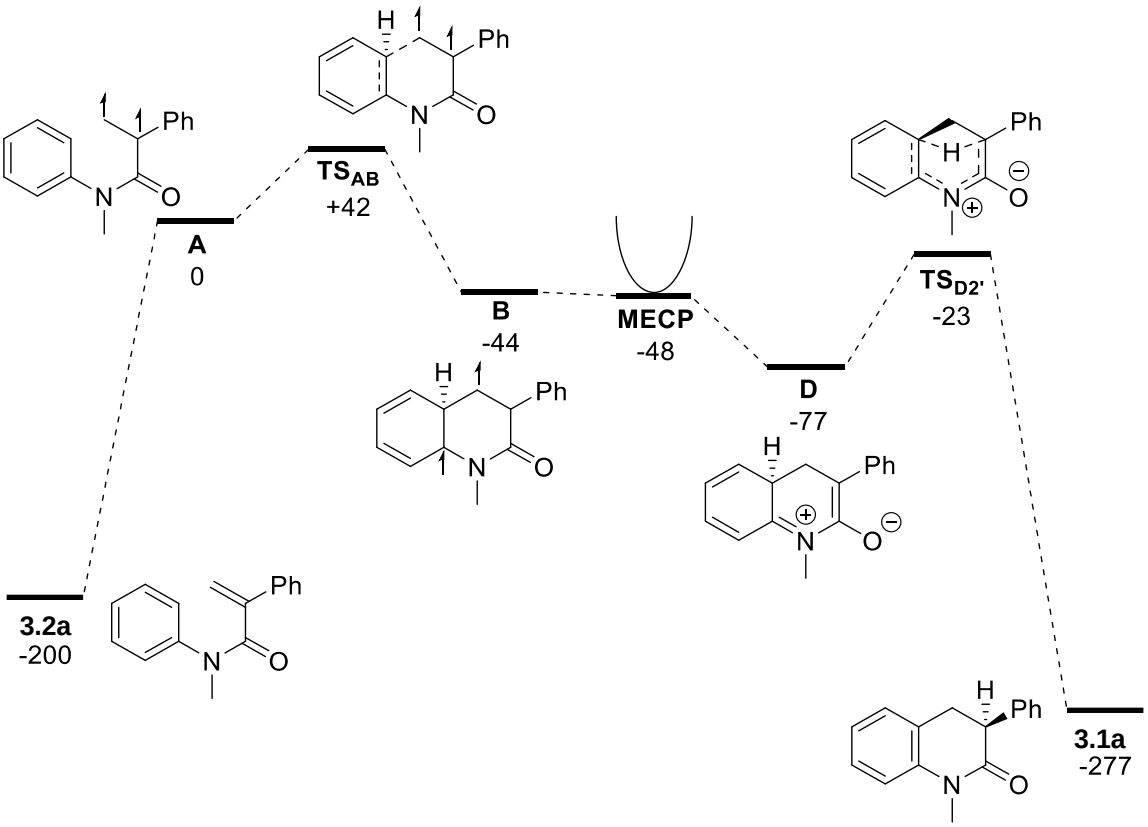

Figure 3.18: DFT studies showing the potential mechanistic pathways for 3,4-dihyroquinolinone **3.1a**. Energies are Gibbs free energies at 298.15 K in kJ mol^{-1} calculated at the D3(BJ)-UB3LYP/def2-TZVPP//UB3LYP/def2-SVP level of theory, with PCM solvent correction in 2,2,2-TFE. The MECP structure and energy was found using Orca, at the D3(BJ)-UB3LYP/G/def2-TZVPP//UB3LYP/G/def2-SVP level of theory, which was compared with Orca calculated energies of **B**.

3.3.5 Explorations in Enantioselective Dihydroquinolin-2-ones via EnT

The above photocyclisation reaction represents a novel, environmentally friendly approach to an array of 3,4-dihydroquinolin-2-one substrates. However, the products are isolated as a racemic mixture. Thus, we turned to investigate improving the stereoselectivity of this photocyclisation.

Traditionally, the stereoselectivity of such reactions can be improved in a number of ways; *1)* either by introducing a chiral co-catalyst; *2)* by attempting the reaction with a chiral thioxanthone photocatalyst (such as the one developed by Bach and coworkers [69]) or *3)* by introducing a chiral, bulky group to the acrylamide starting material in order to direct the photocyclisation stereoselectively.

The novel chiral thioxanthone catalyst first developed by Bach in 2014[69] was a milestone contribution to the field of enantioselective [2+2] cycloadditions (Scheme 3.14). The catalyst consists of a 1,3,5-trimethyl-3-azabicyclo[3.3.1]nonan-2-one moiety attached to a thioxanthone core via an oxazole ring. Hydrogen bonding between an amide group of a substrate and the chiral thioxanthone result in a stable complex which is shielded on one face, allowing the reaction to take place from the other face.

Bach (2014): Enantioselective [2+2] Cycloaddition

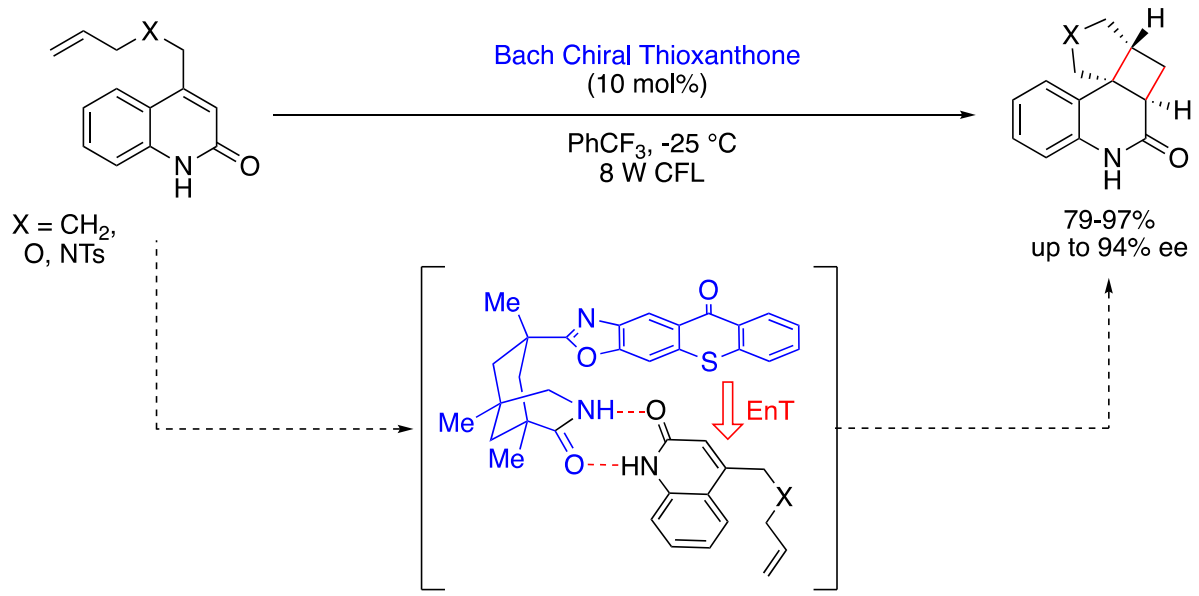

Scheme 3.14: EnT catalysis for enantioselective [2+2] photocycloaddition using a chiral thioxanthone photosensitiser.

Although this catalyst seemed promising as a suitable chiral photosensitiser for our system, the process to synthesise this catalyst includes numerous synthetic steps, as well as a preparative HPLC separation of enantiomers. Additionally, the synthesis starts with Kemp's triacid, which is commercially available, however extremely expensive. Sigma Aldrich quotes

1 gram of Kemp's triacid at ~R14 000 (local currency).[174] Furthermore, since our system required *N*-protection, we reasoned that the Bach thioxanthone would nonetheless be ineffective as our system lacked the key hydrogen bond required for association with the sensitizer. Considering this, we opted to explore a non-covalent chiral co-catalyst approach instead.

When considering a suitable chiral co-catalyst we needed to consider a number of factors; namely a suitable coordination site for the acrylamide such as an amide or thiourea group which facilitates hydrogen bonding and a chiral ligand group that is able to shield one face of the acrylamide in order to direct the photocyclisation on the other face in a similar manner to Bach's chiral catalyst. Admittedly, we were acutely aware that the lack of an N-H hydrogen bond would disadvantage any co-catalyst association. We attempted the cyclisation using the optimised conditions on the standard acrylamide with the addition of a chiral co-catalyst (Table 3.3). The crude reaction mixture was analysed by chiral HPLC in order to determine the enantiomeric excess.

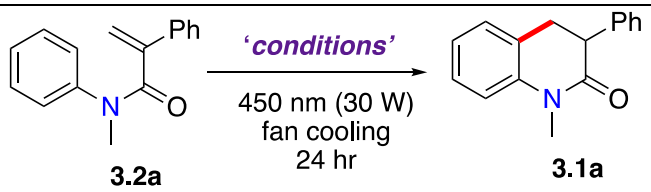

3.2a **3.1a**

Entry	Catalyst (mol %)	Co-catalyst (mol %)	Solvent (M)	ee (%)
1	**2-CTX** (10%)	Jacobsen Organic Thiourea (10%)	EtOH (0.05)	0%
2	**2-CTX** (10%)	Cinchona Thiourea (10%)	EtOH (0.05)	13%
3	**2-CTX** (10%)	R-Trip (10%)	EtOH (0.05)	0%
4	**2-CTX** (10%)	Cinchona Amide (10%)	EtOH (0.05)	2%
5	**2-CTX** (10%)	Cinchona Thiourea (30%)	EtOH (0.05)	14%

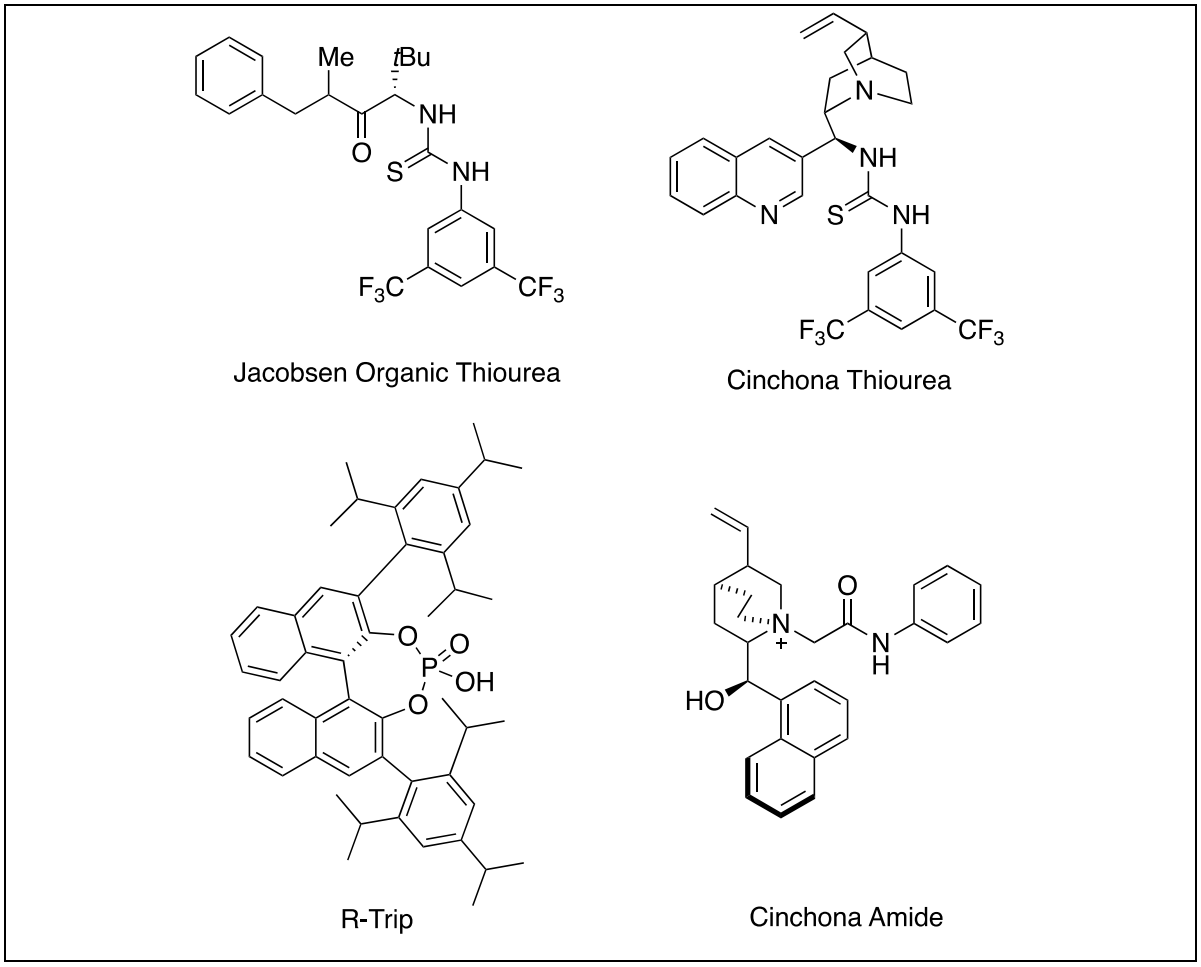

Table 3.3: Optimisation table for stereoselective photocyclisation using a chiral co-catalyst.

When adding 10 mol% of Jacobsen organic thiourea catalyst or R-Trip catalyst, no change in ee was seen (entries 1&3). Additionally, negligible increase was observed when using a cinchona amide catalyst (entry 10). Pleasingly, a small increase in *ee* was seen when using a cinchona thiourea co-catalyst in 10 mol%, albeit only 13% *ee.* This result was presumably due to the coordination abilities of the thiourea group with the acrylamide starting material and the presence of a bulky chiral group in the form of a cinchona group to shield one face of the acrylamide.

Although these results are far from desirable and more work is needed to fully optimize the *ee* of the reaction, these preliminary findings encourage that the stereoselectivity of the photocyclisation can be controlled using a chiral non-covalent co-catalyst.

3.4 Application Toward Quinolin-2-ones

To demonstrate further synthetic utility, we investigated an efficient conversion from 3,4-dihydroquinolin-2-ones to quinoline-2-ones (quinolone). In the past century a variety of quinolone compounds have been extensively studied, several of which possess medicinally interesting properties and have served in the development of many synthetic drugs.[175] More specifically, 2-quinolones represent a privileged molecular scaffold that appears in a number of biologically important natural products and pharmaceuticals (Figure 3.19). For example rebamipide is an antiulcer agent and repirinast has antihistamine properties useful in the treatment of allergic asthma.[176] While screening compounds for potential cancer chemopreventive properties, casimiroine, isolated from the seeds of Casimiroa edulis, was found to have antimutagenic activity.[177]

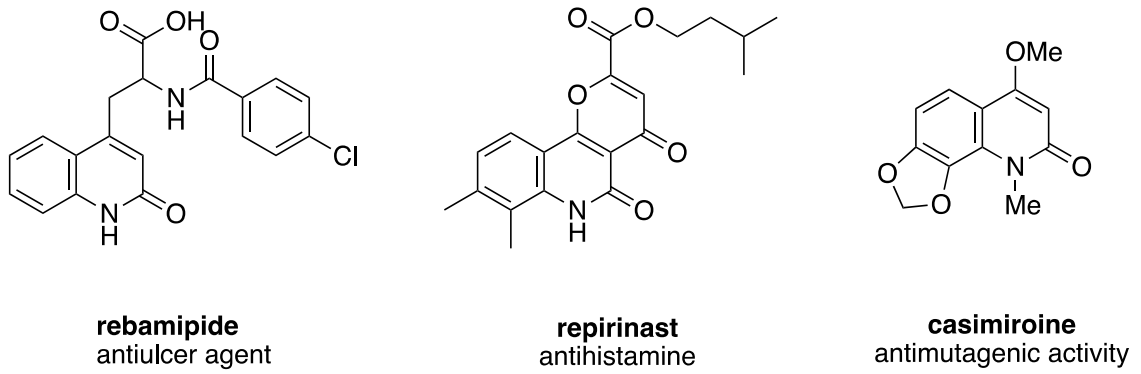

Figure 3.19: Selection of biologically important pharmaceuticals and natural products.

There have been a number of reports describing the synthesis of 2-quinolones.[178] Early synthetic efforts consists mostly of variations on Friedländer and Knorr reactions.

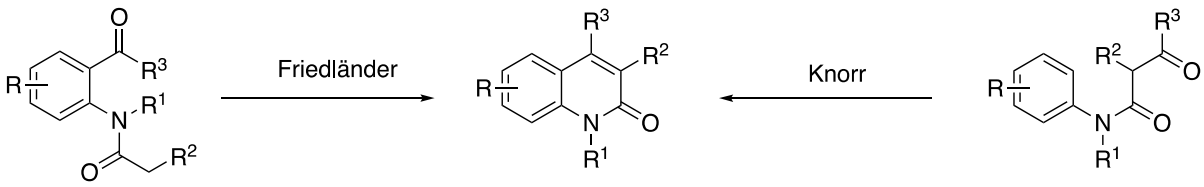

Scheme 3.15: Early synthetic approaches to 2-quinolones.

Recent advances in new bond-forming reactions led to unconventional approaches for 2-quinolone synthesis. However, most of these approaches involve palladium or other rare

transition metals. Some representative examples of metal-free approaches are described below (Scheme 3.16).[179–181]

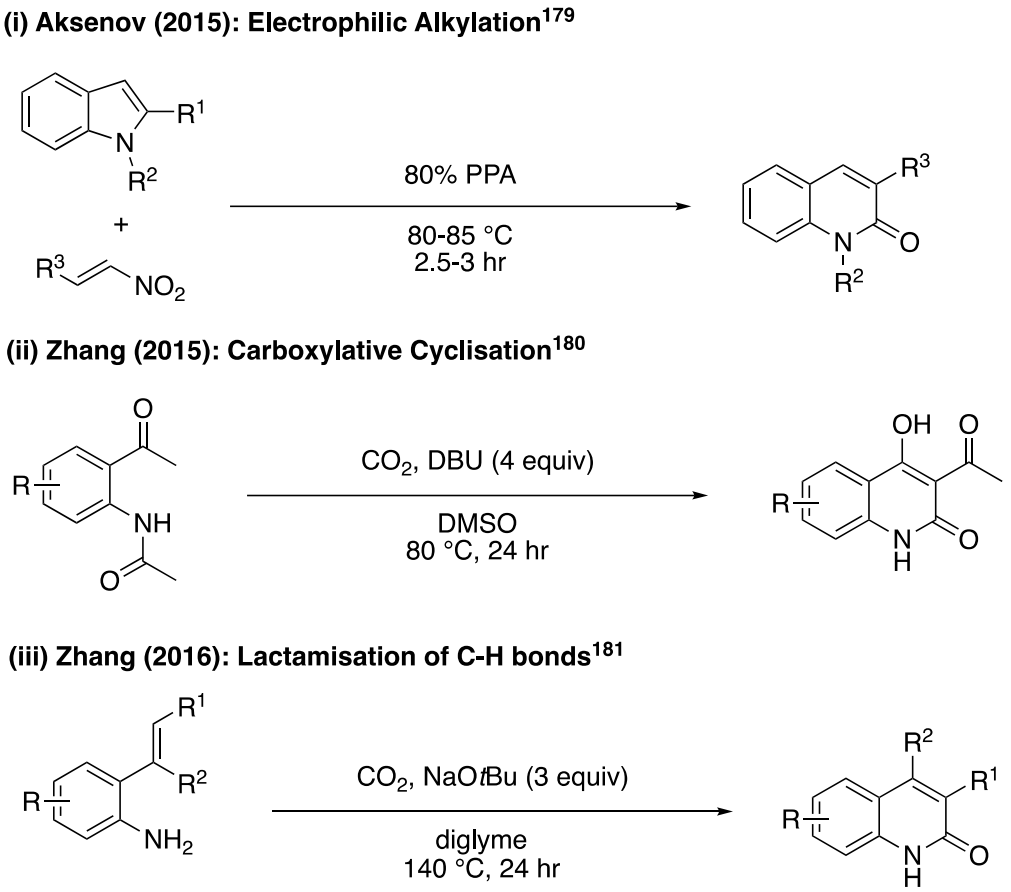

Scheme 3.16: (i) Metal-free approach to 3-substituted 2-quinolones using polyphosphoric acid (PPA). (ii) Metal-free approach to 3-acetyl-4-methoxy-2-quinolones using DBU. (iii) Metal-free approach to 2-quinolones using NaO*t*Bu as a base.

Although the above reactions all have moderate to good yields and decent reaction scope, they all still utilize high reaction temperatures.

With a novel photocatalytic approach to 3,4-dihydroquinolin-2-ones in hand, we set out to investigate dehydrogenation approaches to access these important 2-quinolones. Recently, there have been a number of α,β-dehydrogenation reports, particularly with application to 2-quinolinones (Scheme 3.17).[159,182–184]

(i) Newhouse (2016): Palladium-Catalysed a,b-**Dehydrogenation**[182]

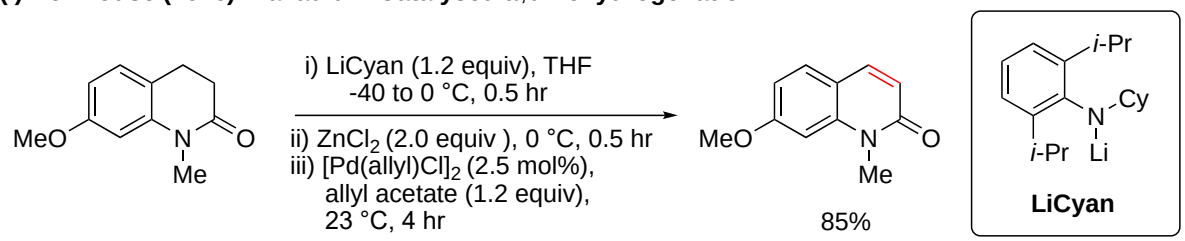

(ii) Li (2020): Base-Mediated Oxidation[159]

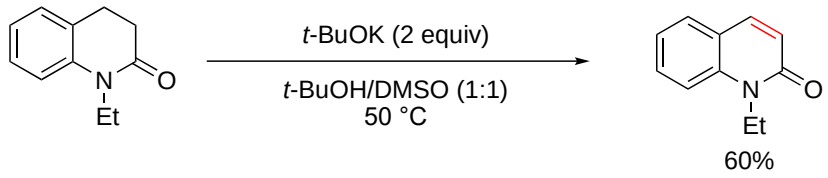

(iii) Kang (2021): Iron-Catalysed a,**β-Dehydrogenation**[183]

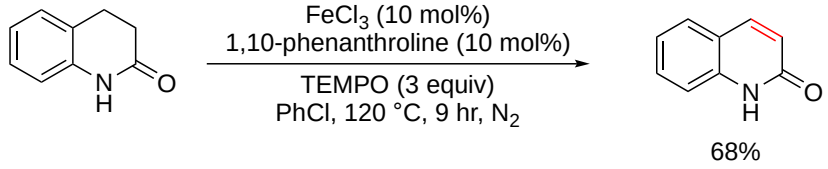

(iv) Huang (2021): Dual Photoredox/Cobalt Dehydrogenation[184]

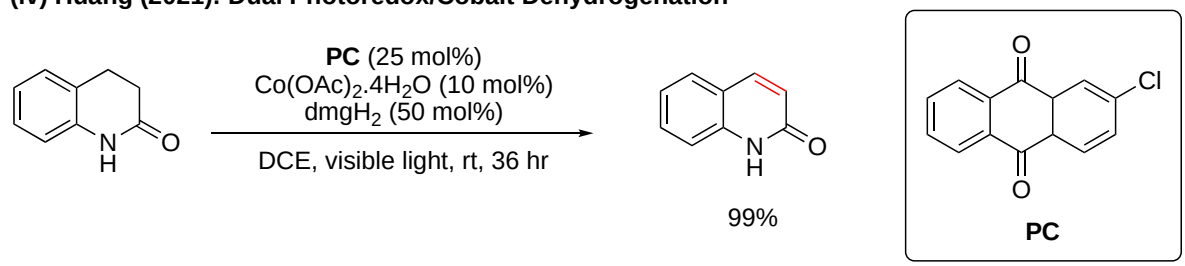

Scheme 3.17: (i) Allyl-palladium catalysed approach for the synthesis of 7-methoxyl-1-methyl-3,4-dihydroquinolin-2-one. (ii) Oxidation of a 3,4-dihydroquinolin-2-one derivative using *t*-BuOK for the formation of 1-ethyl-3,4-dihydroquinolin-2-one. (iii) Iron-catalyzed oxidation of 3,4-dihydroquinolin-2-one for the formation 2-quinolone. (iv) Visible light mediated photocatalytic approach to the oxidation of 3,4-dihydroquinolin-2-one to 2-quinolone.

All of the above approaches to the oxidation of 3,4-dihydroquinolin-2-ones require either harsh reaction conditions or multiple catalysts and additives. We set out to develop a simpler oxidation approach to access these important 2-quinolones from our 3,4-dihydroquinolin-2-ones.

In 2020, Zhang and co-workers[182] reported a copper-catalysed radical *N*-demethylation of amides using *N*-fluorobenzenesulfonimide (NFSI) as an oxidant. The authors proposed the

amide first undergoes an oxidative SET with $Cu(acac)_2$ to reduce Cu^{2+} to Cu^{+}. NFSI is consequently reduced by Cu^{+} resulting in the cleavage of N-F bond to give a nitrogen radical which can undergo a HAT with the amide radical to furnish an iminium cation (Scheme 3.18). This iminium cation is subjected to nucleophilic attack by water, followed by proton transfer, cleavage of C-N bond and additional proton transfer to finally furnish the desired product.

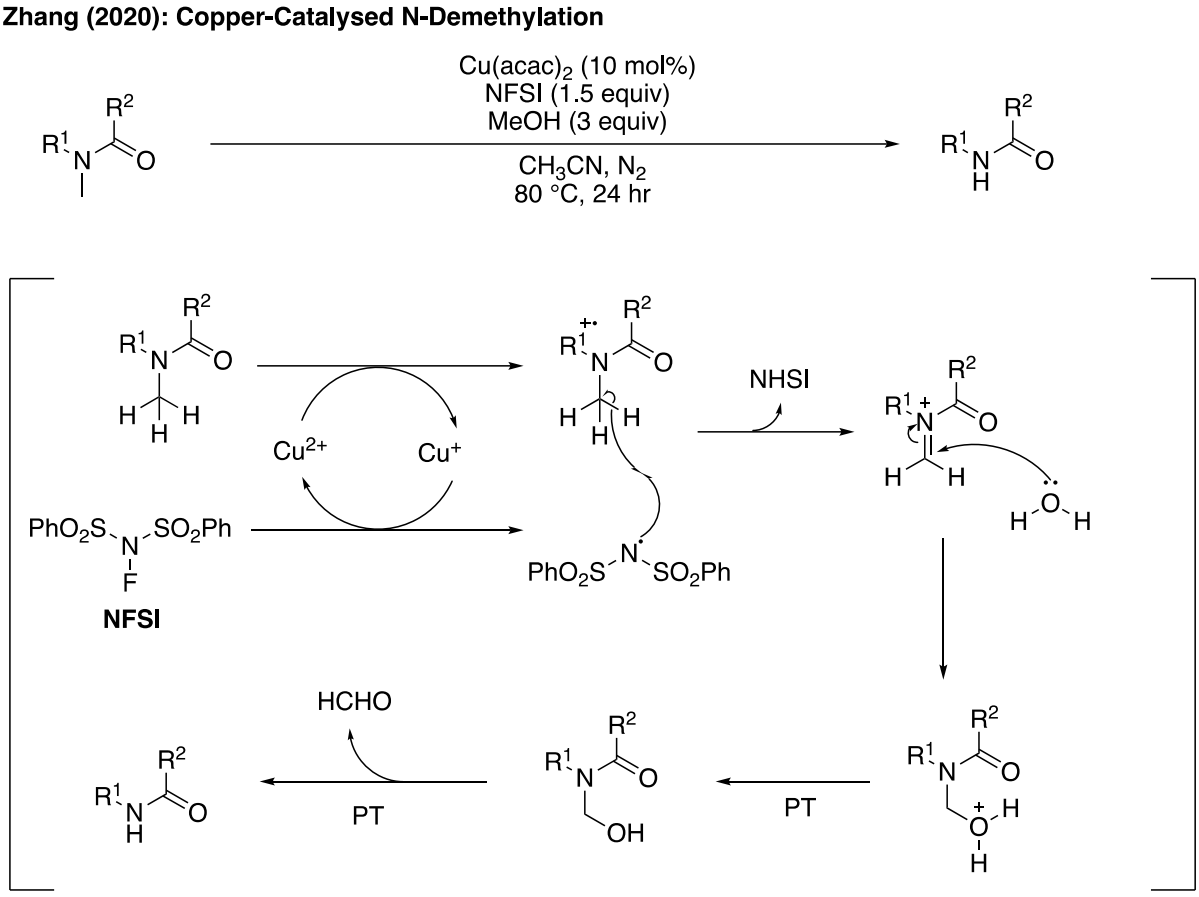

Scheme 3.18: N-demethylation approach using a copper catalyst and NFSI and proposed mechanism.

Inspired by this report, we hypothesized that with our 3,4-dihydroquinolin-2-one core, the HAT would occur preferentially at the benzylic carbon instead of the *N*-methyl carbon, being the most stabilised option (Figure 3.20), and ultimately facilitate double bond formation to produce a quinolin-2-one (vide infra, Scheme 3.24). Abstraction of an *N*-methyl proton would result in a primary radical **A** which is the least stable alkyl radical. Abstraction from a benzylic carbon is the most stabilised as it can undergo resonance stabilisation with the aromatic group. Radicals **B** and **C** are both alpha to an aromatic ring but **C** is a tertiary radical and

therefore more stabilised. Additionally, the tertiary radical **C** is adjacent to the electron-withdrawing carbonyl group which could aid with stabilisation.

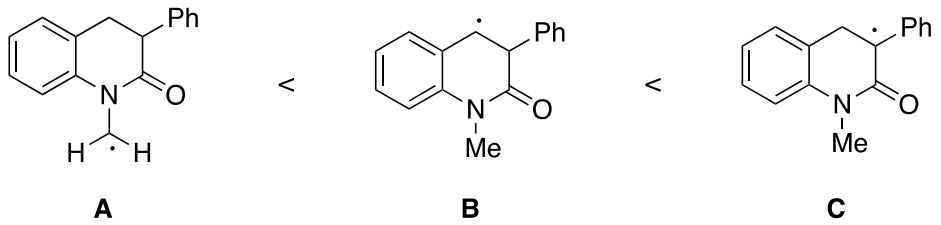

Figure 3.20: Comparison of different 1-methyl-3-phenyl-3,4-dihydroquinolin-2(1*H*)-one radical stabilities.

Accordingly, we envisaged that following the reductive formation of the *N*-centered radical (**3.4)** from NFSI, hydrogen atom abstraction would produce benzylic radical (**3.1a(i)**). Oxidation by the Cu^{2+} — resulting in catalyst turnover — would give rise to cation (**3.1a(ii)**), which would afford the quinolin-2-one following loss of a proton (Scheme 3.19).

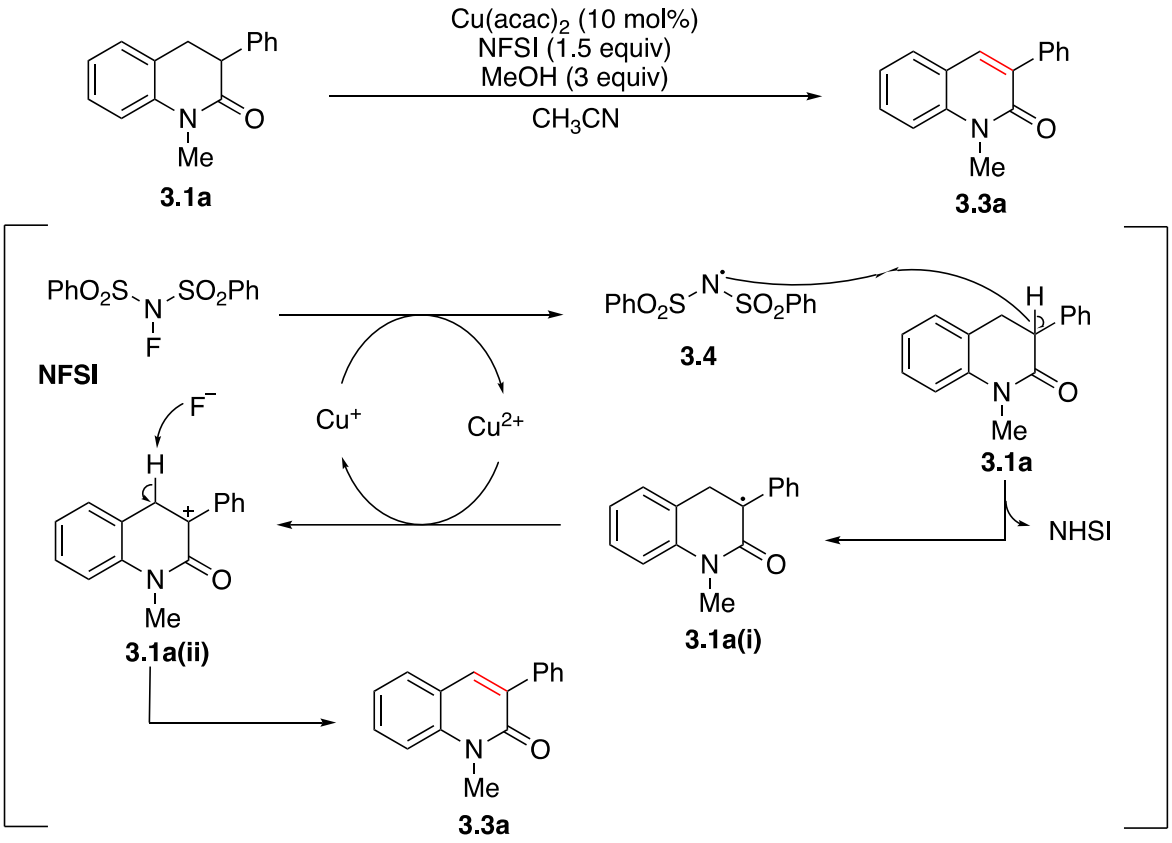

Scheme 3.19: Our proposed mechanism for N-demethylation approach using a copper catalyst and NFSI and proposed mechanism.

After performing the reaction with the same conditions described by Zhang and co-workers,[182] we were pleased to isolate the product **3.3a** in 90% yield. This was confirmed with ^{1}H NMR (Figure 3.21). Due to the extended pi system, the triplet and doublet at the region of 3.00–4.50 ppm (H_a and H_b) are no longer present. Instead, the aromatic proton region now integrates for 10 protons.

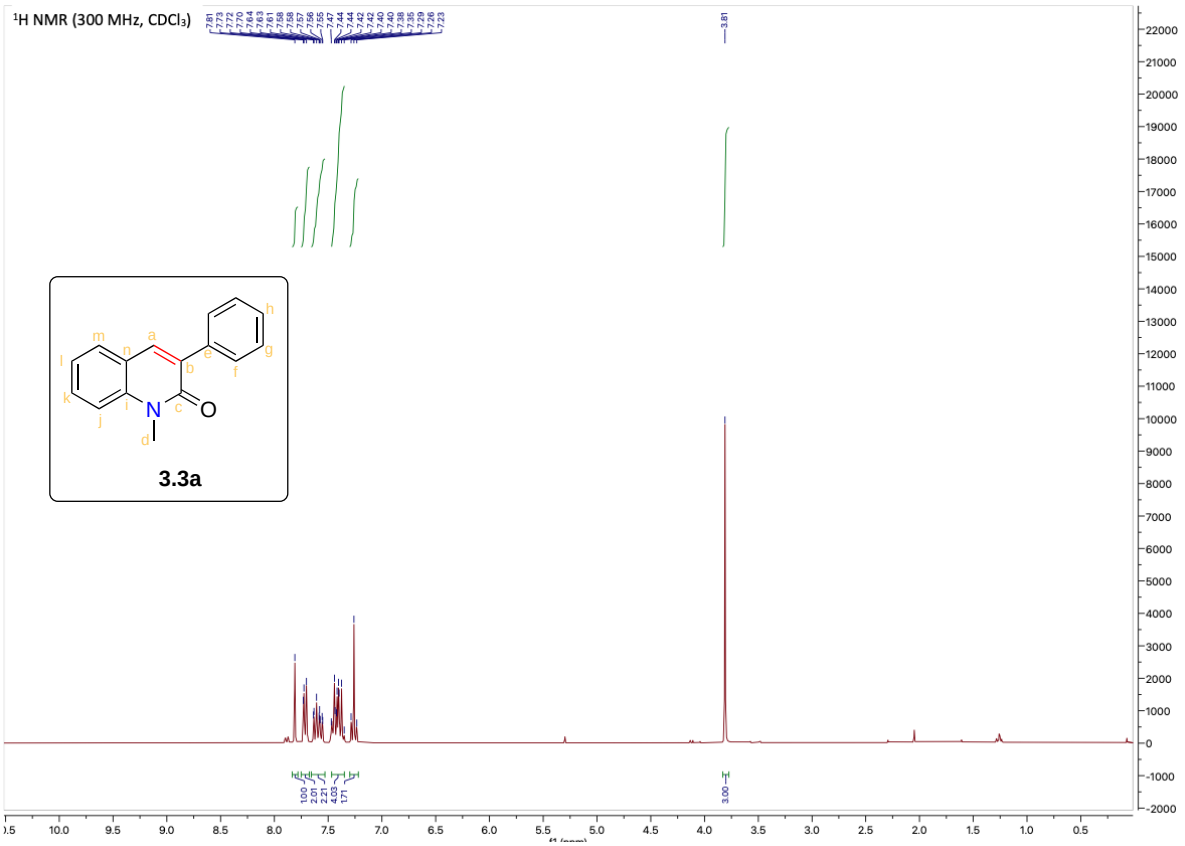

Figure 3.21: ^{1}H NMR spectrum of **3.3a**.

Satisfied we had a working reaction in place, and once again aligned with aiming to develop more sustainable reactions, we turned our attention to developing a photocatalytic variant that would circumvent the heating requirement (Table 3.4). We hypothesized that a suitable reducing photocatalyst would similarly be able to generate the key *N*-radical (**3.4**), and therefore achieve the envisaged dehydrogenation.

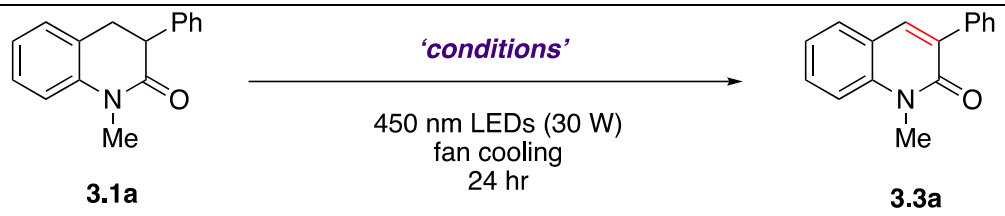

3.1a **3.3a**

Entry	Catalyst	Catalyst mol %	Oxidant (equiv)	Solvent (M)	Yield (%)[a]
1[b]	$Cu(acac)_2$	10%	NFSI (1.5)	MeCN (0.25)	90%[c]
2	**Ir-1**	5%	NFSI (1.5)	MeCN (0.25)	54%
3	$[Cu(dap)_2Cl]$	1%	NFSI (1.5)	MeCN (0.25)	97%
4	$[Cu(dmp)_2Cl]Cl$	1%	NFSI (1.5)	MeCN (0.25)	73%
5	$[Cu(dmp)_2Cl]Cl$	2%	NFSI (1.5)	MeCN (0.17)	99%
6	$[Cu(dmp)_2Cl]Cl$	2%	NFSI (1.5)	THF (0.17)	49%
7	$[Cu(dmp)_2Cl]Cl$	2%	NFSI (1.5)	DCM (0.17)	70%
8	$[Cu(dmp)_2Cl]Cl$	2%	NFSI (1.5)	PhMe (0.17)	17%
9	$[Cu(dmp)_2Cl]Cl$	2%	NFSI (1.5)	EtOH (0.17)	33%
10[d]	$[Cu(dap)_2Cl]$	5%	NFSI (1.5)	MeCN (0.05)	No rxn
11	none	-	NFSI (1.5)	MeCN (0.05)	No rxn
12[e]	none	-	NFSI (1.5)	MeCN (0.05)	65%

Table 3.4: Optimisation table for dehydrogenation of 3,4-dihydroquinolin-2-ones. [a]Determined by ^{1}H NMR against internal standard (methyl 3,5-dinitrobenzoate). [b]Refluxed at 80 °C with no light. [c]Isolated yield. [d]No light. [e]No fan cooling

Preliminary studies with **Ir-1** (as above) using a 450 nm irradiation showed the desired product was forming, albeit in moderate yield of 54% (entry 2). We next focused on varying the catalyst type, loading amount and solvent in order to identify the optimised reaction conditions. Using $[Cu(dap)_2Cl]$ and the cheaper $[Cu(dmp)_2Cl]Cl$ both produced excellent yields at 1 mol% catalyst loading, producing **3a** in 97% and 73% yield, respectively (entries 3 and 4). This was particularly exciting as the most widely utilised photocatalysts are metal complexes based on rare and expensive ruthenium or iridium, while copper is relatively inexpensive and earth abundant. Doubling the catalyst loading of $[Cu(dmp)_2Cl]Cl$ (to 2 mol%) afforded **3a** in 99% yield (entry 5). We next investigated the effect of solvent, but no improvements over MeCN was observed (entries 6–9). To complete the optimisation, control experiments were conducted. No reaction was observed when performing the reaction in the dark (entry 10).

Similarly, no reaction was seen in the absence of a catalyst (entry 11). Interestingly, a 65% yield for **3a** was observed when no catalyst was added but the reaction was irradiated without fan cooling (entry 12). However we know the reaction proceeds under reflux conditions (approx. 80 °C for acetonitrile) and thermometer readings revealed that the photoreactor can reach temperatures of 45 °C without fan cooling. Consistent with entry 1, this result was not too surprising.

In an attempt to get the general sense of this reaction scope, a selected set of unsubstituted and substituted 3,4-dihydroquinolin-2-ones were subjected to the optimised thermal reaction conditions (Figure 3.22).

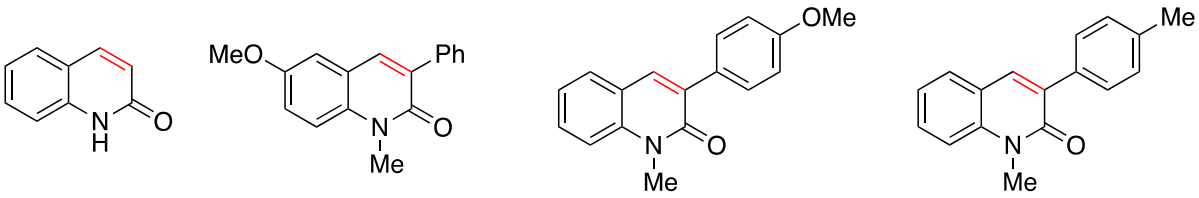

3.3x
54%

3.3c
78%

3.3p
53%

3.3q
88%

Figure 3.22: Expanding the substrate scope of the dehydrogenation reaction.

Firstly, we wanted to show this oxidation could provide facile access to quinolin-2-one, starting from commercially available 3,4-dihydroquinolin-2-one. Pleasingly, product **3.3x** was isolated in 54% yield. The electron withdrawing methoxy substituent produced **3.3c** in 78% yield. Varying the substituent on the phenyl ring with methoxy and methyl groups were also well tolerated, giving **3.3p** and **3.3q** in 53% and 88% yield, respectively.

Holding fast to our vision for reaction developments in photocatalysis, we once again wanted to investigate potential metal-free catalytic approaches for this dehydrogenation reaction (Table 3.5).

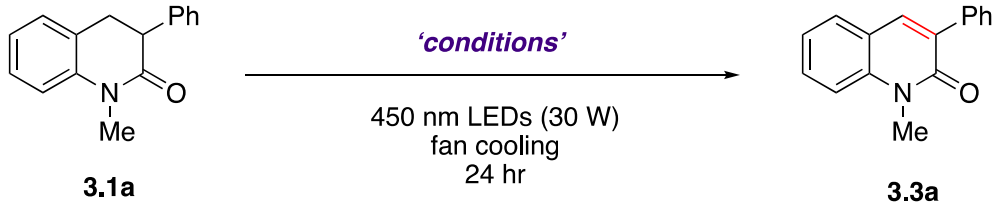

3.1a 3.3a

Entry	Catalyst	Catalyst mol %	Oxidant (equiv)	Solvent (M)	Yield (%)[a]
1	4-CzIPN	3%	NFSI (1.5)	MeCN (0.17)	15%
2	**2-CTX**	20%	NFSI (1.5)	MeCN (0.17)	61%
3	**2-CTX**	20%	NFSI (1.5)	TFE:$CHCl_3$ (0.17)	98%
4	**2-CTX**	20%	NFSI (1.5)	EtOH (0.17)	75%
5	**2-CTX**	20%	NFSI (1.5)	PhMe (0.17)	41%
6	**2-CTX**	10%	NFSI (1.5)	TFE:$CHCl_3$ (0.17)	79%

Table 3.5: Continued optimisation table for metal-free dehydrogenation of 3,4-dihydroquinolin-2-ones. [a]Determined by ^{1}H NMR against internal standard (methyl 3,5-dinitrobenzoate)

The cyanoarene catalyst, **4-CzIPN**, produced **3a** in a modest 15% yield (entry 1). Pleasingly replacing [Cu(dmp)$_2$Cl]Cl with **2-CTX** produced 61% yield according to ^{1}H NMR. Motivated by this result, we investigated different solvents and found near-perfect conversion with TFE:$CHCl_3$ (entry 17), which was unsurprising considering the solvent effects described above. Ethanol and toluene were also investigated but gave 75% and 41% yield, respectively. Finally, lowering the catalyst loading to 10 mol% also lowered the yield to 79% yield.

At this point, the project was handed over to another MSc student, Chipo Magura. The full details of this reaction are beyond the scope of this thesis and will be reported separately.

3.5 Conclusion and Future Work

A successful synthesis for the visible-light mediated metal-free photocatalytic approach to 3,4-dihydroquinolin-2-ones starting from simple *N*-acrylamides is reported. This photocyclisation was performed using the organic class of thioxanthone catalysts which are cheap and readily available. Optimisation studies were performed and identified that 20 mol% **2-CTX** was the optimal catalyst which produced the standard substrate **3.1a** in 95% yield

when irradiated at 450 nm in 2,2,2-TFE:$CHCl_3$ for 24hrs. A total of 22 different substrates were synthesised ranging from yields of 25% to 97%. A number of mechanistic studies including TEMPO radical trapping and fluorescence studies were performed in order to identify the most probable mechanistic pathway. It was determined that the reaction proceeds via a triplet energy transfer to promote a rare example of a metal-free formal C(sp^2)–H/C(sp^3)–H arylation mediated by visible-light.

To demonstrate further synthetic utility, the reaction was performed on a gram scale and the catalysts was recovered and performed on a 2nd gram scale synthesis of a different substrate. Both gram scale reactions produced yields comparable with their lab scale experiments, indicating the ability of this reaction to be scaled up for chemical processes.

Additionally, a novel method for the synthesis of 2-quinolones was reported using a metal-free visible-light mediated photocatalytic dehydrogenation of 3,4-dihydroquinolin-2-ones and this is currently being extended to pursuing a formal Fujiwara-Moritani reaction in the Petersen research group via a two-step, one-pot thioxanthone photocatalysis process (Scheme 3.20).

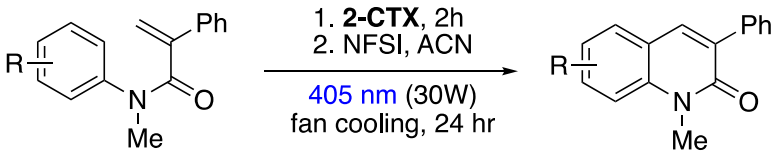

Scheme 3.20: Metal-free one-pot Fujiwara-Moritani transformation using thioxanthone photocatalysis.

Future work in this area will focus on improving the enantioselectivity of the photocyclisation reaction. Preliminary studies showed a slight increase in *ee* when a chiral co-catalyst was added to the reaction. More research is needed to identify a more effective cocatalyst or a potential chiral thioxanthone photocatalyst.

NOTE: Shortly after this work was published, we obtained a 405 nm LED and any future work with the class of thioxanthone photosensitiser was performed with this more optimal wavelength (closer to the absorption maximum of the photosensitiser).

4. Chapter 4 - Thioxanthone Catalysed Triplet Energy Transfer for the Synthesis of β-Lactams

This work was published in Angewandte Chemie (*Angew. Chem. Int. Ed.,* **2022**, 61, e202213086) titled "Visible-Light-Mediated Energy Transfer Enables the Synthesis of β-Lactams via Intramolecular Hydrogen Atom Transfer".[183]

4.1 Background

β-lactams, more formally known as 2-azetidinones, are amongst the most important compound classes in medicinal and biological chemistry.[184,185] The reactive 4-membered β-lactam ring is essential to the bactericidal activity of a large majority of antibiotics, most notably in frontline penicillin antibiotics. β-Lactam derivatives are currently the most widely used antibacterial agents, representing more than half of the antibiotics used worldwide today.[186,187] β-Lactams are divided into several distinct subclasses according to their structure (Figure 4.1). The subclasses of penicillin, cephalosporin, and carbapenem are commonly used for the treatment of a wide range of bacterial infections.

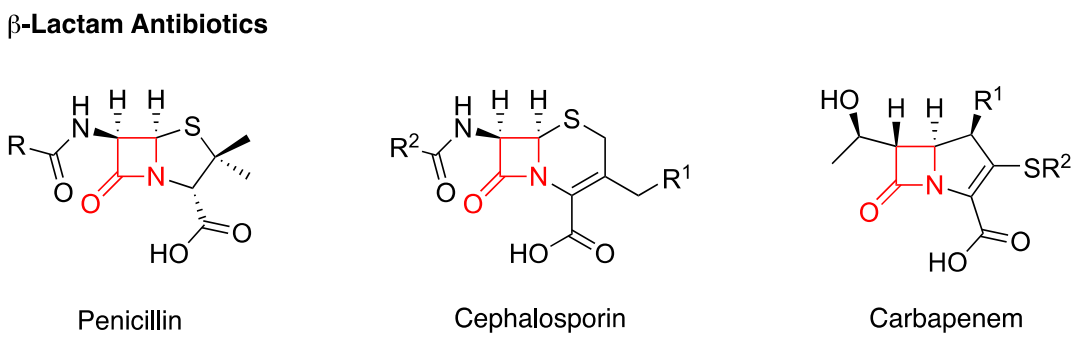

Figure 4.1: Examples of β-lactam antibiotics used for the treatment of bacterial infections.

Until the early 90's, most research into β-lactams was focused on their antibacterial properties, however β-lactam derivatives have also been shown to have diverse pharmacological activities. Some β-lactam derivatives have been shown to possess, among others, anticancer activity, cholesterol absorption inhibitory activity, antidiabetic, anti-inflammatory and anti-HIV activity.[185,188] For example, 1,4-diaryl-2-azetidinone (Figure 4.2)

has shown promising results for antiproliferative activity in HT-29 colon cancer cells,[189] while ezetimibe is used to treat high blood cholesterol and certain other lipid abnormalities.[190] Thus, the versatility of β-lactam compounds in medicinal chemistry makes them a valuable tools for drug discovery across a broad range of therapeutic applications.

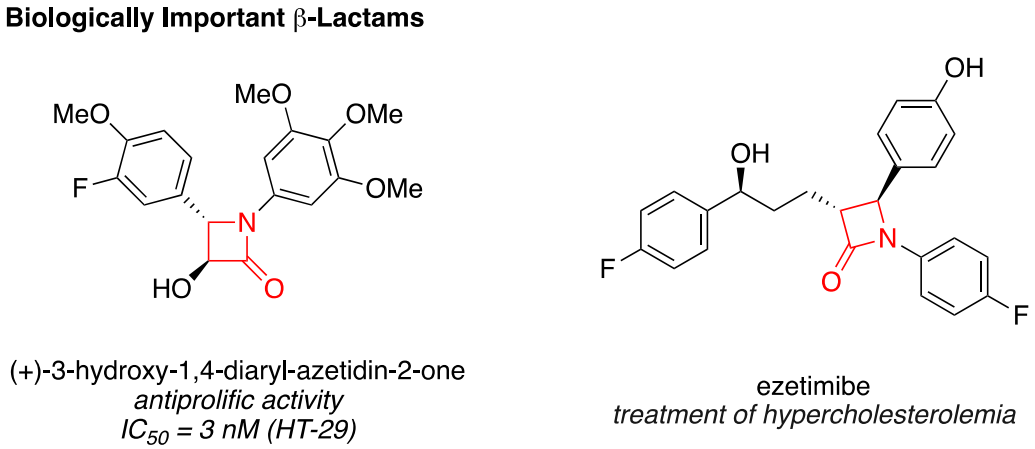

Figure 4.2: Examples of 1,4-Diaryl-2-azetidinone analogues with pharmacological activities.

Additionally, reduction of the lactam carbonyl group also enables the conversion from β-lactams into azetidines, another privileged scaffold with broad utility in medicinal chemistry (Figure 4.3). Derivatives of azetidine have been reported to show antibacterial, anticancer, antifungal, antidiabetic, anti-obesity, analgesic, antimalarial, and antioxidant activities.[191] Some examples of FDA-approved azetidine-based drugs include tebanicline,[192] a potent nicotinic (non-opioid) analgesic drug and azelnidipine,[193] a calcium channel blocker that is used for the treatment of hypertension. BRD9185 is an azetidine-2-carbonitrile derivative which has been shown to have activity against multidrug-resistant malaria.[194] Natural product azetidomonamide A is an azetidine-containing heterobicyclic scaffold, which is relevant in biofilm formation in the Pseudomonas aeruginosa pathogen.[195,196]

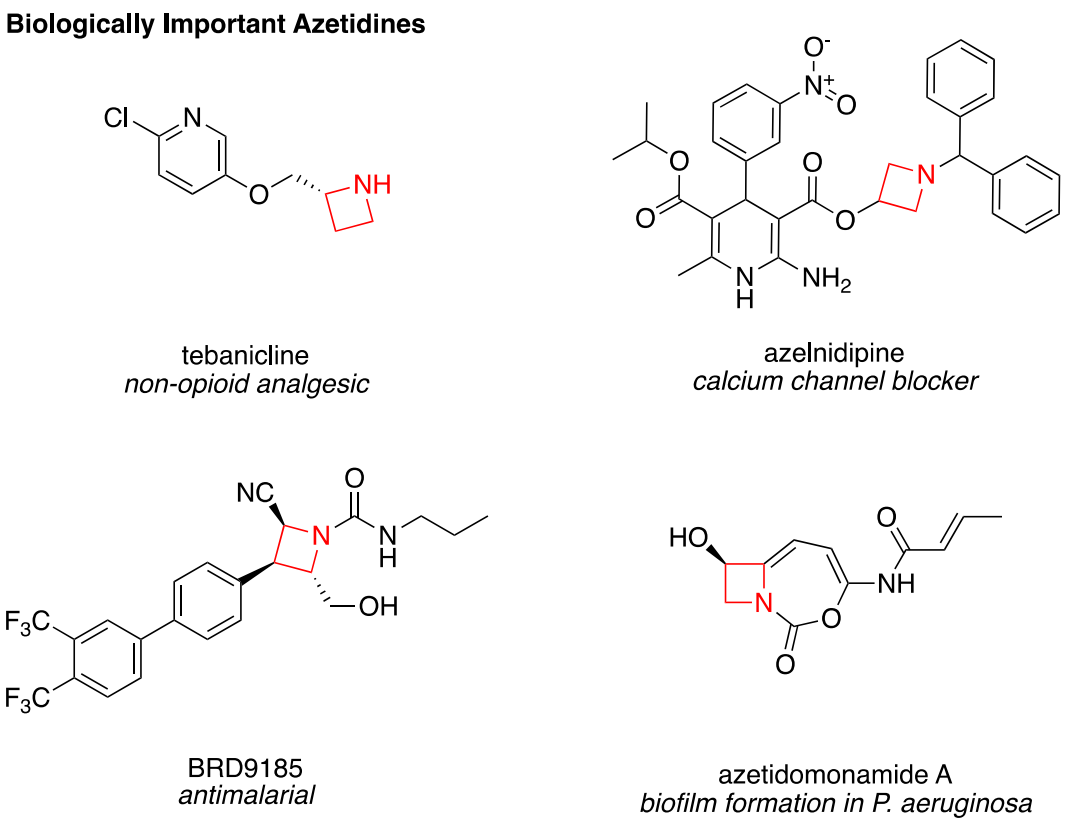

Figure 4.3: Examples of azetidine analogues with biological importance.

Considering this utility, numerous strategies for the formation of β-lactams have been investigated in previous years (Scheme 4.1).[197,198] Traditional methods for β-lactam synthesis usually involve the Staudinger reaction,[198] a stepwise [2+2] cycloaddition reaction between an imine and a ketene (Scheme 4.1(i)), as well as the Kinugasa reaction[199] which involves the dipolar cycloaddition of nitrones and alkynes (Scheme 4.1(ii)). [17]

(i) Staudinger (1907): 2+2 cycloaddition between imine and ketene

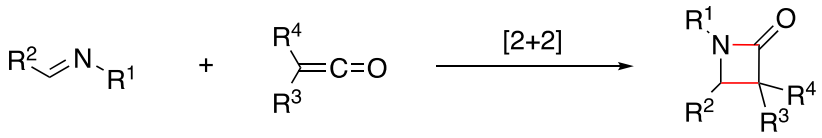

(ii) Kinugasa (1972): Coppr-catalysed reaction between alkyne and nitrone

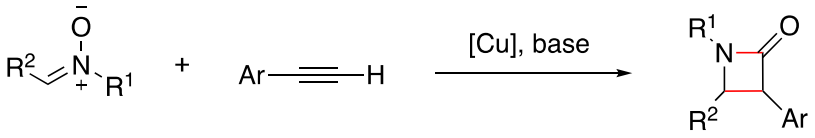

Scheme 4.1: Early approaches to the synthesis of β-lactams.

In recent years, with the advancement of transition metal-catalysis, several new methods have been reported for β-lactam synthesis.[200] When categorising the different methods of synthesis we can consider retrosynthetic strategies for different bond formations (Figure 4.4).

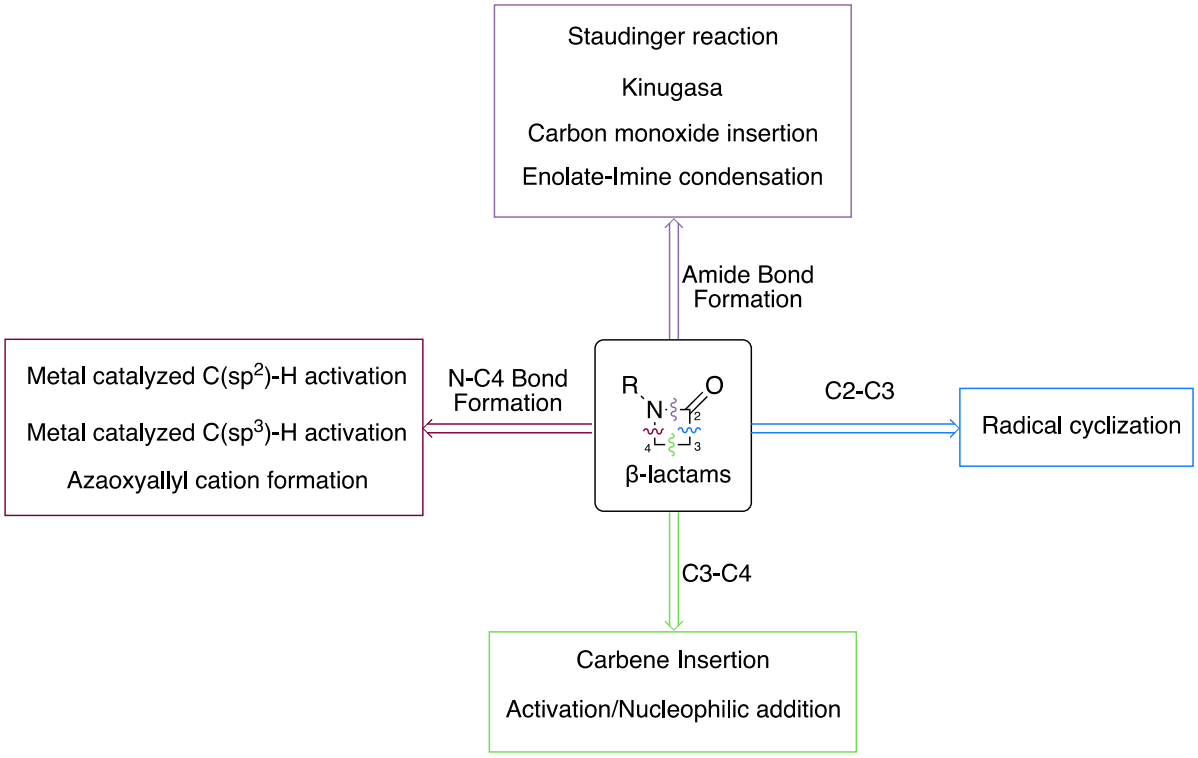

Figure 4.4: Retrosynthetic approaches for the synthesis of β-lactams.

N-C2 Disconnection

Arguably the most common and well investigated approach to β-lactam synthesis is the formation of the amide bond — to which the aforementioned Staudinger and Kinugasa reactions belong. Additional strategies within this retrosynthetic approach include the transition metal catalysed carbonylation of aziridines (Scheme 4.2(i))[201,202] as well as a rhodium catalysed aza-Reformatsky strategy which proceeds via ring closure of an *in situ* generated β-amino ester, as reported by Ando and co-workers (Scheme 4.2(ii)).[203]

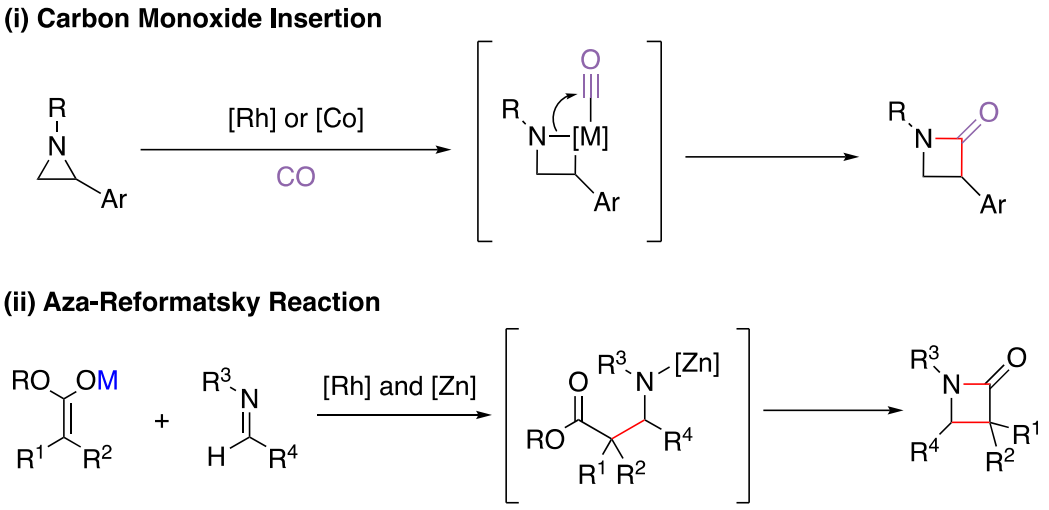

Scheme 4.2: Different approaches for the synthesis of β-lactams via the formation of the amide bond. (i) Metal-catalysed carbon monoxide insertion. (ii) Condensation of α-halo esters and imines in the presence of zinc.

N-C4 Disconnection

Access to the N-C4 bond formation is often enabled by metal or transition metal C-H activation. Palladium-catalysed enantioselective intramolecular C(sp^3)–H activation of amides has been reported by various groups.[197] Most recently, Yu and coworkers[204] described a β-C(sp^3)−H lactamisation of aliphatic amides using common sulfonyl-based protecting groups (Scheme 4.3(i)). Using a Pd catalyst, a suitable ligand and *tert*-butyl hydrogen peroxide (TBHP) as the sole oxidant they were able to synthesis β-lactams from a diverse range of amides.

Liu and Chen[205] reported an interesting alternative method for β-lactam synthesis via an azaoxyallyl cation intermediate, which could be formed in situ using a base from α-halo hydroxamates (Scheme 4.3(ii)). The reaction proceeds via a [3+1]-cycloaddition reaction with sulfur ylide. Interestingly, when the group α to the nitrogen (R^2) was an alkyl group, β-lactam was the major product through the [3+1] reaction, whereas an aromatic group on the nitrogen formed a γ-lactam product through a [3+2]-cycloaddition.

(i) Yu (2022): Metal Catalysed C(sp^3)-H Activation

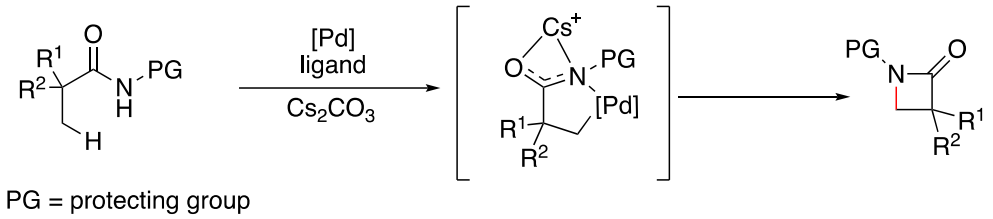

(ii) Chen (2016): 3+1 Cycloaddition

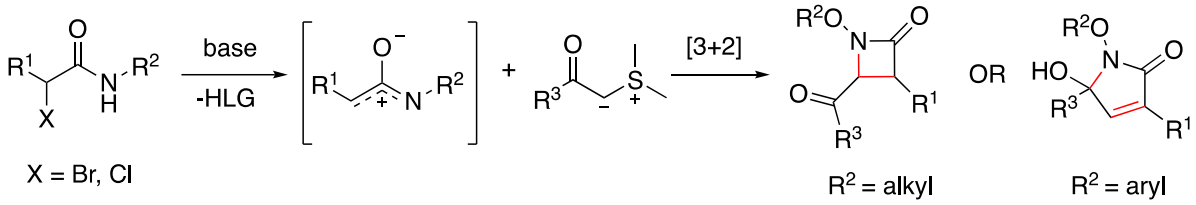

Scheme 4.3: Examples of different approaches to β-lactams synthesis via N-C4 bond formation. (i) Palladium catalysed lactamization of aliphatic amides via C(sp^3)-H activation. (ii) Lactamization of α-halo hydroxamates via a [3+1]-cycloaddition with sulfur ylides.

C3-C4 Disconnection

β-lactams can also be obtained by forming a new C3-C4 bond. A well-studied method for this approach is the metal-catalysed intramolecular C-H bond insertion of diazoamide carbenes. A carbenoid present at the α-position of an amide can undergo C-H insertion to form β-lactams. A major challenge for this type of cyclisations is the competition between 4 and 5 membered rings (β- or γ- lactams).[206] Previous reports have favoured rhodium catalysis for this transformation, however Solé recently published a palladium-catalysed approach starting from α-diazo-α-(methoxycarbonyl)acetamides (Scheme 4.4).[207]

Solé (2018): Carbene C-H Insertion

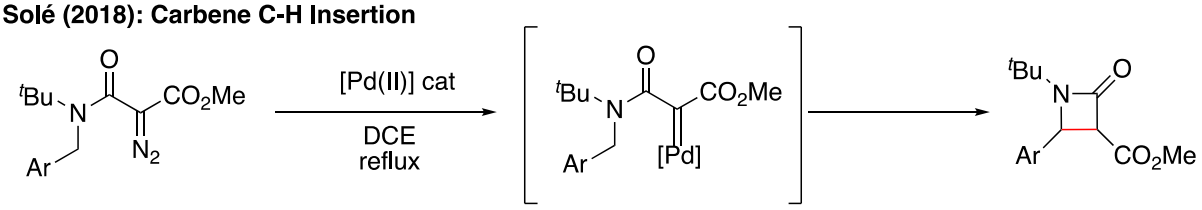

Scheme 4.4: Palladium-catalysed intramolecular diazoamide carbene insertion.

The C3-C4 bond can also be achieved through the activation of unsaturated C-C bonds, followed by nucleophilic addition/ring closure. Some approaches to this strategy include

dearomatisation/cyclisation methods resulting in spiro-β-lactams and cyclisation of propiolamide catalysed by triphenylphosphine.[198]

C2-C3 Disconnection

Formation of a new C-C bond at the carbonyl position (C2-C3) usually requires radical cyclisation. This can be achieved through the formation of a light induced carbamoyl radical which can undergo cyclisation with an alkene moiety, as described by Grainger and co-workers (Scheme 4.5(i)).[208] Norrish-Yang type II photocyclisation reactions have also been employed to access β-lactams. Wencewicz reported a UV light mediated approach to 3-hydroxy-β-lactams, which proceeds via the formation of a carbonyl radical followed by a 1,5-hydrogen abstraction and radical cyclisation (Scheme 4.5(ii)). This reaction was only tolerated by weakly electron donating or withdrawing groups on the *meta* and *para* positions of aromatic groups.[209]

(i) Grainger (2012): 4-Exo Trig Carbamoyl Radical Cyclisation

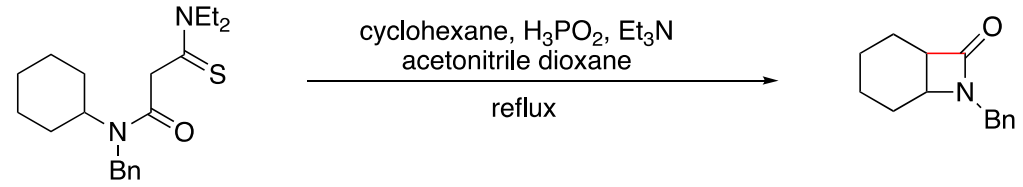

(ii) Wencewicz (2018): Norrish-Yang Type II Photocyclisation

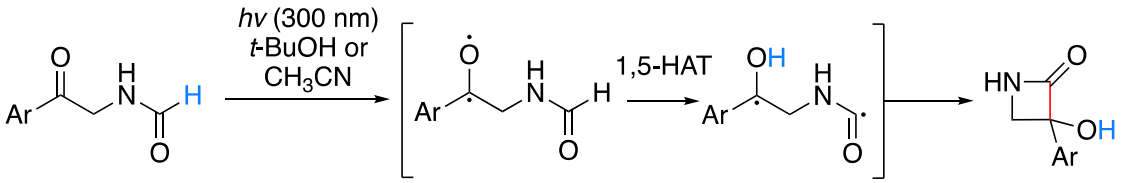

Scheme 4.5: (i) Reduction of dithiocarbamates using Et_3N–H_3PO_2–acetonitrile under thermal conditions. (ii) 1,5-HAT and radical cyclisation mediated by UV light.

This short review highlights that despite the various options for β-lactam synthesis that have been reported, many still require the use of relatively reactive precursors, expensive transition-metal catalysts or harsh reaction conditions such as relatively high reaction temperatures or unselective UV light. On the other hand, visible-light mediated strategies offers viable solutions to these latter restrictions.

To the best of our knowledge, the use of visible-light mediated approaches to β-lactams are rare. In 2021, two independent reports were published which described a Staudinger synthesis of β-lactams in which the reactive ketene intermediate was generated *in situ* from visible-light. The first by Glorius and co-workers who reported a method to generate ketenes from α-ketoacylsilanes via a [1,3]-silyl migration, which could then undergo a formal [2+2] cycloaddition with imines (Scheme 4.6(i)).[210] Jiang and Wei also reported the *in situ* ketene generation via a photoredox catalysed Wolff rearrangement of α-diketones rather than the traditional α-diazoketones (Scheme 4.6(ii)).[211]

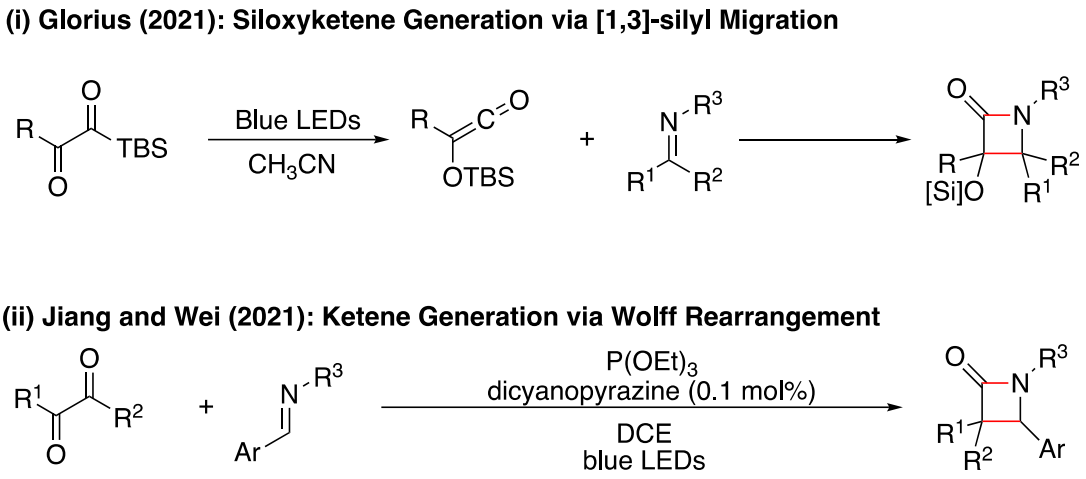

Scheme 4.6: Visible-light mediated approaches towards ketene preparation for β-lactam synthesis via the Staudinger synthesis.

These visible-light mediated strategies still require the use of relatively reactive precursors which can limit their utility in some applications. In Chapter 3 we disclosed the formation of triplet diradicals from simple acrylamides for the synthesis of 3,4-dihydroquinolin-2-ones from visible-light mediated EnT using the class of thioxanthone photosensitisers. We were curious about further applications of this triplet diradical and hypothesized we could access β-lactams via a radical cyclisation of this diradical, using a direct C-H bond functionalisation.

When considering approaches for the synthesis of β-lactams via C-H bond functionalization, the Norrish-Yang-type photocyclisation reactions emerged as a possible approach. [212,213] The mechanism of a Norrish-Yang photocyclisation is initiated with UV light photoexcitation of a γ-hydrogen bearing ketone in which the carbonyl group undergoes n-π* excitation to form a

diradical. The oxygen-centered radical abstracts the γ-hydrogen through a 1,5-HAT to create a reactive C-radical which cyclises by radical recombination to give a cyclic alcohol.

Norrish-Yang-type II photocyclisations

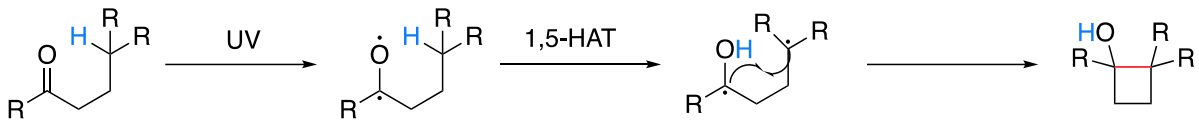

Scheme 4.7: General reaction scheme of Norrish-Yang photocyclisations via a 1,5-HAT from carbon to oxygen.

Norrish-Yang type cyclisations have been used in early reports for the synthesis of β-lactams. In the late 1970s, Aoyama and co-workers published a photochemical approach to β-lactams starting from α-oxoamides (Scheme 4.8(i)).[214,215] Irradiation of these starting α-dicarbonyl compounds with UV light initiates a Norrish-Yang type II cyclisation affording 3-hydroxy-β-lactams. Similarly, in 1980 Wehrli reported the photocyclisation of β-ketoformamides which proceeds via an acyl radical intermediate (Scheme 4.8(ii)).[216]

(i) Aoyama (1978):

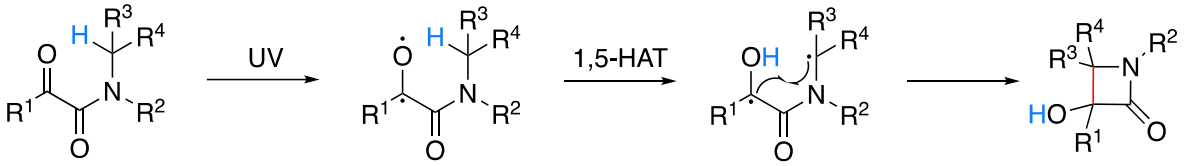

(ii) Wehrli (1980):

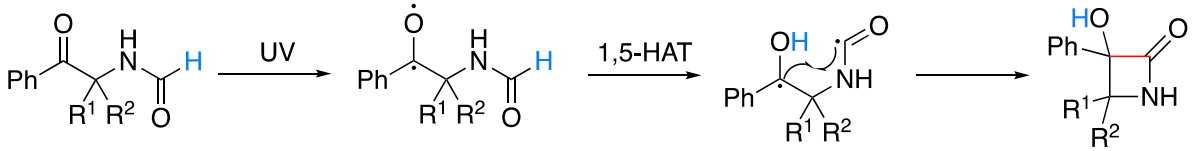

Scheme 4.8: Early reports of Norrish-Yang type II cyclisations mediated by UV light for the synthesis of β-lactams.

A notable variation of the Norrish-Yang cyclisation was reported by Hasegawa and co-workers in 1977. The authors utilized a C=C chromophore to generate a diradical for a rare C-to-C 1,5-HAT variation.[217] In this approach, the authors utilized an alkene to generate a C,C diradical (rather than the typical C,O diradical of the Norrish-Yang cyclisation) from direct UV

irradiation which was then able to undergo a 1,5-HAT and subsequent radical cyclisation to form a new β-lactam.

Hasegawa (1977): C to C HAT

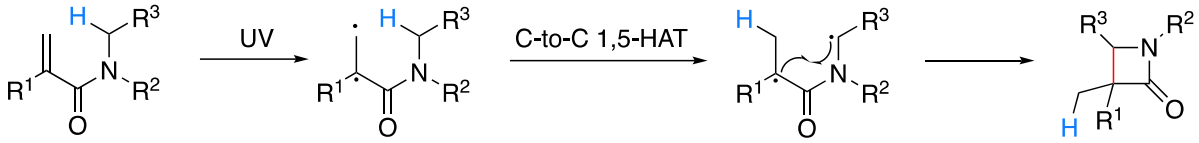

Scheme 4.9: Synthesis of β-lactams via a Norrish-Yang type II variation involving a rare carbon to carbon 1,5-HAT mediated by UV light.

These photochemical 1,5-HAT strategies represent an efficient, metal-free approach towards the synthesis of β-lactams. However they all still require the use of high-power UV light sources which limits the reaction scope/yields and reduces its selectivity. Related methods from other groups have emerged for β-lactam or azetidine synthesis in subsequent years, however all require the use of UV light to form excited triplet states.[218–225] We hypothesized that visible-light mediated photocatalysis could be used to generated β-lactams in a Norrish-Yang type reaction under milder reaction conditions.

Visible-light mediated Norrish-Yang type reactions are rare. To the best of our knowledge, at the time of writing, there had only been one report for the synthesis of β-lactams using visible-light mediated Norrish-Yang type reactions. This report was published in 2016 by Sivaguru and co-workers,[226] who described the formation of a spiro-β-lactam via a TX sensitised visible-light mediated hydrogen abstraction of an enone carboxamide. Using 20 mol% TX with 420 nm light under nitrogen they reported a moderate yield of 48% after 10 hours. This was reported alongside a study of direct irradiation of a variety of these enone carboxamides with UV light.

Sivaguru (2016): Visible-Light Mediated Hydrogen Abstraction

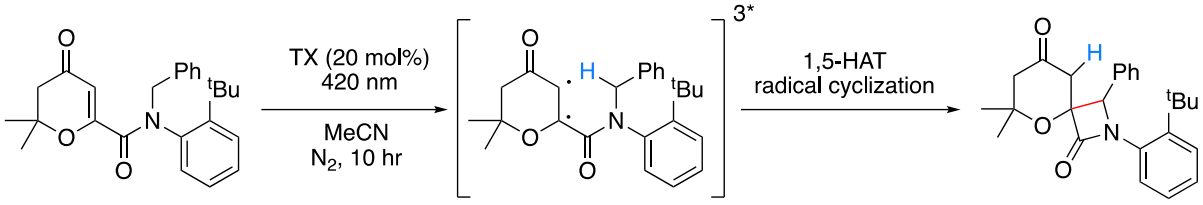

Scheme 4.10: The first known visible-light mediated Norrish-Yang type cyclisation to for spiro-β-lactams.

In 2020, a report to make β-lactam products by direct irradiation with visible-light was described by Sarpong. [227] They reported the cyclisation of keto-amides under direct blue light irradiation for the formation of *N*-fused bicyclic β-lactams (Scheme 4.11i)

A variation of the Norrish-Yang cyclisation, similar to Sivaguru above, was published by Koert and co-workers.[228] They reported a rare C-to-C 1,5-HAT using visible-light to promote an EnT mediated triplet sensitisation. This photocatalytic approach negates the need for UV light, however their conditions required an **[Ir]** photocatalyst, high reaction temperatures (60 – 100 °C) and long reaction times (Scheme 4.11ii).

i) Sarpong (2020): Visible-Light Mediated Norrish-Yang Cyclisation

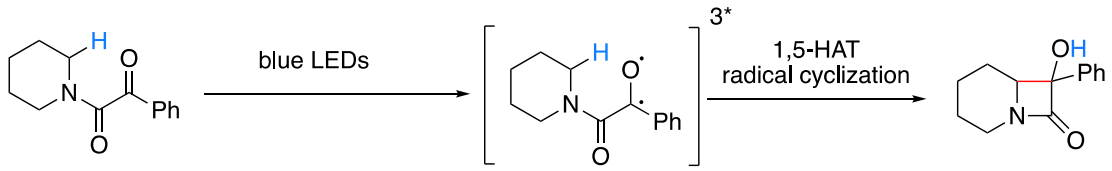

ii) Koert (2019): Visible-Light C-to-C HAT

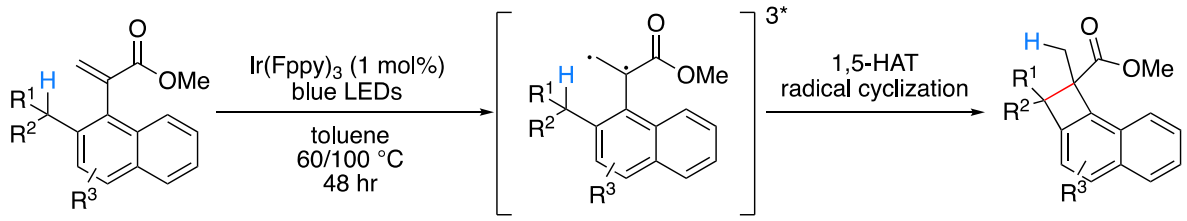

Scheme 4.11: (i) Direct visible-light mediated Norrish-Yang type cyclisation to for N-fused bicyclic β-lactams. (ii) Visible-light mediated photocatalytic Norrish-Yang type cyclisation featuring a C-to-C HAT using an [Ir] catalyst.

As described in Chapter 3, we had reported a visible-light mediated, metal-free EnT approach to triplet diradicals from acrylamides (see chapter 3 Scheme 3.16).

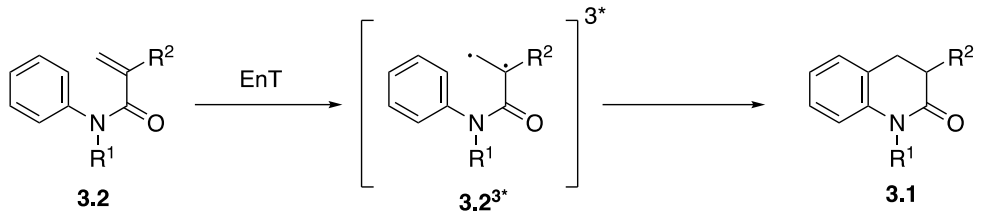

Scheme 3.16: 3,4-dihydroquinolin-2-one synthesis via photocyclisation of acrylamides reported in Chapter 3 above.

We hypothesized that this triplet diradical could initiate a Norrish-Yang type cyclisation via a 1,5-HAT if there was a suitable C(sp^3)-H group at the appropriate distance on the molecule. To this end, we proposed the following approach to β-lactams from *N*-benzyl substituted acrylamides (Scheme 4.12).

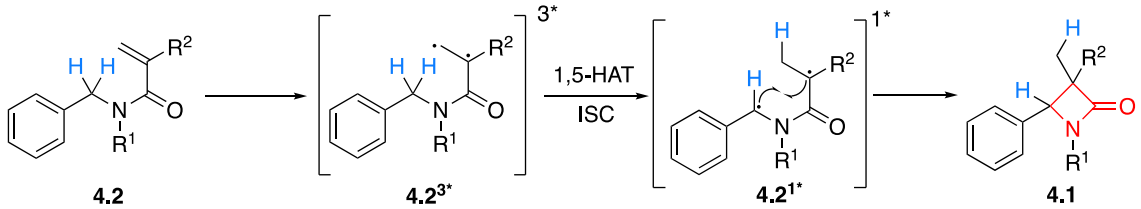

Scheme 4.12: Our proposed EnT approach to β-lactams via a triplet diradical which undergoes 1,5-HAT and radical cyclisation.

A key step in the proposed mechanism involves a direct C-H bond functionalisation via the C-to-C HAT. HAT or hydrogen atom transfer is the concerted movement of a proton and an electron ($H^+ + e^-$) in a single kinetic step from an organic group (R) to a suitable radical species ($X^\bullet$) (Figure 4.5). When considered in terms of C-H functionalisation the hydrogen atom ($H^\bullet$) is abstracted from a C-H bond, resulting in a new carbon-centered radical. This is a particularly powerful tool when used for C(sp^3)-H functionalisation because it allows for the cleavage of inert C-H bonds. There are a number of factors affecting HAT reactions for C-H functionalisation:

(i) Thermodynamic factor: HAT is a thermodynamically favourable process when the bond dissociation energies (BDEs) of the product (X-H) is higher than the initial C-H bond.

(ii) Kinetic factor: Given similar BDE differences, the selectivity of HAT is governed by radical philicity. An electrophilic radical is expected to undergo HAT from an electron-rich C-H bond (ie a hydridic site) as opposed to an electron deficient one (protic site) and *vice versa*.

(iii) Chemoselectivity: Tertiary radicals are more stable than primary and secondary radicals. Additionally, BDE increases going from tertiary to secondary and primary C-H bonds. Therefore, HAT favours more substituted carbons for C-H activation.

(iv) Regioselectivity:[229,230] Intramolecular HAT is referred to as a 1,*n*-HAT where *n* = 4-8. Regioselectivity is dependent on the size of the ring in the cyclic transition structure. 1,5-HAT is the most favoured process because the six-membered transition structure is stabilized by C-H-X angle of 180°.

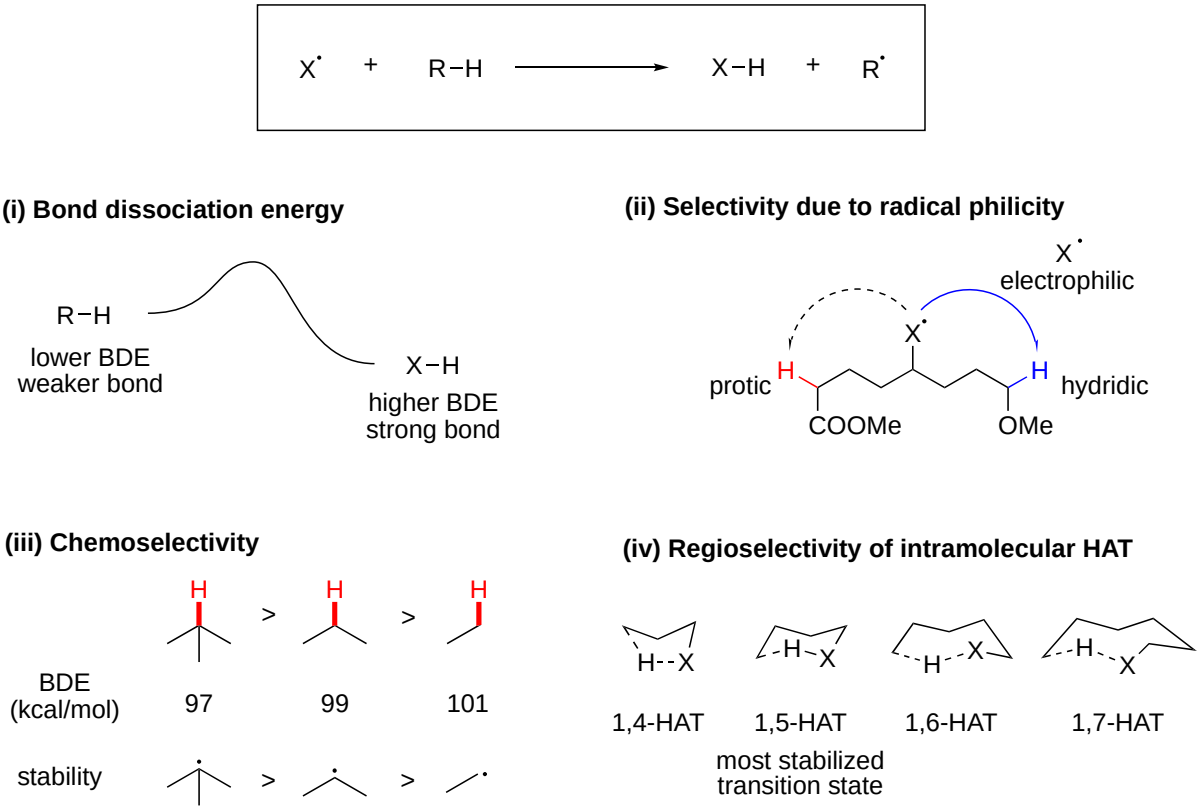

Figure 4.5: The four key factors affecting hydrogen atom transfer reactions.

These factors assisted with our initial selection of the *N*-benzyl fragment for the optimisation studies, particularly with reference to (ii) and (iii). Benzyl radicals are significantly more stabilised, and the combination of the electrophilic primary C-centred radical produced at the

terminus (following sensitisation), together with hydric stabilisation brought about by the adjacent phenyl ring provides the requisite matched radical philicity.

4.2 Aims and Objectives

We recognized an opportunity to develop a novel, visible-light mediated synthesis for β-lactams via an EnT method that allowed for a wide substrate scope and benign reaction conditions. We aimed to develop a method that was metal-free, could be performed at room temperature and negated the need for additives such as oxidants and bases while still producing moderate to excellent yields. Our proposed approach aimed to investigate C(sp^3)-H functionalization using a rare C-to-C HAT via a variation of the Norrish-Yang photocyclisation reaction. We wanted to explore the scope of the reaction by varying the substituents at different positions on the molecule in order to build a comprehensive substrate table. Finally, we planned to perform mechanistic studies such as deuterium labelling and DFT calculations to correctly identify the mechanism of the reaction.

4.3 Results and Discussion

Similarly to Chapter 3, the Mukaiyama peptide coupling could be used to synthesise these *N*-benzyl substituted acrylamides **4.2**. This method was well tolerated for many *N*-benzylaniline derivatives. Conversely to the coupling of *N*-phenylaniline derivatives in chapter 3, strongly electron withdrawing groups on the phenyl ring did not significantly reduce the nucleophilicity of the amine. As a result, an acid chloride synthesis was not required for any acrylamide syntheses.

The majority of the *N*-benzylamine derivatives used when constructing the substrate table were commercially available. When the particular *N*-benzyl amine was not available, a reductive amination from the corresponding aldehyde and amine was first performed (see experimental section). It is worth noting that given the more flexible nature of these systems (as compared to the anilides in Chapter 3), rotamers were evident in the ^{1}H NMR spectra for most acrylamides **4.**2 as seen by a doubling of signals. A representative example is given **for 4.2a** (Figure 4.6).

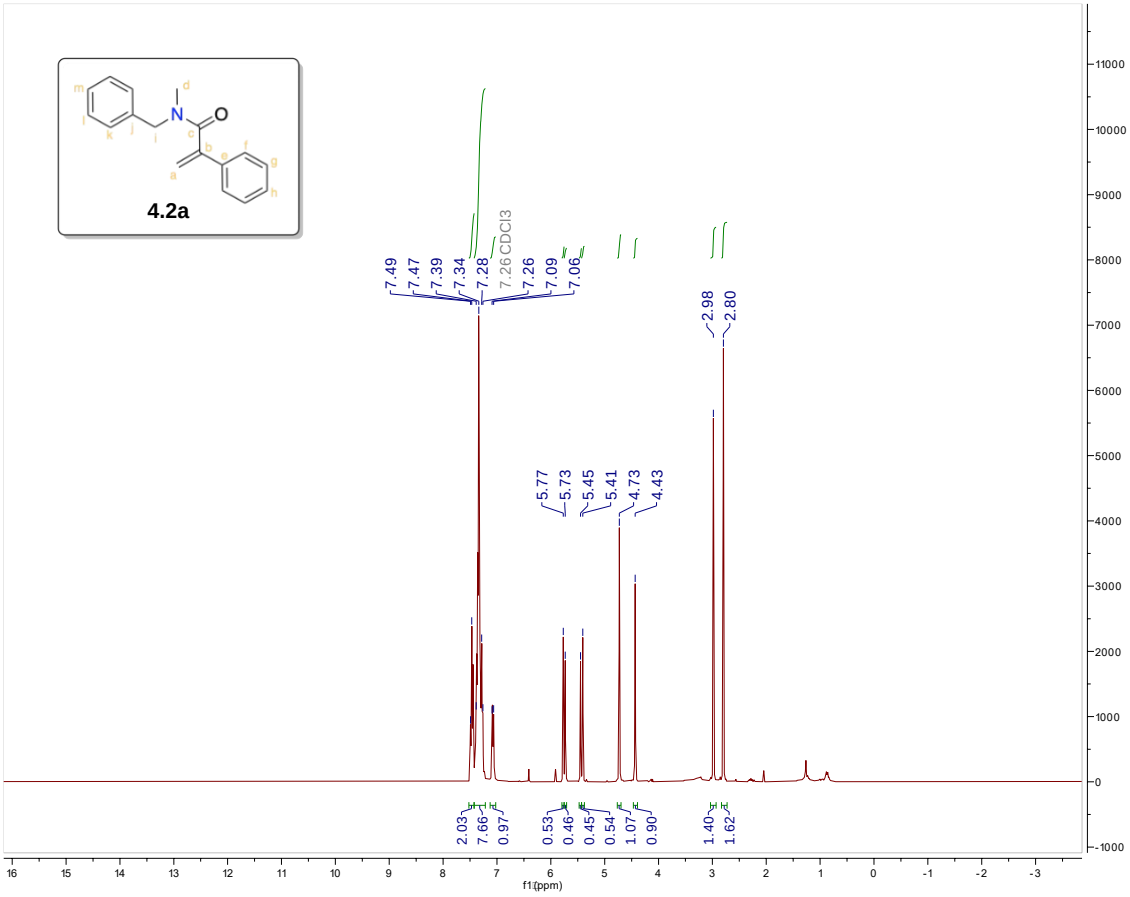

Figure 4.6: ^{1}H NMR spectrum of acrylamide **4.2a**.

Rotamers are conformational isomers where interconversion by rotation around a single bond is restricted and an energy barrier has to be overcome in order to convert one conformer to another. Amides can exist as rotamers due to the hindered rotation of a C-N bond. An amide exhibits partial double bond character around a C-N bond through conjugation of the lone pair at the *N* – centre with the carbonyl moiety (Scheme 4.13).

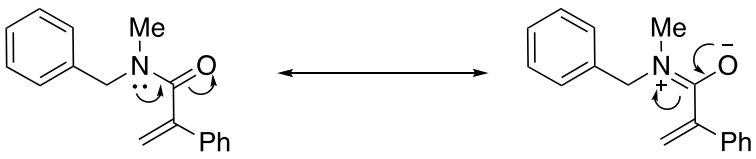

Scheme 4.13: Double bond character of amide C-N bond due to conjugation.

This leads to a high rotation barrier which causes the generation of distinct *cis/trans* isomers (Scheme 4.14). These isomers are detectable through their separate sets of signals in NMR spectra.

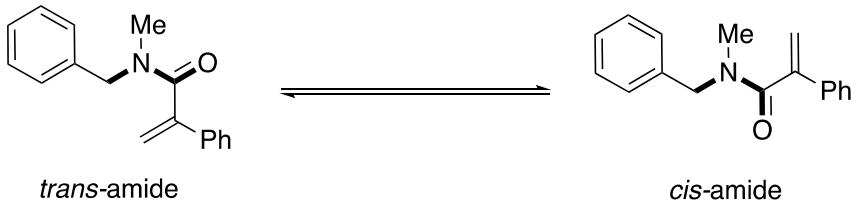

Scheme 4.14: *Cis/trans* isomers arising due to hindered rotation around amide bond.

The ^{1}H NMR spectrum of **4.2a** (Figure 4.6) shows a doubling of signals. The *N*-methyl protons (H_d) are seen as two peaks at 2.80 and 2.98 ppm and integrated for 1.62 and 1.40 protons, respectively. Similarly, the benzyl protons (H_i) appear at 4.43 and 4.73 ppm and integrate for 0.90 and 1.07 protons, respectively. The vinyl protons from the double bond (H_a) are seen at 5.41 and 5.45 ppm, integrating for 0.54 and 0.45 protons as well as at 5.73 and 5.77 ppm, integrating for 0.46 and 0.53, respectively. The aromatic region integrates for a total of 10 protons from the range of 7.06 – 7.49ppm. The doubling of signals is consistent with a 0.55:0.45 ratio of rotamers.

The ^{13}C NMR for **4.2a** also shows a doubling of signals consistent with rotamers.

4.3.1 Optimisation Studies for Photocyclisation

We began our studies by performing preliminary experiments on *N*-benzyl-*N*-methyl-2-phenylacrylamide **4.2a** using the same optimised conditions as the photocyclisation for 3,4-dihydroquinolin-2-ones used in Chapter 3 above but with a 405 nm light source. To our delight, we were able to isolate the desired β-lactam **4.1a** from model *N*-benzyl acrylamide **4.2a** (Scheme 4.15).

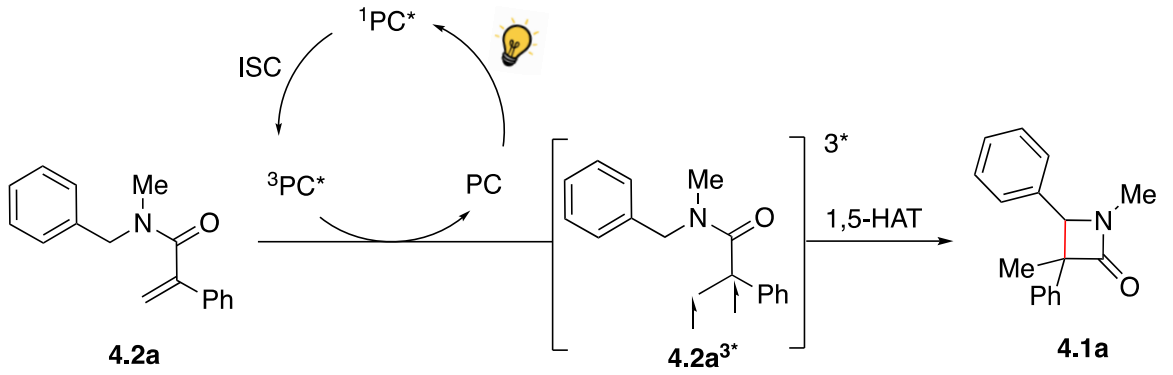

Scheme 4.15: Visible-light mediated EnT approach to model β-lactam **4.1a** via triplet sensitisation of *N*-benzyl acrylamide **4.2a**.

^{1}H NMR spectroscopy confirmed that we were isolating the desired product as two separable diastereomers.

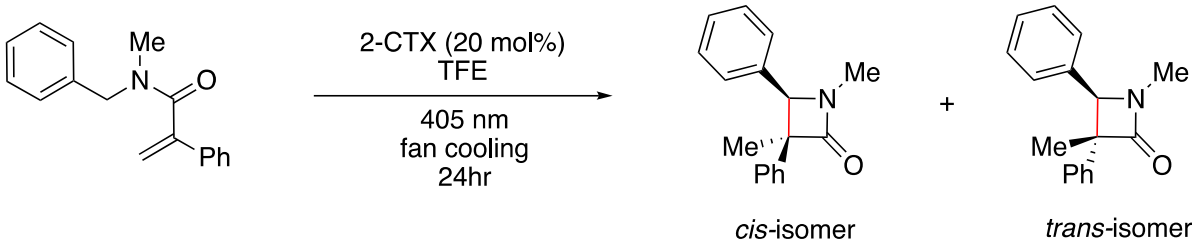

Scheme 4.16: Photocyclisation of *N*-benzyl-*N*-methyl-2-phenylacrylamide using previously optimised conditions.

When studying potential photoproducts for the cyclisation of *N*-benzyl-*N*-methyl-2-phenylacrylamide, we considered the possibility that a photocyclisation could occur onto the aromatic ring as per our 3,4-dihydroquinolin-2-one cyclisation (Scheme 4.17), however we did not observe any of this tetrahydroazepinone product in our studies. This can be attributed to the readily available hydrogens of the benzyl group alpha to the nitrogen. These hydrogens can undergo 1,5-HAT which is likely more favourable than addition to the aromatic ring.

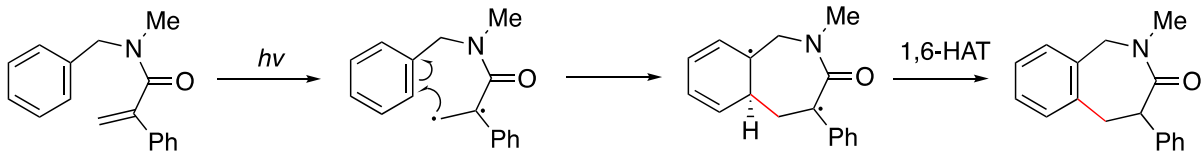

Scheme 4.17: Potential tetrahydroazepin-2-one product not observed.

Satisfied we were producing only the desired β-lactam product, we turned our attention to optimizing the reaction conditions. Since we were performing a similar energy transfer to Chapter 3, we did not require an extensive optimisation table. The results of the optimisation are summarized in Table 4.1 below.

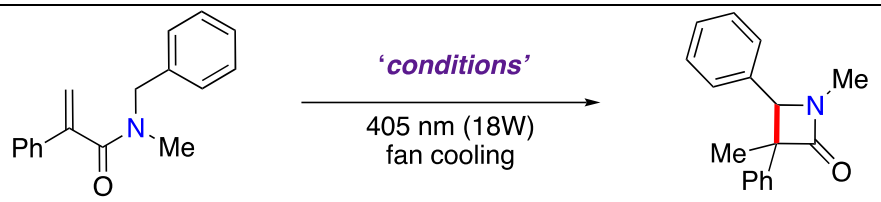

4.2a **4.1a**

Entry	Photocatalyst	Catalyst mol %	Solvent	Reaction Time (hr)	Yield (%)[a]	dr (1st:2nd)
1[a]	**2-CTX**	10%	TFE:$CHCl_3$ (0.03)	18 hr	84%	1.2:1
2[a]	**2-CTX**	10%	EtOH (0.03)	18 hr	72%	1.1:1
3	**2-CTX**	10%	PhMe (0.03)	18 hr	>99%	1.5:1
4	**TX**	10%	PhMe (0.03)	18 hr	75%	1.5:1
5	**4Cz(IPN)**	10%	PhMe (0.03)	18 hr	84%	1.7:1
6[b]	**2-CTX**	10%	PhMe (0.03)	5 hr	89%	1.5:1
7[c]	**2-CTX**	10%	PhMe (0.06)	18 hr	No rxn	-
8	none	-	PhMe (0.06)	18 hr	No rxn	-

Table 4.1: Optimisation table for photocyclisation reaction with organic photosensitisers. [a]Determined by ^{1}H NMR spectroscopy against internal standard (1,3,5-Trimethoxybenzene). [b]Isolated by column chromatography, [c]No light

Using Chapter 3's optimised conditions, we determined an 84% yield after 18 hrs according to ^{1}H NMR yield calculations against an internal standard of 1,3,5-trimethoxybenzene (entry 1). The diastereomeric ratio was determined as 1.2:1. We then investigated different solvents and found that EtOH performed slightly worse with 72% yield in 18 hrs (entry 2). Gratifyingly, we saw near perfect conversion of the starting material when **2-CTX** was used in toluene (entry 3), with a diastereomeric ratio of 1.5:1. Other photosensitisers were also investigated but produced inferior results comparatively; the unsubstituted thioxanthone (**TX**) afforded 75 % yield (entry 4) and 4-CzIPN afforded 84 % yield (entry 5). Satisfied with the **2-CTX** conditions, we investigated the effect of reaction time on yield. We found that **2-CTX** gave 89% conversion after just 4 hours (entry 6). However, we ultimately decided to use a

standardised reaction time of 18 hrs to account for substrates which might have worse conversions.

Finally, we performed control reactions with no light (entry 7) and no catalyst (entry 8) and observed no reaction occurring. This confirmed that a photocatalytic pathway was in use.

Similar to our dihydroquinolin-2-one reaction (Chapter 3), this reaction requires no extended workup; the solvent was removed in vacuo and the resulting residue was purified directly by column chromatography. In most cases the diastereomers could be separated chromatographically, but diastereomeric ratios were determined by ^{1}H NMR analysis of the crude reaction mixture prior to purification.

It is important to mention that concurrent with our studies, a related report by Bach for the thioxanthone mediated production of β spirocyclic azetidine-3,3'-indoline had emerged[231]; similarly following the proposed olefin sensitisation, 1,5-HAT, and radical recombination (Scheme 4.18).

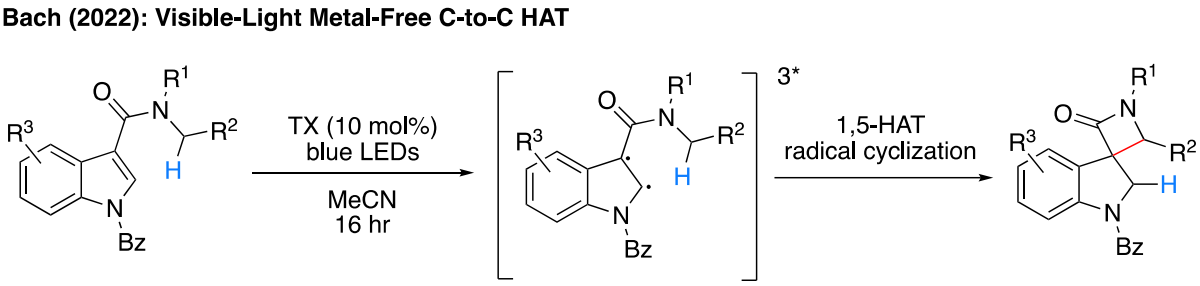

Scheme 4.18: Visible-light mediated metal-free photocatalytic Norrish-Yang type cyclisation for spiro β-lactam synthesis.

4.3.2 Diastereomer Analysis

Since the β-lactam synthesis produced 2 separable diastereomers, we were able to isolate and analyse by NMR spectroscopy two products for each photocyclisation reaction. *Trans* and *cis* β-lactam diastereomers could be assigned from the ^{1}H NMR by comparison of the shielding/deshielding effects experienced by the methyl group on the β-lactam ring (Figure 4.7). In the *trans* product (relative to the phenyl rings), shielding effects by the adjacent phenyl substituent — rotated perpendicular to the methyl due to steric effects — results in

the methyl group occurring at ~1.2 ppm. On the other hand, due to the lack of this shielding effect in the *cis* product, the corresponding methyl resonance is found relatively downfield at ~1.8 ppm. This behaviour is similarly consistent with previous literature.[232]

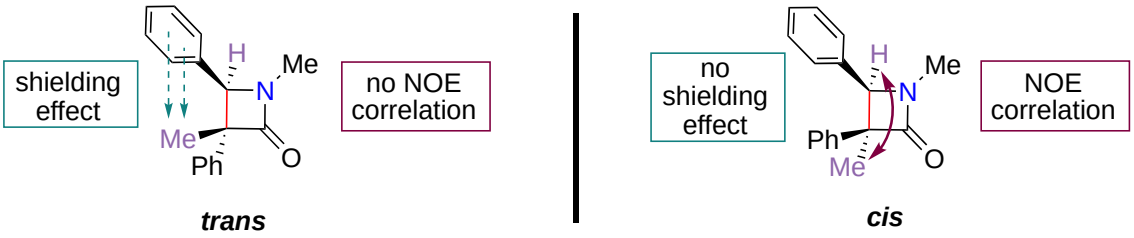

Figure 4.7: Shield effects observed in the ^{1}H NMR used to determine the *trans/cis* stereochemistry of the β-lactam products.

The ^{1}H NMR spectra for the two isolated β-lactam diastereomers of **4.1a** are shown in Figure 4.8 below.

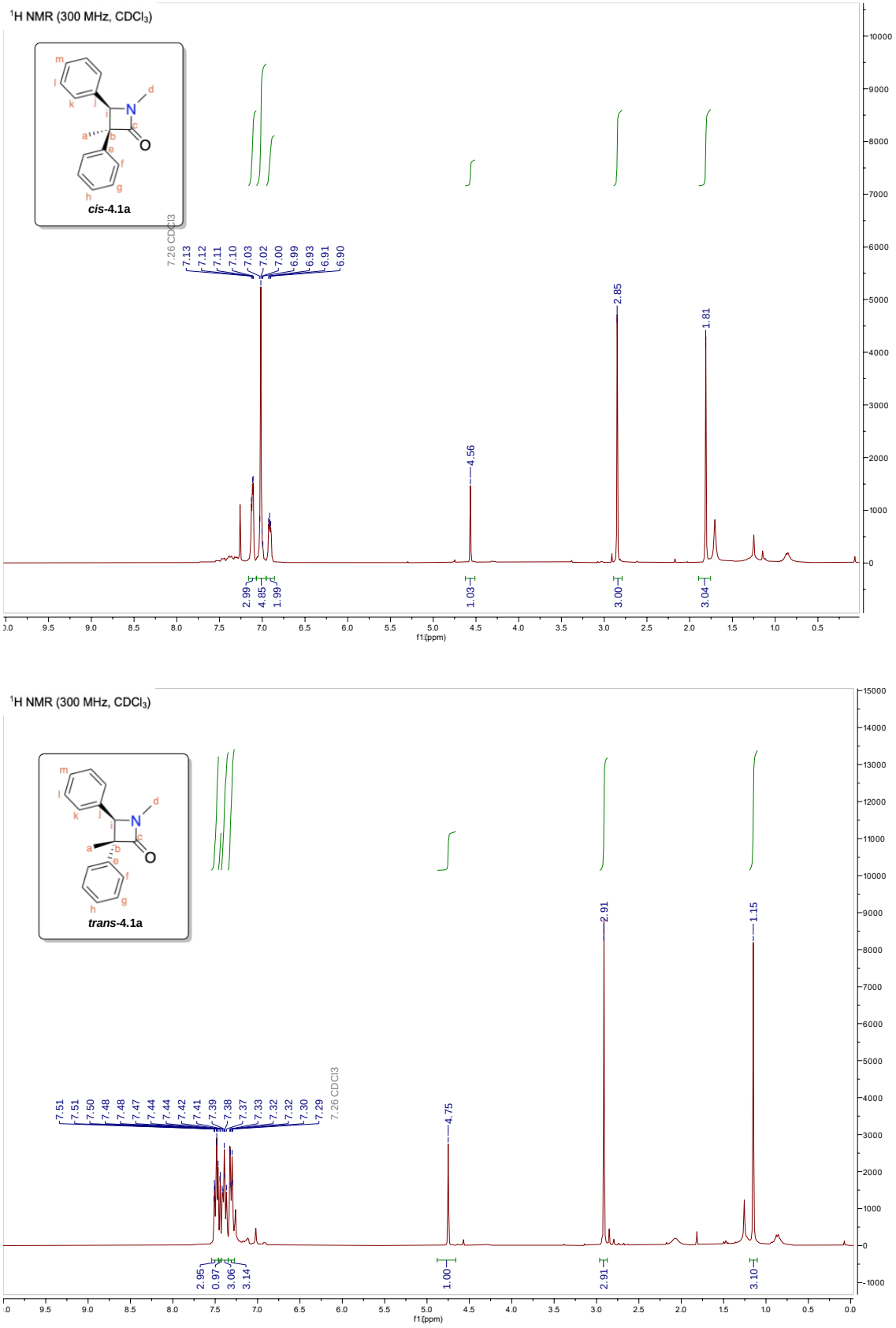

Figure 4.8: ^{1}H NMR spectrum of *cis* and *trans* diastereomer of β-lactam **4.1a**.

The methyl protons H_a of the *cis*-isomer appear at 1.15 ppm and the singlet at 4.75 ppm is assigned to the proton alpha to the nitrogen on the 4 membered ring (H_i). The aromatic region integrates for 10 protons and appears in the range of 7.29-7.51 ppm.

Similarly, the *trans* diastereomer shows the same peaks slightly shifted. The new methyl peak (H_a) appears downfield at 1.81 ppm. The singlet for H_i is shifted upfield to 4.56 ppm. Interestingly, the aromatic region is shifted significantly upfield and appears in the range 6.90 – 7.13 ppm.

NOE experiments for a random selected set of compounds from the substrate scope (**4.1f, 4.1j, 4.1l**) are consistent with this isomer assignment. Additionally, we performed single crystal X-ray analysis on the *trans*-isomer of **4.1j** which is shown below.

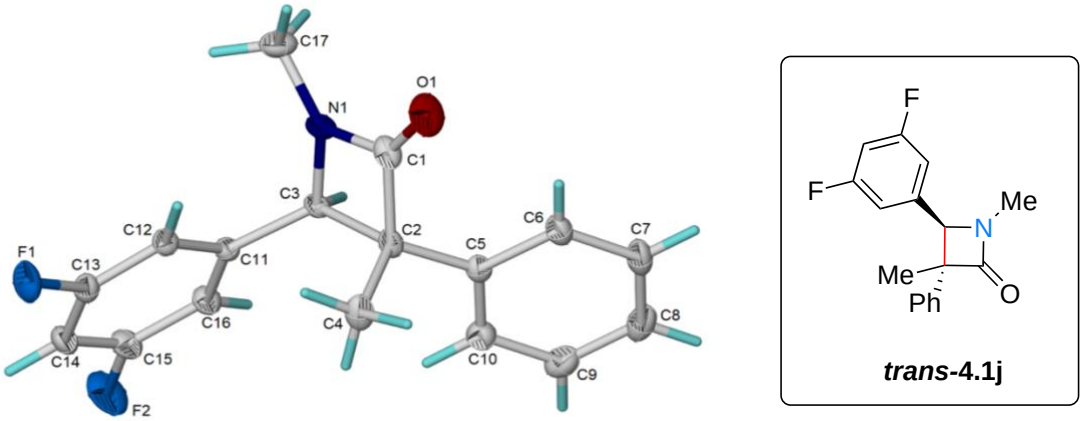

Figure 4.9: Single crystal X-ray structure of ***trans*-4.1j**

4.3.3 Substrate Scope

Pleased with our optimised conditions, we next explored the scope of the reaction. We performed substitutions at 3 positions on the β-lactam ring (Figure 4.10); *purple:* exploring the R^1/R^2 scope by varying the substituents on the phenyl ring alpha to the nitrogen as well as varying the aromatic ring itself; *blue:* modification of the nitrogen protecting group; *green*: substituents on the phenyl group alpha to the carbonyl.

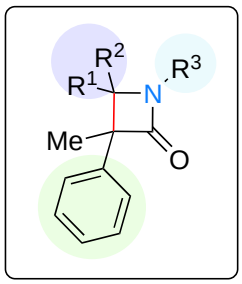

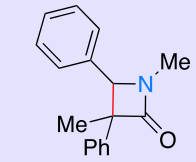

4.1a, 89%
1.5:1 dr

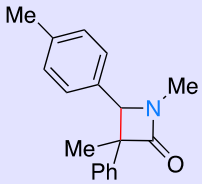

4.1b, 94%
1.6:1 dr

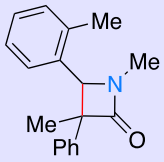

4.1c, 95%
1.5:1 dr

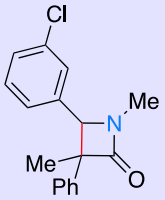

4.1d, 98%
1.4:1 dr

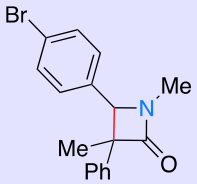

4.1e, 83%
1.5:1 dr

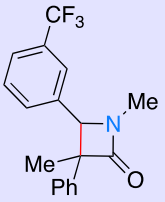

4.1f, 97%
1.6:1 dr

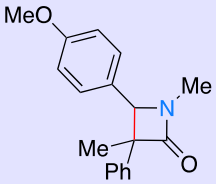

4.1g, 49%
1.5:1 dr

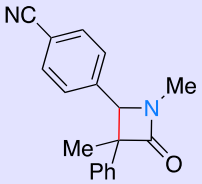

4.1h, 69%
1.3:1 dr

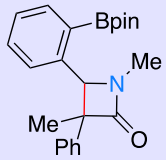

4.1i, 63%
1.8:1 dr

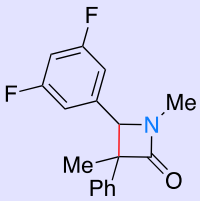

4.1j, 88%
1.4:1 dr

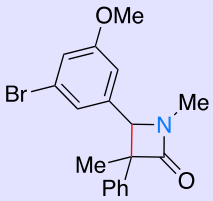

4.1k, 81%
1.7:1 dr

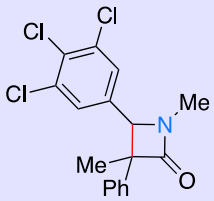

4.1l, 97%
1.3:1 dr

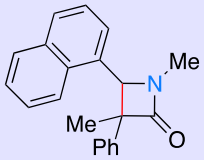

4.1m, 75%
1:5 dr

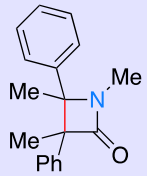

4.1n, 88%
1.7:1 dr

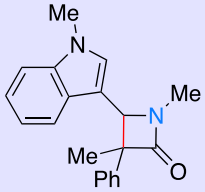

4.1o, 52%
1.6:1 dr

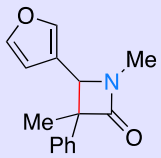

4.1p, 77%
1.5:1 dr

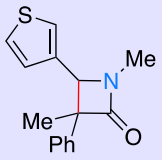

4.1q, 97%
1.3:1 dr

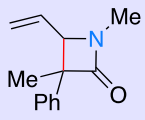

4.1r, 60%
1.4:1 dr

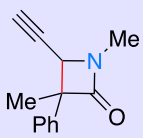

4.1s, 40%
2.3:1 dr

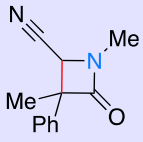

4.1t, 85%
1.4:1 dr

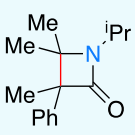

4.1u, 52%

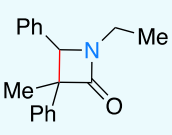

4.1v, 98%
1.4:1 dr

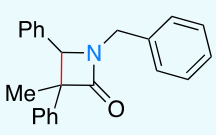

4.1w, 83%
2:1 dr

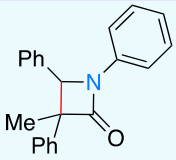

4.1x, 52%
1:1.4 dr

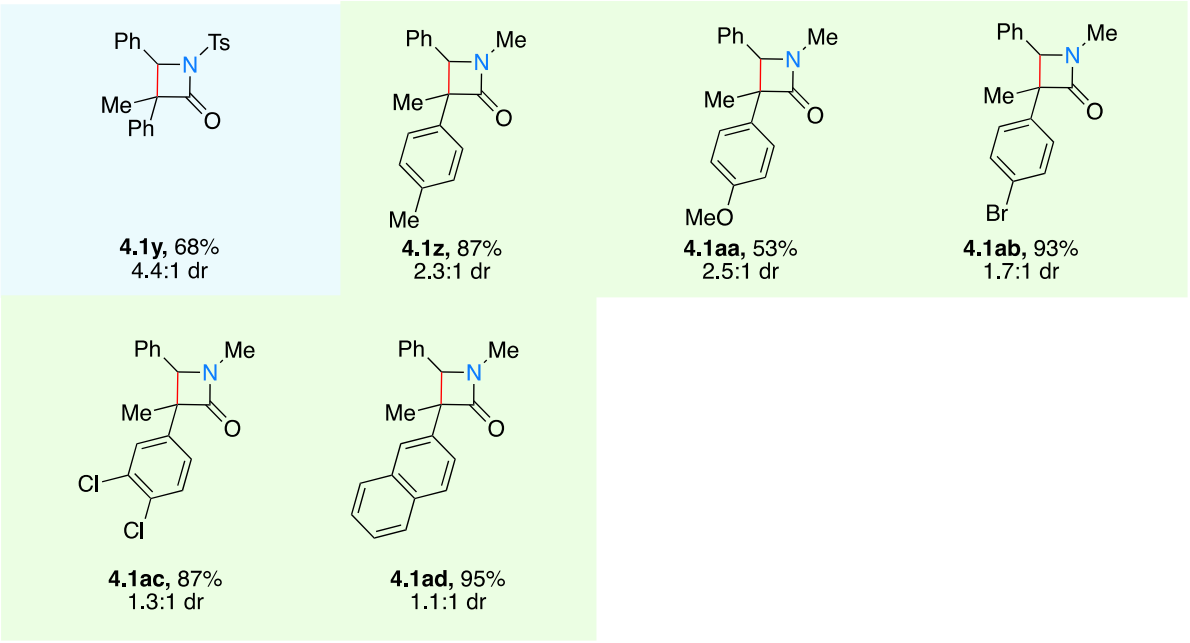

Figure 4.10: Expanding the substrate scope.

The model substrate **4.1a** was isolated in 89% in a ratio of 1.5:1 of separable diastereomers, with the *trans* isomer as the major product. Adding a methyl group at *para* and *meta* position of the aromatic (**4.1b** and **4.1c**) yielded 94% and 95%, respectively with similar dr's (1.5:1). Halogen monosubstituted aromatics were well tolerated with yields of 83%–98% (**4.1d-4.1e**). Strongly electron withdrawing substituents such as CF_3 (**4.1f**) and cyano (**4.1h**) were well tolerated with yields of 97% and 69%, respectively. Contrary, electron donating groups such as methoxy (**4.1g**) were also tolerated (49%). All the above substrates were isolated as 2 separable diastereomers with dr's of between 1.3:1 and 1.6:1. Products featuring aromatic boron esters could also be synthesised, producing **4.1i** in 63% yield, with 1.8:1 dr, however the diastereomers could not be separated by silica gel chromatography. Di- and tri-substituted products were also suitable, affording **4.1j**–**4.1l** in 81–97% yield. The naphthyl derived β-lactam **4.1m** was obtained in 75% yield, but interestingly was isolated with 1:5 dr. This increase in dr can be attributed to the bulkiness of the naphthalene group. Product **4.1n**, featuring a 1,5-HAT from a tertiary carbon centre, was produced in 88% yield. Modification of the aromatic heterocycle was also possible, with indole-, furan-, and thiophene-based products **4.1o**–**4.1q** formed in 52%, 77% and 97% yields, respectively. Pleasingly, extending the 1,5-HAT beyond benzylic amines is possible, with allylic, propargylic, and nitrile products **4.1r**–**4.1t** obtained in 60%, 40%, and 85% yield, respectively. No potential allylic

rearrangement products (such as a δ-lactam) were observed. The reaction is also possible using an amine lacking a radical-stabilising π-system (diisopropylamine), with product **4.1u** formed in 52% yield. This case proceeds via a tertiary radical intermediate, and so has some hyperconjugative stabilisation.

Modifications of the protecting group on the nitrogen atom (blue) were well tolerated, affording ethyl, benzyl and phenyl substituents in 98%, 83% and 52% yields, respectively (**4.1v-4.1x)**. Additionally, a tosyl protecting group produced **4.1y** in 68% with unreacted starting material accounting for the balance of the yield. Interestingly, **4.1y** produced diastereomers in a ratio of 4.4:1 cis to trans, which is possibly due to steric hindrance by the bulky tosyl group.

On varying the acrylic acid aromatic ring (green), monosubstituted aromatics such as methyl (**4.1az**), methoxy (**4.1aa**) and bromo (**4.1ab**) groups produced yields of 87%, 53% and 93%, respectively. Disubstituted chloro- acrylamide was also well tolerated producing **4.1ac** in 87% yield. Substituting the phenyl ring for a naphthalene group produced **4.1ad** in 95% yield. Notably, in most cases the diastereomeric products were easily fully separable using standard silica gel chromatography, with the *trans*-isomer typically obtained in modest excess.

Despite the many substituents that were well tolerated with this method, there were a few limitations that were observed. The products not obtained are shown in Figure 4.11 below.

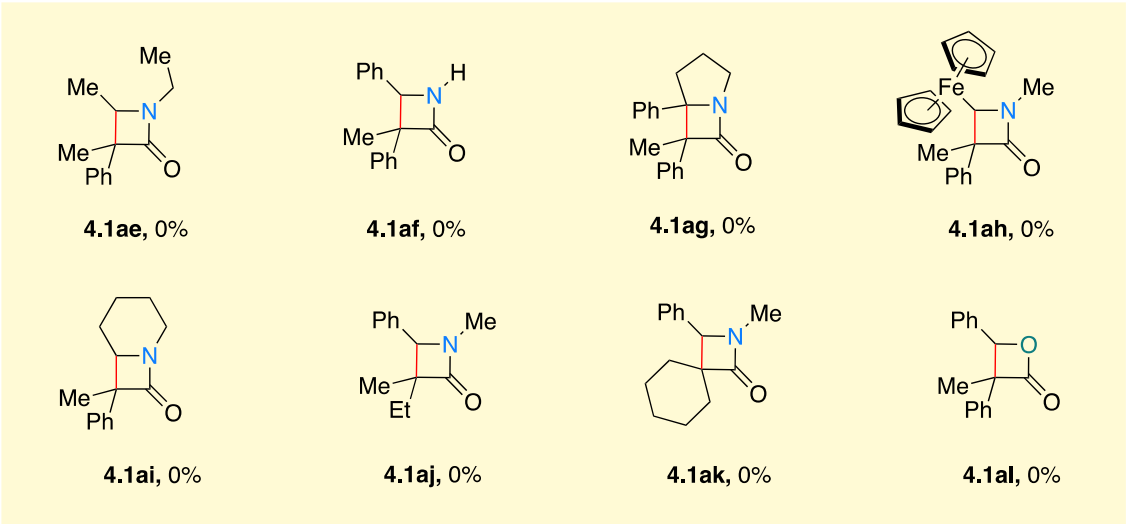

4.1ae, 0% **4.1af**, 0% **4.1ag**, 0% **4.1ah**, 0%

4.1ai, 0% **4.1aj**, 0% **4.1ak**, 0% **4.1al**, 0%

Figure 4.11: Unsuitable substrates

Product **4.1ae**, which utilises diethylamine and would require reaction via an unstabilised secondary radical intermediate was not obtained. Unprotected nitrogen product **4.1af** was also not obtained. Ferrocene-substituted and cyclic modifications to R^1/R^2 did not lead to formation of the corresponding products **4.1ag - 4.1ai**. Acrylic acid moieties featuring nonaromatic substituents (**4.1aj** and **4.1ak**), were also not obtained. Additionally, variation to the benzylic ester did not produce β-butyrolactone **4.1al**. In all of these cases, unreacted starting material was recovered.

4.3.4 Mechanistic Studies

Our proposed mechanism of the reaction is shown in Scheme 4.19 below, in accordance with the aforementioned Norrish-type II process, featuring a C-C HAT.

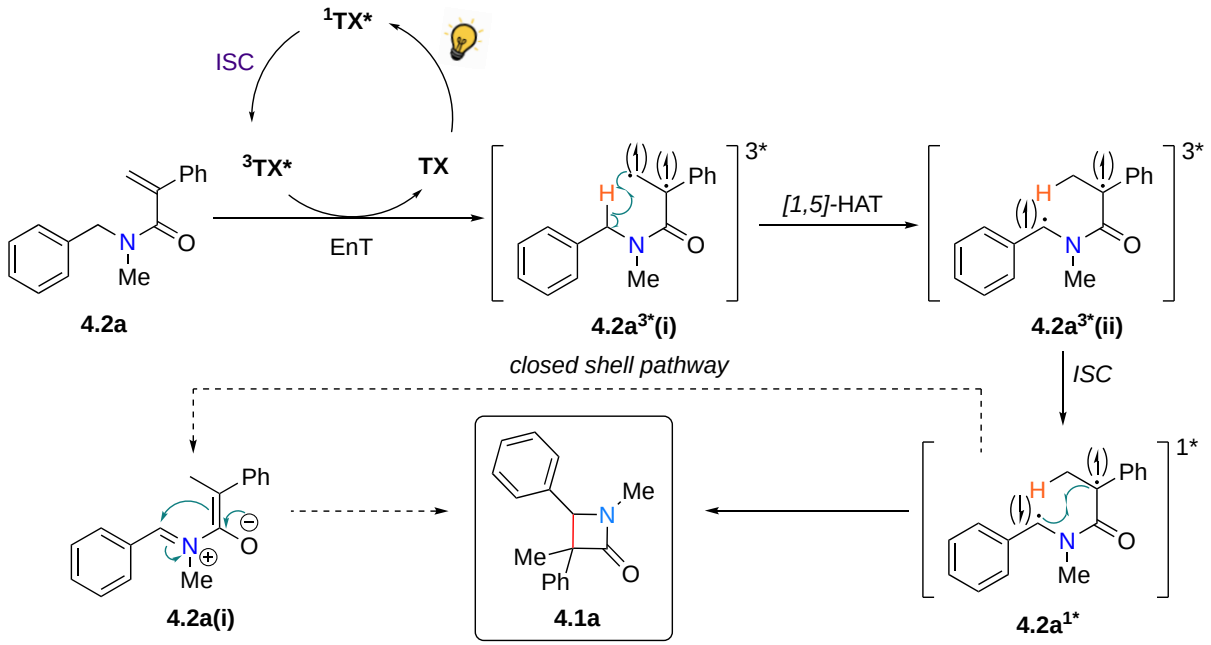

Scheme 4.19: Proposed mechanism for the synthesis of β-lactam **4.1a** via an EnT.

Following energy transfer to the substrate, producing triplet excited state **$4.2a^{3*}$(i)**. A subsequent carbon-to-carbon 1,5-HAT affords triplet intermediate **$4.2a^{3*}$(ii)** which undergoes intersystem crossing (ISC) back to its singlet state **$4.2a^{1*}$**. Finally, radical-radical coupling produces β-lactam **4.1a** as a mixture of diastereomers.

In order to support the proposed 1,5-HAT, deuterium labelling experiments were performed. When deuterated starting material ***d*$_2$-4.2a** was reacted under the standard conditions, both in toluene and ethanol, we saw 100 % deuterium incorporation in product ***d*$_2$-4.1a.**

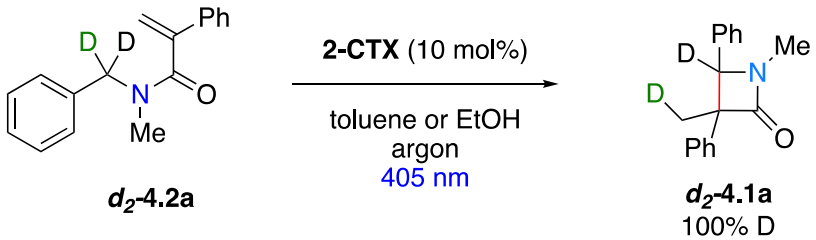

***d*$_2$-4.2a** ***d*$_2$-4.1a** 100% D

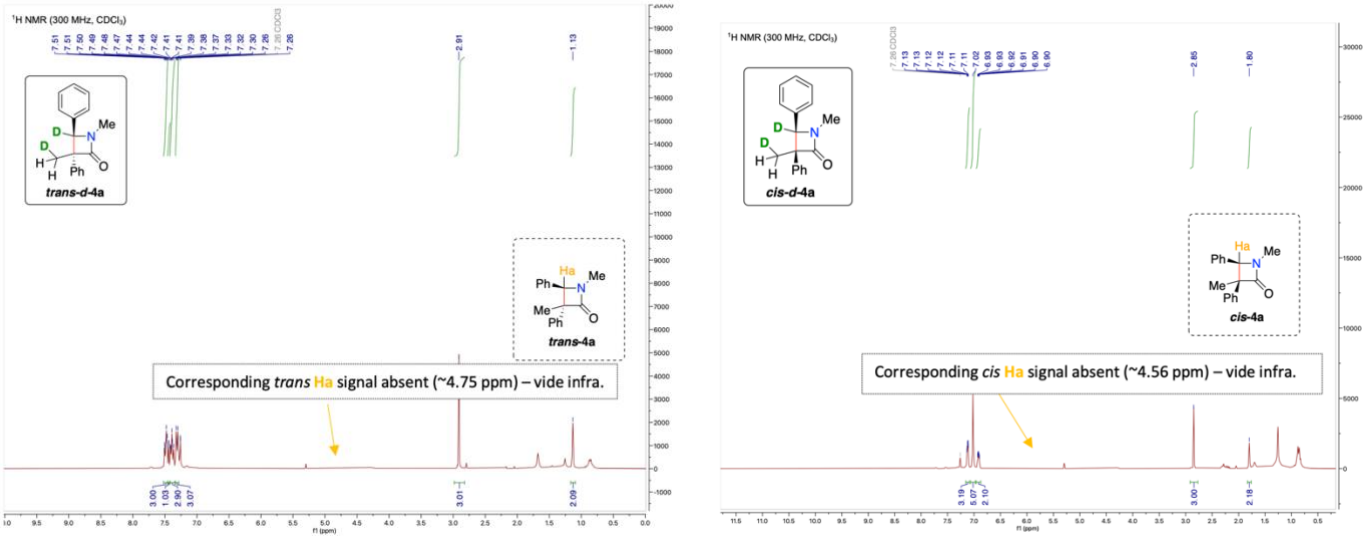

Figure 4.12: Deuterium labelling studies showing 100% deuterium incorporation.

In both the *trans* and *cis* product the corresponding Ha signal was absent, indicating 100% deuterium present at that position. Additionally, the methyl peak integrated for only 2 protons, indicating that the third proton is present as a deuterium atom. This confirms a 1,5-HAT is in operation.

A competition experiment between deuterated and undeuterated acrylamide was also performed in order to determine the primary kinetic isotope effect (KIE). The reaction was stopped after around 25% conversion and the crude reaction mixture was subjected to ^{1}H NMR (Figure 4.13).

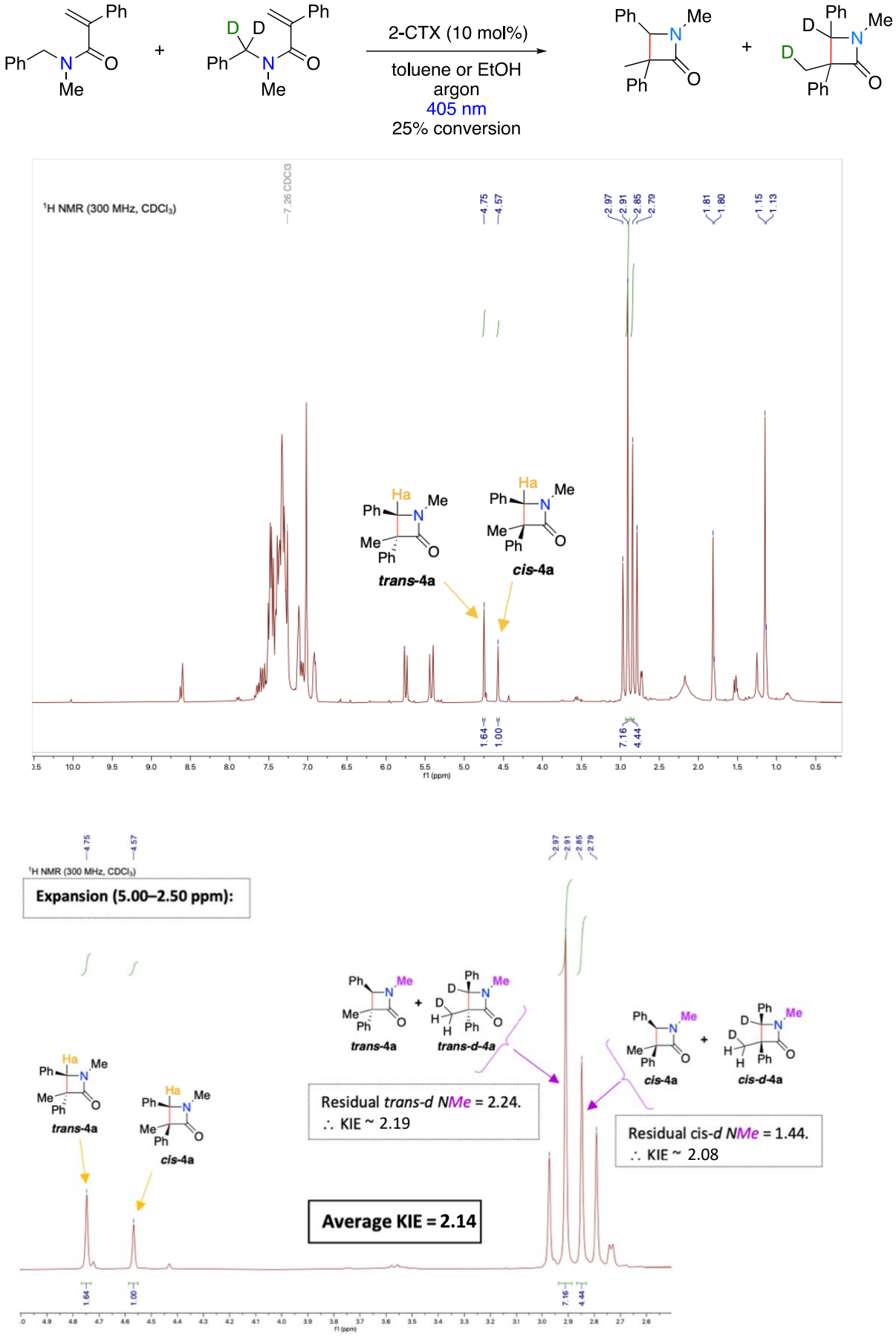

Figure 4.13: Competition experiment for KIE estimation.

It was determined that undeuterated β-lactam was present in a ratio of 1.64:1 of *trans* to *cis* isomers as seen by the integration of the Ha peaks at 4.75 and 4.57 ppm, respectively. The *N*-methyl peaks did not shift for the deuterated β-lactam, so we could determine the ratio of deuterated to undeuterated product by calculating the integration of the *N*-methyl peaks at 2.91 and 2.85 ppm for the *trans* and *cis* diastereomers, respectively. Firstly, considering the *cis N*-methyl peak at 2.85 ppm, this peak integrated for 4.44 protons. If we subtract the 3 protons associated with the undeuterated product, this gives a final integration of 1.44. This integration of 1.44 can be divided by 3 (for the 3 *N*-methyl protons of the deuterated *cis* diastereomer) to give a value of 0.48 for a single proton in the deuterated *cis* diastereomer. Comparing this to the integration of one proton in the undeuterated *cis* diastereomer (1), we get a ratio of 1:0.48, representing a KIE of **2.08**. Similarly, when we look at the *trans* diastereomer, the *N*-methyl peak at 2.91 ppm integrates for 7.16. Subtracting the undeuterated protons (3 x 1.64 = 4.92) we get an integration of 2.24 protons for the deuterated *trans* diastereomers. Dividing this by 3 gives a value of 0.75. This is a ratio of 1.64:0.75 for undeuterated to deuterated β-lactam, which represents a KIE of **2.19**. The average KIE is calculated at **2.14**.

Additionally, this experiment also represents a cross-over experiment which suggests that a chain mechanism proceeding via intermediate **4-exo-*I*** is unlikely as this would lead to mixtures of mono- and di-deuterated products as a result of HAT from competing starting material and/or possibly the solvent. This was not observed.

We were also aware that an alternative closed-shell pathway, via zwitterionic intermediate $\mathbf{C}_{s\text{-}trans}$ was also considered to be a potentially viable pathway. This is a similar mechanism to the Staudinger cyclisation that is a well known method for producing β-lactams. To gain further insight into whether a closed shell or open shell pathway was in operation, we performed DFT calculations. These calculations were performed by Dr William Unsworth, Ryan Epton and Jason Lynam from the University of York in the UK.

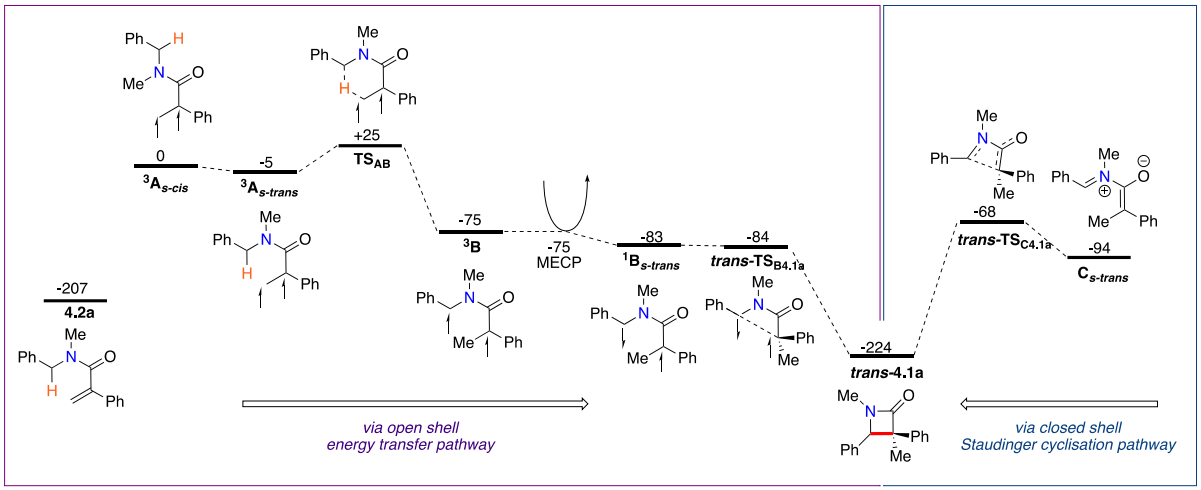

Figure 4.14: DFT studies showing the potential mechanistic pathways for the trans diastereomers. Energies are Gibbs free energies at 298.15 K in kJ mol^{-1} calculated at the D3(BJ)-UB3LYP/def2-TZVPP//UB3LYP/def2-SVP level of theory, with PCM solvent correction in toluene. The MECP structure and energy was found using Orca, at the D3(BJ)-UB3LYP/G/def2-TZVPP//UB3LYP/G/def2-SVP level of theory, which was compared with Orca calculated energies of ^3B and $^1B_{s\text{-}trans}$.

First, the open-shell energy transfer pathway was considered (Figure 4.14, purple box). The conversion of acrylamide **4.2a** into β-lactam **4.1a** was found to be thermodynamically favourable, with the two potential diastereomers ***trans*-4.1a** (shown in Figure 4.14) and ***cis*-4.1a** (not shown) being very close in energy. Energy transfer from the excited **2-CTX** photocatalyst to the ground state acrylamide **4.2a**, results in the triplet excited intermediate $^3\mathbf{A}_{s\text{-}cis}$. This state is located at 207 kJ mol^{-1} higher in energy than **4.2a**. The triplet energy of **2-CTX** is 260 kJ mol^{-1} [233] which implies that it is indeed capable of energy transfer to generate $^3\mathbf{A}$. The *trans* triplet intermediate $^3\mathbf{A}_{s\text{-}trans}$ is located at 5 kJ mol^{-1} lower in energy than the *cis* isomer. A 1,5-hydrogen migration can occur from $^3\mathbf{A}_{s\text{-}trans}$ through a low energy transition state ($\mathbf{TS_{AB}}$) to give $^3\mathbf{B}$. No viable routes to form the lactam ring directly from $^3\mathbf{B}$ were obtained and such a process would be spin-forbidden. Instead, conversion into the singlet is proposed to occur, and a minimum energy crossing point (MECP) was located at −75 kJ mol^{-1}. The singlet diradical $^1\mathbf{B}_{s\text{-}trans}$, was located at −83 kJ mol^{-1} (with respect $^3\mathbf{A}_{s\text{-}cis}$), which can then undergo an essentially barrierless carbon-carbon bond formation through ***trans*-$\mathbf{TS_{B4.1a}}$** to give ***trans*-4.1a**.[234]

The formation of the *cis* diastereomer ***cis*-4.1a** was found to occur through an almost identical and isoenergetic process. This similarity in energy levels of the *cis* and *trans* intermediates

would explain why no significant diastereoselectivity is seen with the experimental results. Although the formation of ***trans*-4.1** from ^{3}**B** is predicted to be essentially barrierless, a mechanistic route corresponding to the closed-shell Staudinger cyclisation pathway was also investigated (Figure 4.14, blue box). In this case, the closed-shell singlet (**C**$_{s\text{-}trans}$) undergoes lactam formation through ***trans*-TS**$_{C4.1a}$ which lies uphill at −68 kJ mol^{-1}. This is consistent with the calculated open-shell pathway being the dominant mechanistic pathway.

4.3.5 Sunlight Experiment

Given the efficiency of our photochemical reaction, we were curious about whether sunlight itself might be able to facilitate this process. If designed in this way, it would offer a highly sustainable strategy for the preparation highly valued medicinal targets. This a particularly powerful tool for Africa: given the limited resource and infrastructure on the continent, photocatalysis has the potential to offer practical solutions for the African continent to produce their own life-saving molecules at a fraction of the cost and powered exclusively by renewable-energy, due to the abundance of sunlight on the African continent in relation to the rest of the world.

The sun emits all colours of visible light as well as all frequencies of the electromagnetic waves except gamma rays (Figure 4.15).[235] It is therefore realistic to assume that irradiation by sunlight would excite the photocatalyst and induce the synthesis of β-lactams.

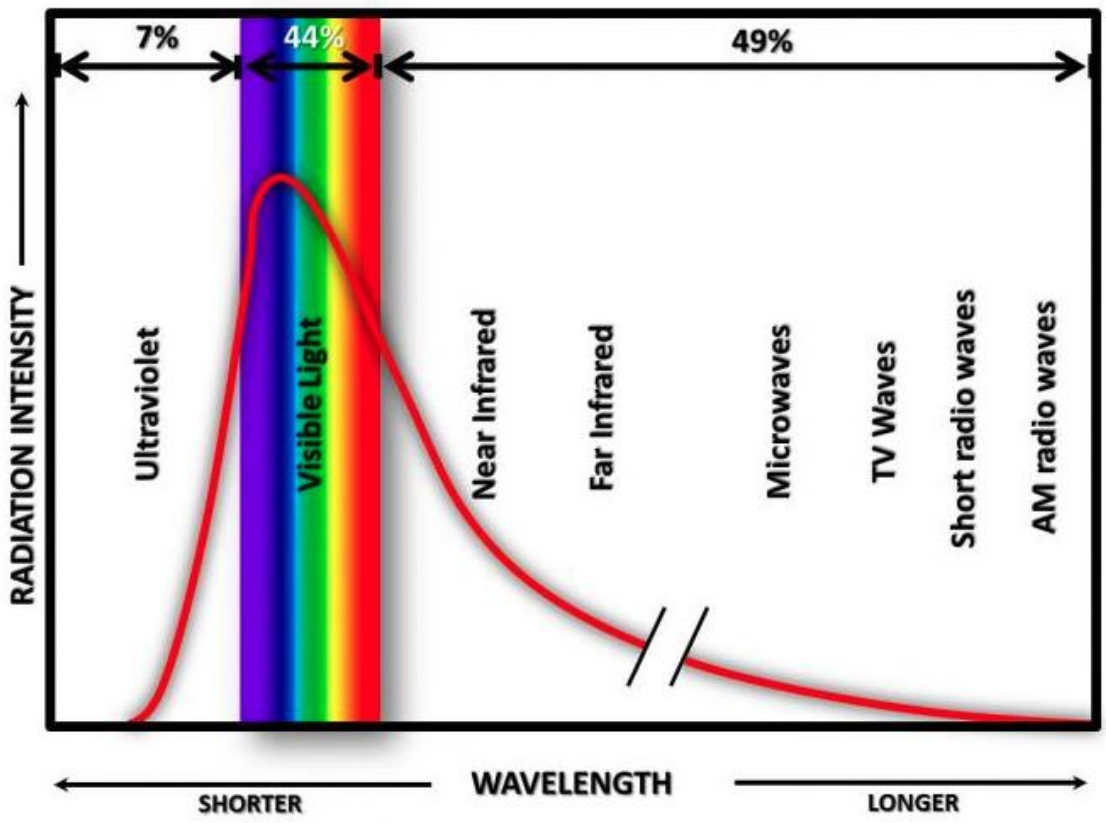

Figure 4.15: Sun's electromagnetic spectrum

To this end, we wanted to experiment with using direct irradiation by sunlight to excite the **2-CTX** photocatalyst. We set up a reaction of acrylamide **4.2a** using 75 mg starting material and 10% CTX in toluene. We used all the same reagents and equipment as the lab experiments but instead of placing the reaction vial in the photoredox box, we placed it on the roof of the Chemistry building. This experiment was performed in June and the reaction was left in the sun for 12 hrs. TLC after 12 hrs indicated that the β-lactam **4.1a** was formed in 68% as determined by crude ^{1}H NMR analysis. This was highly encouraging for us, especially considering this was performed in the South African winter.

4.4 Conclusion and Future Work

We have developed a convenient and straightforward procedure for the synthesis of β-lactams from simple and easily obtained acrylamide precursors using visible-light mediated energy transfer. We demonstrated the scope of the reaction by synthesising 30 substrates, varying the substituents at 3 different positions on the β-lactam ring all with good to excellent yields. The reaction is proposed to proceed via a rare carbon-to-carbon 1,5-HAT and enables

a C(sp^3)−H functionalisation. The proposed mechanism is supported by deuterium labelling experiments and computational studies.

Future work in this area includes developing methods to improve the diastereoselectivity of the reaction. Additionally, further investigation into the feasibility of performing this reaction with sunlight is necessary.

Given the high value of the β-lactam scaffold to the pharmaceutical industry, biological activity and SAR studies of these monobactams are currently being profiled for any interesting data.

5. Chapter 5 - Experimental

5.1 General Information

All reagents and photoinitiators were available by commercial sources (Sigma-Aldrich, Merck) and were used without further purification. Anhydrous solvents were obtained using a solvent purification system drying over 3Å molecular sieves. Photochemical reactions were carried out using an EvoluChemTM PhotoRedOx Box under irradiation at 450 and 405 nm using an EvoluChemTM LED (18 W or 30 W). Standard borosilicate glass vessels were used. Where required, reactions were heated using a standard stirrer/metal heating block combination fitted with a temperature probe. Reactions were monitored by TLC using aluminium-backed Merck silica-gel 60 F_{254} plates and were observed using both ultraviolet and fluorescent light or staining with acidic p-anisaldehyde or ninhydrin solutions. Column chromatography was carried out using Kieselgel 60 silica-gel (Merck). Nuclear Magnetic Resonance spectra were recorded on a Varian Mercury 300 MHz (75 MHz for 13C), Bruker 400 MHz (101 MHz for 13C), Bruker 600 MHz (151 MHz for 13C) instrument. All spectral data were acquired at 295 K. The chemical shifts are reported in parts per million (δ, ppm) downfield from tetramethylsilane (TMS, δ = 0.00 ppm) and are referenced to the residual solvent $CDCl_3$ (7.26 in ^{1}H NMR and 77.0 in ^{13}C). Coupling constants (*J*) are reported in Hertz (Hz). The multiplicity abbreviations used are br broad, s singlet, d doublet, t triplet, q quartet, m multiplet, app apparent. Infrared (IR) spectra were recorded on a PerkinElmer Spectrum 100 FT-IR spectrometer. High-resolution mass spectra were obtained from the University of Stellenbosch Mass Spectrometry Service and recorded in electrospray positive mode with a time-of-flight analyzer system on a Waters Synapt G2 machine. Melting points were determined using a Reichert-Jung Thermovar hot-stage microscope and are uncorrected.

5.2 Chapter 2 – Stereoselective Access to Oxindoles

5.2.1 General Procedure 2A: Synthesis of *N*-hydroxyphthalimido Oxamides

A solution of *N*-hydroxyphthalimide (1 equiv.) in anhydrous THF under argon was cooled to -78 °C and oxalyl chloride (5 equiv.) added dropwise. The reaction mixture was allowed to

slowly reach room temperature and then stirred overnight. The resulting solution was then concentrated on the rotary evaporator and dried under vacuum (to remove excess oxalyl chloride). The residue was re-dissolved in anhydrous THF, cooled to -78 °C followed by the sequential addition of the relevant chiral auxiliary (1 equiv.) in THF and pyridine (1 equiv.). The reaction mixture was once again allowed to reach room temperature and left to stir overnight. The organic solvent was removed in vacuo and the crude residue extracted using aqueous HCl (10%) and 3 washes of EtOAc. The combined organic extracts were then washed with sat. aqueous $NaHCO_3$ solution until the aqueous layer has changed from red to pale yellow. The combined organic extracts were then finally washed with sat. brine, dried over $MgSO_4$, filtered, and the organic solvent was removed in vacuo. The resulting crude white solid was then recrystallised from a minimum amount of hot EtOAc.

5.2.2 General Procedure 2B: Synthesis of *N*-Aryl Acrylamides

To a mixture of *N*-methylaniline (1 equiv.), acrylic acid (1.2 equiv.) and 2-chloro-1-methylpyridinium iodide (1.2 equiv.) in anhydrous CH_2Cl_2 (5 mL/mmol of aniline) at 0 °C under argon, was added triethylamine (3 equiv.) dropwise and the reaction mixture allowed to warm slowly to room temperature. Once the reaction was completed (by TLC) the organic phase was washed with aqueous HCl (1.0 M), followed by sat. aqueous Na_2CO_3 and dried over $MgSO_4$. The organic solvent were removed in vacuo and the resulting crude product was purified by column chromatography on silica gel or neutral alumina (petroleum ether:EtOAc gradient) to give acrylamide **2.1**.

5.2.3 General Procedure 2C: Photoredox Cyclisation

A solution of *N*-aryl acrylamide (1.4 equiv.), phthalimido oxamide (1 equiv.) and $Ir(ppy)_3$ (2 mol%) in toluene was degassed with argon for 10 minutes. The vial was then sealed and irradiated at 450 nm for 24 hours. The reaction solvent was removed under vacuum, and the compounds of interest (diastereomers) were then separated and purified by flash column chromatography from the resulting residue.

5.2.4 Characterisation Data for Compounds

_N_-methyl-_N_-phenylmethacrylamide (2.1a)[236,237]

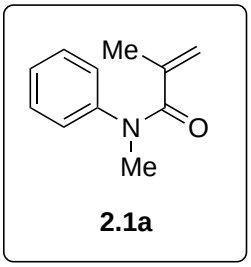

2.1a

Prepared according to general procedure 2B, using *N*-methylaniline (1 g, 9.33 mmol). Chromatography with EtOAc/hexane (10–30%) afforded **2.1a** (0.87 g, 53%) as a yellow oil. **R_f**: 0.32 (30% EtOAc/hexane); **^{1}H-NMR** (300 MHz, $CDCl_3$) δ (ppm) 7.40–7.06 (m, 5H), 5.03 (s, 1H), 5.00 (s, 1H), 3.34 (s, 3H), 1,73 (s, 3H); ^{13}C NMR (101 MHz, $CDCl_3$) δ (ppm) 172.2, 144.5, 140.5, 129.3, 127.0, 126.5, 119.6, 37.8, 20.3. Recorded data in accordance with those previously reported.

_N_-(4-methoxyphenyl)-_N_-methylmethacrylamide (2.1b)[237]

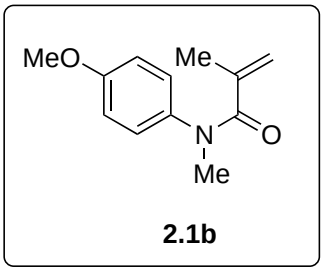

2.1b

Prepared according to general procedure 2B, using 4-methoxy-*N*–methylaniline (1g, 7.28 mmol). Chromatography with EtOAc/hexane (10–30%) afforded **2.1b** (1.2 g, 80%) as an orange oil. **R_f:** 0.15 (20% EtOAc/Hexane); **IR** (film, $\nu_{max/cm^{-1}}$): 1650, 1623; **^{1}H NMR** (300 MHz, $CDCl_3$) δ (ppm) 7.04 (app. d, *J* = 8.9 Hz, 2H), 6.84 (app. d, *J* = 8.9 Hz, 2H), 5.01 (s, 1H), 4.98 (s, 1H), 3.80 (s, 3H), 3.29 (s, 3H), 1.73 (s, 3H); **^{13}C NMR** (101 MHz, $CDCl_3$) δ (ppm) 172.3, 158.5, 141.1, 137.6, 127.9, 119.0, 114.5, 55.6, 38.0, 20.5; HRMS (ESI^+) *m/z*: Calculated for $C_{12}H_{16}NO_2$ (M+H): 206.1176, Found: 206.1182. Recorded data in accordance with those previously reported.

2-((*4S,5R*)-3,4-dimethyl-2-oxo-5-phenylimidazolidin-1-yl)-2-oxoacetic acid (2.2)

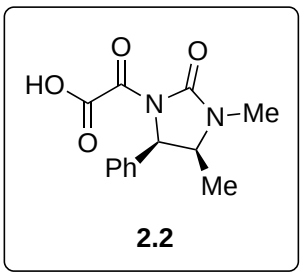

2.2

To a solution of (*4R,5S*)-1,5-dimethyl-4-phenylimidazolidin-2-one[85] (300 mg, 1.58 mmol, 1 equiv.) in anhydrous THF (30 mL) cooled to -78 °C, was added oxalyl chloride (0.26 mL, 3.15 mmol, 2 equiv.) dropwise and the reaction mixture was allowed was allowed to slowly come to room temperature. The reaction was stirred for a further 3 hours, before adding 1M aqueous NaOH (4 mL, 4 mmol, 2.5 equiv.) dropwise. The solution was concentrated under vacuum, and the resulting yellow paste was extracted with sat. $NaHCO_3$ solution and EtOAc. The aqueous layer was acidified with 1 M HCl, and extracted

with EtOAc, and the combined organic washings were dried over $MgSO_4$. The organic solution was then concentrated and dried under vacuum to yield **2.2** (336 mg, 81%) as a white solid. **R_f:** 0.11 (10% MeOH/DCM); **M.P.** 185-188 °C; **IR** (film, $\nu_{max/cm^{-1}}$): 3069, 1758, 1692, 1432, 1335, 1177; **^{1}H NMR** (300 MHz, $CDCl_3$) δ (ppm) 7.42–7.29 (m, 3H), 7.24–7.17 (m, 2H), 5.35 (d, *J* = 6.5 Hz, 1H), 4.15–4.06 (m, 1H), 2.83 (s, 3H), 0.80 (d, *J* = 4.9 Hz, 3H); **^{13}C NMR** (101 MHz, $CDCl_3$) δ (ppm) 164.9, 162.4, 155.9, 136.9, 129.6, 129.4, 128.1, 59.3, 56.5, 28.2, 15.1 **HRMS** (ESI^+) *m/z*: Calculated for $C_{21}H_{18}N_3O_6$ $(M+H)^+$: 263.1026, Found: 263.1036.

3-(2-((4S,5R)-3,4-dimethyl-2-oxo-5-phenylimidazolidin-1-yl)-2-oxoethyl)-1,3-dimethylindolin-2-one (2.3a)

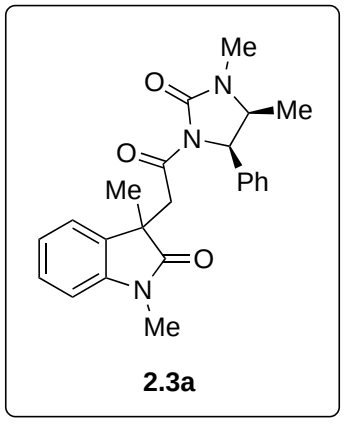

2.3a

Prepared according to general procedure 2C. Using **2.1a** (59.6 mg, 0.34 mmol), **2.5** (100mg, 0.24 mmol) and $Ir(ppy)_3$ (3.21 mg, 2 mol %) was obtained **2.3a** (51.0 mg, 76%; d.r.: 1.3:1).

2.3a-D1: 28.8 mg; yellow amorphous solid; **R_f**: 0.21 (70% EtOAc/Hexane); **IR** (film, $\nu_{max/cm^{-1}}$): 2975, 2924, 1708, 1613, 1380; **^{1}H-NMR** (300 MHz, $CDCl_3$) δ(ppm) 7.40–7.05 (m, 5H), 6.98– 6.91 (m, 1H), 6.80–6.71 (m, 1H), 5.09 (d, *J* = 8.52, 1H), 4.13 (d, *J* = 16.9Hz,1H), 3.89 (dq,J_1 = 8.2Hz, J_2 = 6.6Hz, 1H), 3.37 (d, *J*= 16.8, 1H), 3.12 (s, 3H), 2.76 (s, 3H), 3.34 (s, 3H), 0.76 (d, *J* = 6.5, 3H); **^{13}C-NMR** (101 MHz, $CDCl_3$) δ(ppm) 180.6, 168.7, 155.9, 143.7, 136.0, 128.7, 128.3, 127.7, 127.6, 126.6, 122.1, 108.1, 59.1, 54.0, 45.9, 42.1, 28.3, 26.4, 25.1; HRMS (ESI^+) *m/z*: Calculated for $C_{23}H_{26}N_3O_3$ $(M+H)^+$: 392.1969, Found: 392.1979.

2.3a-D2: 22.1 mg; oil; **R_f:** 0.48 (70% EtOAc/Hexane); **IR** (film, $\nu_{max/cm^{-1}}$): 2923, 2854, 1707, 1611, 1379, 1235; **^{1}H-NMR** (300 MHz, $CDCl_3$) δ(ppm) 7.30–7.18 (m, 5H), 7.16–7.10 (m, 1H), 7.04–6.92 (m, 3H), 6.82–6.77 (m, 1H), 5.01 (d, *J* = 8.4 Hz, 1H), 4.06 (d, *J* = 17.1 Hz, 1H), 3.71 (dq, J_1 = 8.4 Hz, J_2 = 6.7 Hz, 1H), 3.37 (d, *J* = 17.0 Hz, 1H), 3.14 (s, 3H), 2.79 (s, 3H), 1.38 (s, 3H), 0.70 (d, *J* = 6.6 Hz, 3H); **^{13}C-NMR** (101 MHz, $CDCl_3$) δ(ppm) 180.3, 168.7, 156.1, 143.9, 136.1, 134.0, 128.6, 128.1, 127.9, 127.0, 122.0, 108.1, 59.1, 54.1, 45.8, 42.5, 28.2, 26.5, 25.0, ; HRMS (ESI^+) *m/z*: Calculated for $C_{23}H_{26}N_3O_3$ $(M+H)^+$: 392.1969, Found: 392.1974.

3-(2-((*4S,5R*)-3,4-dimethyl-2-oxo-5-phenylimidazolidin-1-yl)-2-oxoethyl)-1,3,5-trimethylindolin-2-one (2.3b)

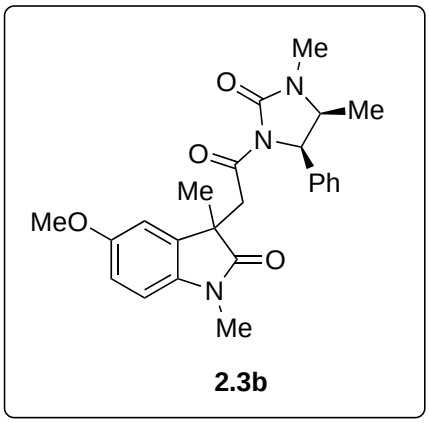

2.3b

Prepared according to general procedure 2C. Using **2.1b** (64.3 mg, 0.34 mmol), **2.5** (100 mg, 0.24 mmol) and $Ir(ppy)_3$ (3.21 mg, 2 mol %) was obtained **2.3b** (83.0 mg, 85%; d.r.: 1.1:1).

2.3b-D1: 43 mg; pale yellow solid; **M.P.** 183-193 °C ; **R_f**: 0.24 (70% EtOAc/Hexane); **IR**: 2965, 2915, 1706, 1607, 1380, 1236; **^{1}H-NMR** (300 MHz, $CDCl_3$) δ(ppm) 7.15–7.06 (m, 3H), 6.99 (s, 1H), 6.92 (d, *J* = 7.9 Hz, 1H), 6.83–6.73 (m, 2H), 6.54 (d, *J* = 7.8 Hz, 1H), 5.09 (d, *J* = 8.4 Hz, 1H), 4.08 (d, *J* = 17.2 Hz, 1H), 3.81 (m, 1H), 3.37 (d, *J* = 17.1 Hz, 1H), 3.10 (s, 3H), 2.77 (s, 3H), 2.29 (s, 3H), 1.34 (s, 3H), 0.68 (d, *J* = 6.5 Hz, 3H); **^{13}C-NMR** (101 MHz, $CDCl_3$) δ(ppm) 180.6, 168.7, 155.9, 141.3, 136.0, 133.7, 131.3, 128.2, 127.9, 127.6, 126.6, 122.8, 107.8, 59.1, 54.0, 45.9, 42.2, 28.2, 26.4, 25.2, 21.3, 15.0; **HRMS** (ESI^+) *m/z*: Calculated for $C_{24}H_{28}N_3O_3$ $(M+H)^+$: 406.2125, Found: 406.2144.

2.3b-D2: 40 mg; orange-yellow amorphous solid; **R_f:** 0.52 (70% EtOAc/Hexane); **IR** (film, ν_{max}/cm^{-1}): 2919, 2852, 1710, 1624, 1374, 1229; **^{1}H-NMR** (300 MHz, $CDCl_3$) δ(ppm) 7.30–7.20 (m, 3H), 7.05-6.65 (m, 5H), 5.03 (d, *J* = 8.4 Hz, 1H), 4.02 (d, *J* = 17.3 Hz, 1H), 3.72 (m, 1H), 3.38 (d, *J* = 17.3 Hz, 1H), 3.12 (s, 3H), 2.79 (s, 3H), 2.28 (s, 3H), 1.35 (s, 1H), 0.70 (d, *J* = 6.6 Hz, 3H); **^{13}C-NMR** (101 MHz, $CDCl_3$) δ(ppm) 180.2, 168.7, 156.1, 141.5, 136.1, 134.0, 131.3, 128.8, 128.5, 128.1, 126.9, 122.9, 107.8, 59.0, 54.1, 45.7, 42.6, 28.2, 26.5, 25.1, 21.3, 14.9; **HRMS** (ESI^+) *m/z*: Calculated for $C_{24}H_{28}N_3O_3$ $(M+H)^+$: 406.2125, Found: 406.2125.

1,3-Dioxoisoindolin-2-yl-2-((*4S,5R*)-3,4-dimethyl-2-oxo-5-phenylimidazolidin-1-yl)-2-oxoacetate (2.5)

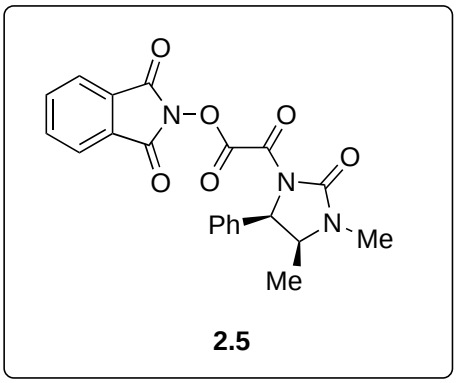

2.5

Prepared according to general procedure 2A, using *N*-hydroxyphthalimide (1.5 g, 9.20 mmol) and (*4R,5S*)-1,5-dimethyl-4-phenylimidazolidin-2-one as the relevant chiral auxiliary. Recrystallisation afforded **2.5** (1.85 g, 49%) as glittery white crystals. **R_f**: 0.43 (70% EtOAc/Hexane); **M.P.** 231-233 °C; **IR** (film, ν_{max}/cm^{-1}): 1824, 1788, 1736, 1694, 1400, 1127, 972, 695; **^{1}H NMR** (300 MHz, $CDCl_3$) δ (ppm) 7.98–7.87 (m, 2H), 7.84–7.75 (m, 2H), 7.41–7.16 (m, 5H), 5.34 (d, *J*

= 8.6 Hz, 1H), 4.18-4.02 (m, 1H), 2.92 (s, 3H), 0.86 (d, *J* = 6.6, 3H); **^{13}C NMR** (101 MHz, $CDCl_3$) δ (ppm) 161.1, 157.4, 155.7, 153.8, 135.0, 134.2, 129.0, 128.9, 128.9, 127.1, 124.3, 58.5, 55.5, 28.3, 15.1; **HRMS** (ESI^+) *m/z:* Calculated for $C_{21}H_{18}N_3O_6$ (M+H): 408.1190, Found: 408.1204.

2,2,6,6-tetramethylpiperidin-1-yl (4S,5R)-3,4-dimethyl-2-oxo-5-phenylimidazolidine-1-carboxylate 2.6

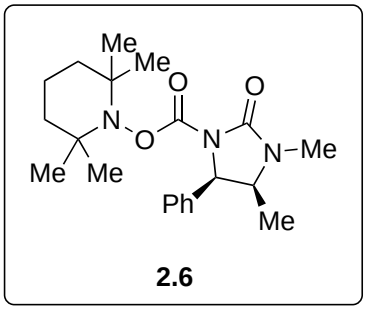

2.6

Prepared according to general procedure 2C using TEMPO (53.1 mg, 0.34 mmol, 1.4 equiv.), NEt_3 (0.05 mL, 0.34 mmol, 1.4 equiv.), **2.1b** (69.8 mg, 0.34 mmol), **2.5** (100 mg, 0.24 mmol) and $Ir(ppy)_3$ (3.2 mg, 2 mol %) was obtained **2.6** (43.6 mg, 48%) as a white solid. **R_f:** 0.50 (EtOAc); **M.P.** 197-210 °C; **IR** (film, $\nu_{max/cm^{-1}}$): 1777, 1697, 1330, 1223; **^{1}H-NMR** (300 MHz, $CDCl_3$) δ(ppm) 7.36–7.14 (m, 5H), 5.14 (d, *J* = 8.5 Hz, 1H), 3.91 (m, 1H), 2.81 (s, 3H), 1.68–1.21 (m, 6H), 1.17 (s, 3H), 0.98 (s, 3H), 0.90 (s, 3H), 0.79 (d, *J* = 6.6 Hz, 3H), 0.76 (s, 3H); **^{13}C-NMR** (101 MHz, $CDCl_3$) δ(ppm) 155.1, 152.5, 137.0, 128.6, 128.3, 127.1, 60.7, 60.5, 60.4, 54.4, 39.2, 39.1, 31.8, 31.7, 28.4, 21.3, 20.5, 17.0, 15.2; **HRMS** (ESI^+) *m/z*: Calculated for $CH_{25}N_4O_3$ $(M+H)^+$: 374,2438, Found: 374.2452.

1,3-dioxoisoindolin-2-yl (R)-2-(5-benzyl-3-methyl-2-oxoimidazolidin-1-yl)-2-oxoacetate (2.7)

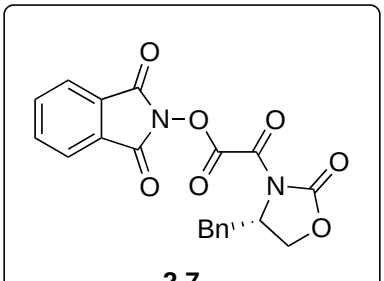

2.7

Prepared according to general procedure 2A, using with *N*-hydroxyphthalimide (0.500 g, 3.07 mmol) and the lithium anion of (*R*)-4-benzyloxazolidin-2-one, generated by stirring in THF (30 mL) with *n*-butyllithium (2.5 M in THF, 1.2 equiv.) for 30 min, afforded **2.7** (880 mg, 50%) as white crystals.

R_f = 0.73 (70% EtOAc/Hexane); white solid; **M.P.** 169-171 °C; **IR** (film, vmax/cm^{-1}): 1793, 1739, 1697, 1388, 1139, 1020; **^{1}H NMR** (300 MHz, $CDCl_3$) δ (ppm) 7.97–7.77 (m, 4H), 7.41–7.14 (m, 5H), 4.77 (m, 1H), 4.51–4.33 (m, 2H), 3.47–3.38 (m, 1H), 3.02–2.91 (m, 1H); **^{13}C NMR** (101 MHz, $CDCl_3$) δ (ppm) 160.8, 156.7, 156.2, 152.4, 135.1, 134.0, 129.6, 129.4, 129.2, 128.9, 127.9, 124.4, 68.2, 54.3, 37.3.

(4R)-3-(2-(1,3-Dimethyl-2-oxoindolin-3-yl)acetyl)-4-(2-oxo-2-phenylethyl)oxazolidin-2-one (2.8)

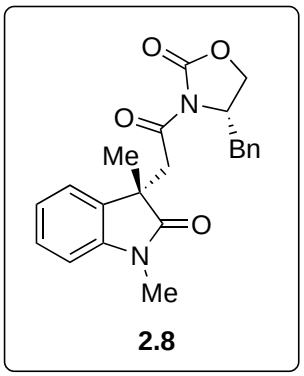

2.8

General procedure 2B on a slightly modified scale, with *N*-methyl-*N*-phenylmethacrylamide (**2.1b**)[134] (31.1 mg, 0.18 mmol), **2.7** (50 mg, 0.13 mmol), and $Ir(ppy)_3$ (1.7 mg, 2.6 ummol), afforded **2.8** (33 mg, 69% yield; 1:1 dr).

2.8-D1: Yield: 16 mg; white amorphous solid; $\mathbf{R_f}$ = 0.51 (1:1 EtOAc:petroleum ether). **IR** (film, $\nu_{max/cm^{-1}}$): 2927, 1767, 1706, 1613, 1383, 1220, 1111 cm^{-1}; **^{1}H NMR** (300 MHz, $CDCl_3$): δ = 7.33–7.21 (m, 4 H), 7.17–7.09 (m, 3 H), 7.06–7.00 (m, 1 H), 6.91–6.88 (m, 1 H), 4.50–4.38 (m, 1 H), 4.10–4.06 (m,2H), 3.83 (d, J=13.4Hz, 1H), 3.47 (d, J=13.4Hz, 1H), 3.30 (s, 3 H), 3.16–3.10 (m, 1 H), 2.74–2.66 (m, 1 H), 1.41 (s, 3 H). **^{13}C NMR** (101 MHz, $CDCl_3$): δ = 180.3, 169.5, 153.7, 144.0, 135.1, 133.7, 129.6, 129.0, 128.2, 127.4, 122.3, 121.8, 108.3, 66.3, 54.8, 45.5, 42.7, 37.6, 26.6, 25.1; **HRMS** (ESI^+): m/z $[M + H]^+$ calcd for $C_{22}H_{25}N_4O_3$: 379.1652; found: 379.1673.

2.8-D2: Yield: 17 mg; colourless oil; $\mathbf{R_f}$ = 0.33 (7:3 EtOAc:petroleum ether); **IR** (film, $\nu_{max/cm^{-1}}$): 2929, 1769, 1701, 1611, 1381, 1219, 1110 cm^{-1}; **^{1}H NMR** (300 MHz, $CDCl_3$): δ = 7.37–7.15 (m, 5 H), 7.10–7.04 (m, 1 H), 6.99–6.94 (m, 2 H), 6.91–6.86 (m, 1 H), 4.54–4.43 (m, 1 H), 4.19–4.02 (m, 2 H), 3.92 (d, J = 13.1 Hz, 1 H), 3.37 (d, J = 13.1 Hz, 1 H), 3.30 (s, 3 H), 2.81–2.74 (m, 1 H), 2.51–2.42 (m, 1 H), 1.42 (s, 3 H); **^{13}C NMR** (101 MHz, $CDCl_3$): δ = 180.4, 169.4, 153.6, 144.1, 135.1, 133.5, 129.5, 129.0, 128.2, 127.4, 122.3, 121.9, 108.4, 66.3, 54.8, 45.8, 42.5, 37.3, 26.6, 25.0; **HRMS** (ESI^+): m/z $[M + H]^+$ calcd for $C_{22}H_{25}N_4O_3$: 379.1652; found: 379.1656.

5.3 Chapter 3 – Thioxanthone Catalysed Triplet Energy Transfer for the Synthesis of 3,4-Dihydroquinolin-2-ones

5.3.1 Synthesis of 2-ITX[238]

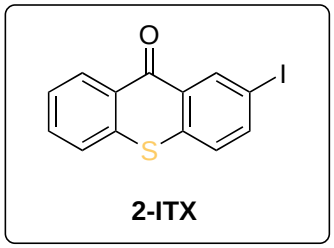

2-ITX

To a mixture of iodobenzene (6.1 mL, 54.0 mmol) in H_2SO_4 (80 mL, 1.50 mol) was added 2-mercaptobenzoic acid (2.00 g, 13.0 mmol) in portions. After stirring at room temperature for 24 h, the reaction mixture was heated at 70 °C for 90 min, cooled, and

then poured over ice (approx. 75–100 g). The mixture was then extracted with CH_2Cl_2 (3 x 50 mL) and washed with brine. The combined organic extracts were removed in vacuo and the crude residue purified by silica gel chromatography eluting with CH_2Cl_2 to afford **2-ITX** as a light yellow solid (1.632 g, 37%). $\mathbf{R_f}$ = 0.79 (CH_2Cl_2); **M.P.** 145 °C; **^{1}H NMR** (300 MHz, $CDCl_3$) δ 8.89 (d, *J* = 2.0 Hz, 1H), 8.57 (dd, *J* = 8.1, 1.1 Hz, 1H), 7.84 (dd, *J* = 8.5, 2.0 Hz, 1H), 7.66–7.42 (m, 3H), 7.28 (d, *J* = 8.5 Hz, 1H); **^{13}C NMR** (75 MHz, $CDCl_3$) δ 178.7, 140.7, 138.7, 136.9, 136.9, 132.7, 130.6, 130.1, 129.0, 127.6, 126.7, 126.2, 90.9. Recorded data in accordance with those previously reported.

5.3.2 General procedure 3A: Synthesis of acrylamides (3.2) using Mukaiyama's reagent

To a mixture of aniline (1 equiv.), carboxylic acid (1.2 equiv.) and 2-chloro-1-methylpyridinium iodide (1.2–1.4 equiv.) in CH_2Cl_2 (5 mL/mmol of aniline) at 0 °C under argon, was added triethylamine (3 equiv.) dropwise and the reaction mixture allowed to warm slowly to room temperature. Once the reaction was completed (by TLC) the organic phase was washed with aqueous HCl (1.0 M), followed by sat. aqueous Na_2CO_3 and dried over $MgSO_4$. The organic solvent were removed in vacuo and the resulting crude product was purified by column chromatography on silica gel or neutral alumina (petroleum ether:EtOAc gradient) to give acrylamide **3.2**.

5.3.3 General procedure 3B: Synthesis of acrylamides (3.2) via acid chlorides

To a mixture of carboxylic acid (1 equiv.) in dry CH_2Cl_2 (5 mL per mmol of atropic acid) was added a catalytic amount of DMF (0.1 mL per mmol of carboxylic acid). At rt, oxalyl chloride (1.5 equiv.) was added dropwise over a period of 30 min. The resulting mixture was stirred for 3 h and the solvent was removed under reduced pressure. The residue was redissolved in dry CH_2Cl_2 (4 mL per mmoL) and a solution of the aniline derivative (0.8–1 equiv.) and triethylamine (2.5 equiv.) in dry CH_2Cl_2 (2 mL per mmol of aniline) was added. The reaction mixture was stirred at rt and monitored by TLC until completion. The mixture was diluted with CH_2Cl_2, washed with sat. aqueous NH_4Cl and sat. aqueous NaCl, and then dried over $MgSO_4$. The solvent was removed under reduced pressure and the resulting residue purified by silica column chromatography (petroleum ether/EtOAc gradient) to afford acrylamide **3.2**.

5.3.4 Characterization data for *N*-acrylamides (3.2)

N-methyl-*N*,2-diphenylacrylamide (3.2a)[239]

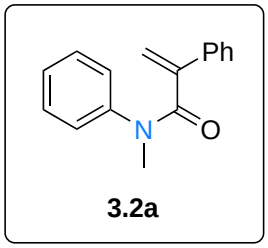

3.2a

Prepared according to general procedure 3A using *N*-methylaniline (0.500 g, 4.66 mmol), 2-phenylacrylic acid (0.828 g, 5.60 mmol), 2-chloro-1-methylpyridinium iodide (1.422 g, 5.56 mmol) and triethylamine (1.94 mL, 13.90 mmol) in CH_2Cl_2 (20 mL). Chromatography on silica gel with EtOAc/petroleum ether (20–40%) afforded **3.2a** as a clear oil (1.138 g, 96% yield). $\mathbf{R_f}$ = 0.18 (2:8 EtOAc: petroleum ether); **IR** (film, vmax/cm^{-1}) 3030, 1645, 1613, 1593, 1494, 1422, 1377, 1305, 1243, 1130, 1095, 1024, 940, 773, 760, 695; **^{1}H NMR** (300 MHz, $CDCl_3$) δ 7.21–7.12 (m, 8H), 6.96–6.94m (m, 2H), 5.48 (s, 1H), 5.37 (s, 1H), 3.39 (s, 3H); **^{13}C NMR** (101 MHz, $CDCl_3$) δ 170.7, 145.9, 143.8, 137.0, 129.0, 128.4, 128.0, 127.1, 127.0, 126.2, 117.9, 37.5; **HRMS** (ESI$^+$) *m/z*: [M + H] calcd for $C_{16}H_{16}NO^+$ 238.1226; found 238.1240. Recorded data in accordance with those previously reported.

N-methyl-2-phenyl-*N*-(phenyl-d_5)acrylamide (d_5-3.2a)

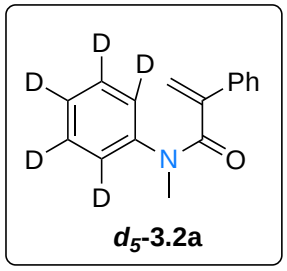

***d*$_5$-3.2a**

Prepared according to general procedure 3A using *N*-methylbenzen-d_5-amine[240] (0.097 g, 0.83 mmol), 2-phenylacrylic acid (0.148 g, 1.00 mmol), 2-chloro-1-methylpyridinium iodide (0.255 g 1.00 mmol) and triethylamine (0.348 mL, 2.50 mmol) in CH_2Cl_2 (10 mL). Chromatography on silica gel with EtOAc/petroleum ether (20–40%) afforded ***d*$_5$-3.2a** as a white solid (0.168 g, 83.8% yield). Recrystallization with CH_2Cl_2:hexane afforded a white crystalline solid. $\mathbf{R_f}$ = 0.22 (2:8 EtOAc:petroleum ether); **M.P.** 31–33°C; **IR** (film, vmax/cm^{-1}) 3055, 2937, 2271, 1638, 1610, 1562, 1497, 1426, 1404, 1368, 1233, 1079, 9322, 779, 693; **^{1}H NMR** (300 MHz, $CDCl_3$) δ 7.28–7.11 (m, 5H), 5.47 (s, 1H), 5.37 (s, 1H), 3.40 (s, 3H); **^{13}C NMR** (101 MHz, $CDCl_3$) δ 170.7, 145.9, 143.7, 137.0, 128.7, 128.4, 128.2, 128.1, 126.7, 126.5, 126.2, 117.9, 37.5; **HRMS** (ESI$^+$) *m/z*: [M + H] calcd for $C_{16}H_{11}D_5NO^+$ 243.1540; found 243.1554.

***N*-methyl-2-phenyl-*N*-(*p*-tolyl)acrylamide (3.2b)**[239]

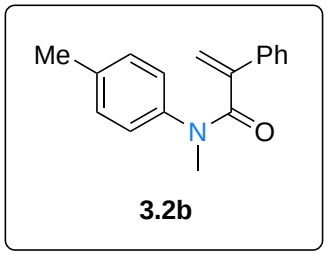

3.2b

Prepared according to general procedure 3A using *N*,4-dimethylaniline (0.206 g, 1.70 mmol), atropic acid (0.302 g, 2.04 mmol), 2-chloro-1-methylpyridinium iodide (0.520 g, 2.04 mmol) and triethylamine (0.71 mL, 5.10 mmol) in CH_2Cl_2 (20 mL). Chromatography on silica gel with EtOAc/petroleum ether (10–25%) afforded **3.2b** as a light yellow oil (0.403 g, 94% yield). $\mathbf{R_f}$ = 0.49 (2:8 EtOAc:petroleum ether); **IR** (film, $\nu_{max/cm^{-1}}$) 3048, 2926, 1646, 1608, 1514, 1496, 1426, 1376, 1254, 1130, 909, 823, 780, 735, 700; **^{1}H NMR** (600 MHz, $CDCl_3$) δ 7.31–7.11 (m, 5H), 7.01–6.71 (m, 4H), 5.45 (bs, 1H), 5.31 (bs, 1H), 3.37 (s, 3H), 2.26 (s, 3H); **^{13}C NMR** (101 MHz, $CDCl_3$) δ 170.8, 145.9, 141.4, 137.2, 136.9, 129.6, 128.3, 128.0, 126.9, 126.2, 117.5, 37.5, 21.1; **HRMS** (ESI^+) *m/z*: [M + H] calcd for $C_{17}H_{18}NO^+$ 252.1383; found 252.1392. Recorded data in accordance with those previously reported.

***N*-(4-methoxyphenyl)-*N*-methyl-2-phenylacrylamide (3.2c)**[239]

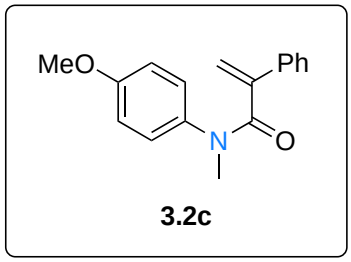

3.2c

Prepared according to general procedure 3A using 4-methoxy-*N*-methylaniline (0.300 g, 2.19 mmol), atropic acid (0.388 g, 2.62 mmol), 2-chloro-1-methylpyridinium iodide (0.670 g, 2.62 mmol) and triethylamine (0.91 mL, 6.56 mmol) in CH_2Cl_2 (20 mL). Chromatography on silica gel with EtOAc/petroleum ether (10–25%) afforded **3.2c** as a colourless oil (0.501 g, 86% yield). $\mathbf{R_f}$ = 0.34 (2:8 EtOAc:petroleum ether); **IR** (film, $\nu_{max/cm^{-1}}$) 2936, 2838, 1644, 1618, 1511, 1444, 1377, 1294, 1247, 1181, 1131, 1107, 1040, 1028, 910, 836, 780; **^{1}H NMR** (600 MHz, $CDCl_3$) δ 7.25–7.12 (m, 5H), 6.80 (d, *J* = 8.7 Hz, 2H), 6.63 (d, *J* = 8.7 Hz, 2H), 5.43 (bs, 1H), 5.33 (bs, 1H), 3.72 (s, 3H), 3.35 (s, 3H); **^{13}C NMR** (101 MHz, $CDCl_3$) δ 171.0, 158.3, 146.0, 137.1, 136.6, 128.3, 128.3, 128.0, 126.1, 117.5, 114.0, 55.5, 37.6. Recorded data in accordance with those previously reported.

***N*-methyl-2-phenyl-*N*-(4-(trifluoromethyl)phenyl)acrylamide (3.2d)**

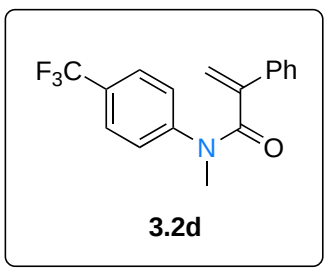

3.2d

Prepared according to general procedure 3B using atropic acid (0.500 g, 3.35 mmol), oxalyl chloride (0.423 mL, 5.00 mmol) and DMF (0.34 mL) in CH_2Cl_2 (15 mL). The residue was redissolved in dry CH_2Cl_2 (10 mL) and a solution of *N*-methyl-4-(trifluoromethyl)aniline (0.525 g, 3.00 mmol) and triethylamine

(1.04 mL, 7.50 mmol) in dry CH_2Cl_2 (10 mL) was added. Chromatography on silica gel with EtOAc/ petroleum ether (20–40%) afforded **3.2d** as a clear oil (0.244 g, 27% yield). $\mathbf{R_f}$ = 0.25 (2:8 EtOAc: petroleum ether); **IR** (film, vmax/cm^{-1}) 2926, 1655, 1611, 1518, 1371, 1325, 1249, 1167, 1125, 1058 848, 774, 702, 603, 532; **^{1}H NMR** (300 MHz, $CDCl_3$) δ 7.44–7.41 (m, 2H), 7.24–7.10 (m, 7H), 5.56 (s, 1H), 5.45 (s, 1H), 3.40 (s, 3H); **^{13}C NMR** (101 MHz, $CDCl_3$) δ 170.6, 146.8, 145.6, 136.6, 128.6 (q, $J_{C\text{-}F}$ = 30.3 Hz), 128.6, 128.4, 127.1, 126.2, 126.1, 123.8 (q, $J_{C\text{-}F}$ = 272.7 Hz), 118.6 (br s), 37.6; **HRMS** (ESI^+) *m/z*: [M + H] calcd for $C_{17}H_{15}F_3NO^+$ 306.1100; found 306.1107.

N-(4-chlorophenyl)-*N*-methyl-2-phenylacrylamide (3.2e)

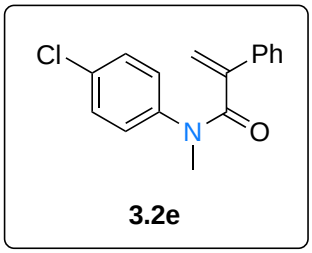

3.2e

Prepared according to general procedure 3A using 4-chloro-*N*-methylaniline (0.141 g, 1.00 mmol), 2-phenylacrylic acid (0.207g, 1.40 mmol), 2-chloro-1-methylpyridinium iodide (0.306 g, 1.20 mmol) and triethylamine (0.418 mL, 3 mmol) in CH_2Cl_2 (10 mL). Chromatography on silica gel with EtOAc/petroleum ether (20–40%) afforded **3.2e** as a white solid (0.185 g, 68% yield). Recrystallization with CH_2Cl_2:hexane afforded a white crystalline solid. $\mathbf{R_f}$ = 0.22 (2:8 EtOAc:petroleum ether); **M.P.** 54–55 °C; **IR** (film, vmax/cm^{-1}) 3057, 1646, 1620, 1495, 1487, 1370, 1242, 1125, 1094, 916, 835, 783, 710, 545, 519; **^{1}H NMR** (300 MHz, $CDCl_3$) δ 7.24–7.10 (m, 7H), 6.91–6.75 (m, 2H), 5.51 (s, 1H), 5.39 (s, 1H), 3.36 (s, 3H); **^{13}C NMR** (101 MHz, $CDCl_3$) δ 170.6, 145.8, 142.3, 136.8, 132.7, 129.1, 128.6, 128.4, 128.3, 126.2, 118.2, 37.6; **HRMS** (ESI^+) *m/z*: [M + H] calcd for $C_{16}H_{15}ClNO^+$ 272.0837; found 272.0846.

N-(4-fluorophenyl)-*N*-methyl-2-phenylacrylamide (3.2f)[239]

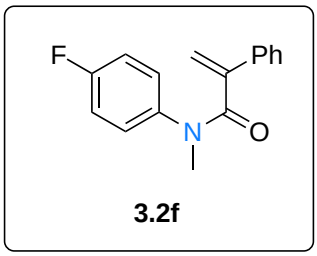

3.2f

Prepared according to general procedure 3A using 4-fluoro-*N*-methylaniline (0.500 g, 4.00 mmol), atropic acid (0.710 g, 4.80 mmol), 2-chloro-1-methylpyridinium iodide (1.23 g, 4.80 mmol) and triethylamine (1.67 mL, 12.0 mmol) in CH_2Cl_2 (50 mL). Chromatography on silica gel with EtOAc/petroleum ether (10–25%) afforded **3.2f** as a colourless oil (0.697 g, 68% yield). $\mathbf{R_f}$ = 0.38 (3:7 EtOAc:petroleum ether); **IR** (film, $\nu_{max/cm^{-1}}$) 3053, 2937, 1644, 1613, 1598, 1504, 1424, 1368, 1219, 1157, 1128, 1092, 1027, 910, 837, 779, 769, 726, 690; **^{1}H NMR** (300 MHz, $CDCl_3$) 7.26–7.00 (m, 5H), 6.97–6.68 (m, 4H), 5.45 (s, 1H), 5.39 (s, 1H), 3.35 (s, 3H); **^{13}C NMR** (75 MHz, $CDCl_3$) δ 170.7,

161.2 (d, $J_{C\text{-}F}$ 246.9 Hz), 145.9, 139.7, 136.9, 128.9 (d, $J_{C\text{-}F}$ = 8.0 Hz), 128.4, 128.1, 126.1, 118.2, 115.7 (d, $J_{C\text{-}F}$ = 2.4 Hz), 37.5; **HRMS** (ESI$^+$) *m/z*: [M + H] calcd for $C_{16}H_{15}FNO^+$ 256.1132; found 256.1147. Recorded data in accordance with those previously reported.

N-(4-bromophenyl)-*N*-methyl-2-phenylacrylamide (3.2g)[239]

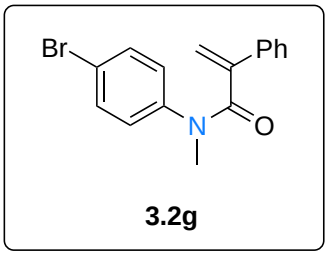

3.2g

Prepared according to general procedure 3A using 4-bromo-*N*-methylaniline (0.500 g, 2.69 mmol), atropic acid (0.477 g, 3.22 mmol), 2-chloro-1-methylpyridinium iodide (0.824 g, 3.22 mmol) and triethylamine (1.12 mL, 8.06 mmol) in CH_2Cl_2 (50 mL). Chromatography on silica gel with EtOAc/petroleum ether (10–25%) afforded **3.2g** as a white solid (0.590 g, 69% yield). Recrystallization with CH_2Cl_2:hexane afforded colourless needles. $\mathbf{R_f}$ = 0.28 (3:7 EtOAc:petroleum ether); **M.P.** 66–68 °C; **IR** (film, ν_{max}/cm^{-1}) 3058, 2931, 1646, 1611, 1585, 1573, 1487, 1424, 1363, 1307, 1247, 1125, 1095, 1067, 1009, 913, 829, 774, 703; **^{1}H NMR** (400 MHz, $CDCl_3$) 7.33–7.08 (m, 7H), 6.80 (bs, 2H), 5.51 (bs, 1H), 5.39 (s, 1H), 3.35 (s, 3H); **^{13}C NMR** (101 MHz, $CDCl_3$) δ 170.6, 145.7, 142.8, 136.7, 132.1, 128.6, 128.6, 128.3, 126.2, 120.6, 118.3, 37.4. Recorded data in accordance with those previously reported.

N-(3-bromophenyl)-*N*-methyl-2-phenylacrylamide (3.2h)

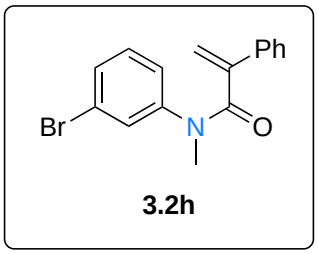

3.2h

Prepared according to general procedure 3A using 3-bromo-*N*-methylaniline (0.251 g, 1.35 mmol), atropic acid (0.200 g, 1.35 mmol), 2-chloro-1-methylpyridinium iodide (0.414 g, 1.62 mmol) and triethylamine (0.57 mL, 4.05 mmol) in CH_2Cl_2 (20 mL). Chromatography on silica gel with EtOAc/petroleum ether (10–20%) afforded **3.2h** as a clear colorless oil (0.218 g, 51% yield). $\mathbf{R_f}$ = 0.55 (4:6 EtOAc:petroleum ether); **IR** (film, vmax/cm^{-1}) 2926, 1729, 1649, 1587, 1571, 1477, 1363, 1242, 1130, 1089, 1070, 1027, 914, 784, 694, 627; **^{1}H NMR** (300 MHz, $CDCl_3$) δ 7.39–6.82 (m, 9H), 5.53 (br s, 1H), 5.45 (s, 1H), 3.36 (s, 3H); **^{13}C NMR** (101 MHz, $CDCl_3$) δ 170.4, 145.7, 144.8, 130.1, 130.0, 129.9, 128.4, 128.1, 126.1, 125.5, 122.0, 37.4. **HRMS** (ESI$^+$) *m/z*: [M + H] calcd for $C_{16}H_{15}{}^{79}BrNO^+$ 316.0332; found 316.0348.

***N*-(4-cyanophenyl)-*N*-methyl-2-phenylacrylamide (3.2i)**

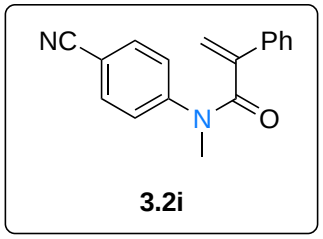

3.2i

Prepared according to general procedure 3A using 4-cyano-*N*-methylaniline (0.500 g, 3.78 mmol), atropic acid (0.670 g, 4.54 mmol), 2-chloro-1-methylpyridinium iodide (1.16 g, 4.54 mmol) and triethylamine (2.11 mL, 15.1 mmol) in CH_2Cl_2 (50 mL). Chromatography on silica gel with EtOAc/petroleum ether (10–40%) afforded **3.2i** an orange gum that solidifies into an orange amorphous solid (0.297 g, 30% yield). $\mathbf{R_f}$ = 0.23 (2:8 EtOAc:petroleum ether); **IR** (film, $\nu_{max/cm^{-1}}$) 3053, 2927, 2228, 1734, 1727, 1649, 1601, 1504, 1426, 1358, 1310, 1237, 1176, 1125, 1092, 1067, 1024, 915, 845, 774, 701; **^{1}H NMR** (300 MHz, $CDCl_3$) 7.46 (d, *J* = 8.8 Hz, 2H), 7.25–7.07 (m, 7H), 5.59 (s, 1H), 5.48 (s, 1H), 3.39 (s, 3H); **^{13}C NMR** (75 MHz, $CDCl_3$) δ 170.4, 147.6, 145.4, 136.2, 132.9, 128.7, 128.5, 127.1, 126.1, 118.9, 118.3, 110.2, 37.4; **HRMS** (ESI^+) *m/z*: [M + H] calcd for $C_{17}H_{15}N_2O^+$ 263.1179; found 263.1194.

***N*-(4-acetylphenyl)-*N*-methyl-2-phenylacrylamide (3.2j)**

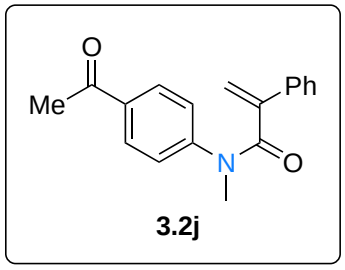

3.2j

Prepared according to general procedure 3A using 1-(4-(methylamino)phenyl)ethan-1-one (0.201 g, 1.35 mmol), atropic acid (0.200 g, 1.35 mmol), 2-chloro-1-methylpyridinium iodide (0.414 g, 1.62 mmol) and triethylamine (0.57 mL, 4.05 mmol) in CH_2Cl_2 (20 mL). Chromatography on silica gel with EtOAc/petroleum ether (10–25%) afforded **3.2j** as a clear colorless oil (0.121 g, 32% yield). $\mathbf{R_f}$ = 0.45 (3:7 EtOAc:petroleum ether); **IR** (film, vmax/cm^{-1}) 2926, 2855, 1680, 1649, 1596, 1359, 1263, 1129, 843, 773, 751, 700, 595; **^{1}H NMR** (300 MHz, $CDCl_3$) δ 7.77 (d, *J* = 8.3 Hz, 2H), 7.25–7.19 (m, 5H), 7.09 (d, *J* = 8.3 Hz, 2H), 5.56 (s, 1H), 5.40 (s, 1H), 3.41 (s, 3H), 2.54 (s, 3H); **^{13}C NMR** (101 MHz, $CDCl_3$) δ 196.9, 170.3, 147.8, 145.4, 136.3, 135.1, 129.0, 128.4, 128.2, 126.4, 126.1, 118.1, 37.3, 26.5; **HRMS** (ESI^+) *m/z*: [M + H] calcd for $C_{18}H_{18}NO_2^+$ 280.1332; found 280.1345.

***N*-(3,5-difluorophenyl)-*N*-methyl-2-phenylacrylamide (3.2k)**

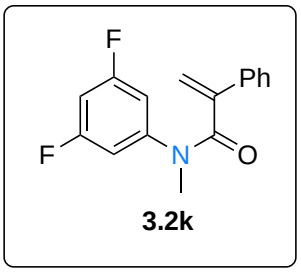

3.2k

Prepared according to general procedure 3B using atropic acid (0.600 g, 3.60 mmol), 3,5-difluoro-*N*-methylaniline (0.429 g, 3.00 mmol) and triethylamine (1.04 mL, 7.50 mmol) in CH_2Cl_2 (12 mL). Chromatography on silica gel with EtOAc/petroleum ether (10–25%) afforded **3.2k** as a clear colorless oil (0.270 g, 33% yield). **R_f** = 0.40 (2:8 EtOAc:petroleum ether); **IR** (film, $\nu_{max/cm^{-1}}$) 3061, 2924, 2852, 1655, 1600, 1496, 1474, 1460, 1447, 1422, 1371, 1344, 1312, 1287, 1263, 1225, 1210, 1118, 1096, 1050, 990, 965, 914, 853, 777, 695; **^{1}H NMR** (300 MHz, $CDCl_3$) δ 7.33–7.18 (m, 5H), 6.67–6.50 (m, 3H), 5.61 (s, 1H), 5.51 (s, 1H), 3.37 (s, 3H); **^{13}C NMR** (151 MHz, $CDCl_3$) δ 170.3, 162.8 (dd, J_{C-F} = 247.8, 14.3 Hz), 145.9 (t, J_{C-F} = 11.0 Hz), 145.7, 136.4, 128.7, 128.5, 126.2, 118.5, 110.2 (d, J_{C-F} = 25.0 Hz), 102.5 (d, J_{C-F} = 25.0 Hz), 37.5; **HRMS** (ESI$^+$) *m/z*: [M + H] calcd for $C_{16}H_{14}F_2NO^+$ 274.1038; found 274.1052.

***N*-methyl-2-phenyl-*N*-(3,4,5-trimethoxyphenyl)acrylamide (3.2l)**

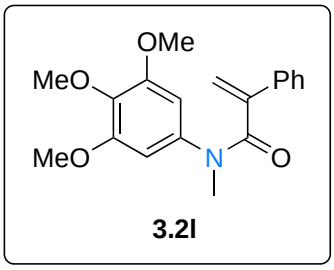

3.2l

Prepared according to general procedure 3B using atropic acid (0.252 g, 1.52 mmol), 3,4,5-trimethoxy-*N*-methylaniline (0.222 g, 1.26 mmol) and triethylamine (0.44 mL, 3.15 mmol) in CH_2Cl_2 (5 mL). Chromatography on silica gel with EtOAc/petroleum ether (10–25%) afforded **3.2l** as a clear colorless oil (0.330 g, 80% yield). **R_f** = 0.2 (2:8 EtOAc:petroleum ether); **IR** (film, vmax/cm^{-1}) 2938, 2840, 1645, 1591, 1502, 1417, 1347, 1229, 1123, 1004, 706; **^{1}H NMR** (300 MHz, $CDCl_3$) δ 7.25–7.11 (m, 5H), 6.05 (s, 2H), 5.45 (s, 1H), 5.40 (s, 1H), 3.76 (s, 3H), 3.57 (s, 6H), 3.37 (s, 3H); **^{13}C NMR** (101 MHz, $CDCl_3$) δ 170.5, 152.9, 146.2, 139.2, 137.3, 136.8, 128.2, 127.8, 126.0, 117.2, 104.8, 60.8, 60.8, 55.9, 37.2; **HRMS** (ESI$^+$) *m/z*: [M + H] calcd for $C_{19}H_{22}NO_4^+$ 328.1543; found 328.1552.

***N*-methyl-2-phenyl-*N*-(pyridine-4-yl)acrylamide (3.2m)**

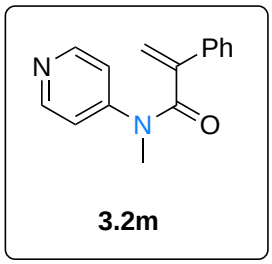

3.2m

Prepared according to general procedure 3A using 4-(methylamino)pyridine (0.500 g, 4.62 mmol), atropic acid (0.821 g, 5.55 mmol), 2-chloro-1-methylpyridinium iodide (1.42 g, 5.55 mmol) and triethylamine (1.93 mL, 13.9 mmol) in CH_2Cl_2 (40 mL). Chromatography on neutral alumina with EtOAc/petroleum ether (25–50%) afforded **3.2m** as a yellow oil (0375 g, 32%). **R_f** (silica) = 0.12 (5:5 EtOAc:petroleum

ether); **R_f** (alumina) = 0.36 (5:5 EtOAc:petroleum ether); **IR** (film, $\nu_{max/cm^{-1}}$) 3032, 2922, 2856, 1679, 1590, 1494, 1454, 1421, 1365, 1340, 1274, 1244, 1188, 1120, 1052, 961, 910, 817; **^{1}H NMR** (300 MHz, $CDCl_3$) 8.38 (d, *J* = 6.4 Hz, 2H); 7.26–7.19 (m, 5H), 7.00 (d, *J* = 6.4 Hz, 2H), 5.61 (s, 1H), 5.42 (s, 1H), 3.35 (s, 3H); **^{13}C NMR** (75 MHz, $CDCl_3$) δ 170.3, 150.7, 150.5, 145.1, 135.9, 128.7, 128.5, 126.1, 120.0, 118.4, 36.7; **HRMS** (ESI^+) *m/z*: [M + H] calcd for $C_{15}H_{15}N_2O^+$ 239.1179; found 239.1196.

1-(indolin-1-yl)-2-phenylprop-2-en-1-one (3.2n)

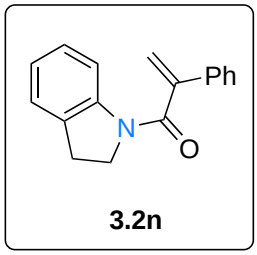

3.2n

Prepared according to general procedure 3A using indoline (0.201 g, 1.68 mmol), atropic acid (0.300 g, 2.02 mmol), 2-chloro-1-methylpyridinium iodide (0.517 g, 3.02 mmol) and triethylamine (0.71 mL, 5.06 mmol) in CH_2Cl_2 (20 mL). Chromatography on silica gel with EtOAc/petroleum ether (5–10%) afforded **3.2n** as a clear oil (0.282 g, 67% yield). **R_f** = 0.25 (1:20 EtOAc:petroleum ether); **IR** (film, $\nu_{max/cm^{-1}}$) 3058, 2957, 1647, 1598, 1483, 1463, 1411, 1399, 1291, 1260, 1075, 1028, 920, 757, 706; **^{1}H NMR** (400 MHz, $CDCl_3$) δ 8.30 (d, *J* = 6 Hz ,1H), 7.45 (d, *J* = 7.8 Hz, 2H), 7.35–7.26 (m, 3H), 7.25–7.17 (m, 1H), 7.13 (d, *J* = 7.6 Hz, 1H), 7.05–6.96 (m, 1H), 5.76 (s, 1H), 5.48 (s, 1H), 4.23 (bs, 0.3H), 3.79 (bs, 1.7H), 3.01 (app t, *J* = 7.8 Hz, 2H); **^{13}C NMR** (101 MHz, $CDCl_3$) δ 168.5, 146.6, 142.7, 135.3, 132.0, 129.1, 128.9 127.7, 126.1, 124.8, 124.4, 117.6, 115.2, 49.5, 28.3; **HRMS** (ESI^+) *m/z*: [M + H] calcd for $C_{17}H_{16}NO^+$ 250.1226; found 250.1239.

1-(6-methoxy-3,4-dihydroquinolin-1(2*H*)-yl)-2-phenylprop-2-en-1-one (3.2o)

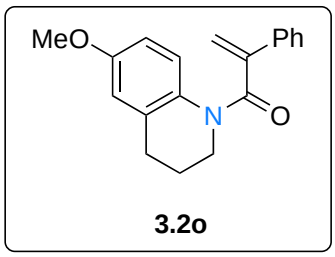

3.2o

Prepared according to general procedure 3A using 6-methoxy-1,2,3,4-tetrahydroquinoline (0.500 g, 3.06 mmol), atropic acid (0.554 g, 3.68 mmol), 2-chloro-1-methylpyridinium iodide (0.939 g, 3.68 mmol) and triethylamine (1.28 mL, 9.19 mmol) in CH_2Cl_2 (40 mL). Chromatography on silica gel with EtOAc/petroleum ether (5–15%) afforded **3.2o** as a white solid (0.696 g, 77% yield). Recrystallization with CH_2Cl_2:hexane afforded colourless needles. **R_f** = 0.45 (2:8 EtOAc:petroleum ether); **M.P.** 82–84 °C **IR** (film, $\nu_{max/cm^{-1}}$) 2937, 2835, 1636, 1606, 1497, 1444, 1383, 1315, 1292, 1247, 1214, 1199, 1156, 1115, 1065, 1034, 961, 905, 872, 837, 809, 779, 731, 606; **^{1}H NMR** (300 MHz, $CDCl_3$) (significant line-broadening) δ 7.91–6.36 (m, 8H), 5.68 (s, 1H), 5.43 (s, 1H), 4.06–3.49 (m, 5H), 2.65 (bs, 2H), 1.93 (bs, 2H); **^{1}H NMR** @ 60 °C (600 MHz, DMSO) δ 7.49–7.25 (m, 6H),

6.70–6.60 (m, 2H), 5.77 (s, 1H), 5.34 (s, 1H), 3.70 (s, 3H), 3.66 (app t, *J* = 6.1 Hz, 2H), 2.68 (t, *J* = 6.8 Hz), 1.86 (m [app pent], 2H); **^{13}C NMR** (75 MHz, $CDCl_3$) (significant line-broadening) δ 169.7, 156.8, 146.0, 128.6 (br), 126.0, 125.5, 113.1 (br), 115.5, 55.4, 27.0, 23.8; **HRMS** (ESI^+) *m/z*: [M + H] calcd for $C_{19}H_{20}NO_2^+$ 294.1489; found 294.1501.

2-(4-methoxyphenyl)-*N*-methyl-*N*-phenylacrylamide (3.2p)[239]

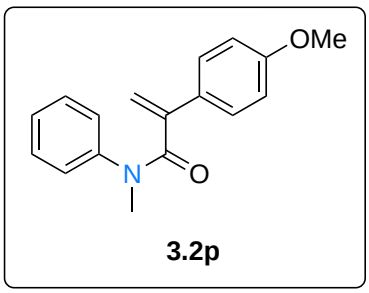

3.2p

Prepared according to general procedure 3A using *N*-methylaniline (0.152 g, 1.42 mmol), 2-(4-methoxyphenyl)acrylic acid[241] (0.304 g, 1.71 mmol), 2-chloro-1-methylpyridinium iodide (0.436 g, 1.71 mmol) and triethylamine (0.59 mL, 4.26 mmol) in CH_2Cl_2 (20 mL). Chromatography on silica gel with EtOAc/petroleum ether (20–40%) afforded **3.2p** as a white solid (0.378 g, 99% yield). Recrystallization with CH_2Cl_2:hexane afforded colourless crystalline solid. **R_f** = 0.24 (2:8 EtOAc:petroleum ether); **M.P.** 80–81 °C; **IR** (film, vmax/cm^{-1}) 2970, 1667, 1601, 1515, 1468, 1250, 1180, 1117, 1050, 1022, 831, 812, 753; **^{1}H NMR** (300 MHz, $CDCl_3$) δ 7.15–6.95 (m, 7H), 6.77–6.74 (m, 2H), 5.37 (s, 1H), 5.22 (s, 1H), 3.78 (s, 3H), 3.39 (s, 3H); **^{13}C NMR** (101 MHz, $CDCl_3$) δ 171.0, 159.6, 145.1, 144.0, 129.6, 129.0, 127.5, 127.0, 115.9, 113.8, 55.4, 37.5 (one carbon peak was missing due to overlapping); **HRMS** (ESI^+) *m/z*: [M + H] calcd for $C_{17}H_{18}NO_2^+$ 268.1332; found 268.1347. Recorded data in accordance with those previously reported.

***N*-methyl-*N*-phenyl-2-(*p*-tolyl)acrylamide (3.2q)**[239]

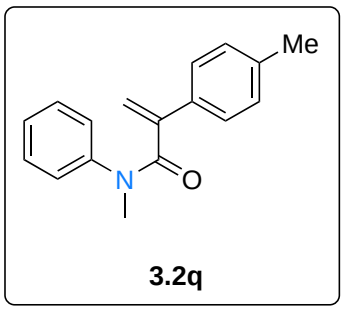

3.2q

Prepared according to general procedure 3A using *N*-methylaniline (0.147 g, 1.37 mmol), 2-(*p*-tolyl)acrylic acid[242] (0.203 g, 1.25 mmol), 2-chloro-1-methylpyridinium iodide (0.383 g, 1.50 mmol) and triethylamine (0.52 mL, 3.75 mmol) in CH_2Cl_2 (10 mL). Chromatography on silica gel with EtOAc/petroleum ether (20–40%) afforded **3.2q** as a white solid (0.273 g, 87% yield). An analytical sample was prepared by recrystallization with CH_2Cl_2:petroleum ether to afford a colorless crystalline solid. **R_f** = 0.25 (4:6 EtOAc:petroleum ether); **M.P.** 69–75°C; **IR** (film, vmax/cm^{-1}) 2922, 1638, 1591, 1494, 1377, 1123, 908, 826, 774, 698, 545; **^{1}H NMR** (300 MHz, $CDCl_3$) δ 7.24–6.68 (m, 9H), 5.43 (brs, 1H), 5.26 (s, 1H), 3.39 (s, 3H), 2.31 (s, 3H); **^{13}C NMR** (101 MHz, $CDCl_3$) δ 170.8, 145.4, 143.8, 137.8, 134.0, 129.0, 128.8,

126.8, 125.9, 116.6, 37.3, 21.1; **HRMS** (ESI$^+$) *m/z*: [M + H] calcd for $C_{17}H_{18}NO^+$ 252.1383; found 252.1400. Recorded data in accordance with those previously reported.

2-(4-bromophenyl)-*N*-methyl-*N*-phenylacrylamide (3.2r)[239]

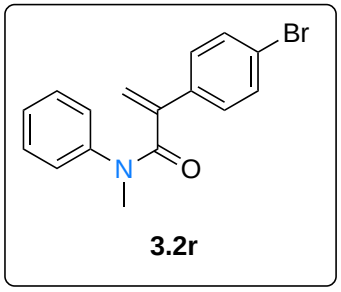

3.2r

Prepared according to general procedure 3A using *N*-methylaniline (0.056 g, 0.518 mmol), 2-(4-bromophenyl)acrylic acid[242] (0.107 g, 0.471 mmol), 2-chloro-1-methylpyridinium iodide (0.144 g, 0.565 mmol) and triethylamine (0.20 mL, 1.41 mmol) in CH_2Cl_2 (5 mL). Chromatography on silica gel with EtOAc/petroleum ether (20–40%) afforded **3.2r** as a white solid (0.115 g, 77% yield). An analytical sample was prepared by recrystallization with CH_2Cl_2:petroleum ether to afford a crystalline solid. $\mathbf{R_f}$ = 0.40 (3:7 EtOAc:petroleum ether); **M.P.** 53–57°C; **IR** (film, vmax/cm^{-1}) 2924, 1645, 1593, 1491, 1372, 1128, 1092, 1071, 1008, 834, 767, 697, 545; **^{1}H NMR** (300 MHz, $CDCl_3$) δ 7.33 (d, *J* = 7.8 Hz, 2H), 7.21–7.10 (m, 3H), 7.04 (app d, *J* = 6.1 Hz, 2H), 6.97–6.81 (m, 2H), 5.45 (s, 1H), 5.38 (s,1H), 3.38 (s, 3H); **HRMS** (ESI$^+$) *m/z*: [M + H] calcd for $C_{16}H_{15}{}^{79}BrNO^+$ 316.0332; found 31.0338. Recorded data in accordance with those previously reported.

***N*-methyl-2-(naphthalen-2-yl)-*N*-phenylacrylamide (3.2s)**

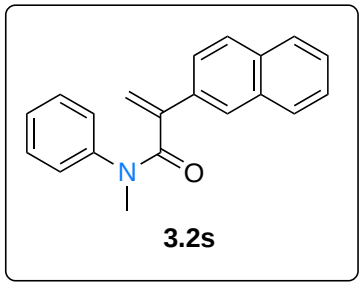

3.2s

Prepared according to general procedure 3A using *N*-methylaniline (0.031 g, 0.289 mmol), 2-(naphthalen-2-yl)acrylic acid[241] (0.052 g, 0.262 mmol), 2-chloro-1-methylpyridinium iodide (0.080 g, 0.315 mmol) and triethylamine (0.11 mL, 0.787 mmol) in CH_2Cl_2 (5 mL). Chromatography on silica gel with EtOAc/petroleum ether (20–40%) afforded **3.2s** as a white solid (0.036 g, 48% yield). An analytical sample was prepared by recrystallization with CH_2Cl_2:petroleum ether to afford a colorless crystalline solid. $\mathbf{R_f}$ = 0.35 (4:6 EtOAc:petroleum ether); **M.P.** 95–98 °C; **IR** (film, vmax/cm^{-1}) 2924, 1646, 1594, 1495, 1376, 1118, 909, 821, 770, 698, 544; **^{1}H NMR** (300 MHz, $CDCl_3$) δ 7.83–7.65 (m, 4H), 7.50–7.42 (m, 2H), 7.39–7.27 (m, 1H), 7.17–7.03 (m, 3H), 7.02–6.85 (m, 2H), 5.60 (s,1H), 5.40 (s, 1H), 3.45 (s, 3H); **^{13}C NMR** (101 MHz, $CDCl_3$) δ 170.58, 145.47, 143.69, 134.07, 133.12,

132.88, 128.85, 128.26, 128.03, 127.48, 126.92, 126.18, 125.44, 123.61, 117.74, 37.31; **HRMS** (ESI^+) *m/z*: [M + H] calcd for $C_{20}H_{18}NO^+$ 288.1383; found 288.1396.

2-(3,4-dichlorophenyl)-*N*-methyl-*N*-phenylacrylamide (3.2t)

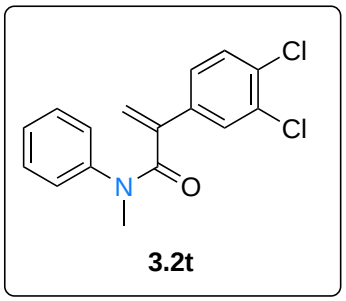

3.2t

Prepared according to general procedure 3A using *N*-methylaniline (0.084 g, 0.784 mmol), 2-(3,4-dichlorophenyl)acrylic acid[243] (0.154 g, 0.713 mmol), 2-chloro-1-methylpyridinium iodide (0.219 g, 0.856 mmol) and triethylamine (0.30 mL, 2.14 mmol) in CH_2Cl_2 (10 mL). Chromatography on silica gel with EtOAc/petroleum ether (20–40%) afforded **3.2t** as a white solid (0.175 g, 80% yield). An analytical sample was prepared by recrystallization with CH_2Cl_2:petroleum ether to afford a colorless crystalline solid; $\mathbf{R_f}$ = 0.6 (1:1 EtOAc:petroleum ether); **M.P.** 75–79 °C; **IR** (film, vmax/cm^{-1}) 2926, 1644, 1593, 1470, 1371, 1127, 1029, 767, 696, 554; **^{1}H NMR** (300 MHz, $CDCl_3$) δ 7.32–7.11 (m, 5H), 7.02 (d, *J* = 7.3 Hz, 1H), 6.91 (s, 2H), 5.46 (brs, 1H), 5.43 (s,1H), 3.39 (s, 3H); **^{13}C NMR** (101 MHz, $CDCl_3$) δ 169.5, 143.7, 143.4, 137.0, 132.4, 131.9, 130.2, 129.0, 128.0, 127.2, 126.9, 125.4, 119.6, 37.4; **HRMS** (ESI^+) *m/z*: [M + H] calcd for $C_{16}H_{14}Cl_2NO^+$ 306.0447; 306.0465.

***N*-methyl-*N*-phenylcyclopent-1-ene-1-carboxamide (3.2u)**

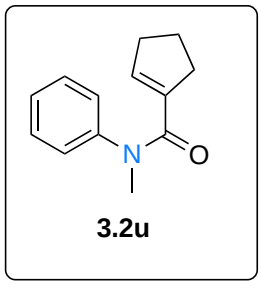

3.2u

Prepared according to general procedure 3A using *N*-methylaniline (0.500 g, 4.66 mmol), cyclopent-1-ene-1-carboxylic acid (0.628 g, 5.60 mmol), 2-chloro-1-methylpyridinium iodide (1.430 g, 5.60 mmol) and triethylamine (1.95 mL, 13.98 mmol) in CH_2Cl_2 (20 mL). Chromatography on silica gel with EtOAc/petroleum ether (20–40%) afforded **3.2u** as a white solid (0.628 g, 67% yield). Recrystallization with CH_2Cl_2:hexane afforded a colourless crystalline solid. $\mathbf{R_f}$ = 0.24 (2:8 EtOAc:petroleum ether); **M.P.** 34–36 °C; **IR** (film, vmax/cm^{-1}) 2936, 2848, 1636, 1615, 1592, 1494, 1365, 1302, 1093, 776, 731, 702, 578; **^{1}H NMR** (300 MHz, $CDCl_3$) δ 7.31–7.25 (m, 2H), 7.22–7.17 (m, 1H), 7.10–7.07 (m, 2H), 5.75 (t, *J* = 3.0 Hz, 1H), 3.28 (s, 3H), 2.19–2.10 (m, 4H), 1.68–1.58 (p, *J* = 7.5 Hz, 2H); **^{13}C NMR** (151 MHz, $CDCl_3$) δ 168.6, 144.8, 139.6, 138.2, 129.3, 127.1, 127.0, 38.0, 33.8, 33.1, 23.4; **HRMS** (ESI^+) *m/z*: [M + H] calcd for $C_{13}H_{16}NO^+$ 202.1226; found 202.1236.

***N*-methyl-*N*-phenylcinnamamide (3.2v)**[152]

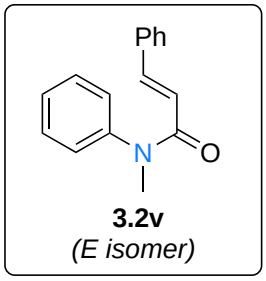

3.2v
(E isomer)

Prepared according to general procedure A using *N*-methylaniline (0.300 g, 2.81 mmol), *trans*-cinnamic acid (0.500 g, 3.37 mmol), 2-chloro-1-methylpyridinium iodide (0.862 g, 3.37 mmol) and triethylamine (1.17 mL, 8.43 mmol) in CH_2Cl_2 (20 mL). Chromatography on silica gel with EtOAc/petroleum ether (10–20%) afforded **3.2v** as a yellow oil (0.569 g, 86% yield). $\mathbf{R_f}$ = 0.29 (2:8 EtOAc:petroleum ether); **IR** (film, ν_{max}/cm^{-1}) 3478, 3059, 3028, 2928, 1738, 1652, 1614, 1592, 1493, 1449 1417, 1367, 1313, 1282, 1244, 1120, 1073, 977, 859, 760, 698; **^{1}H NMR** (300 MHz, $CDCl_3$) δ 7.68 (d, *J* = 15.6 Hz, 1H), 7.48–7.7.20 (m, 10H), 6.38 (d, *J* = 15.6 Hz, 1H), 3.41 (s, 3H); **^{13}C NMR** (151 MHz, $CDCl_3$) δ 166.3, 143.8, 141.8, 135.3, 129.7, 129.6, 128.8, 127.9, 127.7, 127.4, 118.9, 37.7; **HRMS** (ESI^+) *m/z*: [M + H] calcd for $C_{16}H_{16}NO^+$ 238.1226; found 238.1240. Recorded data in accordance with those previously reported.

(*Z*)-*N*-methyl-*N*,3-diphenylacrylamide ((*Z*)-3.1w)

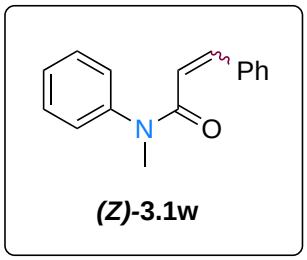

***(Z)*-3.1w**

Recovered starting material during the synthesis of **3.2v** (vide infra). Inseparable from the ***E*** isomer (***Z*:*E*** ~ 2:1). **^{1}H NMR** (300 MHz, $CDCl_3$) δ 7.41–7.14 (m, 8H), 6.98–6.84 (m, 2H), 6.38 (d, *J* = 12.2 Hz, 1H), 5.83 (d, *J* = 12.2 Hz, 1H), 3.32 (s, 3H).

***N*-methyl-*N*-phenylmethacrylamide (3.2ua)**[169]

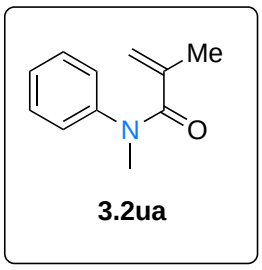

3.2ua

Prepared according to general procedure 3A using *N*-methylaniline (2.000 g, 18.70 mmol), methacrylic acid (1.930 g, 22.40 mmol), 2-chloro-1-methylpyridinium iodide (5.72 g, 22.40 mmol) and triethylamine (7.80 mL, 56.10 mmol) in CH_2Cl_2 (80 mL). Chromatography on silica gel with EtOAc/petroleum ether (20–40%) afforded **3.2ua** as a white solid (1.786 g, 55% yield). Recrystallization with CH_2Cl_2:hexane afforded a white crystalline solid. $\mathbf{R_f}$ = 0.29 (2:8 EtOAc: petroleum ether); **M.P.** 59–61 °C; **IR** (film, vmax/cm^{-1}) 2917, 1651, 1623, 1593, 1496, 1452, 1424, 1379, 1307, 1243, 113, 1039, 925, 903, 783, 708; **^{1}H NMR** (300 MHz, $CDCl_3$) δ 7.35–7.31 (m, 2H), 7.26–7.22 (m, 1H), 7.14–7.12 (m, 2H), 5.02 (s, 1H), 4.98 (s, 1H), 3.34 (s, 3H), 1.75 (s, 3H); **^{13}C NMR** (101 MHz, $CDCl_3$) δ 172.1, 144.7, 140.8, 129.3, 127.0, 126.6, 119.5, 37.8, 20.4; **HRMS** (ESI^+) *m/z*: [M + H] calcd for

$C_{11}H_{14}NO^+$ 176.1070; found 176.1071. Recorded data in accordance with those previously reported.

(*E*)-*N*,2-dimethyl-*N*-phenylbut-2-enamide (3.2ub)

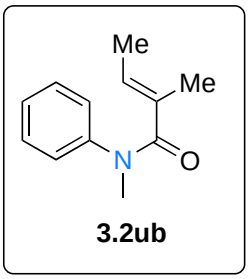

3.2ub

Prepared according to general procedure 3A using *N*-methylaniline (0.446 g, 4.16 mmol), tiglic acid (0.500 g, 4.99 mmol), 2-chloro-1-methylpyridinium iodide (1.27 g, 4.99 mmol) and triethylamine (1.74 mL, 12.5 mmol) in CH_2Cl_2 (25 mL). Chromatography on silica gel with EtOAc/petroleum ether (10–20%) afforded **3.2ub** as a clear liquid (0.400 g, 51% yield). $\mathbf{R_f}$ = 0.18 (3:17 EtOAc:petroleum ether); **IR** (film, ν_{max}/cm^{-1}) 3501, 2920, 1659, 1630, 1594, 1585, 1494, 1456, 1420, 1384, 1358, 1300, 1280, 1194, 1117, 1026, 856,769, 740, 697; **^{1}H NMR** (300 MHz, $CDCl_3$) δ 7.34–7.27 (m, 2H), 7.30–7.16 (m, 1H), 7.11–7.06 (m, 2H), 5.72 (qq, *J* = 6.8, 1.5 Hz, 1H), 3.32 (s, 3H), 1.54, (app quin, *J* = 1.2 Hz, 3H), 1.46 (app dq, *J* = 6.8, 1.2 Hz, 3H); **^{13}C NMR** (101 MHz, $CDCl_3$) δ 173.5, 145.0, 132.7, 130.6, 129., 126.5, 126.5, 37.9, 14.1, 13.4; **HRMS** (ESI^+) *m/z*: [M + H] calcd for $C_{12}H_{16}NO^+$ 190.1226; found 190.1240.

***N*-methyl-*N*-phenylfuran-3-carboxamide (3.2uc)**[244]

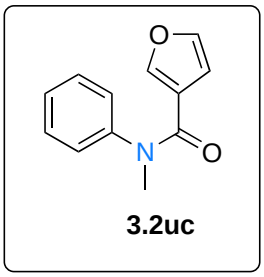

3.2uc

Prepared according to general procedure 3A using *N*-methylaniline (0.500 g, 4.66 mmol), furan-3-carboxylic acid (0.627 g, 5.60 mmol), 2-chloro-1-methylpyridinium iodide (1.430 g, 5.60 mmol) and triethylamine (1.95 mL, 14.0 mmol) in CH_2Cl_2 (20 mL). Chromatography on silica gel with EtOAc/petroleum ether (20–40%) afforded **3.2uc** as a white solid (0.709 g, 76% yield). Recrystallization with CH_2Cl_2:hexane afforded a yellow crystalline solid. $\mathbf{R_f}$ = 0.26 (2:8 EtOAc:petroleum ether); **M.P.** 48–51 °C; **IR** (film, vmax/cm^{-1}) 3146, 3125, 2931, 1623, 1592, 1501, 1378, 1161, 1013, 822, 702, 750, 600, 573 **^{1}H NMR** (300 MHz, $CDCl_3$) δ 7.42–7.35 (m, 3H), 7.22–7.19 (m, 2H), 7.13 (s, 1H), 6.87 (s, 1H), 6.10 (s, 1H), 3.40 (s, 3H); **^{13}C NMR** (101 MHz, $CDCl_3$) δ 163.3, 145.8, 144.2, 142.0, 129.8, 128.1, 127.9, 121.9, 111.1, 38.3; **HRMS** (ESI^+) *m/z*: [M + H] calcd for $C_{12}H_{12}NO_2^+$ 202.0863; found 202.0878. Recorded data in accordance with those previously reported.

***N*-methyl-*N*-phenylthiophene-3-carboxamide (3.2ud)**

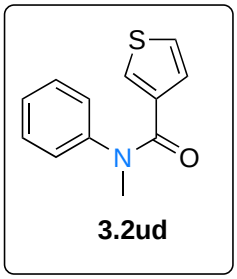

3.2ud

Prepared according to general procedure 3A using *N*-methylaniline (0.174 g, 1.63 mmol), thiophene-3-carboxylic acid (0.250 g, 1.95 mmol), 2-chloro-1-methylpyridinium iodide (0.498 g, 1.95 mmol) and triethylamine (0.68 mL, 4.89 mmol) in CH_2Cl_2 (15 mL). Chromatography on silica gel with EtOAc/petroleum ether (20–40%) afforded **3.2ud** as a clear colorless oil (0.336 g, 95% yield). $\mathbf{R_f}$ = 0.45 (4:6 EtOAc:petroleum ether); **IR** (film, vmax/cm^{-1}) 3103, 2929, 1631, 1591, 1494, 1423, 1346, 1295, 1280, 1103, 845, 771, 736, 696, 559; **^{1}H NMR** (300 MHz, $CDCl_3$) δ 7.36–7.22 (m, 3H), 7.19 (dd, *J* = 3.0, 1.2 Hz, 1H), 7.15–7.09 (m, 2H), 7.02 (dd, *J* = 5.1, 3.0 Hz, 1H), 6.86 (dd, *J* = 5.1, 1.2 Hz, 1H), 3.46 (s, 3H); **^{13}C NMR** (101 MHz, $CDCl_3$) δ 164.8, 144.8, 136.7, 129.8, 129.4, 128.4, 127.1, 127.1, 124.3, 38.4; **HRMS** (ESI^+) *m/z*: [M + H] calcd for $C_{12}H_{12}NOS^+$ 218.0634; found 218.0648.

5.3.5 General procedure 3C: Synthesis of 3,4-dihydroquinolin-2-ones (3.1) via 2-TX photocatalysis

A stirring mixture of acrylamide **3.2** (0.10–0.5 mmol), **2-TX** (20 mol%) in 5 mL TFE:$CHCl_3$ (4:1) was degassed with argon for 10 min before irradiation with 450 nm LEDs (30 W) for 48 h, with fan-cooling. The solvent was then removed in vacuo and the resulting residue purified by silica column chromatography (petroleum ether/EtOAc gradient) to afford 3,4-dihydroquinolin-2-one **3.1**.

5.3.6 General procedure 3D: Synthesis of 3,4-dihydroquinoline-2-ones (3.1) via Ir photocatalysis

A stirring mixture of acrylamide **3.2** (0.10–0.5 mmol), **Ir-1** (2 mol%) in the specified solvent was degassed with argon for 10 min before irradiation with 450 nm LEDs (30 W) for 48 h, with fan-cooling. The solvent was then removed in vacuo and the resulting residue purified by silica column chromatography (petroleum ether/EtOAc gradient) to afford 3,4-dihydroquinolin-2-one **3.1**.

5.3.7 Characterization data for 3,4-dihydroquinolin-2-ones (3.1)

1-methyl-3-phenyl-3,4-dihydroquinolin-2(1*H*)-one (3.1a)[242]

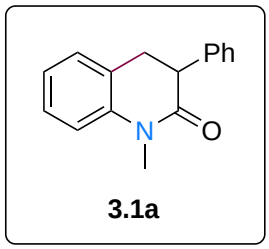

3.1a

Prepared according to general procedure 3C using **3.2a** (0.118 g, 0.50 mmol), **2-CTX** (25 mg, 0.10 mmol), TFE (4 mL). Chromatography on silica gel with EtOAc/petroleum ether (20–40%) afforded **3.1a** a white solid (0.113 g, 95% yield).

Prepared according to general procedure 3D using **3.2a** (0.050 g, 0.21 mmol), **Ir-1** (4.6 mg, 0.004 mmol) and toluene (4 mL). Chromatography on silica gel with EtOAc/petroleum ether (20–40%) afforded **3.1a** a white solid (0.047 g, 94% yield).

Recrystallization with CH_2Cl_2:hexane afforded a white solid. $\mathbf{R_f}$ = 0.28 (2:8 EtOAc:petroleum ether); **M.P.** 91–93 °C; **IR** (film, vmax/cm^{-1}) 1660, 1599, 1500, 1471, 1401, 1370, 1333, 1263, 1113, 746, 721, 696, 685; **^{1}H NMR** (300 MHz, $CDCl_3$) δ 7.34–7.24 (m, 4H), 7.23–7.17 (m, 3H), 7.06–7.01 (m, 2H), 3.87 (t, *J* = 7.5 Hz, 1H), 3.43 (s, 3H), 3.23 (d, *J* = 7.5 Hz, 2H); **^{13}C NMR** (101 MHz, $CDCl_3$) δ 171.0, 140.4, 138.7, 128.6, 128.2, 128.1, 127.7, 127.2, 125.5, 123.1, 114.7, 47.0, 33.1, 30.1; **HRMS** (ESI$^+$) *m/z*: [M + H] calcd for $C_{16}H_{16}NO^+$ 238.1226; found 238.1242. Recorded data in accordance with those previously reported.

1,6-dimethyl-3-phenyl-3,4-dihydroquinolin-2(1*H*)-one (3.1b)

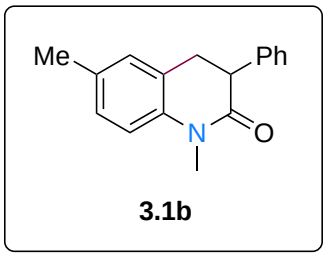

3.1b

Prepared according to general procedure 3C using **3.2b** (0.070 g, 0.28 mmol) and **2-CTX** (14 mg, 0.06 mmol). Chromatography on silica gel with EtOAc/hexanes (0–7%) afforded **3.1b** (0.051 g, 73% yield).

Prepared according to general procedure 3D using **3.2b** (0.075 g, 0.30 mmol) and $[Ir(dF(CF_3)ppy)_2dtbby]PF_6$ (3.4 mg, 0.003 x 10^{-3} mmol). Chromatography on silica gel with EtOAc/hexanes (0–7%) afforded **3.1b** (0.055 g, 73% yield).

Obtained as a white solid. Recrystallization with CH_2Cl_2:hexane afforded white needles. $\mathbf{R_f}$ = 0.27 (1:9 EtOAc:hexane); **M.P.** 113–115 °C; **IR** (film, $\nu_{max/cm^{-1}}$) 3023, 2916, 1666, 1616, 1588, 1507, 1472, 1454, 1454, 1416, 1363, 1340, 1269, 1231, 1115, 809,698; **^{1}H NMR** (400 MHz,

$CDCl_3$) δ 7.30 (d, *J* = 7.1 Hz, 1H), 7.27 (d, *J* = 6.3 Hz, 1H), 7.24 (d, *J* = 6.3 Hz, 1H), 7.20 (app d, *J* = 8.0 Hz, 2H), 7.08 (d, *J* = 8.2 Hz, 1H), 6.99 (s, 1H), 6.09 (d, *J* = 8.2 Hz, 1H), 3.85 (app t, *J* = 7.6 Hz, 1H), 3.41 (s, 3H), 3.19 (app d, *J* = 7.6 Hz, 2H), 2.31 (s, 3H); **^{13}C NMR** (101 MHz, $CDCl_3$) δ 170.8, 138.9, 138.1, 132.6, 128.9, 128.6, 128.2, 128.1, 127.2, 125.3, 114.6, 47.2, 33.1, 30.1, 20.7; **HRMS** (ESI^+) *m/z*: [M + H] calcd for $C_{17}H_{18}NO^+$ 252.1383; found 252.1397.

6-methoxy-1-methyl-3-phenyl-3,4-dihydroquinolin-2(1*H*)-one (3.1c)

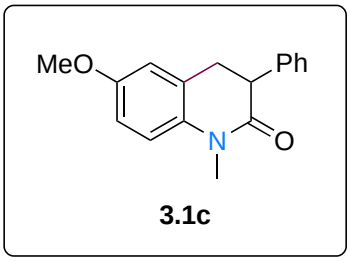

3.1c

Prepared according to general procedure 3C using **3.2c** (0.107 g, 0.40 mmol) and **2-CTX** (20 mg, 0.08 mmol). Chromatography on silica gel with EtOAc/hexanes (0–7%) afforded **3.1c** (0.050 g, 47% yield).

Prepared according to general procedure 3C using **3.2c** (0.054 g, 0.20 mmol) and **2-ITX** (14 mg, 0.04 mmol). Chromatography on silica gel with EtOAc/hexanes (0–7%) afforded **3.1c** (0.028 g, 52% yield).

Prepared according to general procedure 3D using **3.2c** (0,080 g, 0.30 mmol) and $[Ir(dF(CF_3)ppy)_2dtbby]PF_6$ (3.4 mg, 0.003 x 10^{-3} mmol). Chromatography on silica gel with EtOAc/hexanes (0–7%) afforded **3.1c** (0.046 g, 58% yield).

Obtained as a yellow oil. **R_f** = 0.36 (2:8 EtOAc:hexane); **IR** (film, $\nu_{max/cm^{-1}}$) 2922, 2851, 1659, 1590, 1502, 1472, 1454, 1429, 1368, 1282, 1244, 1191, 1166, 1143, 1118, 1057, 1027, 964, 908, 847, 804, 726, 698; **^{1}H NMR** (400 MHz, $CDCl_3$) δ 7.25 (d, *J* = 8.0 Hz, 1H), 7.23–7.17 (m, 2H), 7.15 (app d, *J* = 8.0 Hz, 2H), 6.88 (d, *J* = 8.7 HZ, 1H), 6.75 (dd, *J* = 8.7, 3.2 Hz, 1H), 6.69 (d, *J* = 3.2 Hz, 1H), 3.81 (app t, *J* = 7.4 Hz, 1H), 3.74 (s, 3H), 3.36 (s, 3H), 3.17–3.12 (m, 2H); **^{13}C NMR** (101 MHz, $CDCl_3$) δ 170.5, 155.5, 138.7, 134.0, 128.6, 128.1, 127.2, 126.8, 115.6, 114.3, 112.1, 55.6, 47.0 33.3, 30.2; **HRMS** (ESI^+) *m/z*: [M + H] calcd for $C_{17}H_{18}NO_2^+$ 268.1332; found 268.1346.

1-methyl-3-phenyl-6-(trifluoromethyl)-3,4-dihydroquinolin-2(1*H*)-one (3.1d)

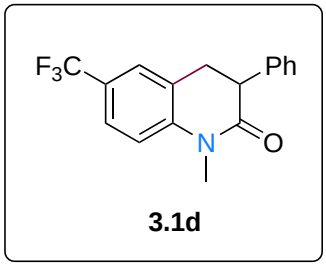

3.1d

Prepared according to general procedure 3C using **3.2d** (0.046 g, 0.150 mmol), **2-CTX** (7 mg, 0.03 mmol), TFE:$CHCl_3$ (4:1 mL). Chromatography on silica gel with EtOAc/petroleum ether (20–40%) afforded **3.1d** as a white solid (0.032 g, 70% yield). Recrystallization with CH_2Cl_2:hexane afforded a colourless crystalline solid. **R_f** = 0.31 (2:8 EtOAc:petroleum ether); **M.P.** 131–133 °C; **IR** (film, vmax/cm^{-1}) 2923, 1667, 1614, 1347, 1325, 1106, 1087, 823, 722, 697, 626, 523 ; **^{1}H NMR** (300 MHz, $CDCl_3$) δ 7.55 (d, *J* = 9.0 Hz, 1H), 7.43 (s, 1H), 7.35–7.23 (m, 3H), 7.21–7.17 (m, 2H), 7.08 (d, *J* = 9.0 Hz, 1H), 3.89 (t, *J* = 7.8 Hz, 1H), 3.45 (s, 3H), 3.28 (d, *J* = 7.8 Hz, 2H); **^{13}C NMR** (151 MHz, $CDCl_3$) δ 170.8, 143.3, 138.0, 128.8, 128.1, 127.6, 125.9, 125.1 (q, J_{C-F} = 32.5 Hz), 125.1, 124.2 (q, J_{C-F} = 272.0 Hz), 114.7, 46.7, 32.9, 30.3, 29.8; **HRMS** (ESI^+) *m/z*: [M + H] calcd for $C_{17}H_{15}F_3NO^+$ 306.1100; found 306.1113.

6-chloro-1-methyl-3-phenyl-3,4-dihydroquinolin-2(1H)-one (3.1e)

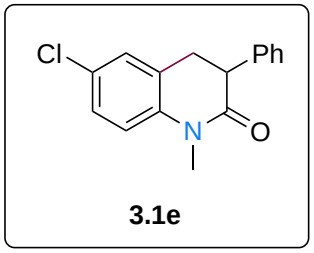

3.1e

Prepared according to general procedure 3C using **3.2e** (0.045 g, 0.16 mmol), **2-CTX** (8 mg, 0.03 mmol) and TFE (4 mL). Chromatography on silica gel with EtOAc/petroleum ether (20–40%) afforded **3.1e** as a white solid (0.038 g, 84% yield). Recrystallization with CH_2Cl_2:hexane afforded a white solid. **R_f** = 0.30 (2:8 EtOAc:petroleum ether); **M.P.** 118–120 °C; **IR** (film, vmax/cm^{-1}) 3032, 2920, 1663, 1598, 1493, 1454, 1423, 1415, 1339, 1261, 1119, 806, 695; **^{1}H NMR** (300 MHz, $CDCl_3$) δ 7.34–7.22 (m, 4H), 6.93 (d, *J* = 8.4 Hz, 1H), 3.86 (t, *J* = 7.5 Hz, 1H), 3.41 (s, 3H), 3.20 (d, *J* = 7.5 Hz, 2H); **^{13}C NMR** (101 MHz, $CDCl_3$) δ 170.6, 139.0, 138.2, 128.8, 128.2, 128.0, 127.6, 127.4, 127.1, 126.2, 115.9, 46.7, 32.8, 30.3; **HRMS** (ESI^+) *m/z*: [M + H] calcd for $C_{16}H_{15}ClNO^+$ 272.0837; found 272.0851.

6-fluoro-1-methyl-3-phenyl-3,4-dihydroquinolin-2(1H)-one (3.1f)

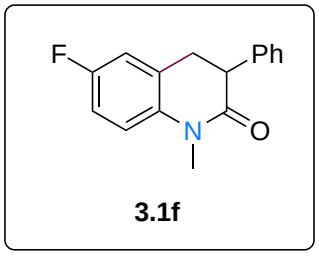

3.1f

Prepared according to general procedure 3C using **3.2f** (0.073 g, 0.29 mmol) and **2-CTX** (14 mg, 0.06 mmol). Chromatography on silica gel with EtOAc/petroleum ether (0–7%) afforded **3.1f** as a white solid (0.065 g, 89% yield). Recrystallization with CH_2Cl_2:hexane afforded a colourless crystalline solid. **R_f** = 0.44 (3:7

EtOAc:petroleum ether); **M.P.** 114–116 °C; **IR** (film, $\nu_{max/cm^{-1}}$) 2922, 1669, 1601, 1502, 1472, 1451, 1439, 1416, 1363, 1272, 1234, 1163, 1153, 1120, 698; **^{1}H NMR** (300 MHz, $CDCl_3$) δ 7.35–7.11 (m, 5H), 6.99–6.82 (m, 3H), 3.86 (app t, *J* = 7.5 Hz, 1H), 3.41 (s, 3H), 3.20 (d, *J* = 7.5 Hz, 2H); **^{13}C NMR** (101 MHz, $CDCl_3$) δ 170.5, 158.6 (d, $J_{C\text{-}F}$ = 243.7 Hz), 138.3, 136.6, 128.7, 128.0, 127.4, 127.4, 115.8 (d, $J_{C\text{-}F}$ = 8.1 Hz), 115.2 (d, $J_{C\text{-}F}$ = 22.8 Hz), 114.0 (d, $J_{C\text{-}F}$ = 22.5 Hz), 46.7, 33.0, 30.4; **HRMS** (ESI^+) *m/z*: [M + H] calcd for $C_{16}H_{15}FNO^+$ 256.1132; found 256.1139.

6-bromo-1-methyl-3-phenyl-3,4-dihydroquinolin-2(1H)-one (3.1g)

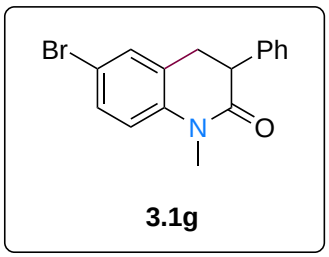

3.1g

Prepared according to general procedure 3C using **3.2g** (0.073 g, 0.23 mmol) and **2-CTX** (11 mg, 0.05 mmol). Chromatography on silica gel with EtOAc/petroleum ether (0–7%) afforded **3.1g** as a white solid (0.064 g, 88% yield). Recrystallization with CH_2Cl_2:hexane afforded a colourless crystalline solid. **R_f** = 0.30 (3:7 EtOAc:petroleum ether); **M.P.** 117–119 °C; **IR** (film, $\nu_{max/cm^{-1}}$) 2922, 2243, 1666, 1593, 1489, 1469, 1451, 1413, 1355, 1335, 1257, 1118, 905, 807, 726, 693; **^{1}H NMR** (300 MHz, $CDCl_3$) δ 7.41–7.35 (m, 1H), 7.33–7.23 (m, 4H), 7.21–7.14 (m, 2H), 6.87 (d, *J* = 8.6 Hz, 1H), 3.86 (app t, *J* = 7.5 Hz, 1H), 3.40 (s, 3H), 3.20 (d, *J* = 7.5 Hz, 2H); **^{13}C NMR** (75 MHz, $CDCl_3$) δ 170.6, 139.5, 138.1, 130.8, 130.5, 128.8, 128.0, 127.5, 127.4, 116.3, 115.7, 46.6, 32.7, 30.2; **HRMS** (ESI^+) *m/z*: [M + H] calcd for $C_{16}H_{15}BrNO^+$ 316.0332; found 316.0346.

5-bromo-1-methyl-3-phenyl-3,4-dihydroquinolin-2(1H)-one & 7-bromo-1-methyl-3-phenyl-3,4-dihydroquinolin-2(1*H*)-one (2h)

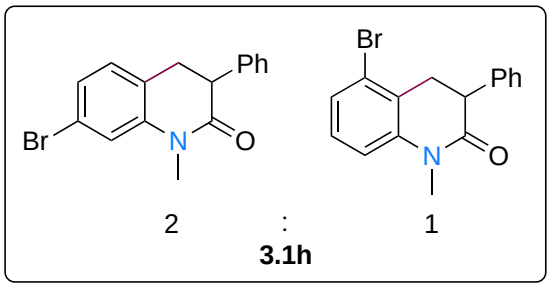

3.1h

Prepared according to general procedure 3C using **1h** (0.097 g, 0.307 mmol) and **2-CTX** (15 mg, 0.061 mmol). Chromatography on silica gel with EtOAc/petroleum ether (0–7%) afforded **3.1h** as a white amorphous solid in an approximate 1:2 mixture of inseparable regioisomers (0.081 g, 84% yield). **R_f** = 0.45 (2:8 EtOAc:petroleum ether); **IR** (film, vmax/cm^{-1}) 2923, 2853, 1674, 1591, 1454, 1362, 1336, 1253, 1122, 773, 750, 698; **^{1}H NMR** (300 MHz, $CDCl_3$) δ 7.36–6.91 (m, 8H), 3.93–3.80 (m, 1H), 3.45–3.34 (m, 4.5H), 3.24–3.12 (m, 0.5H); **^{13}C NMR** (101 MHz, $CDCl_3$) δ 170.6, 170.5, 141.5, 138.0, 137.7, 129.2, 128.6, 128.5, 128.4, 128.0, 127.8, 127.3, 127.1, 125.7, 125.3, 124.1,

123.7, 122.9, 121.0, 117.8, 114.6, 114.0, 46.6, 46.1, 32.4, 32.1, 30.4, 30.0; **HRMS** (ESI^+) *m/z*: [M + H] calcd for $C_{16}H_{15}{}^{79}BrNO^+$ 316.0332; found 316.0344.

1-methyl-2-oxo-3-phenyl-1,2,3,4-tetrahydroquinoline-6-carbonitrile (3.1i)

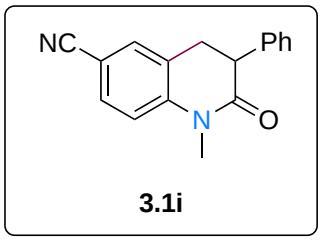

3.1i

Prepared according to general procedure 3C using **3.2i** (0.075 g, 0.29 mmol) and **2-CTX** (14 mg, 0.06 mmol). Chromatography on silica gel with EtOAc/petroleum ether (5–15%) afforded **3.1i** as a white solid (0.034 g, 45% yield). Recrystallization with CH_2Cl_2:hexane afforded fine colourless needles. $\mathbf{R_f}$ = 0.29 (2:8 EtOAc:petroleum ether); **M.P.** 169–171 °C; **IR** (film, $\nu_{max/cm^{-1}}$) 3048, 2922, 2223, 1671, 1603, 1499, 1472, 1451, 1421, 1363, 1338, 1262, 1226, 1108, 827, 733, 698; **^{1}H NMR** (300 MHz, $CDCl_3$) δ 7.58 (dd, *J* = 8.4, 2.0 Hz, 1H), 7.57 (bs, 1H), 7.34–7.23 (m, 3H), 7.19–7.13 (m, 2H), 7.07 (d, *J* = 8.4 Hz, 1H), 3.90 (app t, *J* = 7.6 Hz, 1H), 3.44 (s, 3H), 3.26 (d, *J* = 7.6 Hz, 2H); **^{13}C NMR** (75 MHz, $CDCl_3$) δ 170.7, 144.0, 137.5, 132.3, 131.5, 128.8, 127.9, 127.7, 126.3, 118.9, 115.1, 106.1, 46.43, 32.5, 30.3; **HRMS** (ESI^+) *m/z*: [M + H] calcd for $C_{17}H_{15}N_2O^+$ 263.1179; found 263.1190.

6-acetyl-1-methyl-3-phenyl-3,4-dihydroquinolin-2(1*H*)-one (3.1j)

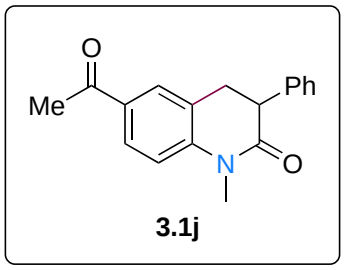

3.1j

Prepared according to general procedure 3C using **3.2j** (0.103 g, 0.369 mmol) and **2-CTX** (18 mg, 0.074 mmol). Chromatography on silica gel with EtOAc/petroleum ether (0–7%) afforded **3.1j** as a white oil (0.026 g, 25% yield). $\mathbf{R_f}$ = 0.50 (3:7 EtOAc:petroleum ether); **IR** (film, vmax/cm^{-1}) 2922, 1671, 1601, 1502, 1358, 1338, 1285, 1272, 1118, 822, 698; **^{1}H NMR** (300 MHz, $CDCl_3$) δ 7.89 (dd, *J* = 8.5, 2.0 Hz, 1H), 7.82–7.78 (m, 1H), 7.37–7.21 (m, 3H), 7.22–7.15 (m, 2H), 7.06 (d, *J* = 8.5 Hz, 1H), 3.91 (t, *J* = 7.6 Hz, 1H), 3.46 (s, 3H), 3.29 (d, *J* = 7.6 Hz, 2H), 2.58 (s, 3H); **^{13}C NMR** (101 MHz, $CDCl_3$) δ 196.8, 170.8, 144.2, 137.9, 131.8, 128.7, 128.6, 128.1, 127.9, 127.3, 125.2, 114.3, 46.6, 32.7, 30.2, 26.4; **HRMS** (ESI^+) *m/z*: [M + H] calcd for $C_{18}H_{18}NO_2^+$ 280.1332; found.

5,7-difluoro-1-methyl-3-phenyl-3,4-dihydroquinolin-2(1H)-one (3.1k)

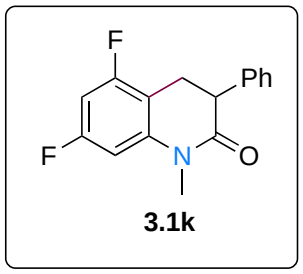

3.1k

Prepared according to general procedure 3C using **3.2k** (0.137 g, 0.501 mmol) and **2-CTX** (25 mg, 0.100 mmol). Chromatography on silica gel with EtOAc/petroleum ether (0–7%) afforded **3.1k** as a white solid (0.111 g, 81% yield). Recrystallization with CH_2Cl_2:petroleum ether afforded colorless needles. $\mathbf{R_f}$ = 0.45 (3:7 EtOAc:petroleum ether); **M.P.** 92–96°C; **IR** (film, vmax/cm^{-1}) 3092, 2925, 1675, 1621, 1601, 1450, 1331, 1273, 1112, 1001, 818, 762, 695, 537; **^{1}H NMR** (300 MHz, $CDCl_3$) δ 7.35–7.23 (m, 3H), 7.23–7.16 (m, 2H), 6.61–6.50 (m, 2H), 3.87 (dd, *J* = 8.5, 6.5 Hz, 1H), 3.39 (s, 3H), 3.29–3.12 (m, 2H); **^{13}C NMR** (101 MHz, $CDCl_3$) δ 170.4, 162.0 (dd, $J_{C\text{-}F}$ = 245.9, 14.6 Hz), 159.6 (dd, $J_{C\text{-}F}$ = 245.8, 14.3 Hz), 142.6 (dd, $J_{C\text{-}F}$ = 12.1, 12.0 Hz), 137.7, 128.7, 127.7, 127.4, 108.1 (dd, $J_{C\text{-}F}$ = 22.0, 3.4 Hz), 98.7 (dd, $J_{C\text{-}F}$ = 26.7, 2.5 Hz), 98.1 (t, $J_{C\text{-}F}$ = 26.2 Hz), 45.8, 30.3, 24.4 (d, $J_{C\text{-}F}$ = 2.0 Hz); **HRMS** (ESI$^+$) *m/z*: [M + H] calcd for $C_{16}H_{14}F_2NO^+$ 274.1038 found 274.1050.

5,6,7-trimethoxy-1-methyl-3-phenyl-3,4-dihydroquinolin-2(1*H*)-one (3.1l)

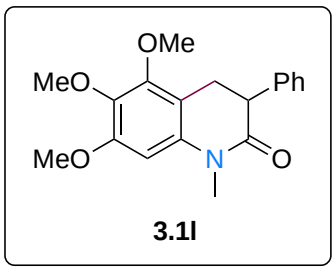

3.1l

Prepared according to general procedure 3C using **3.2l** (0.072 g, 0.220 mmol) and **2-CTX** (11 mg, 0.044 mmol). Chromatography on silica gel with EtOAc/petroleum ether (0–7%) afforded **3.1l** as a clear, colorless oil (0.012 g, 16% yield). $\mathbf{R_f}$ = 0.5 (1:1 EtOAc:petroleum ether); **IR** (film, vmax/cm^{-1}) 2929, 2849, 1667, 1560, 1502, 1464, 1415, 1335, 1255, 1110, 1021, 803, 751, 698; **^{1}H NMR** (300 MHz, $CDCl_3$) δ 7.33–7.17 (m, 5H), 6.37 (s, 1H), 3.89 (s, 3H), 3.84 (s, 3H), 3.83–3.77 (m, 4H), 3.41 (s, 3H), 3.17 (qd, *J* = 15.9, 7.6 Hz, 2H); **^{13}C NMR** (101 MHz, $CDCl_3$) δ 170.9, 152.4, 150.6, 138.6, 138.1, 136.4, 128.5, 127.9, 127.1, 111.3, 96.0, 61.0, 56.3, 56.3, 46.6, 30.3, 25.7.; **HRMS** (ESI$^+$) *m/z*: [M + H] calcd for $C_{19}H_{22}NO_4^+$ 328.1543 found 328.1560.

1-methyl-3-phenyl-3,4-dihydro-1,6-naphthyridin-2(1*H*)-one (3.1m)

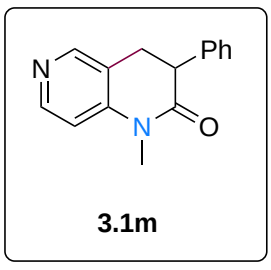

3.1m

Prepared according to general procedure 3C using **3.2m** (0.069 g, 0.29 mmol) and **2-CTX** (14 mg, 0.06 mmol). Chromatography on neutral alumina with EtOAc/petroleum ether (10–50%) afforded **3.1m** as a white solid (0.049 g, 71% yield). Recrystallization with CH_2Cl_2:hexane afforded fine colourless needles. $\mathbf{R_f}$ (alumina) = 0.26 (5:5 EtOAc:petroleum ether); **M.P.** 128–130 °C; **IR** (film, $\nu_{max/cm^{-1}}$) 3033, 2922, 2856, 1679, 1590,

1494, 1467, 1454, 1421, 1365, 1340, 1294, 1274, 1244, 1188, 1120, 1052, 961, 911, 817, 730, 696; **^{1}H NMR** (300 MHz, $CDCl_3$) δ 8.46 (d, *J* = 5.6 Hz, 1H), 8.35 (s, 1H), 7.36–7.24 (m, 3H), 7.22–7.12 (m, 2H), 6.88 (d, *J* = 5.6 Hz, 1H), 3.92 (app t, *J* = 7.8 Hz, 1H), 3.40 (s, 3H), 3.24 (d, *J* = 7.8 Hz, 2H); **^{13}C NMR** (75 MHz, $CDCl_3$) δ 170.8, 149.8, 148.4, 147.0, 137.7, 128.8, 128.0, 127.6, 120.0, 109.1, 46.5, 29.8, 29.6; **HRMS** (ESI^+) *m/z*: [M + H] calcd for $C_{15}H_{15}N_2O^+$ 239.1179; found 239.1194.

5-phenyl-1,2,5,6-tetrahydro-4*H*-pyrrolo[3,2,1-*ij*]quinolin-4-one (3.1n)

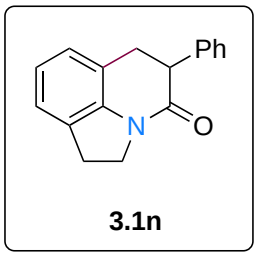

3.1n

Prepared according to general procedure 3C using **3.2n** (0.129 g, 0.52 mmol) and **2-CTX** (0.026 g, 0.1 mmol). Chromatography on silica gel with EtOAc/hexanes (0–7%) afforded **3.1n** a white solid (0.100 g, 78% yield). Recrystallization with CH_2Cl_2:hexane afforded a white crystalline solid. **R_f** = 0.16 (2:8 EtOAc:hexane); **M.P.** 155–157 °C; **IR** (film, ν_{max}/cm^{-1}) 3298, 3039, 2928, 2856, 1652, 1631, 1594, 1481, 1465, 1437, 1392, 1341, 1327, 1298, 1273, 1225, 1077, 1029, 1005, 906, 763, 723, 696; **^{1}H NMR** (300 MHz, $CDCl_3$) δ 7.35–7.20 (m, 5H), 7.11 (d, *J* = 7.3 Hz, 1H), 7.04–6.90 (m, 2H), 4.21–4.05 (m, 2H), 3.93 (app t, *J* = 7.6 Hz, 1H), 3.33 (dd, *J* = 16.4, 7.1 Hz, 1H), 3.27–3.13 (m, 3H); **^{13}C NMR** (151 MHz, $CDCl_3$) δ 168.2, 141.3, 140.0, 129.0, 128.8, 128.1, 127.3, 125.5, 123.6, 123.5, 119.9, 48.2, 45.7, 33.1, 28.0; **HRMS** (ESI^+) *m/z*: [M + H] calcd for $C_{17}H_{16}NO^+$ 250.1226; found 250.1241.

9-methoxy-6-phenyl-2,3,6,7-tetrahydro-1*H*,5*H*-pyrido[3,2,1-*ij*]quinolin-5-one (3.1o)

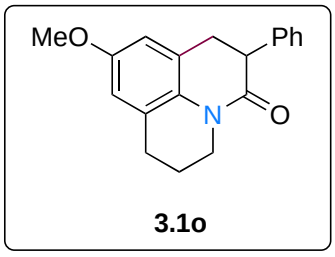

3.1o

Prepared according to general procedure 3C using **3.2o** (0.060 g, 0.2 mmol) and **2-ITX** (14 mg, 0.04 mmol). Chromatography on silica gel with EtOAc/hexanes (0–7%) afforded **3.1o** a white solid (0.058 g, 97% yield). An analytical sample was prepared by recrystallization with CH_2Cl_2:hexane to afford fine white needles. **R_f** = 0.40 (2:8 EtOAc:petroleum ether); **M.P.** 110–112 °C; **IR** (film, ν_{max}/cm^{-1}); **^{1}H NMR** (300 MHz, $CDCl_3$) δ 7.37–7.21 (m, 5H), 6.60 (s, 2H), 4.00–3.91 (m, 2H), 3.88 (app t, *J* = 7.5 Hz, 1H), 3.80 (s, 3H), 3.27–3.10 (m, 2H), 2.83 (t, *J* = 6.3 Hz, 2H), 2.05–1.91 (m, 2H); **^{13}C NMR** (101 MHz, $CDCl_3$) δ 169.5, 155.1, 139.0, 129.5, 128.7, 128.1, 127.2, 126.5, 126.1, 112.5, 112.2, 55.6, 46.9, 41.2, 33.3, 27.6, 21.8; **HRMS** (ESI^+) *m/z*: [M + H] calcd for $C_{19}H_{20}NO_2^+$ 294.1489; found 294.1505.

3-(4-methoxyphenyl)-1-methyl-3,4-dihydroquinolin-2(1*H*)-one (3.1p)

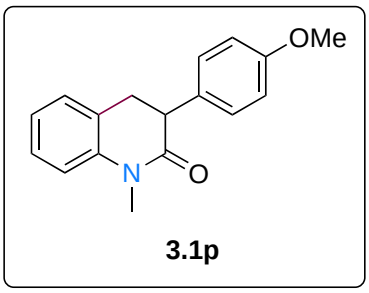

3.1p

Prepared according to general procedure 3C using **3.2p** (0.065 g, 0.24 mmol), **2-CTX** (12 mg, 0.05 mmol) and TFE:$CHCl_3$ (4:1 mL). Chromatography on silica gel with EtOAc/petroleum ether (20–40%) afforded **3.1p** as a white solid (0.058 g, 89% yield). Recrystallization with CH_2Cl_2:hexane afforded a white crystalline solid. $\mathbf{R_f}$ = 0.26 (2:8 EtOAc:petroleum ether); **M.P.** 103–105 °C; **IR** (film, vmax/cm^{-1}) 2970, 1667, 1601, 1515, 1468, 1250, 1181, 1117, 1022, 831, 812, 753, 526; **^{1}H NMR** (300 MHz, $CDCl_3$) δ 7.31–7.25 (m, 1H), 7.20–7.17 (m, 1H), 7.15–7.10 (m, 2H), 7.06–6.99 (m, 2H), 6.86–6.81 (m, 2H), 3.82 (app t, *J* = 7.6 Hz, 1H), 3.77 (s, 3H), 3.42 (s, 3H), 3.20 (d, *J* = 7.6 Hz, 2H); **^{13}C NMR** (101 MHz, $CDCl_3$) δ 171.3, 158.7, 140.4, 130.7, 129.1, 128.1, 127.7, 125.6, 123.0, 114.7, 114.1, 55.3, 46.2, 33.1, 30.1; **HRMS** (ESI^+) *m/z*: [M + H] calcd for $C_{17}H_{18}NO_2^+$ 268.1332; found 268.1348.

1-methyl-3-(*p*-tolyl)-3,4-dihydroquinolin-2(1*H*)-one (3.1q)

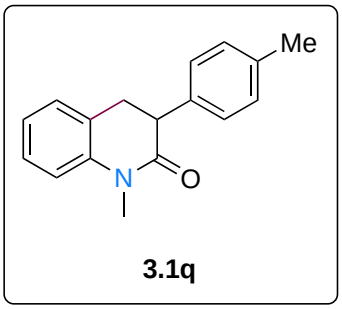

3.1q

Prepared according to general procedure 3C using **3.2q** (0.060 g, 0.24 mmol), **2-CTX** (12 mg, 0.05 mmol) and TFE:$CHCl_3$ (4:1 mL). Chromatography on silica gel with EtOAc/petroleum ether (20–40%) afforded **3.1q** as a white solid (0.049 g, 81% yield). Recrystallization with CH_2Cl_2:hexane afforded white needles. $\mathbf{R_f}$ = 0.35 (2:8 EtOAc:petroleum ether); **M.P.** 64–66 °C; **IR** (film, vmax/cm^{-1}) 2920, 2852, 1671, 1602, 1464, 1365, 1262, 1120, 753; **^{1}H NMR** (300 MHz, $CDCl_3$) δ 7.31–7.25 (m, 1H), 7.20–7.17 (m, 1H), 7.14–7.06 (m, 4H), 7.05–7.00 (m, 2H), 3.83 (app t, *J* = 7.6 Hz, 1H), 3.42 (s, 3H), 3.22 (d, *J* = 7.6 Hz, 2H), 2.31 (s, 3H); **^{13}C NMR** (101 MHz, $CDCl_3$) δ 171.2, 140.4, 136.8, 135.6, 129.4, 128.1, 128.0, 127.7, 125.6, 123.0, 114.7, 46.6, 33.0, 30.1, 21.2; **HRMS** (ESI^+) *m/z*: [M + H] calcd for $C_{17}H_{18}NO^+$ 252.1383; found 252.1391.

3-(4-bromophenyl)-1-methyl-3,4-dihydroquinolin-2(1*H*)-one (3.1r)

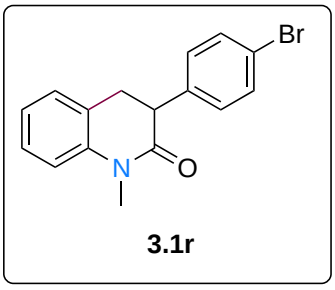

3.1r

Prepared according to general procedure 3C using **3.2r** (0.032 g, 0.101 mmol) and **2-CTX** (5 mg, 0.020 mmol). Chromatography on silica gel with EtOAc/petroleum ether (0–7%) afforded **3.1r** as a white amorphous solid (0.008 g, 26% yield). $\mathbf{R_f}$ = 0.45 (2:8 EtOAc:petroleum ether); **IR** (film, vmax/cm^{-1}) 2924, 1645, 1593,

1491, 1372, 1128, 1092, 1071, 1008, 834, 767, 697, 545; **^{1}H NMR** (300 MHz, $CDCl_3$) δ 7.45–7.38 (m, 2H), 7.33–7.27 (m, 1H), 7.21–7.15 (m, 1H), 7.11–6.99 (m, 4H), 3.82 (app t, *J* = 7.8 Hz, 1H), 3.42 (s, 3H), 3.19 (d, *J* = 7.8 Hz, 2H); **^{13}C NMR** (101 MHz, $CDCl_3$) δ 170.3, 140.1, 137.5, 131.6, 129.8, 128.0, 127.8, 125.0, 123.1, 121.1, 114.7, 46.4, 32.8, 30.1; **HRMS** (ESI^+) *m/z*: [M + H] calcd for $C_{16}H_{15}{}^{79}BrNO^+$ 316.0332; found 316.0298.

1-methyl-3-(naphthalen-2-yl)-3,4-dihydroquinolin-2(1*H*)-one (3.1s)

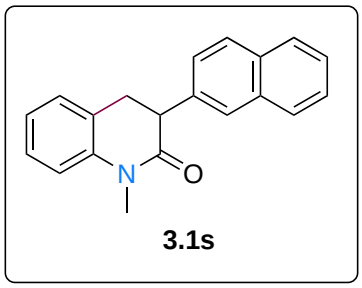

3.1s

Prepared according to general procedure 3C using **3.2s** (0.036 g, 0.125 mmol) and **2-CTX** (6 mg, 0.025 mmol). Chromatography on silica gel with EtOAc/petroleum ether (0–7%) afforded **3.1s** as a white solid (0.027 g, 75% yield). An analytical sample was prepared by recrystallization with CH_2Cl_2:petroleum ether to afford colorless needles. **R_f** = 0.80 (4:6 EtOAc:petroleum ether); **M.P.** 172–177 °C; **IR** (film, vmax/cm^{-1}) 2919, 2850, 1669, 1602, 1470, 1361, 1264, 1118, 752; **^{1}H NMR** (300 MHz, $CDCl_3$) δ 7.85–7.70 (m, 3H), 7.66–7.62 (m, 1H), 7.48–7.41 (m, 2H), 7.41–7.27 (m, 2H), 7.23–7.18 (m, 1H), 7.08–7.00 (m, 2H), 4.04 (dd, *J* = 9.5, 6.2 Hz, 1H), 3.46 (s, 3H), 3.37 (dd, *J* = 15.6, 9.5 Hz, 1H), 3.27 (dd, *J* = 15.6, 6.2 Hz, 1H); **^{13}C NMR** (101 MHz, $CDCl_3$) δ 170.8, 140.2, 136.0, 133.3, 132.5, 128.2, 127.9, 127.8, 127.6, 127.5, 126.7, 126.2, 125.9, 125.7, 125.3, 123.0, 114.7, 47.0, 32.9, 30.1; **HRMS** (ESI^+) *m/z*: [M + H] calcd for $C_{20}H_{18}NO^+$ 288.1383; found 288.1397.

3-(3,4-dichlorophenyl)-1-methyl-3,4-dihydroquinolin-2(1*H*)-one (3.1t)

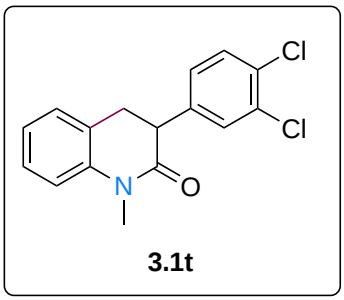

3.1t

Prepared according to general procedure 3C using **3.2t** (0.086 g, 0.281 mmol) and **2-CTX** (14 mg, 0.056 mmol). Chromatography on silica gel with EtOAc/petroleum ether (0–7%) afforded **3.1t** as a white solid (0.081 g, 94% yield). An analytical sample was prepared by recrystallization with CH_2Cl_2:petroleum ether to afford a colorless crystalline solid. **R_f** = 0.80 (4:6 EtOAc:petroleum ether); **M.P.** 89–92 °C; **IR** (film, vmax/cm^{-1}) 2924, 2854, 1669, 1603, 1471, 1368, 1264, 1121, 755; **^{1}H NMR** (300 MHz, $CDCl_3$) δ 7.39–7.27 (m, 3H), 7.19 (app d, *J* = 7.2 Hz, 1H), 7.09–7.00 (m, 3H), 3.84–3.75 (m, 1H), 3.42 (s, 3H), 3.21–3.15 (m, 2H); **^{13}C NMR** (101 MHz, $CDCl_3$) δ 169.8, 140.0, 138.6, 132.5, 131.2, 130.4, 130.2, 127.9, 127.6, 124.8, 123.2, 114.8, 46.2, 32.7, 30.1; **HRMS** (ESI^+) *m/z*: [M + H] calcd for $C_{16}H_{14}Cl_2NO^+$ 306.0447; found 306.0455.

(3aS,9bR)-5-methyl-1,2,3,3a,5,9b-hexahydro-4H-cyclopenta[c]quinolin-4-one (3.1u)[171]

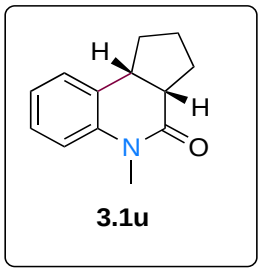

3.1u

Prepared according to general procedure 3C using **3.2u** (0.100 g, 0.50 mmol), **2-CTX** (25 mg, 0.10 mmol) and TFE (4 mL). Chromatography on silica gel with EtOAc/petroleum ether (20–40%) afforded **3.1u** as a yellow oil (0.050 g, 50% yield (75% based on recovered starting material)) as a 2.7:1 ratio of diastereomers (by C-18 HPLC: cis-fused as the major product). $\mathbf{R_f}$ = 0.37 (2:8 EtOAc:petroleum ether); **IR** (film, vmax/cm^{-1}) 2924, 1663, 1601, 1467, 1370, 1344, 1278, 1259, 1128, 1111, 753; **^{1}H NMR** (300 MHz, $CDCl_3$) δ 7.30–7.12 (m, 2H), 7.07–6.96 (m, 2H), 3.37 (s, 3H), 3.18 (q, *J* = 8.4 Hz, 1H) 2.94–2.76 (m, 1H), 2.41–2.21 (m, 1H), 2.11–1.82 (m, 3H), 1.74–1.62 (m, 2H); **^{13}C NMR** (101 MHz, $CDCl_3$) Major Product: δ 171.8, 139.1, 128.3, 127.4, 127.2, 122.8, 114.6, 44.5, 42.0, 33.4, 29.7, 29.2, 22.9; Minor Product: δ 172.9, 141.7, 131.5, 127.2, 124.8, 122.8, 114.9, 48.0, 42.7, 29.8, 27.5, 24.3, 22.8; **HRMS** (ESI$^+$) *m/z*: [M + H] calcd for $C_{13}H_{16}NO^+$ 202.1226; found 202.1239. Recorded data in accordance with those previously reported.

1-methyl-4-phenyl-3,4-dihydroquinolin-2(1*H*)-one (3.1v)[169]

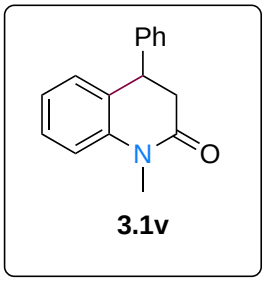

3.1v

Prepared according to general procedure 3C using **3.2v** (0.078 g, 0.33 mmol) and **2-ITX** (0.022 mg, 0.07 mmol). Chromatography on silica gel with EtOAc/hexanes (0–7%) afforded **3.1v** (0.025 g, 32% yield).

Prepared according to general procedure 3D using **3.2v** (0,074 g, 0.31 mmol) and $[Ir(dF(CF_3)ppy)_2dtbby]PF_6$ (3.5 mg, 0.003 x 10^{-3} mmol). Chromatography on silica gel with EtOAc/hexanes (0–10%) afforded **3.1v** (0.047 g, 64% yield).

Obtained as a light yellow solid. $\mathbf{R_f}$ = 0.35 (2:8 EtOAc:petroleum ether); **^{1}H NMR** (300 MHz, $CDCl_3$) δ 7.38–7.24 (m, 4H), 7.20–7.13 (m, 2H), 7.09–6.96 (m, 2H), 6.96–6.88 (m, 1H), 4.28–4.19 (m (app t), 1H), 3.40 (s, 3H), 3.03–2.90 (m, 2H). Recorded data in accordance with those previously reported.

5.3.8 General procedure 3E: Synthesis of quinolin-2-ones (3.3)

A stirring solution of **3.1** (1 equiv.), $[Cu(dmp)_2Cl]Cl$ (2 mol%) and NFSI (1.5 equiv) was heated at 80 °C for 24 h under argon gas. The solvent was removed in vacuo and the crude residue

purified by silica chromatography eluting with EtOAc/petroleum ether to afford quinolin-2-one **3.3**.

5.3.9 Characterization data for quinolin-2-ones (3.3)

1-methyl-3-phenylquinolin-2(1*H*)-one (3.3a)[245]

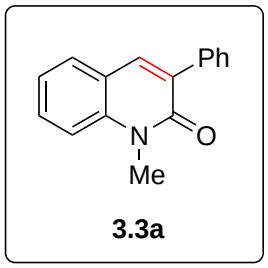

3.3a

Prepared according to general procedure 3E using **3.1a** (0.095 g, 0.40 mmol), Cu(dmp)$_2$Cl]Cl (2.1 mg, 0.008 mol), and NFSI (0.189 g, 0.6 mmol). Chromatography on silica gel with EtOAc/petroleum ether afforded **3.3a** as a white solid (0.085 g, 99% yield). $\mathbf{R_f}$ = 0.15 (2:8 EtOAc:petroleum ether); **^{1}H NMR** (300 MHz, $CDCl_3$) δ 7.81 (s, 1H), 7.73–7.70 (m, 2H), 7.64–7.55 (m, 2H), 7.47–7.35 (m, 4H), 7.29–7.23 (m, 1H), 3.82 (s, 3H). Recorded data in accordance with those previously reported.

quinolin-2(1H)-one (3.3x)[246]

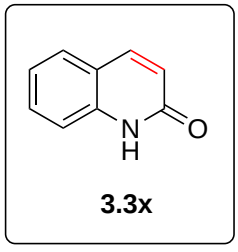

3.3x

Prepared according to general procedure 3E using commercially available quinolinone (0.050 g, 0.339 mmol), Cu(dmp)$_2$Cl]Cl (3.74 mg, 0.007 mmol), and NFSI (0.161 g, 0.509 mmol). Chromatography on silica gel with EtOAc/petroleum ether afforded **3.3x** as a white solid (0.026 g, 53% yield). $\mathbf{R_f}$ = 0.6 (3:7 EtOAc:petroleum ether); **^{1}H NMR** (300 MHz, $CDCl_3$) δ 7.81 (s, 1H), 7.73–7.70 (m, 2H), 7.64–7.55 (m, 2H), 7.47–7.35 (m, 4H), 7.29–7.23 (m, 1H), 3.82 (s, 3H). Recorded data in accordance with those previously reported.

6-methoxy-1-methyl-3-phenylquinolin-2(1*H*)-one (3.3c)[239]

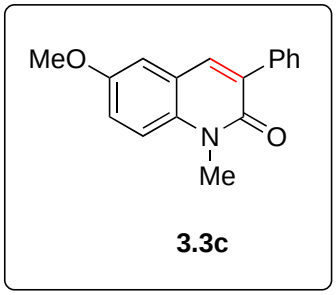

3.3c

Prepared according to general procedure 3E using **3.1c** (0.027 g, 0.10 mmol), Cu(dmp)$_2$Cl]Cl (1.1 mg, 0.002 mol), and NFSI (0.047 g, 0.15 mmol). Chromatography on silica gel with EtOAc/petroleum ether afforded **3.3c** as a white solid (0.021 g, 78% yield). $\mathbf{R_f}$ = 0.33 (2:8 EtOAc:petroleum ether); **^{1}H NMR** (300 MHz, $CDCl_3$) δ 7.74 (s, 1H), 7.71 (m, 2H), 7.47–7.34 (m, 3H), 7.31 (d, *J* = 9.2 Hz, 1H), 7.18, (dd, *J* = 9.2, 2.9 Hz, 1H), 7.05 (d, *J* = 2.9 Hz, 1H), 3.88 (s, 3H), 3.78 (s, 3H). Recorded data in accordance with those previously reported.

3-(4-methoxyphenyl)-1-methylquinolin-2(1H)-one (3.3p)[247]

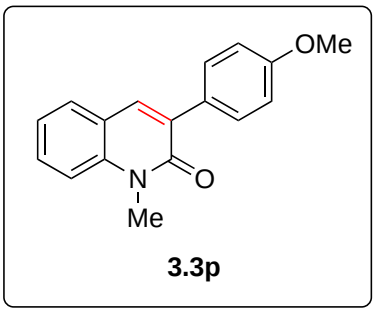

3.3p

Prepared according to general procedure 3E using **3.1p** (0.019 g, 0.07 mmol), $Cu(dmp)_2Cl]Cl$ (1.1 mg, 0.002 mol), and NFSI (0.033 g, 0.107 mmol). Chromatography on silica gel with EtOAc/petroleum ether afforded **3.3p** as a white solid (0.010 g, 53% yield). $\mathbf{R_f}$ = 0.41 (3:7 EtOAc:petroleum ether); **^{1}H NMR** (300 MHz, $CDCl_3$) δ 7.77 (s, 1H), 7.70 (s, 1H), 7.67 (s, 1H), 7.62–7.53 (m, 2H), 7.39–7.36 (m, 1H), 7.27–7.22 (m, 2H), 6.99–6.96 (m, 2H), 3.85 (s, 3H), 3.80 (s, 3H). Recorded data in accordance with those previously reported.

1-methyl-3-(p-tolyl)quinolin-2(1H)-one (3.3q)[239]

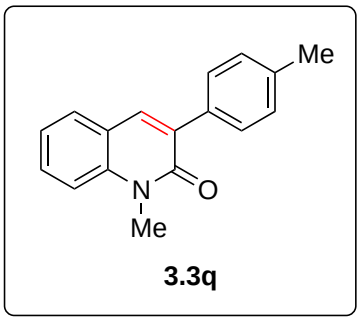

3.3q

Prepared according to general procedure 3E using **3.1q** (0.031 g, 0.123 mmol), $Cu(dmp)_2Cl]Cl$ (1.36 mg, 0.0025 mol), and NFSI (0.058 g, 0.185 mmol). Chromatography on silica gel with EtOAc/petroleum ether afforded **3.3q** as a white solid (0.027 g, 88% yield). $\mathbf{R_f}$ = 0.45 (3:7 EtOAc:petroleum ether); **^{1}H NMR** (300 MHz, $CDCl_3$) δ 7.78 (s, 1H), 7.63–7.53 (m, 4H), 7.38–7.36 (m, 1H), 7.27–7.22 (m, 3H), 3.80 (s, 3H), 2.40 (s, 3H). Recorded data in accordance with those previously reported.

5.4 Chapter 4 - Thioxanthone Catalysed Triplet Energy Transfer for the Synthesis of β-Lactams

5.4.1 General procedure 4A: Synthesis of acrylamides (4.2) using Mukaiyama's reagent

To a mixture of amine (1.1 equiv.), carboxylic acid (1 equiv.) and 2-chloro-1-methylpyridinium iodide (1.2–1.4 equiv.) in CH_2Cl_2 (5 mL/mmol of aniline) at 0 °C under argon, was added triethylamine (3 equiv.) dropwise and the reaction mixture allowed to warm slowly to room temperature. Once the reaction was completed (by TLC) the organic phase was washed with aqueous HCl (1.0 M), followed by sat. aqueous Na_2CO_3 and dried over $MgSO_4$. The organic solvents were removed in vacuo and the resulting crude product was purified by column

chromatography on silica gel or neutral alumina (petroleum ether:EtOAc gradient) to give acrylamide **4.2**.

5.4.2 General procedure 4B: Synthesis of acrylamides (4.2) including reductive amination

To a mixture of aldehyde (1 equiv.), $MgSO_4$ (3 equiv.) in CH_2Cl_2 (5 mL/mmol of aldehyde), was added methylamine 33% in abs. ethanol (3 equiv.) at room temperature and the reaction was stirred overnight. The solvent was evaporated, followed by the addition of $NaBH_4$ (1 equiv.) in MeOH (3.3 mL/mmol of aldehyde) at room temperature and the reaction mixture was stirred for a further 3 hrs, before the addition of water. Excess MeOH was removed under reduced pressure and the product was extracted with 3 x CH_2Cl_2. The combined organic layers were dried over $MgSO_4$ and the organic solvents were removed in vacuo. The resulting crude product was used directly in the subsequent coupling reaction (general procedure 4A).

5.4.3 Characterization data of acrylamides (4.2)

***N*-benzyl-*N*-methyl-2-phenylacrylamide (4.2a)**

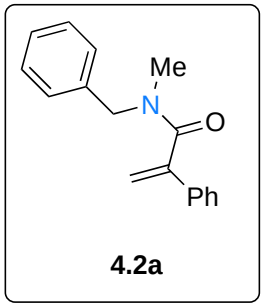

4.2a

Prepared according to general procedure 4A using *N*-methyl-1-phenylmethanamine (0.500 g, 4.12 mmol), 2-phenylacrylic acid (0.856 g, 5.77 mmol), 2-chloro-1-methylpyridinium iodide (1.264 g, 4.95 mmol) and triethylamine (1.72 mL, 12.37 mmol) in CH_2Cl_2 (50 mL). Chromatography on silica gel with EtOAc:petroleum ether (1:9 to 3:7) afforded **4.2a** in a 0.55:0.45 ratio of rotamers as a clear oil (0.685 g, 66% yield). $\mathbf{R_f}$ = 0.15 (2:8 EtOAc:petroleum ether); **IR** (film, ν_{max}/cm^{-1}) 3059, 3029, 2925, 1710, 1684, 1634, 1575, 1492, 1449, 1402, 1253, 1211, 1117, 1075, 1027; **^{1}H NMR** (300 MHz, $CDCl_3$) 7.50–7.44 (m, 2H), 7.39–7.28 (m, 7H), 7.09–7.06 (m, 1H), 5.77 (s, 0.55 H), 5.73 (s, 0.45H), 5.45 (s, 0.45H), 5.41 (s, 0.55H) 4.73 (s, 1.1H), 4.43 (s, 0.9H), 2.98 (s, 1.35H), 2.80 (s, 1.65H); **^{13}C NMR** (101 MHz, $CDCl_3$) δ 171.4, 171.0, 145.2, 145.0, 137.0, 136.3, 135.7, 135.6, 129.0, 128.9, 128.8, 128.8, 128.7, 128.4, 128.3, 128.1, 127.7, 127.6, 127.1, 125.8, 125.7, 114.4, 114.3, 54.5, 50.3, 36.0, 32.3; **HRMS** (ESI^+) *m/z*: [M + H] calcd for $C_{17}H_{18}NO^+$ 252.1383; found 252.1396.

***N*-methyl-*N*-(4-methylbenzyl)-2-phenylacrylamide (4.2b)**

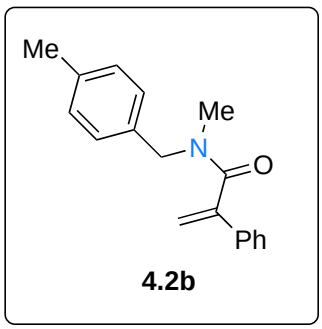

4.2b

Prepared according to general procedure 4A using *N*-methyl-1-(*p*-tolyl)methanamine (0.297 g, 2.2 mmol), 2-phenylacrylic acid (0.297 g, 2 mmol), 2-chloro-1-methylpyridinium iodide (0.665 g, 2.6 mmol) and triethylamine (0.836 mL, 6 mmol) in CH_2Cl_2 (25 mL). Chromatography on silica gel with EtOAc:petroleum ether (1:9 to 4:6) afforded **4.2b** in a 0.55:0.45 ratio of rotamers as a clear oil (0.355 g, 67% yield). **R_f** = 0.26 (3:7 EtOAc:petroleum ether); **IR** (film, ν_{max}/cm^{-1}) 3053, 3024, 2922, 2864, 1712, 1682, 1635, 1574, 1514, 1490, 1445, 1401, 1252, 1210, 1118, 1075, 1025; **^{1}H NMR** (300 MHz, $CDCl_3$) 7.49–7.43 (m, 2H), 7.37–7.33 (m, 3H), 7.24–7.09 (m, 3H), 6.97–6.94 (m, 1H), 5.75 (s, 0.55H), 5.73 (s, 0.45H), 5.44 (s, 0.45H), 5.38 (s, 0.55H), 4.68 (s, 1.1H), 4.39 (s, 0.9H), 2.96 (s, 1.35H), 2.78 (s, 1.65H), 2.35 (s, 1.65H), 2.32 (s, 1.35H); **^{13}C NMR** (101 MHz, $CDCl_3$) δ 171.3, 170.9, 145.3, 145.1, 137.5, 137.3, 135.8, 135.6, 134.0, 133.3, 129.5, 129.4, 129.0, 128.9, 128.8, 128.6, 128.4, 127.1, 125.8, 125.8, 114.3, 114.1, 54.3, 50.0, 35.9, 32.2, 21.2, 21.2; **HRMS** (ESI^+) *m/z*: [M + H] calcd for $C_{18}H_{20}NO^+$ 266.1539; found 266.1548.

***N*-methyl-*N*-(2-methylbenzyl)-2-phenylacrylamide (4.2c)**

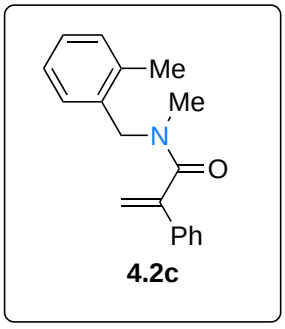

4.2c

Prepared according to general procedure 4A using *N*-methyl-1-(*o*-tolyl)methanamine (0.297 g, 2.2 mmol), 2-phenylacrylic acid (0.297 g, 2 mmol), 2-chloro-1-methylpyridinium iodide (0.665 g, 2.6 mmol) and triethylamine (0.836 mL, 6 mmol) in CH_2Cl_2 (25 mL). Chromatography on silica gel with EtOAc:petroleum ether (1:9 to 4:6) afforded **4.2c** in a 0.58:0.42 ratio of rotamers as a clear oil (0.393 g, 74% yield). **R_f** = 0.33 (3:7 EtOAc:petroleum ether); **IR** (film, ν_{max}/cm^{-1}) 3057, 3023, 2923, 1636, 1548, 1490, 1453, 1400, 1307, 1284, 1245, 1217, 1125, 1076; **^{1}H NMR** (300 MHz, $CDCl_3$) δ 7.51–7.45 (m, 2H), 7.41–7.32 (m, 3H), 7.20–7.06 (m, 4H), 5.77 (s, 0.58H), 5.64 (s, 0.42H), 5.41 (s, 0.58H), 5.38 (s, 0.42H), 4.76 (s, 1.16H), 4.40 (s, 0.84H), 3.02 (s, 1.26H), 2.77 (s, 1.74H), 2.36 (s, 1.74H), 2.14 (s, 1.26H); **^{13}C NMR** (101 MHz, $CDCl_3$) δ 171.6, 170.8, 145.5, 144.8, 136.7, 135.7, 135.7, 135.6, 134.5, 134.3, 130.6, 130.6, 128.9, 128.7, 128.3, 127.6, 127.4, 126.3, 126.2, 125.9, 125.8, 114.3, 114.3, 114.2, 52.3, 48.0, 35.8, 32.8, 19.3, 19.1; **HRMS** (ESI^+) *m/z*: [M + H] calcd for $C_{18}H_{20}NO^+$ 266.1539; found 266.1551

***N*-(3-chlorobenzyl)-*N*-methyl-2-phenylacrylamide (4.2d)**

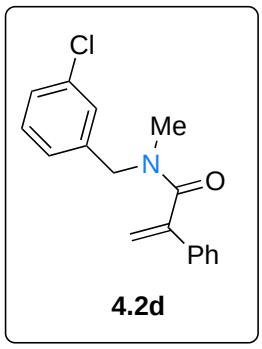

4.2d

Prepared according to general procedure 4A using 1-(3-chlorophenyl)-*N*-methylmethanamine (0.342 g, 2.2 mmol), 2-phenylacrylic acid (0.297 g, 2 mmol), 2-chloro-1-methylpyridinium iodide (0.665 g, 2.6 mmol) and triethylamine (0.836 mL, 6 mmol) in CH_2Cl_2 (25 mL). Chromatography on silica gel with EtOAc:petroleum ether (1:9 to 3:7) afforded **4.2d** in a 0.6:0.4 ratio of rotamers as a clear oil (0.335 g, 59% yield). **R_f** = 0.19 (2:8 EtOAc:petroleum ether); **IR** (film, ν_{max}/cm^{-1}) 3058, 3027, 2926, 1638, 1565, 1568, 1478, 1429, 1400, 1357, 1287, 1253, 1205, 1122, 1078, 1028; **^{1}H NMR** (300 MHz, $CDCl_3$) δ 7.47–7.19 (m, 8.2H), 7.00–6.93 (m, 0.8H), 5.77 (s, 0.6H), 5.72 (s, 0.4H), 5.42 (s, 0.4H), 5.40 (s, 0.6H), 4.68 (s, 1.2H), 4.39 (s, 0.8H), 2.97 (s, 1.2H), 2.79 (s, 1.8H); **^{13}C NMR** (101 MHz, $CDCl_3$) δ 171.3, 171.1, 145.1, 145.0, 139.1, 138.5, 135.6, 135.5, 134.8, 134.6, 130.1 (2C), 129.0, 129.0, 128.9, 128.8, 128.2, 127.9, 127.8, 127.2, 126.4, 125.8, 125.8, 125.2, 114.6, 114.5, 54.0, 49.8, 36.2, 32.5; **HRMS** (ESI^+) *m/z*: [M + H] calcd for $C_{17}H_{17}{}^{35}ClNO^+$ 286.0993; found 286.1004.

***N*-(4-bromobenzyl)-*N*-methyl-2-phenylacrylamide (4.2e)**

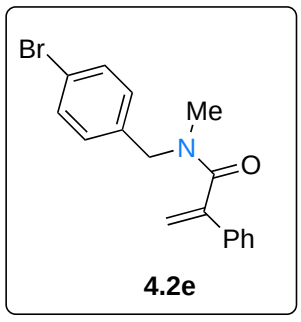

4.2e

Prepared according to general procedure 4A using 1-(4-bromophenyl)-*N*-methylmethanamine (0.440 g, 2.2 mmol), 2-phenylacrylic acid (0.297 g, 2 mmol), 2-chloro-1-methylpyridinium iodide (0.665 g, 2.6 mmol) and triethylamine (0.836 mL, 6 mmol) in CH_2Cl_2 (25 mL). Chromatography on silica gel with EtOAc:petroleum ether (1:9 to 3:7) afforded **4.2e** in a 0.6:0.4 ratio of rotamers as a clear oil (0.495 g, 75% yield). **R_f** = 0.14 (2:8 EtOAc:petroleum ether); **IR** (film, ν_{max}/cm^{-1}) 3056, 3028, 2925, 1698, 1634, 1486, 1441, 1399, 1282, 1253, 1209, 1120, 1071, 1010; **^{1}H NMR** (300 MHz, $CDCl_3$) δ 7.47–7.29 (m, 7H), 7.21–7.18 (m, 1.2H), 6.91– 6.89 (m, 0.8H), 5.75 (s, 0.6H), 5.70 (s, 0.4H), 5.39 (s, 0.4H), 5.37 (s, 0.6H), 4.64 (s, 1.2H), 4.36 (s, 0.8H), 2.94 (s, 1.2H), 2.77 (s, 1.8H); **^{13}C NMR** (101 MHz, $CDCl_3$) δ 171.1, 170.9, 144.9, 144.9, 136.0, 135.5, 135.4, 135.3, 131.8, 131.7, 129.9, 128.9, 128.8, 128.7, 128.7, 128.6, 125.7, 125.6, 121.4, 121.4, 114.3, 114.3, 53.8, 49.6, 35.9, 32.2; **HRMS** (ESI^+) *m/z*: [M + H] calcd for $C_{17}H_{17}{}^{79}BrNO^+$ 330.0488; found 330.0484.

***N*-methyl-2-phenyl-*N*-(3-(trifluoromethyl)benzyl)acrylamide (4.2f)**

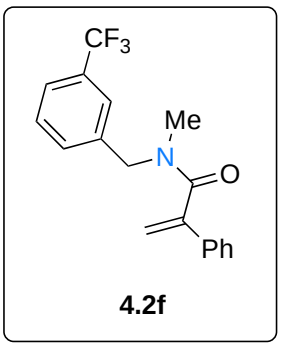

4.2f

Prepared according to general procedure 4A using *N*-methyl-1-(3-(trifluoromethyl)phenyl)methanamine (0.416 g, 2.2 mmol), 2-phenylacrylic acid (0.297 g, 2 mmol), 2-chloro-1-methylpyridinium iodide (0.665 g, 2.6 mmol) and triethylamine (0.836 mL, 6 mmol) in CH_2Cl_2 (25 mL). Chromatography on silica gel with EtOAc:petroleum ether (1:9 to 4:6) afforded **4.2f** in a 0.6:0.4 ratio of rotamers as a clear oil (0.491 g, 77% yield). $\mathbf{R_f}$ = 0.23 (3:7 EtOAc:petroleum ether; **IR** (film, ν_{max}/cm^{-1}) 2926, 1658, 1679, 1612, 1519, 1425, 1364, 1322, 1271, 1165, 1115, 1069, 1017; **^{1}H NMR** (300 MHz, $CDCl_3$) δ 7.57–7.23 (m, 9H), 5.78 (s, 0.6H), 5.73 (s, 0.4H), 5.43 (s, 0.4H), 5.41 (s, 0.6H), 4.77 (s, 1.2H), 4.48 (s, 0.8H), 2.99 (s, 1.2H), 2.81 (s, 1.8H); **^{13}C NMR** (151 MHz, $CDCl_3$) δ 171.4, 171.2, 145.2, 138.3, 137.6, 135.6, 135.6, 131.6, 131.3 (q, $J_{C\text{-}F}$ = 32.0 Hz), 131.2 (q, $J_{C\text{-}F}$ = 32.2 Hz), 130.4, 129.3, 129.1, 129.0, 129.0, 128.8, 125.9, 125.8, 124.7 (q, $J_{C\text{-}F}$ = 3.9 Hz), 124.7, 124.6, 124.5 (q, $J_{C\text{-}F}$ = 3.9 Hz), 124.2 (q, $J_{C\text{-}F}$ = 272.7 Hz), 124.0 (q, $J_{C\text{-}F}$ = 272.1 Hz), 123.9, 123.9, 114.6, 114.5, 54.2, 50.0, 36.2, 32.5; **^{19}F NMR** (377 MHz, $CDCl_3$) δ -62.62; **HRMS** (ESI^+) *m/z*: [M + H] calcd for $C_{18}H_{17}F_3NO^+$ 320.1257; found 320.1274.

***N*-(4-methoxybenzyl)-*N*-methyl-2-phenylacrylamide (4.2g)**

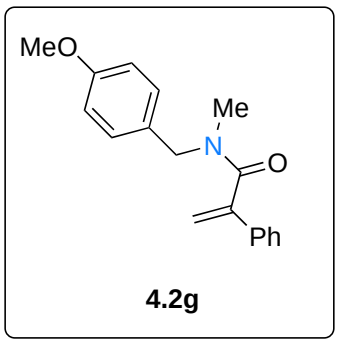

4.2g

Prepared according to general procedure A using 1-(4-methoxyphenyl)-*N*-methylmethanamine (201 mg, 1.33 mmol), 2-phenylacrylic acid (179 mg, 1.21 mmol), 2-chloro-1-methylpyridinium iodide (402 mg, 1.57 mmol) and triethylamine (0.51 mL, 3.63 mmol) in CH_2Cl_2 (7 mL). Chromatography on silica gel with EtOAc:petroleum ether (1:9 to 1:4) afforded **4.2g** in a 0.55:0.45 ratio of rotamers as a clear oil (276 mg, 81% yield). $\mathbf{R_f}$ = 0.38 (3:7 EtOAc:petroleum ether); **IR** (film, ν_{max}/cm^{-1}) 2922, 2851, 1632, 1511, 1443, 1400, 1299, 1245, 1176, 1119, 1076, 1031; **^{1}H NMR** (300 MHz, $CDCl_3$) δ 7.49–7.25 (m, 6H), 6.99–6.80 (m, 3H), 5.75 (s, 1H), 5.44 (s, 0.45H), 5.37 (s, 0.55H), 4.65 (s, 1.1H), 4.36 (s, 0.9H), 3.81 (s, 1.65H), 3.78 (s, 1.35H), 2.94 (s, 1.35H), 2.77 (s, 1.65H); **^{13}C NMR** (101 MHz, $CDCl_3$) 171.2, 170.9, 159.2, 159.2, 145.2, 145.2, 135.8, 135.6, 129.8, 129.1, 129.0, 128.9, 128.8, 128.7, 128.6, 128.2, 125.9, 125.8, 114.5,

114.2, 114.1, 55.4, 55.4, 54.0, 49.7, 35.8, 35.8, 32.1; **HRMS** (ESI^+) *m/z*: [M + H] calcd for $C_{18}H_{20}NO_2^+$ 282.1498; found 282.1495.

***N*-(4-cyanobenzyl)-*N*-methyl-2-phenylacrylamide (4.2h)**

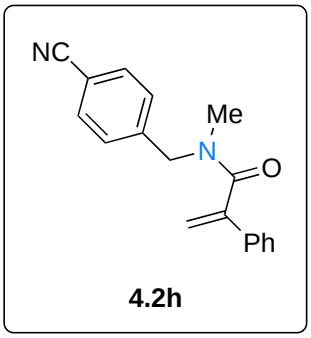

4.2h

Prepared according to general procedure 4A using 4-((methylamino)methyl)benzonitrile (322 mg, 2,20 mmol), 2-phenylacrylic acid (296 mg, 2.00 mmol), 2-chloro-1-methylpyridinium iodide (664 mg, 2.60 mmol) and triethylamine (0.84 mL, 6.00 mmol) in CH_2Cl_2 (10 mL). Chromatography on silica gel with EtOAc:petroleum ether (1:9 to 1:4) afforded **4.2h** in a 0.65:0.35 ratio of rotamers as a clear oil (426 mg, 77% yield). $\mathbf{R_f}$ = 0.48 (6:4 EtOAc:petroleum ether); **IR** (film, ν_{max}/cm^{-1}) 3010, 2929, 2228, 1633, 1493, 1446, 1401, 1214, 1123, 1024; **^{1}H NMR** (300 MHz, $CDCl_3$) δ 7.65 (d, *J* = 8.0 Hz, 1.3H), 7.58 (d, *J* = 8.0 Hz, 0.7H), 7.44–7.35 (m, 6.30H), 7.15 (d, *J* = 8.0 Hz, 0.7H), 5.78 (s, 0.65H), 5.71 (s, 0.35H), 5.41 (s, 0.65H), 5.40 (s, 0.35H), 4.75 (s, 1.30H), 4.48 (s, 0.65H), 2.99 (s, 1.05H), 2.83 (s, 1.95H); **^{13}C NMR** (101 MHz, $CDCl_3$) δ 171.4, 171.3, 145.0, 142.7, 142.1, 135.6, 132.7, 129.1, 129.1, 128.9, 128.8, 127.7, 125.9, 125.8, 118.8, 118.5, 114.8, 111.8, 111.7, 54.3, 50.3, 36.5, 32.8; **HRMS** (ESI^+) *m/z*: [M + H] calcd for $C_{18}H_{17}N_2O^+$ 277.1335; found 277.1353.

***N*-methyl-2-phenyl-*N*-(2-(4,4,5,5-tetramethyl-1,3,2-dioxaborolan-2-yl)benzyl)acrylamide (4.2i)**

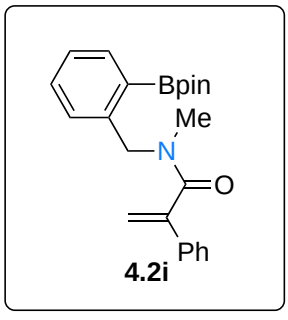

4.2i

Prepared according to general procedure 4A using *N*-methyl-1 (2-(4,4,5,5-tetramethyl-1,3,2-dioxaborolan-2-yl)phenyl)methanamine (408 mg, 1.65 mmol), 2-phenylacrylic acid (222 mg, 1.50 mmol), 2-chloro-1-methylpyridinium iodide (498 mg, 1.95 mmol) and triethylamine (0.63 mL, 4.50 mmol) in CH_2Cl_2 (8 mL). Chromatography on silica gel with EtOAc:petroleum ether (1:9 to 1:4) afforded **4.2i** in a 0.55:0.45 ratio of rotamers as a clear oil (385 mg, 68% yield). $\mathbf{R_f}$ = 0.4 (3:7 EtOAc:petroleum ether); **IR** (film, ν_{max}/cm^{-1}) 2981, 2933, 1634, 1492, 1444, 1378, 1345, 1317, 1265, 1216, 1143, 1114, 1068, 1042; **^{1}H NMR** (300 MHz, $CDCl_3$) δ 7.82 (dd, *J* = 13.9, 7.6 Hz, 1H), 7.50–7.21 (m, 7.55H), 7.09 (d, *J* = 7.6 Hz, 0.45H), 5.76 (s, 0.55H), 5.60 (s, 0.45H), 5.41 (s, 0.55H), 5.33 (s, 0.45H), 5.09 (s, 1.1H), 4.75 (s, 0.9H), 3.04 (s, 1.35H), 2.81 (s, 1.65H), 1.34 (s, 6.6H), 1.25 (s, 5.4H); **^{13}C NMR** (101 MHz, $CDCl_3$) δ 171.7, 171.1, 145.7, 145.2, 143.8, 143.5,

136.5, 136.3, 136.2, 135.9, 131.7, 131.5, 128.9, 128.8, 128.6, 128.6, 127.7, 126.6, 126.5, 126.1, 126.0, 125.7, 114.4, 114.0, 83.9, 83.9, 53.7, 48.7, 36.1, 33.1, 25.1, 24.9; **HRMS** (ESI^+) *m/z*: [M + H] calcd for $C_{23}H_{29}BNO_3^+$ 378.2235; found 378.2247.

***N*-(3,5-difluorobenzyl)-*N*-methyl-2-phenylacrylamide (4.2j)**

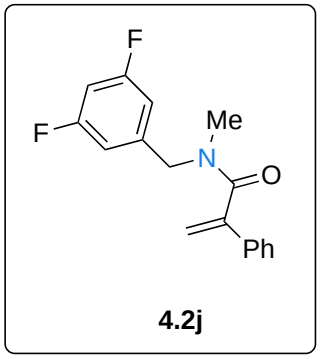

4.2j

Prepared according to general procedure 4A using 1-(3,5-difluorophenyl)-*N*-methylmethanamine (0.246 g, 1.57 mmol), 2-phenylacrylic acid (0.212 g, 1.43 mmol), 2-chloro-1-methylpyridinium iodide (0.475, 1.85 mmol) and triethylamine (0.6 mL, 4.29 mmol) in CH_2Cl_2 (15 mL). Chromatography on silica gel with EtOAc:petroleum ether (1:9 to 3:7) afforded **4.2j** in a 0.6:0.4 ratio of rotamers as a yellow oil (0.270 g, 66% yield). $\mathbf{R_f}$ = 0.20 (3:7 EtOAc:petroleum ether); **IR** (film, ν_{max}/cm^{-1}) 3059, 2926, 1627, 1599, 1550, 1492, 1453, 1340, 1354, 1315, 1202, 1118, 1079; **^{1}H NMR** (300 MHz, $CDCl_3$) δ 7.46–7.33 (m, 5H), 6.85– 6.55 (m, 3H), 5.78 (s, 0.6H), 5.72 (s, 0.4H), 5.42 (s, 1H), 4.68 (s, 1.2H), 4.39 (s, 0.8H), 2.99 (s, 1.2H), 2.82 (s, 1.8H); **^{13}C NMR** (151 MHz, $CDCl_3$) δ 171.4, 171.2, 163.5 (d, $J_{C\text{-}F}$ = 249.8 Hz), 163.4 (d, $J_{C\text{-}F}$ = 249.2 Hz), 145.1, 145.1, 141.2 (t, $J_{C\text{-}F}$ = 8.8Hz), 140.8 (t, $J_{C\text{-}F}$ = 8.2 Hz), 135.6, 135.6, 129.1, 129.1, 129.0, 128.9, 125.9, 125.8, 114.8, 110.9 (dd, $J_{C\text{-}F}$ = 20.6, 5.2 Hz), 109.9 (dd, $J_{C\text{-}F}$ = 20.6, 4.8 Hz), 103.3 (t, $J_{C\text{-}F}$ = 25.1 Hz), 103.2 (t, $J_{C\text{-}F}$ = 25.2 Hz), 54.0, 49.9, 36.4, 32.7; **^{19}F NMR** (377 MHz, $CDCl_3$) *δ* -108.81, -109.30; **HRMS** (ESI^+) *m/z*: [M + H] calcd for $C_{17}H_{16}F_2NO^+$ 288.1194; found 288.1203.

***N*-(3-bromo-5-methoxybenzyl)-*N*-methyl-2-phenylacrylamide (4.2k)**

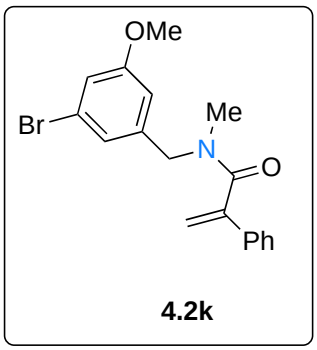

4.2k

Prepared according to general procedure 4A using 1-(3-bromo-5-methoxyphenyl)-*N*-methylmethanamine (759 mg, 3.30 mmol), 2-phenylacrylic acid (444 mg, 3.00 mmol), 2-chloro-1-methylpyridinium iodide (996 mg, 3.90 mmol) and triethylamine (1.25 mL, 9.00 mmol) in CH_2Cl_2 (17 mL). Chromatography on silica gel with EtOAc:petroleum ether (1:9 to 1:4) afforded **4.2k** in a 0.6:0.4 ratio of rotamers as a yellow solid (367 mg, 34% yield). $\mathbf{R_f}$ = 0.31 (3:7 EtOAc:petroleum ether); **M.P.** 72–75 °C; **IR** (film, ν_{max}/cm^{-1}) 3002, 2932, 1633, 1601, 1571, 1456, 1427, 1399, 1268, 1050; **^{1}H NMR** (300 MHz, $CDCl_3$) δ 7.46–7.30 (m, 5H), 7.03 (s, 0.6H), 6.97 (s, 0.6H), 6.92 (s, 0.4H), 6.79 (s, 0.6H), 6.76 (s, 0.4H), 6.48 (s, 0.4H), 5.77 (s, 0.6H), 5.72 (s, 0.4H), 5.42 (s, 0.4H), 5.40 (s, 0.6H), 4.64 (s, 1.2H), 4.36 (s, 0.8H), 3.78 (s, 1.8H),

3.69 (s, 1.2H), 2.97 (s, 1.2H), 2.80 (s, 1.8H); **^{13}C NMR** (101 MHz, $CDCl_3$) δ 171.4, 171.2, 160.8, 160.8, 145.1, 145.0, 140.3, 139.7, 135.7, 135.6, 129.1, 129.0, 128.9, 128.8, 125.9, 125.8, 123.4, 123.3, 123.1, 122.5, 116.6, 116.5, 114.8, 114.6, 112.8, 111.9, 55.6, 55.6, 54.1, 49.9, 36.2, 32.5; **HRMS** (ESI^+) *m/z*: [M + H] calcd for $C_{18}H_{19}{}^{79}BrNO_2^+$ 360.0594; found 360.0601.

***N*-methyl-2-phenyl-*N*-(3,4,5-trichlorobenzyl)acrylamide (4.2l)**

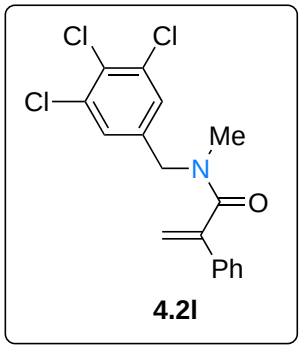

4.2l

Prepared according to general procedure 4A using *N*-methyl-1-(3,4,5-trichlorophenyl)methanamine (0.186 g, 0.83 mmol), 2-phenylacrylic acid (0.112 g, 0.753 mmol), 2-chloro-1-methylpyridinium iodide (250 mg, 0.98 mmol) and triethylamine (0.31 mL, 2.26 mmol) in CH_2Cl_2 (10 mL). Chromatography on silica gel with EtOAc:petroleum ether (1:9 to 3:7) afforded **4.2l** in a 0.65:0.35 ratio of rotamers as a white solid (0.202 g, 91% yield). **R_f** = 0.24 (2:8 EtOAc:petroleum ether); **M.P.** 101–102 °C; **IR** (film, ν_{max}/cm^{-1}) 3059, 2935, 1620, 1554, 1492, 1431, 1397, 1346, 1275, 1250, 1202, 1157, 1115, 1075, 1030; **^{1}H NMR** (300 MHz, $CDCl_3$) δ 7.44–7.34 (m, 6.35H), 6.99 (s, 0.65H), 5.78 (s, 0.65H), 5.72 (s, 0.35H), 5.42 (s, 1H), 4.65 (s, 1.3H), 4.35 (s, 0.7H), 2.98 (s, 1.05H), 2.82 (1.95H); **^{13}C NMR** (151 MHz, $CDCl_3$) δ 171.3, 171.2, 145.1, 145.0, 137.7, 137.0, 135.6, 135.5, 134.7, 134.6, 130.8, 130.7, 129.2, 129.1, 128.9, 128.3, 127.3, 125.9, 125.8, 115.0, 114.9, 53.3, 49.3, 36.4, 32.7; **HRMS** (ESI^+) *m/z*: [M + H] calcd for $C_{17}H_{15}{}^{35}Cl_3NO^+$ 354.0214; found 354.0223.

***N*-methyl-*N*-(naphthalen-1-ylmethyl)-2-phenylacrylamide (4.2m)**

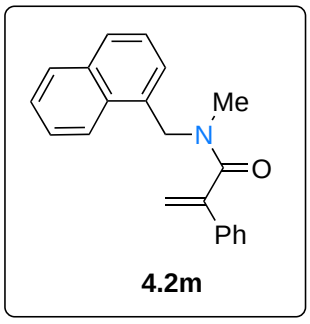

4.2m

Prepared according to general procedure 4A using *N*-methyl-1-(naphthalen-1-yl)methanamine (377 mg, 2.20 mmol), 2-phenylacrylic acid (296 mg, 2.00 mmol), 2-chloro-1-methylpyridinium iodide (664 mg, 2.60 mmol) and triethylamine (0.84 mL, 6.00 mmol) in CH_2Cl_2 (11 mL). Chromatography on silica gel with EtOAc:petroleum ether (1:9 to 1:4) afforded **4.2m** in a 0.7:0.3 ratio of rotamers as a white solid (476 mg, 79% yield). **R_f** = 0.46 (3:7 EtOAc:petroleum ether); **M.P.** 105–107 °C; **IR** (film, ν_{max}/cm^{-1}) 2920, 2864, 1689, 1459, 1377, 1077, 1049; **^{1}H NMR** (300 MHz, $CDCl_3$) δ 8.26 (d, *J* = 8.2 Hz, 0.7H), 7.90–7.30 (m, 11.3H), 5.75 (s, 0.7H), 5.63 (s, 0.3H), 5.42 (s, 0.3H), 5.39 (s, 0.7H), 5.22 (s, 1.4H), 4.92 (s, 0.6H), 3.10 (s, 0.9H), 2.71 (s, 2.1H); **^{13}C NMR** (101 MHz, $CDCl_3$) δ 171.8, 170.7, 145.5, 144.9, 135.8, 135.7, 134.1, 133.8,

132.5, 131.9, 131.8, 131.0, 129.1, 129.0, 128.9, 128.8, 128.8, 128.7, 128.3, 127.7, 126.7, 126.5, 126.2, 126.1, 126.0, 125.9, 125.5, 125.3, 124.2, 124.2, 122.4, 114.3, 114.2, 52.4, 48.3, 35.6, 33.2 (one rotameric signal not reliably assigned due to overlapping signals); **HRMS** (ESI^+) *m/z*: [M + H] calcd for $C_{21}H_{20}NO^+$ 302.1539; found 302.1550.

***N*-methyl-2-phenyl-*N*-(1-phenylethyl)acrylamide (4.2n)**

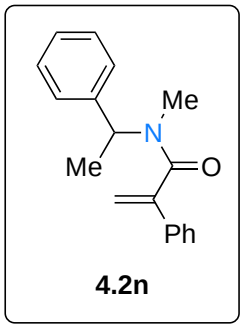

4.2n

Prepared according to general procedure 4A using *N*-methyl-1-phenylethan-1-amine (0.297 g, 2.2 mmol), 2-phenylacrylic acid (0.297 g, 2 mmol), 2-chloro-1-methylpyridinium iodide (0.665 g, 2.6 mmol) and triethylamine (0.836 mL, 6 mmol) in CH_2Cl_2 (25 mL). Chromatography on silica gel with EtOAc:petroleum ether (1:9 to 4:6) afforded **4.2n** in a 0.5:0.5 ratio of rotamers as a clear oil (0.481 g, 59% yield). $\mathbf{R_f}$ = 0.37 (3:7 EtOAc:petroleum ether); **IR** (film, ν_{max}/cm^{-1}) 3057, 3029, 2976, 2936, 1630, 1492, 1445, 1398, 1340, 1124, 1078, 1028; **^{1}H NMR** (300 MHz, $CDCl_3$) δ 7.53–7.51 (m, 1H), 7.46–7.23 (m, 8H), 7.10–7.07 (m, 1H), 6.20 (q, *J* = 6.0 Hz, 0.5H), 5.75 (s, 1H), 5.47 (s, 0.5H), 5.37 (s, 0.5H), 5.12 (q, *J* = 6.0 Hz, 0.5H), 2.75 (s, 1.5H), 2.54 (s, 1.5H), 1.57 (d, *J* = 6.0 Hz, 1.5H), 1.38 (d, *J* = 6.0 Hz, 1.5H); **^{13}C NMR** (151 MHz, $CDCl_3$) δ 170.9, 170.8, 145.8, 145.7, 140.2, 139.7, 135.9, 135.6, 129.1, 128.9, 128.8, 128.7, 128.4, 128.6, 127.5, 127.4, 127.4, 126.8, 126.0, 125.7, 113.9, 113.7, 56.0, 50.2, 30.6, 27.1, 16.8, 15.5; **HRMS** (ESI^+) *m/z*: [M + H] calcd for $C_{18}H_{20}NO^+$ 266.1539; found 266.1547.

***N*-methyl-*N*-((1-methyl-1H-indol-3-yl)methyl)-2-phenylacrylamide (4.2o)**

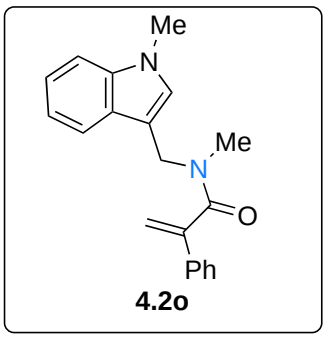

4.2o

Prepared according to general procedure 4A using *N*-methyl-1-(1-methyl-1*H*-indol-3-yl)methanamine (0.061 g, 0.35 mmol), 2-phenylacrylic acid (0.47 g, 0.32 mmol), 2-chloro-1-methylpyridinium iodide (0.106 g, 0.41 mmol) and triethylamine (0.133 mL, 0.95 mmol) in CH_2Cl_2 (10 mL). Chromatography on silica gel with EtOAc:petroleum ether (1:9 to 3:7) afforded **4.2o** in a 0.65:0.35 ratio of rotamers as a clear oil (0.057 g, 59% yield). $\mathbf{R_f}$ = 0.14 (3:7 EtOAc:petroleum ether); **IR** (film, ν_{max}/cm^{-1}) 3055, 2923, 1681, 1625, 1552, 1475, 1445, 1401, 1377, 1331, 1253, 1125, 1071; **^{1}H NMR** (300 MHz, $CDCl_3$) δ 7.82–7.79 (m, 0.65H), 7.53–6.62 (m, 9H), 6.62 (s, 0.35H), 5.78 (s, 0.35H), 5.72 (s, 0.65H), 5.52 (s, 0.35H), 5.33 (s, 0.65H), 4.87 (s, 1.3H), 4.59 (s, 0.7H), 3.78 (s, 1.95H), 3.70 (s, 1.05), 3.02 (s, 1.05H), 2.80 (s, 1.95H); **^{13}C NMR**

(101 MHz, $CDCl_3$) δ 168.0, 168.0, 144.7, 144.7, 137.3, 137.3, 136.1, 136.1, 128.9, 128.9, 128.7, 128.7, 128.4, 128.4, 125.7, 125.7, 122.7, 122.7, 120.9, 120.9, 119.0, 119.0, 117.4, 117.4, 109.0, 109.0, 107.1, 107.1, 34.0, 29.8, 26.8, 26.3, 20.6, 20.6; **HRMS** (ESI^+) *m/z*: [M + H] calcd for $C_{20}H_{21}N_2O^+$ 305.1648; found 305.1646.

N-(furan-3-ylmethyl)-*N*-methyl-2-phenylacrylamide (4.2p)

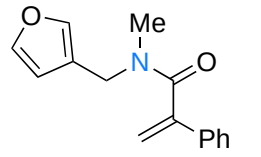

4.2p

Prepared according to general procedure 4A using 1-(furan-3-yl)-*N*-methylmethanamine (0.556 g, 5 mmol), 2-phenylacrylic acid (0.674 g, 4.54 mmol), 2-chloro-1-methylpyridinium iodide (1.507 g, 5.90 mmol) and triethylamine (1.89 mL, 13.62 mmol) in CH_2Cl_2 (20 mL). Chromatography on silica gel with EtOAc:petroleum ether (1:9 to 4:6) afforded **4.2p** in a 0.55:0.45 ratio of rotamers as a clear oil (0.457 g, 42% yield). $\mathbf{R_f}$ = 0.23 (3:7 EtOAc:petroleum ether); **IR** (film, ν_{max}/cm^{-1}) 2925, 1692, 1632, 1493, 1442, 1400, 1205, 1158, 1120, 1071, 1022; **^{1}H NMR** (300 MHz, $CDCl_3$) δ 7.48–7.30 (m, 6.55H), 7.16 (s, 0.45H), 6.44 (s, 0.55H), 6.00 (s, 0.45H), 5.74 (s, 1H), 5.41 (s, 0.45H), 5.35 (s, 0.55H), 4.53 (s, 1.1H), 4.25 (s, 0.9H), 2.98 (s, 1.35H), 2.81 (s, 1.65H); **^{13}C NMR** (101 MHz, $CDCl_3$) δ 170.9 (2C), 145.2 (2C) 143.7, 143.7, 140.9, 140.5, 135.8, 135.6, 129.0, 129.0, 128.9, 128.7, 125.9, 125.7, 120.8, 120.7, 114.5, 114.3, 110.8, 109.8, 45.7, 41.3, 35.9, 32.0; **HRMS** (ESI^+) *m/z*: [M + H] calcd for $C_{15}H_{16}NO_2^+$ 242.1176; found 242.1188.

N-methyl-2-phenyl-*N*-(thiophen-3-ylmethyl)acrylamide (4.2q)

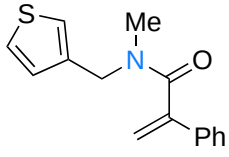

4.2q

Prepared according to general procedure 4A using *N*-methyl-1-(thiophen-3-yl)methanamine (0.200 g, 1.57 mmol), 2-phenylacrylic acid (0.212 g, 1.43 mmol), 2-chloro-1-methylpyridinium iodide (0.473 g, 1.85 mmol) and triethylamine (0.597 mL, 4.29 mmol) in CH_2Cl_2 (20 mL). Chromatography on silica gel with EtOAc:petroleum ether (1:9 to 4:6) afforded **4.2q** in a 0.55:0.45 ratio of rotamers as a clear oil (0.245 g, 67% yield). $\mathbf{R_f}$ = 0.29 (3:7 EtOAc:petroleum ether); **IR** (film, ν_{max}/cm^{-1}) 3088, 2924, 1631, 1549, 1488, 1442, 1399, 1281, 1259, 1233, 1203, 1120, 11076, 1028; **^{1}H NMR** (300 MHz, $CDCl_3$) δ 7.48–7.18 (m, 6H), 7.19 (br s, 0.55H), 7.10 (d, *J* = 4.8 Hz, 0.55H), 6.95–6.94 (br s, 0.45H), 6.73 (d, *J* = 4.8 Hz, 0.45H), 5.75 (s, 0.55H), 5.74 (s, 0.45H), 5.42 (s, 0.45H), 5.37 (s, 0.55H), 4.70 (s, 1.1H), 4.41 (s, 0.9H), 2.99 (s, 1.35H), 2.81 (s, 1.65H); **^{13}C NMR** (101 MHz, $CDCl_3$) δ 171.0, 170.8, 145.4, 145.3, 137.8, 137.6, 135.9, 135.7, 129.0, 129.0, 128.9, 128.7, 127.9,

126.7, 126.7, 126.4, 125.9, 125.8, 123.2, 122.6, 114.4, 114.2, 50.1, 45.6, 36.1, 32.3; **HRMS** (ESI^+) *m/z*: [M + H] calcd for $C_{15}H_{16}NOS^+$ 258.0947; found 258.0966.

***N*-allyl-*N*-methyl-2-phenylacrylamide (4.2r)**

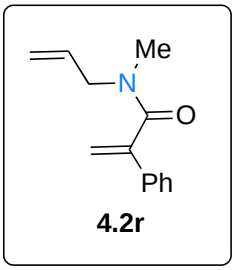

4.2r

Prepared according to general procedure 4A using *N*-methylprop-2-en-1-amine (156 mg, 2.20 mmol), 2-phenylacrylic acid (296 mg, 2.00 mmol), 2-chloro-1-methylpyridinium iodide (664 mg, 2.60 mmol) and triethylamine (0.84 mL, 6.00 mmol) in CH_2Cl_2 (11 mL). Chromatography on silica gel with EtOAc:petroleum ether (1:9 to 1:3) afforded **4.2r** in a 0.55:0.45 ratio of rotamers as a clear oil (105 mg, 26% yield). $\mathbf{R_f}$ = 0.52 (6:4 EtOAc:petroleum ether); **IR** (film, ν_{max}/cm^{-1}) 2986, 2924, 1708, 1630, 1491, 1441, 1400, 1217, 1142, 1075; **^{1}H NMR** (300 MHz, $CDCl_3$) δ 7.43–7.29 (m, 5H), 5.88–5.75 (m, 0.45H), 5.73 (s, 0.45H), 5.69 (s, 0.55H), 5.60–5.47 (m, 0.55H), 5.35 (s, 0.55H), 5.34 (s, 0.45H), 5.22–5.06 (m, 2H), 4.11 (d, *J* = 5.8Hz, 0.9H), 3.80 (d, *J* = 5.8 Hz, 1.1H), 2.99 (s, 1.65H), 2.82 (s, 1.35H); **^{13}C NMR** (101 MHz, $CDCl_3$) δ 171.1, 170.7, 145.4, 145.1, 135.7, 135.6, 132.8, 132.6, 128.9, 128.9, 128.7, 128.6, 125.8, 125.7, 117.9, 117.8, 114.1, 113.9, 53.5, 49.4, 36.0, 32.2; **HRMS** (ESI^+) *m/z*: [M + H] calcd for $C_{13}H_{16}NO^+$ 202.1226; found 202.1238.

***N*-methyl-2-phenyl-*N*-(prop-2-yn-1-yl)acrylamide (4.2s)**

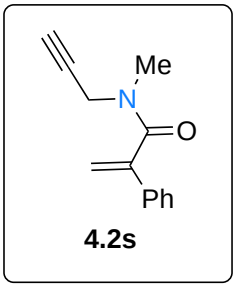

4.2s

Prepared according to general procedure 4A using *N*-methylprop-2-yn-1-amine (228 mg, 3.30 mmol), 2-phenylacrylic acid (444 mg, 3.00 mmol), 2-chloro-1-methylpyridinium iodide (996 mg, 3.90 mmol) and triethylamine (1.25 mL, 9.00 mmol) in CH_2Cl_2 (17 mL). Chromatography on silica gel with EtOAc:petroleum ether (1:9 to 1:3) afforded **4.2s** in a 0.6:0.4 ratio of rotamers as a white solid (287 mg, 48% yield). $\mathbf{R_f}$ = 0.58 (6:4 EtOAc:petroleum ether); **M.P.** 60–62 °C; **IR** (film, ν_{max}/cm^{-1}) 3288, 3237, 2925, 1635, 1488, 1444, 1397, 1256, 1216, 1124, 1076, 1029; **^{1}H NMR** (300 MHz, $CDCl_3$) δ 7.44–7.29 (m, 5H), 5.79 (s, 0.4H), 5.77 (s, 0.6H), 5.45 (s, 0.4H), 5.39 (s, 1H), 4.35 (d, *J* = 2.5 Hz, 1.2H), 4.01 (d, *J* = 2.5 Hz, 0.8H), 3.13 (s, 1.2H), 2.95 (s, 1.8H), 2.26–2.23 (m, 1H); **^{13}C NMR** (101 MHz, $CDCl_3$) δ 170.7, 170.6, 144.7, 144.2, 153.3, 129.0, 128.9, 128.8, 128.7, 125.9, 125.9, 125.7, 114.6, 114.6, 78.3, 78.0, 72.3, 72.2, 40.8, 35.9, 35.7, 32.1; **HRMS** (ESI^+) *m/z*: [M + H] calcd for $C_{13}H_{14}NO^+$ 200.1070; found 200.1084.

***N*-(cyanomethyl)-*N*-methyl-2-phenylacrylamide (4.2t)**

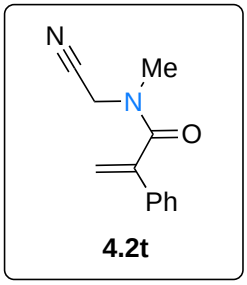

4.2t

Prepared according to general procedure 4A using 2-(methylamino)acetonitrile (0.154 g, 2.2 mmol), 2-phenylacrylic acid (0.297 g, 2 mmol), 2-chloro-1-methylpyridinium iodide (0.665 g, 2.6 mmol) and triethylamine (0.836 mL, 6 mmol) in CH_2Cl_2 (25 mL). Chromatography on silica gel with EtOAc:petroleum ether (1:9 to 4:6) afforded **4.2t** in a 0.75:0.25 ratio of rotamers as a yellow oil (0.358 g, 90% yield). $\mathbf{R_f}$ = 0.39 (3:7 EtOAc:petroleum ether); **IR** (film, ν_{max}/cm^{-1}) 3058, 3027, 2984, 2931, 1647, 1558, 1486, 1448, 1395, 1343, 1263, 1200, 1128, 1077, 1028; **^{1}H NMR** (300 MHz, $CDCl_3$) δ 7.39–7.33 (m, 5H), 5.87 (s, 0.25H), 5.83 (s, 0.75H), 5.52 (s, 0.25H), 5.45 (s, 0.75H), 4.48 (s, 1.5H), 4.15 (s, 0.5H), 3.18 (s, 0.75H), 3.00 (s, 2.25H); **^{13}C NMR** (101 MHz, $CDCl_3$) δ (major rotamer) 171.0, 143.7, 134.8, 129.4, 129.2, 129.1, 125.7, 116.0, 36.6, 34.9 (diagnostic signals for the minor rotamer can be seen at 115.0, 39.6, 33.0); **HRMS** (ESI$^+$) *m/z*: [M + H] calcd for $C_{12}H_{13}N_2O^+$ 201.1022; found 201.1035.

***N*,*N*-diisopropyl-2-phenylacrylamide (4.2u)**

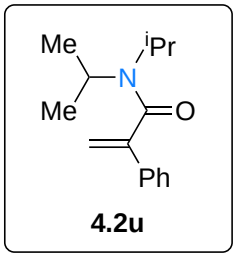

4.2u

Prepared according to general procedure 4A using diisopropylamine (278 mg, 2.75 mmol), 2-phenylacrylic acid (370 mg, 2.50 mmol), 2-chloro-1-methylpyridinium iodide (830 mg, 3.25 mmol) and triethylamine (1.05 mL, 7.50 mmol) in CH_2Cl_2 (14 mL). Chromatography on silica gel with EtOAc:petroleum ether (1:9 to 1:4) afforded **4.2u** as a white solid (538 mg, 93% yield). $\mathbf{R_f}$ = 0.45 (2:8 EtOAc:petroleum ether); **M.P.** 70–73 °C; **IR** (film, ν_{max}/cm^{-1}) 2967, 2928, 1630, 1442, 1372, 1345, 1256, 1214, 1155, 1135, 1039; **^{1}H NMR** (300 MHz, $CDCl_3$) δ 7.45–7.28 (m, 5H), 5.61 (s, 1H), 5.24 (s, 1H), 3.97 (h, *J* = 6.3 Hz, 1H), 3.42 (h, *J* = 6.3 Hz, 1H), 1.53 (d, *J* = 6.8 Hz, 6H), 0.99 (d, *J* = 6.8 Hz, 6H); **^{13}C NMR** (101 MHz, $CDCl_3$) δ 170.2, 146.8, 135.9, 128.8, 128.5, 125.7, 111.6, 50.8, 45.6, 20.5, 20.5; **HRMS** (ESI$^+$) *m/z*: [M + H] calcd for $C_{15}H_{22}NO^+$ 232.1696; found 232.1708.

***N*-benzyl-*N*-ethyl-2-phenylacrylamide (4.2v)**

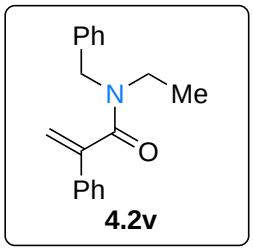

4.2v

Prepared according to general procedure 4A using *N*-benzylethanamine (0.297 g, 2.2 mmol), 2-phenylacrylic acid (0.297 g, 2 mmol), 2-chloro-1-methylpyridinium iodide (0.665 g, 2.6 mmol) and triethylamine (0.836 mL, 6 mmol) in CH_2Cl_2 (25 mL). Chromatography on silica gel with EtOAc:petroleum ether (1:9 to 3:7) afforded **4.2v** in a 0.55:0.45 ratio of as a colourless oil (0.510 g, 96% yield). $\mathbf{R_f}$ = 0.51 (3:7 EtOAc:petroleum ether); **IR** (film, ν_{max}/cm^{-1}) 3059, 3029, 2973, 2931, 1692, 1634, 1549, 1495, 1430, 1366, 1309, 1285, 1235, 1207, 1178, 1125, 1077, 1028; **^{1}H NMR** (300 MHz, $CDCl_3$) δ 7.49–7.45 (m, 2H), 7.40–7.25 (m, 7H), 7.10–7.08 (m, 1H), 5.73 (s, 0.55H), 5.70 (s, 0.45H), 5.40 (s, 1H), 4.73 (s, 1.1H), 4.42 (s, 0.9H), 3.47 (q, *J* = 7.1 Hz, 0.9H), 3.18 (q, *J* = 7.1 Hz, 1.1H), 1.17 (t, *J* = 7.1 Hz, 1.35H), 0.97 (t, *J* = 7.1 Hz, 1.65H); **^{13}C NMR** (101 MHz, $CDCl_3$) δ 171.0, 170.8, 145.4, 145.1, 137.5, 136.7, 135.8, 135.7, 129.0, 128.9, 128.7, 128.7, 128.2, 127.6, 127.5, 127.1, 125.8, 125.7, 113.9, 113.6, 51.5, 46.5, 42.3, 38.9, 13.4, 12.1; **HRMS** (ESI^+) *m/z*: [M + H] calcd for $C_{18}H_{20}NO^+$ 266.1539; found 266.1550.

***N*,*N*-dibenzyl-2-phenylacrylamide (4.2w)**

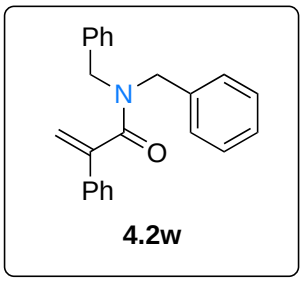

4.2w

Prepared according to general procedure 4A using dibenzylamine (434 mg, 2.20 mmol), 2-phenylacrylic acid (296 mg, 2.00 mmol), 2-chloro-1-methylpyridinium iodide (664 mg, 2.60 mmol) and triethylamine (0.84 mL, 6.00 mmol) in CH_2Cl_2 (11 mL). Chromatography on silica gel with EtOAc:petroleum ether (1:9 to 1:4) afforded **4.2w** as a white solid (524 mg, 80% yield). $\mathbf{R_f}$ = 0.59 (3:7 EtOAc:petroleum ether); **M.P.** 54–55 °C; **IR** (film, ν_{max}/cm^{-1}) 3060, 2926, 1635, 1495, 1423, 1362, 1322, 1206, 1077, 1022; **^{1}H NMR** (300 MHz, $CDCl_3$) δ 7.51–7.48 (m, 2H), 7.40–7.26 (m, 11H), 7.09–7.06 (m, 2H), 5.74 (s, 1H), 5.50 (s, 1H), 4.66 (s, 2H), 4.34 (s, 2H); **^{13}C NMR** (101 MHz, $CDCl_3$) δ 171.3, 145.1, 136.9, 136.2, 135.9, 129.0, 128.8, 128.8, 128.7, 128.7, 127.8, 127.7, 127.4, 125.9, 114.5, 51.0, 46.4; **HRMS** (ESI^+) *m/z*: [M + H] calcd for $C_{23}H_{22}NO^+$ 328.1696; found 328.1701.

***N*-benzyl-*N*,2-diphenylacrylamide (4.2x)**

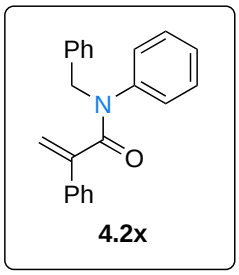

4.2x

Prepared according to general procedure 4A using *N*-benzylaniline (0.200 mg, 1.09 mmol), 2-phenylacrylic acid (0.226 mg, 1.53 mmol), 2-chloro-1-methylpyridinium iodide (0.334 mg, 1.31 mmol) and triethylamine (0.456 mL, 3.27 mmol) in CH_2Cl_2 (10 mL). Chromatography on silica gel with EtOAc:petroleum ether (1:9 to 3:7) afforded **4.2x** as a colourless oil (0.222 g, 65% yield). **R_f** = 0.42 (2:8 EtOAc:petroleum ether); **IR** (film, ν_{max}/cm^{-1}) 3058, 3030, 2929, 1645, 1592, 1493, 1448, 1390, 1329, 1284, 1240, 1205, 1076, 1027, 1004; **^{1}H NMR** (300 MHz, $CDCl_3$) δ 7.29–7.06 (m, 13H), 6.76–6.73 (m, 2H), 5.46 (s, 1H), 5.38 (s, 1H), 5.02 (s, 2H); **^{13}C NMR** (101 MHz, $CDCl_3$) δ 170.6, 145.9, 142.2, 137.5, 137.2, 128.9, 128.8, 128.7, 128.6, 128.4, 128.0, 127.6, 127.2, 126.2, 117.9, 53.2; **HRMS** (ESI^+) *m/z*: [M + H] calcd for $C_{22}H_{20}NO^+$ 314.1539; found 314.1551.

***N*-benzyl-2-phenyl-*N*-tosylacrylamide (4.2y)**

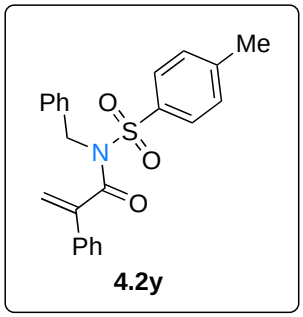

4.2y

Prepared according to general procedure 4A using *N*-benzyl-4-methylbenzenesulfonamide (862 mg, 3.30 mmol), 2-phenylacrylic acid (444 mg, 3.00 mmol), 2-chloro-1-methylpyridinium iodide (996 mg, 3.90 mmol) and triethylamine (1.25 mL, 9.00 mmol) in CH_2Cl_2 (17 mL). Chromatography on silica gel with EtOAc:petroleum ether (1:9 to 1:4) afforded **4.2y** as a clear oil (446 mg, 38% yield). **R_f** = 0.58 (2:8 EtOAc:petroleum ether); **M.P.** 120–122 °C; **IR** (film, ν_{max}/cm^{-1}) 3060, 3032, 2923, 1687, 1598, 1495, 1449, 1405, 1355, 1163, 1123, 1082, 1030; **^{1}H NMR** (300 MHz, $CDCl_3$) δ 7.65 (d, *J* = 8.1 Hz, 2H), 7.46–6.98 (m, 12H), 5.65 (s, 1H), 5.28 (s, 1H), 4.88 (s, 2H), 2.42 (s, 3H); **^{13}C NMR** (101 MHz, $CDCl_3$) δ 170.5, 145.0, 144.4, 136.6, 136.1, 134.8, 129.4, 129.0, 129.0, 129.0, 128.7, 127.8, 127.7, 125.9, 118.2, 50.5, 21.8; **HRMS** (ESI^+) *m/z*: [M + H] calcd for $C_{23}H_{22}NO_3S^+$ 392.1315; found 392.1324.

***N*-benzyl-*N*-methyl-2-(p-tolyl)acrylamide (4.2z)**

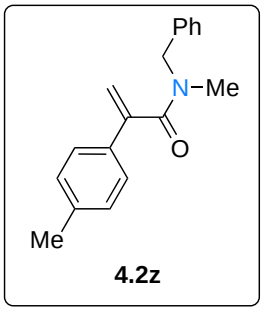

4.2z

Prepared according to general procedure 4A using *N*-methyl-1-phenylmethanamine (0.152 g, 1.25 mmol), 2-(*p*-tolyl)acrylic acid[12] (0.185 g, 1.14 mmol), 2-chloro-1-methylpyridinium iodide (0.379 g, 1.482 mmol) and triethylamine (0.476 mL, 3.42 mmol) in CH_2Cl_2 (10 mL). Chromatography on silica gel with EtOAc:petroleum ether (1:9 to

3:7) afforded **4.2z** in a 0.55:0.45 ratio of rotamers as a clear oil (0.187 g, 62% yield). $\mathbf{R_f}$ = 0.26 (2:8 EtOAc:petroleum ether); **IR** (film, ν_{max}/cm^{-1}) 3027, 2921, 1637, 1564, 1511, 1488, 1450, 1361, 1305, 1256, 1212, 1185, 1119, 1077, 1028; **^{1}H NMR** (300 MHz, $CDCl_3$) δ 7.38–7.26 (m, 6H), 7.19 –7.15 (m, 2H), 7.10–7.07 (m, 1H), 5.72 (s, 0.55H), 5.69 (s, 0.45H), 5.38 (s, 0.45H), 5.34 (s, 0.55H), 4.72 (s, 1.1H), 4.42 (s, 0.9H), 2.97 (s, 1.35H), 2.79 (s, 1.65H), 2.36 (s, 1.35H), 2.35 (s, 1.65H); **^{13}C NMR** (151 MHz, $CDCl_3$) δ 171.6, 171.2, 145.3, 145.1, 138.8, 138.7, 137.2, 136.6, 133.0, 132.9, 129.7, 129.7, 128.8, 128.8, 128.4, 127.8, 127.6, 127.2, 125.8, 125.7, 113.5, 113.3, 54.6, 50.3, 36.0, 32.4, 21.3, 21.3; **HRMS** (ESI$^+$) *m/z*: [M + H] calcd for $C_{18}H_{20}NO^+$ 266.1539; found 266.1553.

N-benzyl-2-(4-methoxyphenyl)-*N*-methylacrylamide (4.2aa)

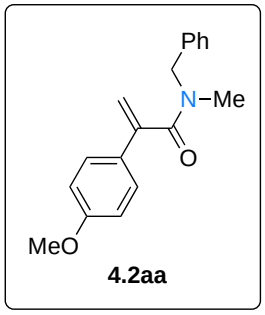

4.2aa

Prepared according to general procedure 4A using *N*-methyl-1-phenylmethanamine (44.0 mg, 0.36 mmol), 2-(4-methoxyphenyl)acrylic acid[248] (58.8 mg, 0.33 mmol), 2-chloro-1-methylpyridinium iodide (110 mg, 0.43 mmol) and triethylamine (0.14 mL, 0.99 mmol) in CH_2Cl_2 (2 mL). Chromatography on silica gel with EtOAc:petroleum ether (1:9 to 1:5) afforded **4.2aa** in a 0.55:0.45 ratio of rotamers as a clear oil (23.2 mg, 25% yield). $\mathbf{R_f}$ = 0.21 (2:8 EtOAc:petroleum ether); **IR** (film, ν_{max}/cm^{-1}) 3031, 2923, 2855, 1789, 1740, 1638, 1498, 1456, 1367, 1248, 1169, 1087, 1055, 1030; **^{1}H NMR** (300 MHz, $CDCl_3$) δ 7.42–7.26 (m, 6H), 7.09–6.86 (m, 3H), 5.65 (s, 0.55H), 5.61 (s, 0.45H), 5.32 (s, 0.45H), 5.27 (s, 0.55H), 4.71 (s, 1.1H), 4.43 (s, 0.9H), 3.82 (s, 1.35H), 3.81 (s, 1.65H), 2.97 (s, 1.35H), 2.80 (s, 1.65H); **^{13}C NMR** (101 MHz, $CDCl_3$) δ 171.6, 171.3, 160.0, 159.9, 144.6, 144.3, 137.0, 136.4, 128.8, 128.8, 128.4, 128.2, 128.1, 127.7, 127.6, 127.1, 127.1, 114.3, 114.2, 112.3, 112.1, 55.4, 55.4, 54.5, 50.2, 36.0, 32.3 (one rotameric signal not reliably assigned due to overlapping signals); **HRMS** (ESI$^+$) *m/z*: [M + H] calcd for $C_{18}H_{20}NO_2^+$ 282.1489; found 282.1502.

N-benzyl-2-(4-bromophenyl)-*N*-methylacrylamide (4.2ab)

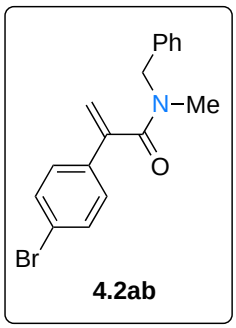

4.2ab

Prepared according to general procedure 4A using *N*-methyl-1-phenylmethanamine (595 mg, 4.91 mmol), 2-(4-bromophenyl)acrylic acid[248] (1013 mg, 4.46 mmol), 2-chloro-1-methylpyridinium iodide (1481 mg, 5.80 mmol) and triethylamine (1.86 mL, 13.38 mmol) in CH_2Cl_2 (25 mL). Chromatography on silica gel with EtOAc:petroleum ether (1:9 to

1:4) afforded **8c** in a 0.55:0.45 ratio of rotamers as a clear oil (560 mg, 38% yield). $\mathbf{R_f}$ = 0.56 (3:7 EtOAc:petroleum ether); **IR** (film, ν_{max}/cm^{-1}) 2923, 2859, 1635, 1487, 1450, 1397, 1259, 1210, 1185, 1113, 1075, 1009; **^{1}H NMR** (300 MHz, $CDCl_3$) δ 7.50–7.46 (m, 2H), 7.38–7.24 (m, 6H), 7.08–7.05 (m, 1H), 5.76 (s, 0.55H), 5.72 (s, 0.45H), 5.45 (s, 0.45H), 5.41 (s, 0.55H), 4.70 (s, 1.1H), 4.42 (s, 0.9H), 2.97 (s, 1.35H), 2.79 (s, 1.65H); **^{13}C NMR** (101 MHz, $CDCl_3$) δ 170.8, 170.4, 144.3, 144.1, 136.9, 136.2, 134.8, 134.7, 132.1 (2C), 128.9, 128.8, 128.3, 127.9, 127.7, 127.5, 127.5, 127.1, 123.0, 122.8, 115.0, 114.8, 54.6, 50.4, 36.1, 32.5; **HRMS** (ESI$^+$) *m/z*: [M + H] calcd for $C_{17}H_{17}{}^{79}BrNO^+$ 330.0488; found 330.0496.

N-benzyl-2-(3,4-dichlorophenyl)-*N*-methylacrylamide (4.2ac)

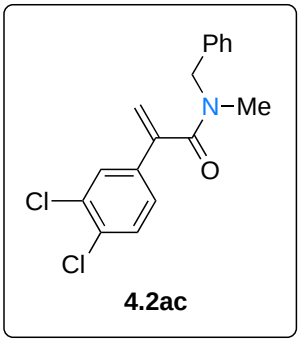

4.2ac

Prepared according to general procedure 4A using *N*-methyl-1-phenylmethanamine (0.046 g, 0.38 mmol), 2-(3,4-dichlorophenyl)acrylic acid[243] (0.075 g, 0.35 mmol), 2-chloro-1-methylpyridinium iodide (0.114 g, 0.45 mmol) and triethylamine (0.144 mL, 1.04 mmol) in CH_2Cl_2 (10 mL). Chromatography on silica gel with EtOAc:petroleum ether (1:9 to 4:6) afforded **4.2ac** in a 0.55:0.45 ratio of rotamers as a clear oil (0.053 g, 48% yield). $\mathbf{R_f}$ = 0.17 (2:8 EtOAc:petroleum ether); **IR** (film, ν_{max}/cm^{-1}) 3062, 3029, 2924, 1716, 1636, 1549, 1472, 1399, 1263, 1208, 1136, 1080, 1029; **^{1}H NMR** (300 MHz, $CDCl_3$) δ 7.56–7.53 (m, 1H), 7.44–7.26 (m, 7H), 7.09–7.06 (m, 1H), 5.77 (s, 0.55H), 5.72 (s, 0.45H), 5.48 (s, 0.45H), 5.45 (s, 0.55H), 4.70 (s, 1.1H), 4.44 (s, 0.9H), 3.00 (s, 1.35H), 2.80 (s, 1.65H); **^{13}C NMR** (151 MHz, $CDCl_3$) δ 170.3, 169.9, 143.3, 143.0, 136.8, 136.1, 135.9, 135.8, 133.3, 132.9, 132.8, 130.9, 129.2, 129.0, 128.9, 128.8, 128.4, 128.1, 128.0, 127.9, 127.9, 127.0, 125.3, 125.2, 116.0, 115.8, 54.6, 50.5, 36.1, 32.7; **HRMS** (ESI$^+$) *m/z*: [M + H] calcd for $C_{17}H_{16}{}^{35}Cl_2NO^+$ 320.0603; found 320.0622.

N-benzyl-*N*-methyl-2-(naphthalen-2-yl)acrylamide (4.2ad)

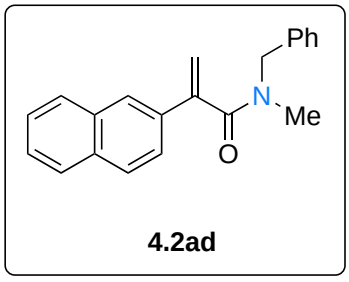

4.2ad

Prepared according to general procedure 4A using *N*-methyl-1-phenylmethanamine (0.151 g, 0.76 mmol), 2-(naphthalen-2-yl)acrylic acid[248] (0.101 g, 0.84 mmol), 2-chloro-1-methylpyridinium iodide (0.252 g, 0.99 mmol) and triethylamine (0.32 mL, 2.28 mmol) in CH_2Cl_2 (10 mL). Chromatography on silica gel with EtOAc:petroleum ether (1:9 to 3:7) afforded **4.2ad** in a 0.55:0.45 ratio of rotamers as a clear oil (0.144 g, 48% yield). $\mathbf{R_f}$ = 0.63 (2:8 EtOAc:petroleum ether); **IR** (film,

ν_{max}/cm^{-1}) 355, 3030, 2924, 1716, 1685, 1632, 1575, 1489, 1451, 1400, 1360, 1317, 1267, 1191, 1107, 1073, 1026; **^{1}H NMR** (300 MHz, $CDCl_3$) δ 7.87–7.74 (m, 4H), 7.66–7.62 (m, 1H), 7.51– 7.46 (m, 2H), 7.39–7.24 (m, 4H), 7.10–7.08 (m, 1H), 5.90 (s, 0.55H), 5.87 (s, 0.45H), 5.54 (s, 0.45H), 5.50 (s, 0.55H), 4.78 (s,1.1H), 4.45 (s, 0.9H), 3.04 (s, 1.35H), 2.82 (s, 1.65H); **^{13}C NMR** (151 MHz, $CDCl_3$) δ 171.5, 171.1, 145.4, 145.2, 137.2, 136.5, 133.5, 133.5, 133.5, 133.4, 133.1, 132.9, 128.9, 128.8, 128.8, 128.6, 128.5, 128.5, 127.8, 127.7, 127.2, 126.7, 126.6, 126.6, 125.6, 125.5, 123.2, 123.1, 114.8, 114.4, 54.6, 50.5, 36.1, 32.5 (overlapping peaks in the ^{13}C NMR spectrum meant that some rotameric signals could not be reliably assigned); **HRMS** (ESI$^+$) *m/z*: [M + H] calcd for $C_{21}H_{20}NO^+$ 302.1539; found 302.1550.

N,*N*-diethyl-2-phenylacrylamide (4.2ae)

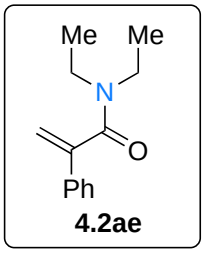

4.2ae

Prepared according to general procedure 4A using diethylamine (241 mg, 3.30 mmol), 2-phenylacrylic acid (444 mg, 3.00 mmol), 2-chloro-1-methylpyridinium iodide (996 mg, 3.90 mmol) and triethylamine (1.25 mL, 9.00 mmol) in CH_2Cl_2 (17 mL). Chromatography on silica gel with EtOAc:petroleum ether (1:9 to 1:4) afforded **4.2v** as a clear oil (506 mg, 83% yield). **R_f** = 0.32 (3:7 EtOAc:petroleum ether); **IR** (film, ν_{max}/cm^{-1}) 2976, 2935, 1626, 1433, 1378, 1312, 1284, 1247, 1220, 1144, 1091, 908, 780, 753, 699; **^{1}H NMR** (300 MHz, $CDCl_3$) δ 7.43–7.28 (m, 5H), 5.68 (s, 1H), 5.31 (s, 1H), 3.49 (q, *J* = 7.1 Hz, 2H), 3.21 (q, *J* = 7.1 Hz, 2H), 1.20 (t, *J* = 7.1 Hz, 3H), 0.98 (d, *J* = 7.1 Hz, 3H); **^{13}C NMR** (101 MHz, $CDCl_3$) δ 170.3, 145.6, 135.8, 128.8, 128.5, 125.6, 113.0, 42.8, 38.8, 14.0, 12.8; **HRMS** (ESI$^+$) *m/z*: [M + H] calcd for $C_{13}H_{18}NO^+$ 204.1383; found 204.1396.

N-benzyl-2-phenylacrylamide (4.2af)[249]

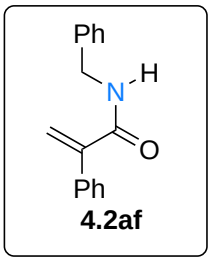

4.2af

Prepared according to general procedure 4A using phenylmethanamine (490 mg, 4.58 mmol), 2-phenylacrylic acid (616 mg, 4.16 mmol), 2-chloro-1-methylpyridinium iodide (1382 mg, 5.41 mmol) and triethylamine (1.74 mL, 12.5 mmol) in CH_2Cl_2 (23 mL). Chromatography on silica gel with EtOAc:petroleum ether (1:9 to 3:10) afforded **4.2af** as a clear oil (612 mg, 62% yield). **R_f** = 0.66 (4:6 EtOAc:petroleum ether); **M.P.** 70–72 °C; **IR** (film, ν_{max}/cm^{-1}) 3315, 3062, 3032, 2970, 2926, 1734, 1704, 1655, 1607, 1528, 1449, 1356, 1305, 1328, 1229, 1077, 1047; **^{1}H NMR** (300 MHz, $CDCl_3$) δ 7.37–7.24 (m, 10H), 6.18 (s, 1H), 6.01 (brs, 1H), 5.63 (s, 1H), 4.52 (d, *J* = 5,8 Hz, 2H); **^{13}C NMR** (101 MHz, $CDCl_3$) δ 167.3, 144.8, 138.2, 137.1, 128.9, 128.9,

128.7, 128.3, 127.8, 127.7, 122.7, 44.1; **HRMS** (ESI$^+$) *m/z*: [M + H] calcd for $C_{16}H_{16}NO^+$ 238.1226; found 238.1228. Recorded data in accordance with those previously reported.

2-phenyl-1-(2-phenylpyrrolidin-1-yl)prop-2-en-1-one (4.2ag)

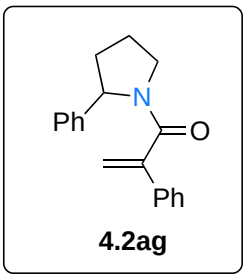

4.2ag

Prepared according to general procedure 4A using 2-phenylpyrrolidine (0.324 g, 2.2 mmol), 2-phenylacrylic acid (0.297 g, 2 mmol), 2-chloro-1-methylpyridinium iodide (0.665 g, 2.6 mmol) and triethylamine (0.836 mL, 6 mmol) in CH_2Cl_2 (25 mL). Chromatography on silica gel with EtOAc:petroleum ether (1:9 to 3:7) afforded **4.2w** in a 1:1 ratio of rotamers as a yellow oil (0.313 g, 56% yield). $\mathbf{R_f}$ = 0.19 (3:7 EtOAc:petroleum ether); **IR** (film, ν_{max}/cm^{-1}) 3057, 3028, 2970, 2877, 1711, 1634, 1517, 1493, 1424, 1313, 1255, 1206, 1173, 1076, 1027; **^{1}H NMR** (300 MHz, $CDCl_3$) δ 7.49–7.19 (m, 9H), 7.05–7.02 (m, 1H), 5.75 (s, 0.5H), 5.52 (s, 0.5H), 5.38 (s, 0.5H), 5.35–5.31 (m, 0.5H), 4.98 (s, 0.5H), 4.74 (d, *J* = 6.6 Hz, 0.5H), 3.94–3.88 (m, 1H), 3.53–3.42 (m, 1H), 2.41–2.28 (m, 0.5H), 2.25–2.18 (m, 0.5H), 1.97–1.80 (m, 3H); **^{13}C NMR** (101 MHz, $CDCl_3$) δ 170.2, 169.3, 146.3, 145.1, 143.5, 143.2, 135.9, 135.6, 128.8, 128.6, 128.5, 128.4, 128.3, 128.0, 128.0, 127.0, 126.9, 126.2, 125.7, 125.7, 125.6, 115.3, 62.4, 60.5, 49.3, 46.8, 35.7, 34.5, 24.1, 21.7; **HRMS** (ESI$^+$) *m/z*: [M + H] calcd for $C_{19}H_{20}NO^+$ 278.1539; found 278.1553.

***N*-methyl-2-phenyl-*N*-(ferrocene)acrylamide (4.2ah)**

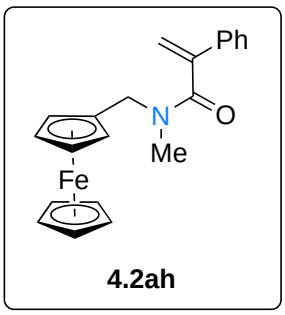

4.2ah

Prepared according to general procedure 4A using *N*-methyl-1-(ferrocene)methanamine (1.145 g, 5 mmol), 2-phenylacrylic acid (0.674, 4.54 mmol), 2-chloro-1-methylpyridinium iodide (1.507 g, 5.90 mmol) and triethylamine (1.9 mL, 13.62 mmol) in CH_2Cl_2 (25 mL). Chromatography on silica gel with EtOAc:petroleum ether (1:9 to 3:7) afforded **4.2ah** in a 1:1 ratio of rotamers as an orange oil (0.340 g, 21% yield). $\mathbf{R_f}$ = 0.19 (3:7 EtOAc:petroleum ether); **IR** (film, ν_{max}/cm^{-1}) 3086, 2922, 2860, 1583, 1631, 1488, 1440, 1396, 1301, 1280, 1257, 1233, 1182, 1104, 1075, 1029, 1001; **^{1}H NMR** (300 MHz, $CDCl_3$) δ 7.51–7.29 (m, 5H), 5.82 (s, 0.5H), 5.72 (s, 0.5H), 5.44 (s, 0.5H), 5.28 (s, 0.5H), 4.60 (m, 5H), 4.18–3.92 (m, 6H), 2.94–2.87 (m, 3H); **^{13}C NMR** (151 MHz, $CDCl_3$) δ 170.3, 145.4, 136.2, 135.5, 129.0, 128.9, 128.5, 126.0, 125.7, 114.6, 114.0, 69.5, 69.0, 68.7, 50.4, 46.3, 36.3, 31.6; **HRMS** (ESI$^+$) *m/z*: [M + H] calcd for $C_{21}H_{22}FeNO^+$ 360.1045; found 360.1053.

2-phenyl-1-(piperidin-1-yl)prop-2-en-1-one (4.2ai)[250]

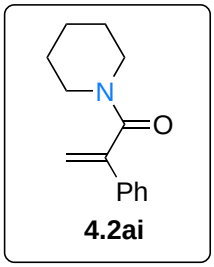

4.2ai

Prepared according to general procedure 4A using piperidine (0.187 g, 2.2 mmol), 2-phenylacrylic acid (0.297 g, 2 mmol), 2-chloro-1-methylpyridinium iodide (0.665 g, 2.6 mmol) and triethylamine (0.836 mL, 6 mmol) in CH_2Cl_2 (25 mL). Chromatography on silica gel with EtOAc:petroleum ether (1:9 to 4:6) afforded **4.2ai** as a yellow oil (0.115 g, 27% yield). **R_f** = 0.21 (3:7 EtOAc:petroleum ether); **IR** (film, ν_{max}/cm^{-1}) 2932, 2857, 1635, 1441, 1279, 1248, 1218, 1132, 1069, 1013; **^{1}H NMR** (300 MHz, $CDCl_3$) δ 7.45–7.41 (m, 2H), 7.37–7.30 (m, 3H), 5.71 (s, 1H), 5.33 (s, 1H), 3.69–3.66 (m, 2H), 3.30 (app t, *J* = 5.7 Hz, 2H), 1.63–1.59 (m, 4H), 1.38–1.34 (m, 2H); **HRMS** (ESI$^+$) *m/z*: [M + H] calcd for $C_{14}H_{18}NO^+$ 216.1383; found 216.1391. Recorded data in accordance with those previously reported.

(*E*)-*N*-benzyl-*N*,2-dimethylbut-2-enamide (4.2aj)

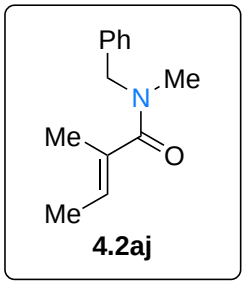

4.2aj

Prepared according to general procedure 4A using *N*-methyl-1-phenylmethanamine (235 mg, 1.55 mmol), (*E*)-2-methylbut-2-enoic acid (141 mg, 1.41 mmol), 2-chloro-1-methylpyridinium iodide (468 mg, 1.83 mmol) and triethylamine (0.59 mL, 4.23 mmol) in CH_2Cl_2 (8 mL). Chromatography on silica gel with EtOAc:petroleum ether (1:9 to 1:4) afforded **4.2aj** as a clear oil (166 mg, 58% yield). **R_f** = 0.41 (3:7 EtOAc:petroleum ether); **IR** (film, ν_{max}/cm^{-1}) 2926, 2859, 1769, 1712, 1647, 1440, 1383, 1277, 1220, 1010; **^{1}H NMR** (300 MHz, $CDCl_3$) δ 7.35–7.21 (m, 5H), 5.68 (q, *J* = 6.6 Hz, 1H), 4.58 (s, 2H), 2.87 (s, 3H), 1.86 (s, 3H), 1.67 (d, *J* = 6.6 Hz, 3H); **^{13}C NMR** (101 MHz, $CDCl_3$) δ 174.3, 137.1, 132.2, 128.8, 127.5, 54.6, 50.4, 36.2, 32.8, 126.0, 14.3, 13.3 (overlapping peaks in the ^{13}C NMR spectrum meant that some rotameric signals could not be reliably assigned); **HRMS** (ESI$^+$) *m/z*: [M + H] calcd for $C_{13}H_{18}NO^+$ 204.1383; found 204.1398.

***N*-benzyl-*N*-methylcyclohex-1-ene-1-carboxamide (4.2ak)**

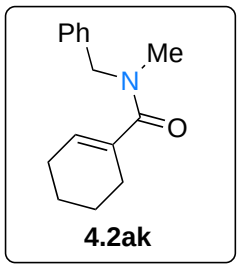

4.2ak

Prepared according to general procedure 4A using *N*-methyl-1-phenylmethanamine (267 mg, 2.20 mmol), cyclohex-1-ene-1-carboxylic acid (252 mg, 2.00 mmol), 2-chloro-1-methylpyridinium iodide (664 mg, 2.60 mmol) and triethylamine (0.84 mL, 6.00 mmol) in CH_2Cl_2 (11 mL). Chromatography on silica gel with EtOAc:petroleum ether (1:9 to 1:3) afforded **4.2ak** as a clear oil (271 mg, 59% yield). **R_f** = 0.30 (4:6 EtOAc:petroleum ether); **IR**

(film, ν_{max}/cm^{-1}) 2927, 2860, 1611, 1493, 1449, 1397, 1242, 1062, 1032, 734, 699; **^{1}H NMR** (300 MHz, $CDCl_3$) δ 7.36–7.19 (m, 5H), 5.88–5.85 (m, 1H), 4.59 (s, 2H), 2.88 (s, 3H), 2.28-2.19 (m, 2H), 2.13–2.02 (m, 2H), 1.68–1.60 (m, 4H); **^{13}C NMR** (101 MHz, $CDCl_3$) δ 173.7, 137.1, 134.5, 128.8, 127.9, 127.5, 54.7, 50.3, 36.3, 32.8, 26.1, 24.7, 22.2, 21.7 (overlapping peaks in the ^{13}C NMR spectrum meant that some rotameric signals could not be reliably assigned); **HRMS** (ESI$^+$) *m/z*: [M + H] calcd for $C_{15}H_{20}NO^+$ 230.1539; found 230.1554.

Synthesis and characterisation data of benzyl 2-phenylacrylate (4.2al)[251]

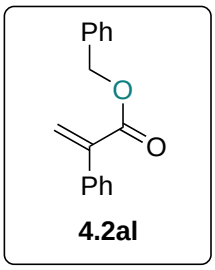

4.2al

To a mixture of phenylmethanol (433 mg, 4.00 mmol, 2 equiv.), 2-phenylacrylic acid (296 mg, 2.00 mmol, 1 equiv.), *N*,*N*'-dicyclohexylmethanediimine (908 mg, 2.2 mmol, 1.1 equiv.) and *N*,*N*-dimethylpyridin-4-amine (33.7 mg, 0.20 mmol, 0.1 equiv.) in CH_2Cl_2 (40 mL) at 0 °C under argon and the reaction mixture allowed to warm slowly to room temperature. Once the reaction was completed (by TLC) the mixture was cooled to -20 °C for 2 hours then filtered through Celite. The organic solvents were removed in vacuo and the resulting crude product was purified by column chromatography on silica gel with EtOAc:petroleum ether (1:9 to 1:3) and afforded **4.2al** as a clear oil (162 mg, 34% yield). **R_f** = 0.48 (3:7 EtOAc:petroleum ether); **IR** (film, ν_{max}/cm^{-1}) 3033, 2930, 2856, 2117, 1718, 1615, 1496, 1451, 1400, 1378, 1309, 1277, 1177, 1086; **^{1}H NMR** (300 MHz, $CDCl_3$) δ 7.45–7.36 (m, 10H), 6.42 (s, 1H), 5.94 (s, 1H), 5.29 (s, 2H); **^{13}C NMR** (101 MHz, $CDCl_3$) δ 166.7, 141.4, 136.8, 136.1, 128.7, 128.4, 128.3, 128.3, 128.3, 128.2, 127.1, 66.9. Reported data in accordance with those previously reported.

5.4.4 General procedure 4C: Synthesis of β-lactams (4.1) via 2-CTX mediated photocatalysis

A stirring mixture of acrylamide **4.2** (0.10–0.5 mmol), **2-CTX** (10 mol%) in 5 mL PhMe was degassed with argon for 10 min before irradiation with 405 nm LEDs (18 W) overnight, with fan-cooling. The solvent was then removed in vacuo and the resulting residue purified by silica column chromatography (petroleum ether/EtOAc gradient) to afford β-lactam **4.1**. *Diastereomeric ratios reported were determined by ^{1}H NMR analysis of the crude reaction mixture prior to purification.*

5.4.5 Characterization data for β-lactams (4.1)

1,3-dimethyl-3,4-diphenylazetidin-2-one (4.1a)

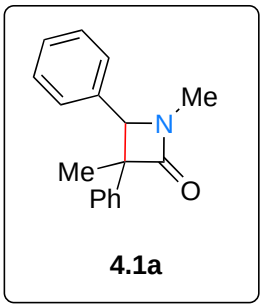

4.1a

Prepared according to general procedure 4C using **4.2a** (0.050 g, 0.20 mmol) and **2-CTX** (0.0049 g, 0.02 mmol). Chromatography on silica gel with EtOAc:petroleum ether (1:9 to 2:8) afforded **4.1a** as 2 separable diastereomers (0.044 g, 89% yield, 1.5:1 dr). **HRMS** (ESI^+) *m/z*: [M + H] calcd for $C_{17}H_{18}NO^+$ 252.1383; found 252.1388.

***trans*-Diastereomer:** 0.026 g; white solid; R_f = 0.61 (4:6 EtOAc:petroleum ether); **M.P.** 101–102 °C; **IR** (film, ν_{max}/cm^{-1}) 2969, 2903, 1742, 1494, 1448, 1420, 1390, 1357, 1179, 1027; **^{1}H NMR** (300 MHz, $CDCl_3$) δ 7.51–7.45 (m, 3H), 7.44 (m, 1H), 7.42–7.37 (m, 3H), 7.33–7.29 (m, 3H), 4.75 (s, 1H), 2.91 (s, 3H), 1.15 (s, 3H); **^{13}C NMR** (101 MHz, $CDCl_3$) δ 172.1, 142.4, 135.6, 129.0, 128.9, 128.4, 127.2, 127.2, 126.1, 69.1, 63.8, 27.1, 19.8.

***cis*-Diastereomer:** 0.018 g; yellow oil; R_f = 0.33 (4:6 EtOAc:petroleum ether); **IR** (film, ν_{max}/cm^{-1}) 2958, 2922, 1744, 1673, 1451, 1422, 1390, 1362, 1282, 1027; **^{1}H NMR** (300 MHz, $CDCl_3$) δ 7.13–7.10 (m, 3H), 7.03–6.99 (m, 5H), 6.93–6.90 (m, 2H), 4.56 (s, 1H), 2.85 (s, 3H), 1.81 (s, 3H); **^{13}C NMR** (101 MHz, $CDCl_3$) δ 172.0, 138.3, 135.7, 128.3, 128.1, 128.0, 127.6, 127.3, 126.6, 70.8, 66.2, 27.1, 24.5.

1-methyl-3-(methyl-*d*)-3,4-diphenylazetidin-2-one-4-*d* (*d*-4.1a)

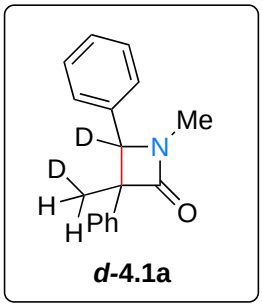

***d*-4.1a**

Prepared according to general procedure 4C using *d*-**4.2a** (0.050 g, 0.20 mmol) and **2-CTX** (0.0049 g, 0.02 mmol). Chromatography on silica gel with EtOAc:petroleum ether (1:9 to 2:8) afforded *d*-**4.1a** as 2 separable diastereomers (0.043 g, 86% yield, 1.1:1 dr).

***trans*-Diastereomer:** 0.022 g; white solid; R_f = 0.61 (4:6 EtOAc:petroleum ether); **^{1}H NMR** (300 MHz, $CDCl_3$) δ 7.51–7.45 (m, 3H), 7.44 (m, 1H), 7.42–7.37 (m, 3H), 7.33–7.30 (m, 3H), 2.91 (s, 3H), 1.13 (s, 2H).

***cis*-Diastereomer:** 0.021 g; yellow oil; R_f = 0.33 (4:6 EtOAc:petroleum ether); **^{1}H NMR** (300 MHz, $CDCl_3$) δ 7.13–7.11 (m, 3H), 7.03–6.99 (m, 5H), 6.93–6.90 (m, 2H), 2.85 (s, 3H), 1.80 (s, 2H).

1,3-dimethyl-3-phenyl-4-(*p*-tolyl)azetidin-2-one (4.1b)

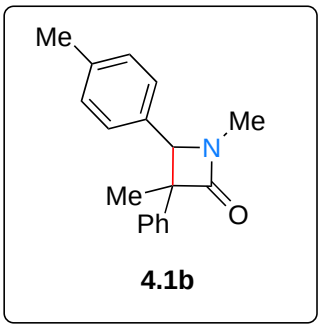

4.1b

Prepared according to general procedure 4C using **4.2b** (90 mg, 0.34 mmol) and **2-CTX** (8.3 mg, 0.03 mmol). Chromatography on silica gel with EtOAc:petroleum ether (1:9 to 2:8) afforded **4.1b** as 2 separable diastereomers (85 mg, 94% yield, 1.6:1 dr). **HRMS** (ESI^+) *m/z*: [M + H] calcd for $C_{18}H_{20}NO^+$ 266.1539; found 266.1542. ***trans*-Diastereomer:** 0.053 g; yellow oil; R_f = 0.68 (3:7 EtOAc:petroleum ether); **IR** (film, ν_{max}/cm^{-1}) 2966, 2922, 1443, 1426, 1387, 1279, 1178, 1027; **^{1}H NMR** (300 MHz, $CDCl_3$) δ 7.51–7.50 (m, 2H), 7.41 (t, *J* = 7.5 Hz, 2H), 7.31–7.26 (m, 3H), 7.22–7.19 (m, 2H), 4.72 (s, 1H), 2.90 (s, 3H), 2.40 (s, 3H), 1.16 (s, 3H); **^{13}C NMR** (101 MHz, $CDCl_3$) δ 172.1, 142.5, 138.2, 132.4, 129.6, 128.8, 127.2, 127.2, 126.1, 68.9, 63.7, 27.0, 21.3, 19.8.

***cis*-Diastereomer:** 0.032 g; white solid; R_f = 0.48 (3:7 EtOAc:petroleum ether); **M.P.** 105–107 °C; **IR** (film, ν_{max}/cm^{-1}) 2955, 2924, 1742, 1638, 1446, 1391, 1280, 1122, 1069, 1027; **^{1}H NMR** (300 MHz, $CDCl_3$) δ 7.08–7.03 (m, 5H), 6.92 (d, *J* = 7.8 Hz, 2H), 6.79 (d, *J* = 7.8 Hz, 2H), 4.53 (s, 1H), 2.82 (s, 3H), 2.21 (s, 3H), 1.79 (s, 3H); **^{13}C NMR** (101 MHz, $CDCl_3$) δ 172.1, 138.5, 137.8, 132.5, 129.0, 127.9, 127.5, 127.3, 126.5, 70.6, 65.8, 27.0, 24.6, 21.2.

1,3-dimethyl-3-phenyl-4-(*o*-tolyl)azetidin-2-one (4.1c)

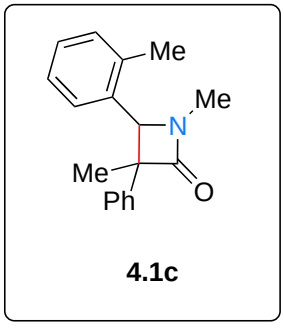

4.1c

Prepared according to general procedure 4C using **4.2c** (100 mg, 0.38 mmol) and **2-CTX** (9.3 mg, 0.04 mmol). Chromatography on silica gel with EtOAc:petroleum ether (1:9 to 2:8) afforded **4.1c** as 2 separable diastereomers (95 mg, 95% yield, 1.5:1 dr). **HRMS** (ESI^+) *m/z*: [M + H] calcd for $C_{18}H_{20}NO^+$ 266.1539; found 266.1549.

***trans*-Diastereomer:** 0.057 g; white solid; R_f = 0.42 (4:6 EtOAc:petroleum ether); **M.P.** 92–94 °C; **IR** (film, ν_{max}/cm^{-1}) 2961, 2927, 1747, 1454, 1415, 1389, 1027; **^{1}H NMR** (300 MHz, $CDCl_3$) δ 7.45–7.37 (m, 4H), 7.33–7.20 (m, 5H), 4.82 (s, 1H), 3.01 (s, 3H), 2.12 (s, 3H), 1.19 (s, 3H); **^{13}C NMR** (101 MHz, $CDCl_3$) δ 172.9, 141.1, 136.5, 134.1, 131.0, 128.9, 127.9, 127.4, 126.2, 126.0, 125.9, 67.5, 63.4, 27.4, 19.8, 16.2.

***cis*-Diastereomer:** 0.038 g; colourless oil; R_f = 0.28 (4:6 EtOAc:petroleum ether); **IR** (film, ν_{max}/cm^{-1}) 2961, 2924, 1744, 1448, 1422, 1388, 1352, 1028; **^{1}H NMR** (300 MHz, $CDCl_3$) δ 7.05–6.96 (m, 7H), 6.89 (t, *J* = 7.5 Hz, 1H), 6.72 (d, *J* = 7.8Hz, 1H), 4.84 (s, 1H), 2.91 (s, 1H), 2.39 (s,

3H), 1.89 (s, 3H); **^{13}C NMR** (101 MHz, $CDCl_3$) δ 172.4, 137.8, 135.7, 133.9, 130.3, 128.0, 127.5, 127.0, 126.8, 126.0, 125.8, 67.2, 65.9, 27.6, 23.6, 19.8.

4-(3-chlorophenyl)-1,3-dimethyl-3-phenylazetidin-2-one (4.1d)

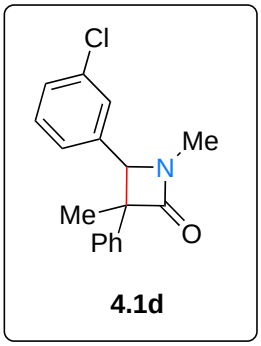

4.1d

Prepared according to general procedure 4C using **4.2d** (100 mg, 0.35 mmol) and **2-CTX** (8.6 mg, 0.04 mmol). Chromatography on silica gel with EtOAc:petroleum ether (1:9 to 2:8) afforded **4.1d** as 2 separable diastereomers (98 mg, 98% yield, 1.4:1 dr). **HRMS** (ESI^+) *m/z*: [M + H] calcd for $C_{17}H_{17}{}^{35}ClNO^+$ 286.0993; found 286.0999.

***trans*-Diastereomer:** 0.057 g; white solid; R_f = 0.30 (3:7 EtOAc:petroleum ether); **M.P.** 104–106 °C; **IR** (film, ν_{max}/cm^{-1}) 2958, 2924, 1737, 1435, 1390, 1274, 1125, 1073,, 1030; **^{1}H NMR** (300 MHz, $CDCl_3$) δ 7.49–7.45 (m, 2H), 7.43–7.26 (m, 6H), 7.20 (d, *J* = 7.2 Hz, 1H), 4.70 (s, 1H), 2.90 (s, 3H), 1.16 (s, 3H); **^{13}C NMR** (151 MHz, $CDCl_3$) δ 171.8, 142.0, 138.0, 135.2, 130.3, 129.0, 128.6, 127.4, 127.3, 126.0, 125.3, 68.6, 64.1, 27.2, 19.8.

***cis*-Diastereomer:** 0.042 g; yellow oil; R_f = 0.17 (3:7 EtOAc:petroleum ether); **IR** (film, ν_{max}/cm^{-1}) 2960, 2922, 1744, 1435, 1388, 1278, 1072, 1030; **^{1}H NMR** (300 MHz, $CDCl_3$) δ 7.10–6.99 (m, 7H), 6.93 (s, 1H), 6.76 (d, *J* = 7.5 Hz, 1H), 4.51 (s, 1H), 2.84 (s, 3H), 1.81 (s, 3H); **^{13}C NMR** (151 MHz, $CDCl_3$) δ 171.8, 138.0, 137.8, 134.4, 129.6, 128.2, 128.1, 127.8, 127.3, 126.9, 125.5, 70.1, 66.5, 27.2, 24.2.

4-(4-bromophenyl)-1,3-dimethyl-3-phenylazetidin-2-one (4.1e)

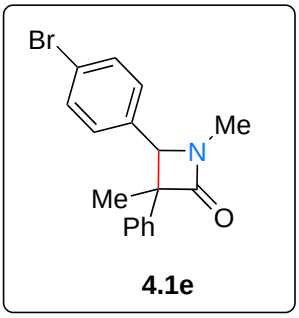

4.1e

Prepared according to general procedure 4C using **4.2e** (120 mg, 0.36 mmol) and **2-CTX** (8.9 mg, 0.04 mmol). Chromatography on silica gel with EtOAc:petroleum ether (1:9 to 2:8) afforded **4.1e** as 2 separable diastereomers (100 mg, 83% yield, 1.5:1 dr). **HRMS** (ESI^+) *m/z*: [M + H] calcd for $C_{17}H_{17}{}^{79}BrNO^+$ 330.0488; found 330.0499.

***trans*-Diastereomer:** 0.060 g; oil; R_f = 0.65 (3:7 EtOAc:petroleum ether); **IR** (film, ν_{max}/cm^{-1}) 2965, 2921, 1746, 1487, 1443, 1424, 1386, 1069, 1028, 1008; **^{1}H NMR** (300 MHz, $CDCl_3$) δ 7.59 (d, *J* = 8.1 Hz, 2H), 7.47–7.44 (m, 2H), 7.39 (t, *J* = 7.2 Hz, 2H), 7.32–7.27 (m, 1H), 7.19 (d, *J* = 8.1 Hz, 2H), 4.69 (s, 1H), 2.89 (s, 3H), 1.14 (s, 3H); **^{13}C NMR** (101 MHz, $CDCl_3$) δ 171.9, 142.0, 134.7, 132.2, 129.0, 128.8, 127.4, 126.0, 122.4, 68.6, 63.9, 27.1, 19.8.

***cis*-Diastereomer:** 0.040 g; white solid; R_f = 0.35 (3:7 EtOAc:petroleum ether); **M.P.** 105–106 °C; **IR** (film, ν_{max}/cm^{-1}) 2956, 2923, 1742, 1640, 1487, 1445, 1423, 1389, 1278, 1068, 1008; **^{1}H NMR** (300 MHz, $CDCl_3$) δ 7.28 (d, *J* = 7.5 Hz, 2H), 7.10–7.06 (m, 3H), 7.04–7.00 (m, 2H), 6.81 (d, *J* = 8.4 Hz, 2H), 4.54 (s, 1H), 2.84 (s, 3H), 1.83 (s, 3H); **^{13}C NMR** (101 MHz, $CDCl_3$) δ 171.8, 137.9, 134.8, 131.5, 129.2, 128.2, 127.3, 126.9, 122.1, 70.1, 66.3, 27.1, 24.4;

1,3-dimethyl-3-phenyl-4-(3-(trifluoromethyl)phenyl)azetidin-2-one (4.1f)

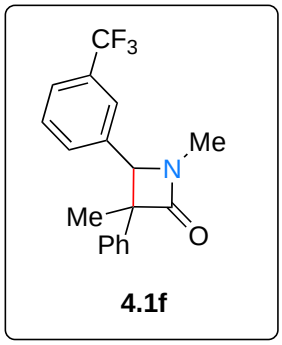

4.1f

Prepared according to general procedure 4C using **4.2f** (100 mg, 0.31 mmol) and **2-CTX** (7.7 mg, 0.03 mmol). Chromatography on silica gel with EtOAc:petroleum ether (1:9 to 2:8) afforded **4.1f** as 2 separable diastereomers (97 mg, 97% yield, 1.6:1 dr). **HRMS** (ESI$^+$) *m/z*: [M + H] calcd for $C_{18}H_{17}F_3NO^+$ 320.1257; found 320.1273.

***trans*-Diastereomer:** 0.062 g; yellow soild; R_f = 0.32 (3:7 EtOAc:petroleum ether); **M.P.** 108–109 °C; **IR** (film, ν_{max}/cm^{-1}) 2955, 2922, 1741, 1448, 1326, 1284, 1260, 1163, 1123, 1072, 1032; **^{1}H NMR** (300 MHz, $CDCl_3$) δ 7.68–7.58 (m, 2H), 7.55–7.44 (m, 4H), 7.41 (t, *J* = 7.5 Hz, 2H), 7.34–7.29 (m, 1H), 4.80 (s, 1H), 2.92 (s, 3H), 1.14 (s, 3H); **^{13}C NMR** (101 MHz, $CDCl_3$) δ 171.9, 141.8, 137.1, 131.6 (q, J_{C-F} = 32.6 Hz), 130.5, 129.6, 129.1, 127.5, 126.0, 125.3 (q, J_{C-F} = 3.9 Hz), 124.0 (q, J_{C-F} = 273.4 Hz), 123.8 (q, J_{C-F} = 3.8 Hz), 68.7, 64.2, 27.2, 19.8; **^{19}F NMR** (377 MHz, $CDCl_3$) δ –62.64.

***cis*-Diastereomer:** 0.035 g; oil; R_f = 0.19 (3:7 EtOAc:petroleum ether); **IR** (film, ν_{max}/cm^{-1}) 2968, 2927, 1738, 1392, 1326, 1156, 1116, 1071, 1083; **^{1}H NMR** (300 MHz, $CDCl_3$) δ 7.36 (d, *J* = 7.8 Hz, 1H), 7.22 (t, *J* = 7.8 Hz, 1H), 7.16 (s, 1H), 7.11–6.93 (m, 6H), 4.61 (s, 1H), 2.86 (s, 3H), 1.84 (s, 3H); **^{13}C NMR** (101 MHz, $CDCl_3$) δ 171.7, 137.6, 137.1, 130.8 (q, J_{C-F} = 32.5 Hz), 130.6, 128.8, 128.2, 127.2, 126.9, 126.6 (q, J_{C-F} = 273.5 Hz), 124.9, 124.4, 70.2, 66.8, 27.3, 24.0; **^{19}F NMR** (377 MHz, $CDCl_3$) δ –62.90.

4-(4-methoxyphenyl)-1,3-dimethyl-3-phenylazetidin-2-one (4.1g)

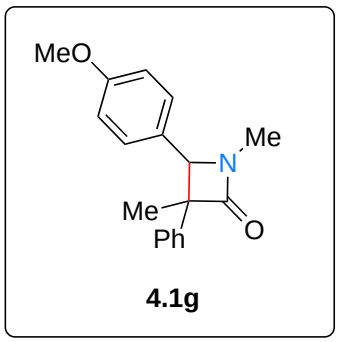

4.1g

Prepared according to general procedure 4C using **4.2g** (137.9 mg, 0.49 mmol) and **2-CTX** (12.1 mg, 0.05 mmol). Chromatography on silica gel with EtOAc:petroleum ether (0:1 to 1:7) afforded **4.1g** as 2 separable diastereomers (67.6 mg, 49% yield, 1.5:1 dr). **HRMS** (ESI$^+$) *m/z*: [M + H] calcd for $C_{18}H_{20}NO_2^+$ 282.1489; found 282.1502.

***trans*-Diastereomer:** 40.6 mg; clear oil; R_f = 0.46 (3:7 EtOAc:petroleum ether); **IR** (film, ν_{max}/cm^{-1}) 2957, 2924, 1745, 1611, 1513, 1444, 1389, 1298, 1248, 1176, 1028; **^{1}H NMR** (300 MHz, $CDCl_3$) 7.47 (d, *J* = 7.8 Hz, 2H), 7.38 (t, *J* = 7.5 Hz, 2H), 7.32–7.19 (m, 3H), 6.99 (d, *J* = 8.3 Hz, 2H), 4.69 (s, 1H), 3.85 (s, 3H), 2.88 (s, 3H), 1.16 (s, 3H); **^{13}C NMR** (101 MHz, $CDCl_3$) δ 172.2, 159.8, 142.6, 128.9, 128.5, 127.5, 127.2, 126.1, 114.5, 68.8, 63.8, 55.5, 27.0, 19.8.

***cis*-Diastereomer:** 27.0 mg; clear oil; R_f = 0.34 (3:7 EtOAc:petroleum ether; **IR** (film, ν_{max}/cm^{-1}) 2956, 2923, 2856, 1744, 1612, 1513, 1445, 1390, 1248, 1176, 1030; **^{1}H NMR** (300 MHz, $CDCl_3$) 7.11–6.96 (m, 5H), 6.82 (d, *J* = 8.5 Hz, 2H), 6.65 (d, *J* = 8.5 Hz, 2H), 4.51 (s, 1H), 3.70 (s, 3H), 2.81 (s, 3H), 1.78 (s, 3H); **^{13}C NMR** (101 MHz, $CDCl_3$) δ 172.1, 159.5, 138.6, 128.8, 128.0, 127.6, 127.4, 126.6, 113.8, 70.4, 65.9, 55.3, 26.9, 24.7.

4-(1,3-dimethyl-4-oxo-3-phenylazetidin-2-yl)benzonitrile (4.1h)

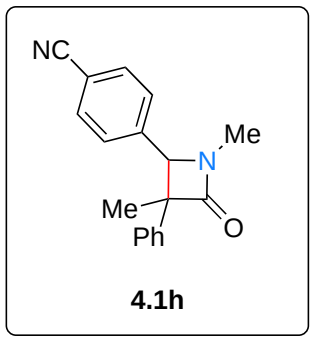

4.1h

Prepared according to general procedure 4C using **4.2h** (77.4 mg, 0.28 mmol) and **2-CTX** (6.9 mg, 0.03 mmol). Chromatography on silica gel with EtOAc:petroleum ether (0:1 to 1:7) afforded **4.1h** as 2 separable diastereomers (53.4 mg, 69% yield, 1.25:1 dr). **HRMS** (ESI$^+$) *m/z*: [M + H] calcd for $C_{18}H_{17}N_2O^+$ 277.1335; found 277.1340.

***trans*-Diastereomer:** 29.7 mg, clear oil; R_f = 0.43 (3:7 EtOAc:petroleum ether); **IR** (film, ν_{max}/cm^{-1}) 2965, 2923, 2855, 2228, 1748, 1607, 1443, 1426, 1389, 1346, 1171, 1028; **^{1}H NMR** (300 MHz, $CDCl_3$) δ 7.77 (d, *J* = 7.9 Hz, 2H), 7.46–7.28 (m, 7H), 4.78 (s, 1H), 2.92 (d, *J* = 1.2 Hz, 3H), 1.12 (s, 3H); **^{13}C NMR** (101 MHz, $CDCl_3$) δ 171.6, 141.5, 135.8, 132.8, 129.1, 127.9, 127.6, 126.0, 118.5, 112.5, 68.7, 64.6, 27.4, 19.7.

***cis*-Diastereomer:** 23.7 mg, white solid; R_f = 0.22 (3:7 EtOAc:petroleum ether; **M.P.** 180–182 °C; **IR** (film, ν_{max}/cm^{-1}) 3016, 2966, 2924, 2227, 1744, 1609, 1498, 1425, 1390, 1353, 1216, 1030; **^{1}H NMR** (300 MHz, $CDCl_3$) δ 7.40 (d, *J* = 8.0 Hz, 2H), 7.04–6.95 (m, 7H), 4.60 (s, 1H), 2.85

(s, 3H), 1.83 (s, 3H).; **^{13}C NMR** (101 MHz, $CDCl_3$) δ 171.5, 141.6, 137.4, 132.1, 128.3, 128.1, 127.2, 127.2, 118.5, 111.9, 70.2, 67.1, 27.4, 24.1.

1,3-dimethyl-3-phenyl-4-(2-(4,4,5,5-tetramethyl-1,3,2-dioxaborolan-2-yl)phenyl)azetidin-2-one (4.1i)

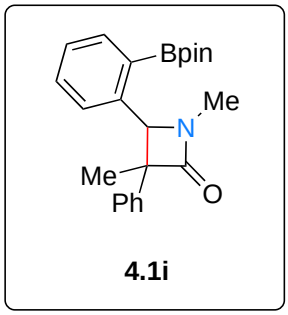

4.1i

Prepared according to general procedure 4C using **4.2i** (166 mg, 0.44 mmol) and **2-CTX** (10.9 mg, 0.04 mmol). Chromatography on silica gel with EtOAc:petroleum ether (0:1 to 1:7) afforded **4.1i** as 2 inseparable diastereomers (105 mg, 63% yield, 1.8:1 dr). **HRMS** (ESI^+) *m/z*: [M + H] calcd for $C_{23}H_{29}BNO_3^+$ 378.2235; found 378.2254. **Combined Diastereomers (~2:1 after chromatography):** clear oil; **R_f** = 0.53 (3:7 EtOAc:petroleum ether); **IR** (film, ν_{max}/cm^{-1}) 2979, 2932, 1749, 1445, 1422, 1382, 1347, 1320, 1263, 1144, 1115, 1069, 1027; **^{1}H NMR** (300 MHz, $CDCl_3$) 5.47 (s, 0.6H), 5.38 (s, 0.3H), 2.96 (s, 2H), 2.87 (s, 1H), 1.89 (s, 1H), 1.44 (s, 4H), 1.14 (s, 2H), 1.10 (s, 4H), 1.03 (s, 4H); **^{13}C NMR** (101 MHz, $CDCl_3$) 173.1, 172.8, 142.3, 141.7, 141.7, 138.7, 136.8, 136.2, 131.0, 130.98, 128.5, 127.8, 127.3, 127.3, 127.0, 126.7, 126.4, 126.3, 126.3, 125.8, 84.2, 83.9, 68.6, 68.1, 66.5, 63.8, 27.2, 26.9, 25.2, 25.0, 24.8, 24.4, 24.3, 16.2. Overlapping peaks in the ^{13}C NMR spectrum meant that some of the signals in this diastereomeric mixture could not be reliably assigned.

4-(3,5-difluorophenyl)-1,3-dimethyl-3-phenylazetidin-2-one (4.1j)

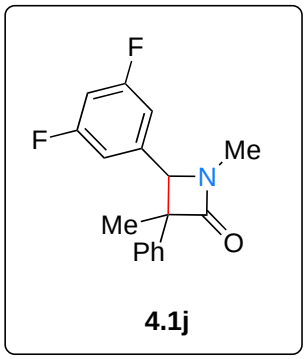

4.1j

Prepared according to general procedure 4C using **4.2j** (101 mg, 0.35 mmol) and **2-CTX** (8.7 mg, 0.035 mmol). Chromatography on silica gel with EtOAc:petroleum ether (1:9 to 2:8) afforded **4.1j** as 2 separable diastereomers (89 mg, 88% yield, 1.4:1 dr). **HRMS** (ESI^+) *m/z*: [M + H] calcd for $C_{17}H_{16}F_2NO^+$ 288.1194; found 288.1205. ***trans*-Diastereomer:** 0.052 g; white solid **R_f** = 0.31 (2:8 EtOAc:petroleum ether); **M.P.** 153–155 °C; **IR** (film, ν_{max}/cm^{-1}) 3059, 2916, 1744, 1624, 1596, 1460, 1443, 1393, 1341, 1115, 1038; **^{1}H NMR** (300 MHz, $CDCl_3$) δ 7.47–7.37 (m, 4H), 7.33–7.28 (m, 1H), 6.86–6.83 (m, 3H), 4.69 (s, 1H), 2.92 (s, 3H), 1.18 (s, 3H); **^{13}C NMR** (151 MHz, $CDCl_3$) δ 171.7, 163.6 (dd, $J_{C\text{-}F}$ = 250.5, 12.6 Hz), 141.6, 140.3 (t, $J_{C\text{-}F}$ = 8.2 Hz), 129.1, 127.6, 126.0, 110.0 (dd, $J_{C\text{-}F}$ = 20.4, 5.6 Hz), 104.0 (t, $J_{C\text{-}F}$ = 25.4 Hz), 68.4, 64.4, 27.4, 19.6; **^{19}F NMR** (377 MHz, CDCl3) δ -108.04.

***cis*-Diastereomer::** 0.037 g; white solid; R_f = 0.11 (2:8 EtOAc:petroleum ether); **M.P.** 113–115 °C; **IR** (film, ν_{max}/cm^{-1}) 2958, 2924, 2867, 1748, 1625, 1597, 1459, 1390, 1346, 1318, 1117; **^{1}H NMR** (300 MHz, $CDCl_3$) δ 7.12–7.00 (m, 5H), 6.57–6.51 (m, 1H), 6.47–6.44 (m, 2H), 4.50 (s, 1H), 2.86 (s, 3H), 1.81 (s, 3H); **^{13}C NMR** (151 MHz, $CDCl_3$) δ 171.5, 163.0 (dd, J_{C-F} = 249.7, 12.8 Hz), 140.4 (t, J_{C-F} = 8.5 Hz), 137.5, 128.3, 127.2, 127.1, 110.3 (d, J_{C-F} = 20.5, 5.4 Hz), 103.5 (t, J_{C-F} = 25.4 Hz), 69.9, 66.9, 27.4, 24.0; **^{19}F NMR** (377 MHz, CDCl3) δ -109.37;

4-(3-bromo-5-methoxyphenyl)-1,3-dimethyl-3-phenylazetidin-2-one (4.1k)

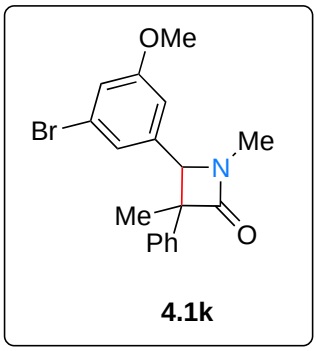

4.1k

Prepared according to general procedure 4C using **4.2k** (75.7 mg, 0.21 mmol) and **2-CTX** (5.2 mg, 0.02 mmol). Chromatography on silica gel with EtOAc:petroleum ether (0:1 to 1:5) afforded **4.1k** as 2 separable diastereomers (61.3 mg, 69% yield, 1.7:1 dr). **IR** (film, ν_{max}/cm^{-1}) 2965, 2926, 1746, 1598, 1570, 1458, 1431, 1389, 1339, 1314, 1270, 1156, 1051, 1029; **HRMS** (ESI^+) *m/z*: [M + H] calcd for $C_{18}H_{19}{}^{79}BrNO_2^+$ 360.0594; found 360.0610.

***trans*-Diastereomer:** 38.6 mg; R_f = 0.50 (4:6 EtOAc:petroleum ether); **^{1}H NMR** (300 MHz, $CDCl_3$) 7.45 (d, *J* = 7.7 Hz, 2H), 7.38 (t, *J* = 7.5 Hz, 2H), 7.33–7.27 (m, 1H), 7.07–7.00 (m, 2H), 6.75 (s, 1H), 4.64 (s, 1H), 3.83 (s, 3H), 2.89 (s, 3H), 1.19 (s, 3H); **^{13}C NMR** (101 MHz, $CDCl_3$) 171.8, 160.9, 141.9, 139.2, 129.0, 127.4, 126.0, 123.6, 122.4, 116.6, 112.4, 68.5, 64.2, 55.8, 27.3, 19.6.

***cis*-Diastereomer:** 22.7 mg; R_f = 0.29 (4:6 EtOAc:petroleum ether; **^{1}H NMR** (300 MHz, $CDCl_3$) 7.12–6.02 (m, 5H), 6.79 (s, 1H), 6.73 (s, 1H), 6.24 (s, 1H), 4.44 (s, 1H), 3.54 (s, 3H), 2.83 (s, 3H), 1.80 (s, 3H); **^{13}C NMR** (101 MHz, $CDCl_3$) 171.7, 160.3, 139.1, 137.9, 128.2, 127.2, 127.0, 123.4, 122.6, 117.3, 111.7, 70.0, 66.5, 55.6, 27.3, 24.2.

1,3-dimethyl-3-phenyl-4-(3,4,5-trichlorophenyl)azetidin-2-one (4.1l)

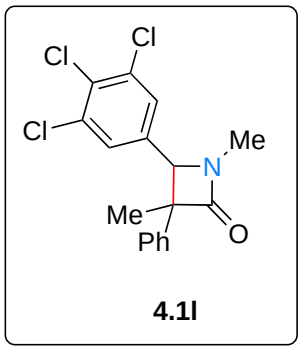

4.1l

Prepared according to general procedure 4C using **4.2l** (100 mg, 0.28 mmol) and **2-CTX** (7.0 mg, 0.03 mmol). Chromatography on silica gel with EtOAc:petroleum ether (1:9 to 2:8) afforded **4.1l** as 2 separable diastereomers (97 mg, 97% yield, 1.3:1 dr). **HRMS** (ESI^+) *m/z*: [M + H] calcd for $C_{17}H_{15}{}^{35}Cl_3NO^+$ 354.0214; found 354.0225.

***trans*-Diastereomer:** 0.054 g; white solid; R_f = 0.26 (3:7 EtOAc:petroleum ether); **M.P.** 187–189 °C; **IR** (film, ν_{max}/cm^{-1}) 2957,

2923, 1746, 1641, 1425, 1392, 1265, 1033; **^{1}H NMR** (300 MHz, $CDCl_3$) δ 7.42–7.35 (m, 4H), 7.30–7.23 (m, 3H), 4.62 (s, 1H), 2.88 (s, 3H), 1.17 (s, 3H); **^{13}C NMR** (151 MHz, $CDCl_3$) δ 171.6, 141.4, 136.7, 135.2, 131.6, 129.1, 127.7, 127.2, 126.0, 67.9, 64.6, 27.4, 19.8.

***cis*-Diastereomer:** 0.043 g; white solid; **R_f** = 0.18 (3:7 EtOAc: petroleum ether); **M.P.** 138–140 °C; **IR** (film, ν_{max}/cm^{-1}) 2955, 2925, 2856, 1742, 1639, 1426, 1388, 1333, 1271, 1224, 1032; **^{1}H NMR** (300 MHz, $CDCl_3$) δ 7.16–7.09 (m, 3H), 7.02 (d, *J* = 7.8 Hz, 2H), 6.92 (s, 2H), 4.44 (s, 1H), 2.84 (s, 3H), 1.82 (s, 3H); **^{13}C NMR** (151 MHz, $CDCl_3$) δ 171.4, 137.2, 136.7, 134.3, 130.9, 128.5, 127.6, 127.5, 127.1, 69.3, 67.1, 27.4, 23.9.

1,3-dimethyl-4-(naphthalen-1-yl)-3-phenylazetidin-2-one (4.1m)

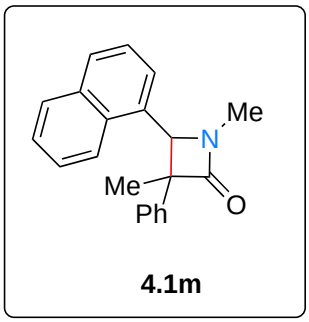

4.1m

Prepared according to general procedure 4C using **4.2m** (101 mg, 0.34 mmol) and **2-CTX** (8.3 mg, 0.03 mmol). Chromatography on silica gel with EtOAc:petroleum ether (0:1 to 1:7) afforded **4.1m** as 2 separable diastereomers (76.0 mg, 75% yield, 1:5 dr). **HRMS** (ESI^+) *m/z*: [M + H] calcd for $C_{21}H_{20}NO^+$ 302.1539; found 302.1541.

***trans*-Diastereomer:** 12.7 mg, clear oil, **R_f** = 0.54 (3:7 EtOAc:petroleum ether); **IR** (film, ν_{max}/cm^{-1}) 2919, 2855, 1457, 1376, 1067; **^{1}H NMR** (300 MHz, $CDCl_3$) 7.92 (d, *J* = 8.1 Hz, 1H), 7.86 (d, *J* = 8.1 Hz, 1H), 7.59–7.36 (m, 10H), 5.32 (s, 1H), 3.12 (s, 3H), 1.61 (s, 3H), 1.13 (s, 3H); **^{13}C NMR** (101 MHz, $CDCl_3$) 173.1, 140.9, 134.0, 132.0, 131.7, 129.2, 129.1, 128.6, 127.7, 126.7, 126.2, 126.2, 125.4, 123.8, 123.2, 67.7, 64.1, 27.8, 16.0.

***cis*-Diastereomer:** 63.3 mg, clear oil, **R_f** = 0.46 (3:7 EtOAc:petroleum ether; **IR** (film, ν_{max}/cm^{-1}) 2959, 2922, 2858, 1748, 1447, 1386, 1259 1231, 1049; **^{1}H NMR** (300 MHz, $CDCl_3$) 8.06 (d, *J* = 8.7 Hz, 1H), 7.80 (d, *J* = 8.1 Hz, 1H), 7.64–7.50 (m, 3H), 7.18 (t, *J* = 8.1 Hz, 1H), 6.98 (d, *J* = 7.4 Hz, 1H), 6.92–6.82 (m, 5H), 5.42 (s, 1H), 3.00 (s, 3H), 2.02 (s, 3H); **^{13}C NMR** (101 MHz, $CDCl_3$) 172.5, 137.7, 133.6, 131.7, 131.6, 129.2, 128.1, 127.7, 126.9, 126.7, 126.6, 125.8, 125.1, 123.9, 122.4, 67.0, 66.6, 27.7, 23.4.

1,3,4-trimethyl-3,4-diphenylazetidin-2-one (4.1n)

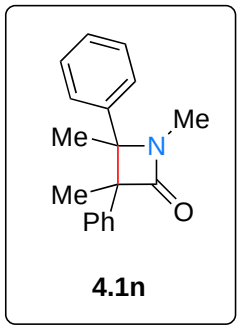

4.1n

Prepared according to general procedure 4C using **4.2n** (100 mg, 0.37 mmol) and **2-CTX** (9.3 mg, 0.037 mmol). Chromatography on silica gel with EtOAc:petroleum ether (1:9 to 2:8) afforded **4.1n** as 2 separable diastereomers (88 mg, 88% yield, 1.7:1 dr). **HRMS** (ESI$^+$) *m/z*: [M + H] calcd for $C_{18}H_{20}NO^+$ 266.1539; found 266.1552.

***trans*-Diastereomer:** 0.056 g; white solid; R_f = 0.39 (3:7 EtOAc:petroleum ether); **M.P.** 138–139 °C; **IR** (film, ν_{max}/cm^{-1}) 2972, 2925, 1735, 1492, 1445, 1419, 1386, 1260, 1064, 1023; **^{1}H NMR** (300 MHz, $CDCl_3$) δ 7.47–7.28 (m, 10H), 2.94 (s, 3H), 1.27 (s, 3H), 1.12 (s, 3H); **^{13}C NMR** (101 MHz, $CDCl_3$) δ 172.2, 141.0, 140.0, 128.8, 128.6, 127.5, 127.2, 126.9, 126.1, 69.0, 66.4, 24.8, 22.7, 21.7.

***cis*-Diastereomer:** 0.032 g; white solid; R_f = 0.25 (3:7 EtOAc:petroleum ether); **M.P.** 138–140 °C; **IR** (film, ν_{max}/cm^{-1}) 2975, 2941, 1727, 1494, 1447, 1422, 1392, 1266, 1285, 1069, 1028; **^{1}H NMR** (300 MHz, $CDCl_3$) δ 7.09–6.89 (m, 10H), 2.84 (s, 3H), 1.90 (s, 3H), 1.71 (s, 3H); **^{13}C NMR** (101 MHz, $CDCl_3$) δ 172.0, 140.6, 140.1, 127.9, 127.7, 127.1, 126.9, 126.6, 126.2, 68.5, 67.9, 24.3, 20.5, 19.8.

1,3-dimethyl-4-(1-methyl-1*H*-indol-3-yl)-3-phenylazetidin-2-one (4.1o)

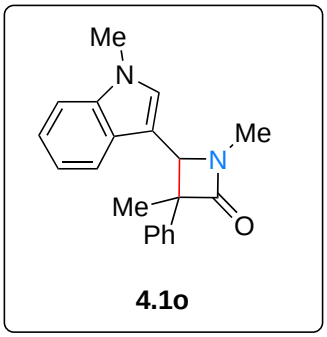

4.1o

Prepared according to general procedure 4C using **4.2o** (48 mg, 0.16 mmol) and **2-CTX** (3.87 mg, 0.02 mmol). Chromatography on silica gel with EtOAc:petroleum ether (1:9 to 2:8) afforded colourless oil **4.1o** as 2 inseparable diastereomers (25 mg, 52% yield, 1.6:1 dr).

Combined diastereomers: R_f = 0.14 (3:7 EtOAc:petroleum ether); **IR** (film, ν_{max}/cm^{-1}) 3057, 2960, 2922, 1737, 1664, 1545, 1668, 1424, 1387, 1241, 1068; **^{1}H NMR** (300 MHz, $CDCl_3$) δ 7.65–7.59 (m, 0.6H), 7.54–7.51 (m, 1.2H), 7.43–7.26 (m, 3.8H), 7.21–6.96 (m, 4H), 6.50 (s, 0.4H), 5.00 (s, 0.6H), 4.90 (s, 0.4H), 3.85 (s, 1.8H), 3.60 (s, 1.2H), 2.90 (s, 1.8H), 2.83 (s, 1.2H), 1.84 (s, 1.2H), 1.32 (s, 1.8H); **^{13}C NMR** (101 MHz, $CDCl_3$) δ 172.4, 172.2, 142.8, 139.5, 137.5, 137.0, 128.9, 128.2, 127.9, 127.8, 127.3, 127.2, 127.1, 127.0, 126.5, 126.0, 122.3, 121.8, 120.1, 119.6, 119.5, 118.9, 109.9, 109.4, 109.0, 65.3, 64.1, 63.9, 63.8, 33.2, 32.9, 26.9, 24.8, 19.6; **HRMS** (ESI$^+$) *m/z*: [M + H] calcd for $C_{20}H_{21}N_2O^+$ 305.1648; found 305.1660.

4-(furan-3-yl)-1,3-dimethyl-3-phenylazetidin-2-one (4.1p)

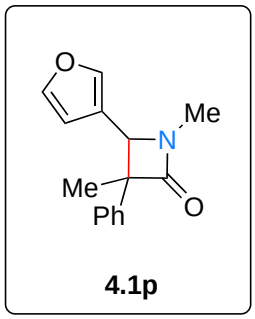

4.1p

Prepared according to general procedure 4C using **4.2p** (100 mg, 0.41 mmol) and **2-CTX** (10.2 mg, 0.04 mmol). Chromatography on silica gel with EtOAc:petroleum ether (1:9 to 2:8) afforded **4.1p** as 2 separable diastereomers (77 mg, 77% yield, 1.5:1 dr). **HRMS** (ESI$^+$) *m/z*: [M + H] calcd for $C_{15}H_{16}NO_2^+$ 242.1176; found 242.1192.

***trans*-Diastereomer:** 0.046 g; colourless oil; R_f = 0.40 (3:7 EtOAc:petroleum ether); **IR** (film, ν_{max}/cm^{-1}) 3124, 2905, 1743, 1497, 1445, 1425, 1389, 1163, 1026; **^{1}H NMR** (300 MHz, $CDCl_3$) δ 7.52–7.48 (m, 2H), 7.45–7.34 (m, 4H), 7.30–7.25 (m, 1H), 6.42 (s, 1H), 4.65 (s, 1H), 2.85 (s, 3H), 1.32 (s, 3H); **^{13}C NMR** (101 MHz, $CDCl_3$) δ 171.9, 144.1, 142.1, 140.9, 128.9, 127.3, 126.0, 120.9, 109.6, 63.2, 61.7, 26.8, 20.2.

***cis*-Diastereomer:** 0.031 g; white solid; R_f = 0.23 (3:7 EtOAc:petroleum ether); **M.P.** 104–106 °C; **IR** (film, ν_{max}/cm^{-1}) 2960, 2914, 1743, 1444, 1423, 1392, 1372, 1154, 1022; **^{1}H NMR** (300 MHz, $CDCl_3$) δ 7.26 (s, 1H), 7.18–7.12 (m, 5H), 7.09 (m, 1H), 5.61 (s, 1H), 4.49 (s, 1H), 2.78 (s, 3H), 1.76 (s, 3H); **^{13}C NMR** (101 MHz, $CDCl_3$) δ 171.6, 143.5, 141.4, 138.7, 128.2, 127.2, 127.0, 121.5, 109.0, 64.8, 62.5, 26.8, 24.2;

1,3-dimethyl-3-phenyl-4-(thiophen-3-yl)azetidin-2-one (4.1q)

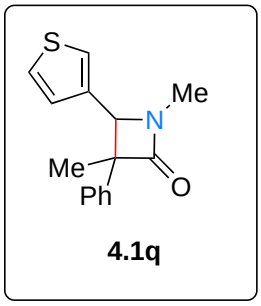

4.1q

Prepared according to general procedure 4C using **4.2q** (100 mg, 0.39 mmol) and **2-CTX** (9.6 mg, 0.04 mmol). Chromatography on silica gel with EtOAc:petroleum ether (1:9 to 2:8) afforded **4.1q** as 2 separable diastereomers (97 mg, 97% yield, 1.3:1 dr). **HRMS** (ESI$^+$) *m/z*: [M + H] calcd for $C_{15}H_{16}NOS^+$ 258.0947; found 258.0961.

***trans*-Diastereomer:** 0.056 g; yellow soild; R_f = 0.20 (3:7 EtOAc:petroleum ether); **M.P.** 96–97 °C; **IR** (film, ν_{max}/cm^{-1}) 3083, 2965, 2907, 1735, 1647, 1492, 1442, 1423, 1388, 1321, 1257, 1027; **^{1}H NMR** (300 MHz, $CDCl_3$) δ 7.48–7.36 (m, 5H), 7.31–7.23 (m, 2H), 7.07 (d, *J* = 5.1 Hz, 1H), 4.81 (s, 1H), 2.90 (s, 3H), 1.22 (s, 3H); **^{13}C NMR** (101 MHz, $CDCl_3$) δ 172.0, 142.2, 137.5, 128.9, 127.3, 127.0, 126.5, 126.0, 122.8, 65.4, 63.8, 27.1, 19.9.

***cis*-Diastereomer:** 0.042 g; yellow solid; R_f = 0.10 (3:7 EtOAc:petroleum ether); **M.P.** 103–104 °C; **IR** (film, ν_{max}/cm^{-1}) 2959, 2922, 1740, 1641, 1444, 1423, 1390, 1372, 1261, 1073, 1026; **^{1}H NMR** (300 MHz, $CDCl_3$) δ 7.12–7.06 (m, 5H), 7.03–7.01 (m, 1H), 6.95–6.93 (m, 1H), 6.46 (d, *J*

= 4.8 Hz, 1H), 4.66 (s, 1H), 2.83 (s, 3H), 1.78 (s, 3H); **^{13}C NMR** (101 MHz, $CDCl_3$) δ 171.8, 138.7, 137.9, 128.1, 127.1, 126.8, 126.4, 126.0, 123.5, 66.5, 65.7, 27.1, 24.4.

1,3-dimethyl-3-phenyl-4-vinylazetidin-2-one (4.1r)

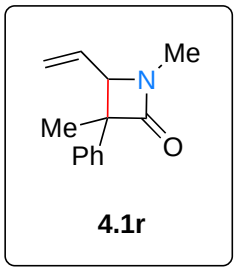

4.1r

Prepared according to general procedure 4C using **4.2r** (50.3 mg, 0.25 mmol) and **2-CTX** (6.2 mg, 0.03 mmol). Chromatography on silica gel with EtOAc:petroleum ether (0:1 to 1:4) afforded **4.1r** as 2 inseparable diastereomers (30.2 mg, 60% yield, 1.4:1 dr). **IR** (film, ν_{max}/cm^{-1}) 2969, 2921, 1742, 1494, 1423, 1389, 1251, 1177, 1067, 1028; **HRMS** (ESI$^+$) *m/z*: [M + H] calcd for $C_{13}H_{16}NO^+$ 202.1226; found 202.1236.

Combined diastereomers (~1.5:1): R_f = 0.64 (6:4 EtOAc:petroleum ether); **^{1}H NMR** (300 MHz, $CDCl_3$) 7.41–7.15 (m, 5H), 5.96–5.79 (m, 0.6H), 5.49–5.37 (m, 1.2H), 5.33–5.20 (m, 0.4H), 5.18–5.02 (m, 0.8H), 4.04 (d, *J* = 7.7 Hz, 0.6H), 3.84 (d, *J* = 7.4 Hz, 0.4H), 2.77 (s, 3H), 1.68 (s, 1.2H), 1.43 (s, 1.8H); **^{13}C NMR** (101 MHz, $CDCl_3$) 171.7, 171.4, 142.3, 138.4, 135.0, 133.5, 128.8, 128.4, 127.3, 127.1, 127.1, 125.9, 121.4, 120.6, 69.3, 67.7, 63.6, 62.7, 26.7, 26.7, 23.7, 19.9.

4-ethynyl-1,3-dimethyl-3-phenylazetidin-2-one (4.1s)

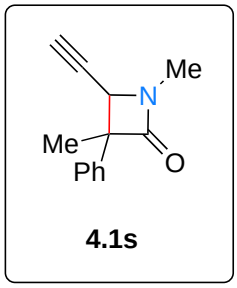

4.1s

Prepared according to general procedure 4C using **4.2s** (93.6 mg, 0.47 mmol) and **2-CTX** (11.6 mg, 0.05 mmol). Chromatography on silica gel with EtOAc:petroleum ether (0:1 to 1:4) afforded **4.1s** as 2 separable diastereomers (37.5 mg, 40% yield, 2.3:1 dr). **HRMS** (ESI$^+$) *m/z*: [M + H] calcd for $C_{13}H_{14}NO^+$ 200.1070; found 200.1085.

***trans*-Diastereomer:** 26.1 mg, R_f = 0.70 (3:7 EtOAc:petroleum ether); **IR** (film, ν_{max}/cm^{-1}) 3283, 3237, 2972, 2923, 1746, 1495, 1444, 1421, 1388, 1331, 1248, 1166, 1035; **^{1}H NMR** (300 MHz, $CDCl_3$) δ 7.41–7.24 (m, 5H), 4.28 (d, *J* = 2.1 Hz, 1H), 2.86 (s, 3H), 2.66 (d, *J* = 2.1 Hz, 1H), 1.67 (s, 3H); **^{13}C NMR** (101 MHz, $CDCl_3$) δ 170.7, 140.8, 128.9, 127.5, 126.0, 77.7, 76.9, 63.2, 56.1, 26.6, 21.1.

***cis*-Diastereomer:** 11.4 mg, R_f = 0.46 (3:7 EtOAc:petroleum ether; **IR** (film, ν_{max}/cm^{-1}) 3287, 3235, 2964, 2923, 1744, 1445, 1423, 1389, 1384, 1257, 1071, 1036; **^{1}H NMR** (300 MHz, $CDCl_3$) δ 7.41–7.28 (m, 5H), 4.16 (d, *J* = 1.8 Hz, 1H), 2.91 (s, 3H), 2.30 (d, *J* = 1.8 Hz, 1H), 1.74 (s, 3H); **^{13}C NMR** (101 MHz, $CDCl_3$) δ 170.7, 137.9, 128.3, 127.6, 127.2, 78.5, 78.0, 64.9, 57.2, 26.9, 22.9.

1,3-dimethyl-4-oxo-3-phenylazetidine-2-carbonitrile (4.1t)

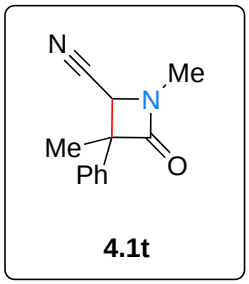

4.1t

Prepared according to general procedure 4C using **4.2t** (100 mg, 0.50 mmol) and **2-CTX** (12.3 mg, 0.05 mmol). Chromatography on silica gel with EtOAc:petroleum ether (1:9 to 2:8) afforded **4.1t** as 2 separable diastereomers (85 mg, 85% yield, 1.4:1 dr). **HRMS** (ESI$^+$) *m/z*: [M + H] calcd for $C_{12}H_{13}N_2O^+$ 201.1022; found 201.1026.

Diastereomer 1: 0.050 g; yellow oil; $\mathbf{R_f}$ = 0.48 (3:7 EtOAc:petroleum ether); **IR** (film, ν_{max}/cm^{-1}) 2973, 2934, 2540, 1753, 1655, 1448, 1424, 1383, 1033; **^{1}H NMR** (300 MHz, $CDCl_3$) δ 7.41–7.30 (m, 5H), 4.33 (s, 1H), 2.97 (s, 3H), 1.82 (s, 3H); **^{13}C NMR** (101 MHz, $CDCl_3$) δ 169.3, 138.6, 129.2, 128.3, 125.8, 115.3, 64.8, 54.5, 27.8, 21.6.

Diastereomer 2: 0.035 g; yellow solid; $\mathbf{R_f}$ = 0.18 (3:7 EtOAc:petroleum ether); **M.P.** 111–113 °C; **IR** (film, ν_{max}/cm^{-1}) 2959, 2922, 2243, 1740, 1641, 1491, 1444, 1422, 1390, 13721261, 1026; **^{1}H NMR** (300 MHz, $CDCl_3$) δ 7.45–7.34 (m, 5H), 4.23 (s, 1H), 3.00 (s, 3H), 1.80 (s, 3H); **^{13}C NMR** (101 MHz, $CDCl_3$) δ 169.4, 136.1, 129.1, 128.8, 126.6, 115.1, 66.2, 55.7, 28.0, 22.5.

1-isopropyl-3,4,4-trimethyl-3-phenylazetidin-2-one (4.1u)

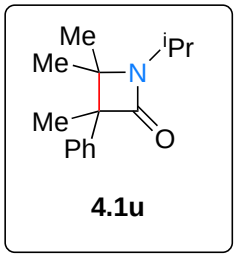

4.1u

Prepared according to general procedure 4C using **4.2u** (139 mg, 0.60 mmol) and **2-CTX** (14.8 mg, 0.06 mmol). Chromatography on silica gel with EtOAc:petroleum ether (0:1 to 1:7) afforded **4.1u** as a clear oil (72.2 mg, 52% yield). $\mathbf{R_f}$ = 0.73 (3:7 EtOAc:petroleum ether); **IR** (film, ν_{max}/cm^{-1}) 2972, 2927, 1729, 1453, 1405, 1379, 1343, 1244, 1127, 1068, 1030; **^{1}H NMR** (300 MHz, $CDCl_3$) δ 7.34–7.17 (m, 5H), 3.62 (hept, *J* = 6.7 Hz, 1H), 1.58 (s, 3H), 1.45 (s, 3H), 1.34 (s, 3H), 1.36 (s,3H), 0.90 (s, 3H); **^{13}C NMR** (101 MHz, $CDCl_3$) δ 170.6, 141.1, 128.5, 127.0, 126.9, 64.1, 63.2, 43.9, 26.1, 23.1, 22.2, 22.1, 20.0; **HRMS** (ESI$^+$) *m/z*: [M + H] calcd for $C_{15}H_{22}NO^+$ 232.1696; found 232.1712.

1-ethyl-3-methyl-3,4-diphenylazetidin-2-one (4.1v)

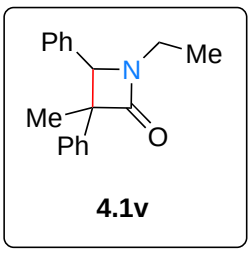

4.1v

Prepared according to general procedure 4C using **4.2v** (100 mg, 0.38 mmol) and **2-CTX** (9.3 mg, 0.038 mmol). Chromatography on silica gel with EtOAc:petroleum ether (1:9 to 2:8) afforded **4.1v** as 2 separable diastereomers (98 mg, 98% yield, 1.4:1 dr). **HRMS** (ESI$^+$) *m/z*: [M + H] calcd for $C_{18}H_{20}NO^+$ 266.1539; found 266.1555.

***trans*-Diastereomer:** 0.057 g; white solid; R_f = 0.44 (3:7 EtOAc:petroleum ether); **M.P.** 96–98 °C; **IR** (film, ν_{max}/cm^{-1}) 2973, 2929, 1739, 1643, 1494, 1451, 1400, 1354, 1311, 1272, 1272, 1169, 1049; **^{1}H NMR** (300 MHz, $CDCl_3$) δ 7.51–7.27 (m, 10H), 4.80 (s, 1H), 3.78–3.70 (m 1H), 3.08–3.01 (m, 1H), 1.16 (s, 3H), 1.14 (t, *J* = 7.2 Hz, 3H); **^{13}C NMR** (151 MHz, $CDCl_3$) δ 171.9, 142.4, 136.0, 128.9, 128.9, 128.4, 127.3, 127.2, 126.0, 66.9, 62.9, 35.3, 19.5, 13.0.

***cis*-Diastereomer:** 0.041 g; colourless oil; R_f = 0.36 (3:7 EtOAc:petroleum ether); **IR** (film, ν_{max}/cm^{-1}) 2963, 2926, 1733, 1494, 1451, 1405, 1356, 1300, 1065; **^{1}H NMR** (300 MHz, $CDCl_3$) δ 7.12–7.09 (m, 3H), 7.02 (s, 5H), 6.95–6.92 (m, 2H), 4.63 (s, 1H), 3.66–3.59 (m, 1H), 3.01–2.94 (m, 1H), 1.80 (s, 3H), 1.14, (t, *J* = 7.3 Hz, 3H); **^{13}C NMR** (151 MHz, $CDCl_3$) δ 171.8, 138.4, 136.1, 128.2, 128.0, 128.0, 127.7, 127.4, 126.6, 68.5, 65.2, 35.2, 24.5, 12.9.

1-benzyl-3-methyl-3,4-diphenylazetidin-2-one (4.1w)

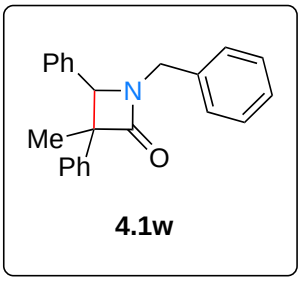

4.1w

Prepared according to general procedure 4C using **4.2w** (115 mg, 0.35 mmol) and **2-CTX** (8.6 mg, 0.04 mmol). Chromatography on silica gel with EtOAc:petroleum ether (0:1 to 1:7) afforded **4.1w** as 2 inseparable diastereomers (95.1 mg, 83% yield, 2:1 dr). **IR** (film, ν_{max}/cm^{-1}) 3029, 2969, 2923, 1742, 1495, 1452, 1398, 1354, 1216, 1175, 1073; **HRMS** (ESI$^+$) *m/z*: [M + H] calcd for $C_{23}H_{22}NO^+$ 328.1696; found 328.1705.

Combined diastereomers: clear oil; R_f = 0.45 (2:8 EtOAc:petroleum ether); **^{1}H NMR** (300 MHz, $CDCl_3$) δ 7.47–6.91 (m, 15H), 5.06 (d, *J* = 14.9 Hz, 0.66H), 5.03 (d, *J* = 14.9 Hz, 0.33H), 4.65 (s, 0.66H), 4.44 (s, 0.33H), 4.03 (d, *J* = 14.9 Hz, 0.66H), 3.82 (d, *J* = 14.9 Hz, 0.33H), 1.77 (s, 1H), 1.23 (s, 2H); **^{13}C NMR** (101 MHz, $CDCl_3$) δ 172.1, 171.8, 142.2, 138.3, 135.8, 135.6, 135.6, 135.5, 128.9, 128.9, 128.8, 128.7, 128.5, 128.4, 128.2, 128.0, 128.0, 127.9, 127.8, 127.8, 127.4, 127.3, 127.2, 126.6, 126.0, 68.0, 67.0, 65.7, 63.4, 44.4, 44.3, 24.3, 19.5.

3-methyl-1,3,4-triphenylazetidin-2-one (4.1x)[252]

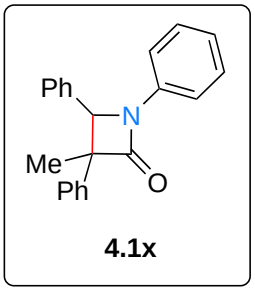

4.1x

Prepared according to general procedure 4C using **4.2x** (60 mg, 0.19 mmol) and **2-CTX** (4.72 mg, 0.02 mmol). Chromatography on silica gel with EtOAc:petroleum ether (1:9 to 3:7) afforded **4.1x** as 2 inseparable diastereomers (25 mg, 52% yield, 1:1.4 dr).

R_f = 0.60 (2:8 EtOAc:petroleum ether); **IR** (film, ν_{max}/cm^{-1}) 3030, 2925, 1731, 1598, 1493, 1453, 1382, 1351, 1273, 1151, 1062, 1025; **^{1}H NMR**

(300 MHz, $CDCl_3$) δ 7.57–7.54 (m, 2H), 7.43–7.29 (m, 14.25H), 7.10–6.99 (m, 10H), 5.24 (s, 1H), 5.06 (s, 0.75H), 1.92 (s, 2.25H), 1.23 (s, 3H); **^{13}C NMR** (101 MHz, $CDCl_3$) 169.4, 169.3, 142.0, 137.9, 137.7, 137.6, 135.4, 135.0, 131.1, 129.9, 129.2, 129.1, 129.0, 128.5, 128.4, 128.1, 128.1, 127.5, 127.4, 127.3, 127.1, 126.8, 126.1, 124.1, 68.8, 67.1, 64.8, 62.7, 24.6, 19.9 (overlapping peaks in the ^{13}C NMR spectrum meant that some of the signals in this diastereomeric mixture could not be reliably assigned); **HRMS** (ESI^+) *m/z*: [M + H] calcd for $C_{22}H_{20}NO^+$ 314.1539; found 314.1547. Recorded data in accordance with those previously reported.

3-methyl-3,4-diphenyl-1-tosylazetidin-2-one (4.1y)

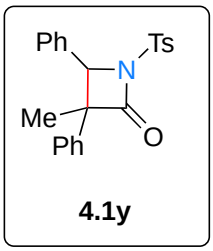

4.1y

Prepared according to general procedure 4C using **4.2y** (114 mg, 0.29 mmol) and **2-CTX** (7.2 mg, 0.03 mmol). Chromatography on silica gel with EtOAc:petroleum ether (0:1 to 1:7) afforded **4.1y** as partially separable diastereomers (77.2 mg, 68% yield, 4.4:1 dr). **HRMS** (ESI^+) *m/z*: [M + H] calcd for $C_{23}H_{22}NO_3S^+$ 392.1315; found 392.1329.

***trans*-Diastereomers (as a mixture with *cis-diastereomer*):** 24.9 mg (1.6:1 *cis*:*trans*); colourless oil; $\mathbf{R_f}$ = 0.53 (2:8 EtOAc:petroleum ether); **IR** (film, ν_{max}/cm^{-1}) 3030, 2964, 2925, 1787, 1598, 1496, 1451, 1365, 1249, 1216, 1165, 1087, 1053, 1028; **^{1}H NMR** (300 MHz, $CDCl_3$) (only *trans* signals reported) δ 7.85 (d, *J* = 8.0 Hz, 2H), 7.39–7.15 (m, 13H), 5.18 (s, 1H), 2.46 (s, 3H), 1.15 (s, 3H); **^{13}C NMR** (101 MHz, $CDCl_3$) (only *trans* signals reported) δ 169.4, 145.5, 134.0, 135.7, 134.3, 130.0, 129.2, 128.8, 128.8, 127.9, 127.9, 127.0, 125.6, 69.8, 63.5, 29.8, 19.4.

***cis*-Diastereomer (completely separated):** 52.3 mg; white solid, $\mathbf{R_f}$ = 0.45 (2:8 EtOAc:petroleum ether; **M.P.** 152–153 °C; **IR** (film, ν_{max}/cm^{-1}) 3061, 3032, 2965, 2926, 1786, 1597, 1496, 1451, 1364, 1247, 119, 1184, 1088, 1053, 1028; **^{1}H NMR** (300 MHz, $CDCl_3$) δ 7.76 (d, *J* = 7.9 Hz, 2H), 7.30–6.82 (m, 13H), 4.99 (s, 0.87H), 4.29 (s, 0.13H), 2.44 (s, 3H), 1.70 (s, 3H); **^{13}C NMR** (101 MHz, $CDCl_3$) δ 168.9, 145.4, 136.2, 135.5, 134.4, 130.0, 128.4, 128.2, 128.1, 127.8, 127.7, 127.3, 126.9, 70.7, 65.6, 24.6, 21.8.

1,3-dimethyl-4-phenyl-3-(*p*-tolyl)azetidin-2-one (4.1z)

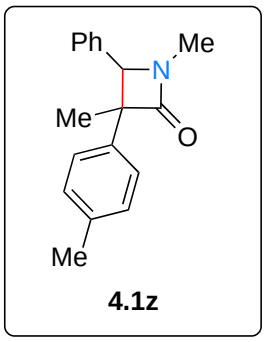

4.1z

Prepared according to general procedure 4C using **4.2z** (89 mg, 0.34 mmol) and **2-CTX** (8.3 mg, 0.03 mmol). Chromatography on silica gel with EtOAc:petroleum ether (1:9 to 2:8) afforded **4.1z** as 2 separable diastereomers (77 mg, 87% yield, 2.3:1 dr). **HRMS** (ESI$^+$) *m/z*: [M + H] calcd for $C_{18}H_{20}NO^+$ 266.1539; found 266.1553.

***trans*-Diastereomer:** 0.054 g; colourless oil; R_f = 0.27 (2:8 EtOAc:petroleum ether); **IR** (film, ν_{max}/cm^{-1}) 2969, 2921, 1745, 1636, 1514, 1452, 1420, 1387, 1352, 1179, 1024; **^{1}H NMR** (300 MHz, $CDCl_3$) δ 749–7.44 (m, 2H), 7.40–7.37 (m, 3H), 7.32–7.30 (m, 2H), 7.22–7.19 (m, 2H), 4.72 (s, 1H), 2.91 (s, 3H), 2.36 (s, 3H), 1.13 (s, 3H); **^{13}C NMR** (101 MHz, $CDCl_3$) δ 172.3, 139.4, 136.9, 135.8, 129.5, 128.9, 128.3, 127.2, 126.0, 69.3, 63.6, 27.1, 21.2, 19.7.

***cis*-Diastereomer:** 0.023 g; colourless oil; R_f = 0.13 (2:8 EtOAc:petroleum ether); **M.P.** 111–113 °C; **IR** (film, ν_{max}/cm^{-1}) 2959, 2921, 1744, 1633, 1452, 1420, 1390, 1361, 1280, 1260, 1067, 1026; **^{1}H NMR** (300 MHz, $CDCl_3$) δ 7.38–7.35 (m, 1H), 7.14–7.11 (m, 3H), 6.93–6.82 (m, 5H), 4.54 (s, 1H), 2.84 (s, 3H), 2.16 (s, 3H), 1.78 (s, 3H); **^{13}C NMR** (101 MHz, $CDCl_3$) δ 172.2, 136.1, 135.8, 135.3, 128.7, 128.3, 128.0, 127.6, 127.2, 70.8, 65.9, 27.1, 24.7, 21.1.

3-(4-methoxyphenyl)-1,3-dimethyl-4-phenylazetidin-2-one (4.1aa)

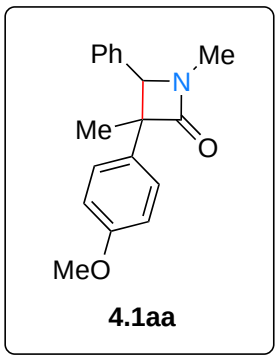

4.1aa

Prepared according to general procedure 4C using **4.2aa** (30.1 mg, 0.11 mmol) and **2-CTX** (2.6 mg, 0.01 mmol). Chromatography on silica gel with EtOAc:petroleum ether (0:1 to 1:7) afforded **4.1aa** as 2 separable diastereomers (16.0 mg, 53% yield, 2.5:1 dr). **IR** (film, ν_{max}/cm^{-1}) 2957, 2924, 2858, 1745, 1611, 1513, 1456, 1391, 1296, 1249, 1181, 1030; **HRMS** (ESI$^+$) *m/z*: [M + H] calcd for $C_{18}H_{20}NO_2^+$ 282.1489; found 282.1486.

***trans*-Diastereomer:** 11.4 mg; colourless oil; R_f = 0.50 (3:7 EtOAc:petroleum ether); **^{1}H NMR** (300 MHz, $CDCl_3$) δ 7.45–7.28 (m, 7H), 6.92 (d, *J* = 9.1 Hz, 2H), 4.69 (s, 1H), 3.82 (s, 3H), 2.91 (s, 3H), 1.11 (s, 3H); **^{13}C NMR** (101 MHz, $CDCl_3$) δ 172.4, 158.8, 135.8, 134.6, 129.0, 128.4, 127.2 (2C), 114.3, 69.4, 63.3, 55.5, 27.2, 19.7.

***cis*-Diastereomer:** 4.6 mg; colourless oil; R_f = 0.39 (3:7 EtOAc:petroleum ether; **^{1}H NMR** (300 MHz, $CDCl_3$) δ 7.14–7.12 (m, 3H), 6.94–6.90 (m, 4H), 6.57 (d, *J* = 8.6 Hz, 2H), 4.53 (s, 1H), 3.67

(s, 3H), 2.84 (s, 3H), 1.77 (s, 3H); **^{13}C NMR** (101 MHz, $CDCl_3$) δ 172.1, 158.0, 135.6, 130.4, 128.3, 128.2, 127.9, 127.4, 113.2, 70.6, 65.4, 55.0, 26.9, 24.5.

3-(4-bromophenyl)-1,3-dimethyl-4-phenylazetidin-2-one (4.1ab)

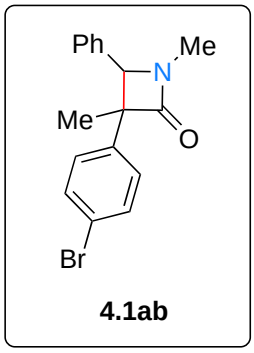

4.1ab

Prepared according to general procedure 4C using **4.2ab** (104 mg, 0.32 mmol) and **2-CTX** (7.8 mg, 0.03 mmol). Chromatography on silica gel with EtOAc:petroleum ether (0:1 to 1:7) afforded **4.1ab** as 2 separable diastereomers (97.0 mg, 93% yield, 1.7:1 dr). **IR** (film, ν_{max}/cm^{-1}) 2956, 2923, 2857, 1750, 1644, 1490, 1455, 1422, 1392, 1076, 1012; **HRMS** (ESI^+) *m/z*: [M + H] calcd for $C_{17}H_{17}{}^{79}BrNO^+$ 330.0488; found 330.0497.

***trans*-Diastereomer:** 61.1 mg; clear oil; R_f = 0.56 (3:7 EtOAc:petroleum ether); **IR** (film, ν_{max}/cm^{-1}) 2923, 2856, 1751, 1489, 1455, 1422, 1391, 1354, 1178, 1077, 1012; **^{1}H NMR** (300 MHz, $CDCl_3$) δ 7.52–7.27 (m, 9H), 4.69 (s, 1H), 2.90 (s, 3H), 1.12 (s, 3H); **^{13}C NMR** (101 MHz, $CDCl_3$) δ 171.5, 141.4, 135.3, 132.0, 129.1, 128.6, 127.9, 127.2, 121.2, 69.0, 63.4, 27.2, 19.7.

***cis*-Diastereomer:** 35.9 mg; colourless oil; R_f = 0.39 (3:7 EtOAc:petroleum ether; **^{1}H NMR** (300 MHz, $CDCl_3$) δ 7.17–7.14 (m, 5H), 6.92–6.87 (d, 4H), 4.56 (s, 1H), 2.83 (s, 3H), 1.77 (s, 3H); **^{13}C NMR** (101 MHz, $CDCl_3$) δ 171.5, 137.6, 135.3, 131.1, 129.1, 128.5, 128.4, 127.5, 120.7, 70.5, 65.5, 27.1, 24.6.

3-(3,4-dichlorophenyl)-1,3-dimethyl-4-phenylazetidin-2-one (4.1ac)

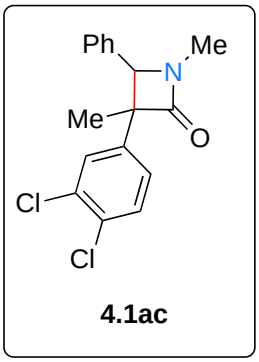

4.1ac

Prepared according to general procedure 4C using **4.2ac** (46 mg, 0.14 mmol) and **2-CTX** (3.5 mg, 0.014 mmol). Chromatography on silica gel with EtOAc:petroleum ether (1:9 to 2:8) afforded **4.1ac** as 2 separable diastereomers (40 mg, 87% yield, 1.3:1 dr). **HRMS** (ESI^+) *m/z*: [M + H] calcd for $C_{17}H_{16}{}^{35}Cl_2NO^+$ 320.0603; found 320.0614.

***trans*-Diastereomer:** 0.022 g; oil; R_f = 0.32 (2:8 EtOAc:petroleum ether); **IR** (film, ν_{max}/cm^{-1}) 2971, 2923, 1747, 1643, 1461, 1423, 1386, 1354, 1134, 1026; **^{1}H NMR** (300 MHz, $CDCl_3$) δ 7.56 (s, 1H), 7.50–7.37 (m, 4H), 7.33–7.27 (m, 3H), 4.68 (s, 1H), 2.91 (s, 3H), 1.12 (s, 3H); **^{13}C NMR** (151 MHz, $CDCl_3$) δ 171.0, 142.5, 135.0, 133.1, 131.5, 130.9, 129.2, 128.8, 128.3, 127.2, 125.7, 69.0, 63.1, 27.3, 19.6.

***cis*-Diastereomer:** 0.018 g; oil; R_f = 0.26 (2:8 EtOAc:petroleum ether); **IR** (film, ν_{max}/cm^{-1}) 2964, 2924, 1745, 1643, 1468, 1422, 1389, 1136, 1028; **^{1}H NMR** (300 MHz, $CDCl_3$) δ 7.20–7.14 (m,

4H), 7.08 (d, *J* = 8.4 Hz, 1H), 6.94–6.91 (m, 2H), 6.83–6.79 (m, 1H), 4.57 (s, 1H), 2.85 (s, 3H), 1.77 (s, 3H); **^{13}C NMR** (151 MHz, $CDCl_3$) δ 170.9, 138.8, 135.1, 132.1, 130.8, 129.9, 129.5, 128.7, 128.6, 127.4, 126.8, 70.5, 65.1, 27.2, 24.5.

1,3-dimethyl-3-(naphthalen-2-yl)-4-phenylazetidin-2-one (4.1ad)

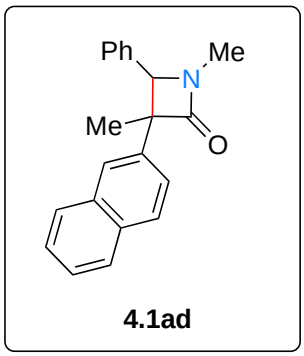

4.1ad

Prepared according to general procedure 4C using **4.2ad** (115 mg, 0.39 mmol) and **2-CTX** (9.65 mg, 0.04 mmol). Chromatography on silica gel with EtOAc:petroleum ether (1:9 to 2:8) afforded **4.1ad** as 2 separable diastereomers (109 mg, 95% yield, 1.1:1 dr). **HRMS** (ESI^+) *m/z*: [M + H] calcd for $C_{21}H_{20}NO^+$ 302.1539; found 302.1548.

***trans*-Diastereomer:** 0.056 g; oil; R_f = 0.22 (2:8 EtOAc:petroleum ether); **IR** (film, ν_{max}/cm^{-1}) 2967, 2921, 1742, 1633, 1600, 1499, 1453, 1389, 1276, 1185, 1026; **^{1}H NMR** (300 MHz, $CDCl_3$) δ 8.02 (s, 1H), 7.91–7.83 (m, 3H), 7.56–7.47 (m, 5H), 7.44–7.35 (m, 3H), 4.81 (s, 1H), 2.95 (s, 3H), 1.26 (s, 3H); **^{13}C NMR** (151 MHz, $CDCl_3$) δ 172.0, 139.6, 135.6, 133.5, 132.5, 129.0, 128.8, 128.4, 128.2, 127.7, 127.2, 126.5, 126.1, 124.6, 124.3, 69.1, 64.0, 27.1, 19.5.

***cis*-Diastereomer:** 0.053 g; white solid; R_f = 0.11 (2:8 EtOAc:petroleum ether); **M.P.** 128–130 °C; **IR** (film, ν_{max}/cm^{-1}) 2958, 2924, 1740, 1633, 1451, 1392, 1274, 1068, 1027; **^{1}H NMR** (300 MHz, $CDCl_3$) δ 7.87 (s, 1H), 7.75–7.72 (m, 1H), 7.64–7.61 (m, 1H), 7.43–7.36 (m, 3H), 7.08–7.03 (m, 3H), 6.98–6.94 (m, 2H), 6.81–6.78 (m 1H), 4.65 (s, 1H), 2.88 (s, 3H), 1.88 (s, 3H); **^{13}C NMR** (151 MHz, $CDCl_3$) δ 171.9, 135.9, 135.5, 133.0, 132.0, 128.3, 128.1, 128.1, 127.6, 127.5, 127.5, 126.1, 125.9, 125.7, 125.2, 70.6, 66.1, 27.0, 24.7.

References

1 A. D. McNaught and A. Wilkinson, *IUPAC. Compendium of Chemical Terminology (the 'Gold Book')*, Blackwell Scientific Publications, Oxford, 2nd Edition., 1997.

2 A. G. Griesbeck, *Angew. Chem. Int. Ed.*, 2009, **48**, 4671–4672.

3 N. Hoffmann, *Chem. Rev.*, 2008, **108**, 1052–1103.

4 P. T. Anastas and J. C. Warner, *Green chemistry: theory and practice*, Oxford University Press, Oxford, 1998.

5 A. Mermer, T. Keles and Y. Sirin, *Bioorg. Chem.*, 2021, **114**, 105076.

6 N. Kerru, L. Gummidi, S. Maddila, K. K. Gangu and S. B. Jonnalagadda, *Molecules*, 2020, **25**, 1909.

7 C. T. Walsh, *Tetrahedron Lett*, 2015, **56**, 3075–3081.

8 P. N. Kalaria, S. C. Karad and D. K. Raval, *Eur. J. Med. Chem.*, 2018, 158, 917–936.

9 R. D. Taylor, M. Maccoss and A. D. G. Lawson, *J. Med. Chem.*, 2014, 57, 5845–5859.

10 J. Jampilek, *Molecules*, 2019, 24, 3839.

11 X. Zhou, A. E. Hohman and W. H. Hsu, *J. Vet. Pharmacol. Ther.*, 2022, **45**, 1–15.

12 Y. M. Khetmalis, M. Shivani, S. Murugesan and K. V. G. Chandra Sekhar, *Biomedicine & Pharmacotherapy*, 2021, **141**, 111842.

13 P. Bhutani, G. Joshi, N. Raja, N. Bachhav, P. K. Rajanna, H. Bhutani, A. T. Paul and R. Kumar, *J. Med. Chem.*, 2021, 64, 2339–2381.

14 M. M. Heravi and V. Zadsirjan, *RSC Adv*, 2020, **10**, 44247–44311.

15 A. P. Taylor, R. P. Robinson, Y. M. Fobian, D. C. Blakemore, L. H. Jones and O. Fadeyi, *Org. Biomol. Chem.*, 2016, **14**, 6611–6637.

16 J. Liu, J. Jiang, L. Zheng and Z. Liu, *Adv. Synth. Catal.*, 2020, **362**, 4876–4895.

17 R. Nishanth Rao, S. Jena, M. Mukherjee, B. Maiti and K. Chanda, *Environ. Chem. Lett.*, 2021, **19**, 3315–3358.

18 H. Wang, J. Li, Z. Guo, H. Zheng and W. Wei, *ChemSusChem*, 2021, **14**, 4658–4670.

19 S. Deketelaere, T. Van Nguyen, C. V. Stevens and M. D'hooghe, *ChemistryOpen*, 2017, **6**, 301–319.

20 B. König, *Eur. J. Org. Chem.*, 2017, 1979–1981.

21 D. Cambié, C. Bottecchia, N. J. W. Straathof, V. Hessel and T. Noël, *Chem. Rev.*, 2016, **116**, 10276–10341.

22 G. Ciamician, *Science* , 1912, **36**, 385–394.

23 D. M. Hedstrand, W. H. Kruizinga and R. M. Kellogg, *Tetrahedron Lett.*, 1978, **14**, 1255–1258.

24 T. J. Van Bergen, David M. Hedstrand, Wim H. Kruizinga and Richard M. Kellogg, *J. Org. Chem.*, 1979, **44**, 4953–4962.

25 H. Cano-Yelo and A. Deronzier, *J. Chem. Soc. Perkin Trans. II*, 1984, 1093–1098.

26 K. Okada, K. Okamoto, N. Morita, K. Okubo and M. Oda, *J. Am. Chem. Soc*., 1991, **113**, 9401–9402.

27 B. Giese, J. A. González-Gómez and T. Witzel, *Angew. Chem. Int. Ed.*, 1984, **23**, 69–70.

28 K. Okada, K. Okubo, N. Morita and M. Oda, *Tetrahedron Lett.*, 1992, **33**, 7377–7380.

29 K. Okada, K. Okubo, N. Morita and M. Oda, *Chem. Lett.*, 1993, **22**, 2021–2024.

30 G. Pandey, S. Hajra, M. K. Ghorai and K. R. Kumar, *J. Am. Chem. Soc.*, 1997, **119**, 8777–8787.

31 D. A. Nicewicz and D. W. C. MacMillan, *Science (1979)*, 2008, **322**, 77–80.

32 N. Hoffmann, *Journal of Photochemistry and Photobiology C: Photochemistry Reviews*, 2008, **9**, 43–60.

33 K. Dreier, What are Fluorescence and Phosphorescence?, https://www.chemistryviews.org/details/education/10468955/What_are_Fluorescence_and_Phosphorescence/, (accessed 6 October 2022).

34 N. A. Romero and D. A. Nicewicz, *Chem. Rev.*, 2016, **116**, 10075–10166.

35 A. Ito and K. Tanaka, *Applications of Carbon Nanotubes and Graphene in Spin Electronics*, Elsevier, 2nd Edition., 2014.

36 F. Strieth-Kalthoff, M. J. James, M. Teders, L. Pitzer and F. Glorius, *Chem. Soc. Rev.*, 2018, **47**, 7190–7202.

37 T. Rigotti and J. Alemán, *Chem. Commun.*, 2020, **56**, 11169–11190.

38 J. W. Tucker and C. R. J. Stephenson, *J. Org. Chem.*, 2012, **77**, 1617–1622.

39 K. L. Skubi, T. R. Blum and T. P. Yoon, *Chem. Rev.*, 2016, **116**, 10035–10074.

40 S. Reischauer and B. Pieber, *iScience*.

41 S. Campagna, F. Puntoriero, F. Nastasi, G. Bergamini and V. Balzani, *Top Curr. Chem.*, 2007, **280**, 117–214.

42 L. Flamigni, A. Barbieri, C. Sabatini, B. Ventura and F. Barigelletti, *Top Curr. Chem.*, 2007, **281**, 143–203.

43 D. Rehm and A. Weller, *Israel J. Chem.*, 1970, **8**, 259–271.

44 R. A. Marcus, *J. Chem. Phys.*, 1956, **24**, 966–978.

45 R. A. Marcus and N. Sutin, *Biochimica et Biophysica Acta (BBA) - Reviews on Bioenergetics*, 1985, **811**, 265–322.

46 J. R. Miller, L. T. Calcaterra and G. L. Closs, *J. Am. Chem. Soc.*, 1984, **106**, 3047–3049.

47 G. L. Closs, L. T. Calcaterra, N. J. Green, K. W. Penfield and J. R. Miller, *J. Phys. Chem.*, 1986, **90**, 3673–3683.

48 G. L. Closs and J. R. Miller, *Science*, 1988, **240**, 440–447.

49 A. McNally, C. K. Prier and D. W. C. MacMillan, *Science*, 2011, **334**, 1114–1117.

50 Merck Photocatalysis Chart, https://macmillan.princeton.edu/wp-content/uploads/Merck-Photocatalysis-Chart.pdf, (accessed 13 October 2022).

51 H. Roth, N. Romero and D. Nicewicz, *Synlett*, 2015, **27**, 714–723.

52 J. Zoller, D. C. Fabry, M. A. Ronge and M. Rueping, *Angew. Chem. Int. Ed*, 2014, **53**, 13264–13268.

53 M. A. Ischay, M. E. Anzovino, J. Du and T. P. Yoon, *J. Am. Chem. Soc.*, 2008, **130**, 12886–12887.

54 J. W. Verhoeven, *Glossary Of Terms Used In Photochemistry*, 1996, vol. 68.

55 A. Kaur, P. Kaur and S. Ahuja, *Anal. Methods*, 2020, **12**, 5532–5550.

56 T. Förster, *Ann. Phys.*, 1948, **437**, 55–75.

57 D. L. Dexter, *J. Chem. Phys.*, 1953, **21**, 836–850.

58 J. B. Birks, *Nature*, 1967, **214**, 1187–1190.

59 F. Scandola and V. Balzani, *J. Chem. Educ.*, 1983, **60**, 814.

60 P. J. Wagner and I. Kochevar, *J. Am. Chem. Soc.*, 1968, **90**, 2232–2238.

61 S. L. Murov, G. L. Hug and Carmichael Ian, *Handbook of photochemistry*, M. Dekker, New York, 2nd ed., 1993.

62 W. Rothman, A. Case and D. R. Kearns, *J. Chem. Phys.*, 1965, **43**, 1067–1068.

63 C. Adamo and D. Jacquemin, *Chem. Soc. Rev.*, 2013, **42**, 845–856.

64 F. Strieth-Kalthoff and F. Glorius, *Chem.*, 2020, **6**, 1888–1903.

65 M. Montalti, A. Credi, L. Prodi and M. T. Gandolfi, *Handbook of Photochemistry*, CRC Press, 2006.

66 C. Ruckebusch, M. Sliwa, P. Pernot, A. de Juan and R. Tauler, *Journal of Photochemistry and Photobiology C: Photochemistry Reviews*, 2012, **13**, 1–27.

67 V. Balzani, P. Ceroni and A. Juris, *Photochemistry and Photophysics: Concepts, Research, Applications*, Wiley-VCH, Weinheim, 2014.

68 Z. Lu and T. P. Yoon, *Angew. Chem. Int. Ed.*, 2012, **51**, 10329–10332.

69 R. Alonso and T. Bach, *Angew. Chem. Int. Ed.*, 2014, **53**, 4368–4371.

70 T. R. Blum, Z. D. Miller, D. M. Bates, I. A. Guzei and T. P. Yoon, *Science (1979)*, 2016, **354**, 1391–1395.

71 N. Münster, N. A. Parker, L. van Dijk, R. S. Paton and M. D. Smith, *Angew. Chem. Int. Ed.*, 2017, **56**, 9468–9472.

72 T. Neveselý, M. Wienhold, J. J. Molloy and R. Gilmour, *Chem. Rev.*, 2022, **122**, 2650–2694.

73 K. Singh, S. J. Staig and J. D. Weaver, *J. Am. Chem. Soc.*, 2014, **136**, 5275–5278.

74 J. B. Metternich and R. Gilmour, *J. Am. Chem. Soc.*, 2015, **137**, 11254–11257.

75 A. Hölzl-Hobmeier, A. Bauer, A. V. Silva, S. M. Huber, C. Bannwarth and T. Bach, *Nature*, 2018, **564**, 240–243.

76 E. P. Farney and T. P. Yoon, *Angew. Chem. Int. Ed.*, 2014, **53**, 793–797.

77 E. Brachet, T. Ghosh, I. Ghosh and B. König, *Chem. Sci.*, 2015, **6**, 987–992.

78 M. Teders, C. Henkel, L. Anhäuser, F. Strieth-Kalthoff, A. Gómez-Suárez, R. Kleinmans, A. Kahnt, A. Rentmeister, D. Guldi and F. Glorius, *Nat. Chem.*, 2018, **10**, 981–988.

79 T. Patra, S. Mukherjee, J. Ma, F. Strieth-Kalthoff and F. Glorius, *Angew. Chem. Int. Ed.*, 2019, **58**, 10514–10520.

80 T. Patra, P. Bellotti, F. Strieth-Kalthoff and F. Glorius, *Angew. Chem. Int. Ed.*, 2020, **132**, 3198–3203.

81 D. R. Heitz, J. C. Tellis and G. A. Molander, *J. Am. Chem. Soc.*, 2016, **138**, 12715–12718.

82 E. R. Welin, C. Le, D. M. Arias-Rotondo, J. K. McCusker and D. W. C. MacMillan, *Science (1979)*, 2017, **355**, 380–385.

83 T. Kim, S. J. McCarver, C. Lee and D. W. C. MacMillan, *Angew. Chem. Int. Ed.*, 2018, **57**, 3488–3492.

84 J. Späth, M. J. Oddy, R. Hunter and W. F. Petersen, *Synthesis*, 2023, **55**, 1736–1743.

85 P. Ruiz-Sanchis, S. A. Savina, F. Albericio and M. Álvarez, *Chemistry – A European Journal*, 2011, **17**, 1388–1408.

86 D. J. Triggle, J. M. Mitchell and R. Filler, *CNS Drug Rev*, 1998, **4**, 87–136.

87 A. Proudfoot, *Toxicol Rev*, 2006, **25**, 99–138.

88 V. N. Dubrovskii, A. D. Shalabodov and A. V. Belkin, *Bull. Exp. Biol. Med.*, 2018, **166**, 50–53.

89 Q. Yu, C. Liu, M. Brzostowska, L. Chrisey, A. Brossi, N. H. Greig, J. R. Atack, T. T. Soncrant, S. I. Rapoport and H. Radunz, *Helv. Chim. Acta.*, 1991, **74**, 761–766.

90 Z.-Y. Cao, F. Zhou and J. Zhou, *Acc. Chem. Res.*, 2018, **51**, 1443–1454.

91 J. E. M. N. Klein and R. J. K. Taylor, *European J. Org. Chem.*, 2011, **2011**, 6821–6841.

92 N. Radhoff and A. Studer, *Chem. Sci.*, 2022, **13**, 3875–3879.

93 J. Singh and A. Sharma, *Adv. Synth. Catal.*, 2021, **363**, 4284–4308.

94 Y.-L. Liu, X.-P. Wang, J. Wei and Y. Li, *Org. Biomol. Chem.*, 2022, **20**, 538–552.

95 H.-M. Huang, M. H. Garduño-Castro, C. Morrill and D. J. Procter, *Chem. Soc. Rev.*, 2019, **48**, 4626–4638.

96 J. Liao, X. Yang, L. Ouyang, Y. Lai, J. Huang and R. Luo, *Organic Chemistry Frontiers*, 2021, **8**, 1345–1363.

97 K. Hung, X. Hu and T. J. Maimone, *Nat. Prod. Rep.*, 2018, **35**, 174–202.

98 S. R. S. Rudrangi, V. K. Bontha and V. R. Manda, B. Srinivas, *Asian Journal of Research in Chemistry*, 2011, **4**, 335–338.

99 S. Peddibhotla, *Curr. Bioact. Compd.*, 2009, **5**, 20–38.

100 S. Sharma, Y. Monga, A. Gupta and S. Singh, *RSC Adv.*, 2023, **13**, 14249–14267.

101 A. D. Marchese, E. M. Larin, B. Mirabi and M. Lautens, *Acc. Chem. Res.*, 2020, **53**, 1605–1619.

102 P. V. Saranya, M. Neetha, T. Aneeja and G. Anilkumar, *RSC Adv.*, 2021, **11**, 7146–7179.

103 J.-R. Chen, X.-Y. Yu and W.-J. Xiao, *Synthesis (Stuttg)*, 2014, **47**, 604–629.

104 C.-C. Li and S.-D. Yang, *Org. Biomol. Chem.*, 2016, **14**, 4365–4377.

105 X. Ju, Y. Liang, P. Jia, W. Li and W. Yu, *Org. Biomol. Chem.*, 2012, **10**, 498–501.

106 S. Bhunia, S. Ghosh, D. Dey and A. Bisai, *Org. Lett.*, 2013, **15**, 2426–2429.

107 S. Ghosh, S. De, B. N. Kakde, S. Bhunia, A. Adhikary and A. Bisai, *Org. Lett.*, 2012, **14**, 5864–5867.

108 N. Kumar, S. Ghosh, S. Bhunia and A. Bisai, *Beilstein J. Org. Chem.*, 2016, **12**, 1153–1169.

109 J. E. M. N. Klein, A. Perry, D. S. Pugh and R. J. K. Taylor, *Org. Lett.*, 2010, **12**, 3446–3449.

110 Y. Jia and E. P. Kündig, *Angew. Chem. Int. Ed.*, 2009, **48**, 1636–1639.

111 A. Teichert, K. Jantos, K. Harms and A. Studer, *Org. Lett.*, 2004, **6**, 3477–3480.

112 J. R. Donald, R. J. K. Taylor and W. F. Petersen, *J. Org. Chem.*, 2017, **82**, 11288–11294.

113 Y. Wang, W. Lin, J. Zou, W. Yu and X. Liu, *Adv. Synth. Catal.*, 2020, **362**, 3116–3120.

114 M. Zhang, X. Ding, A. Lu, J. Kang, Y. Gao, Z. Wang, H. Li and Q. Wang, *Organic Chemistry Frontiers*, 2021, **8**, 961–967.

115 X. Li, M.-Y. Han, B. Wang, L. Wang and M. Wang, *Org. Biomol. Chem*., 2019, **17**, 6612–6619.

116 G. Bergonzini, C. Cassani and C. Wallentin, *Angew. Chem. Int. Ed.*, 2015, **54**, 14066–14069.

117 A. Banerjee, Z. Lei and M.-Y. Ngai, *Synthesis (Stuttg)*, 2019, **51**, 303–333.

118 Y.-L. Liu, Y.-J. Ouyang, H. Zheng, H. Liu and W.-T. Wei, *Chem. Commun.*, 2021, **57**, 6111–6120.

119 D. M. Kitcatt, S. Nicolle and A.-L. Lee, *Chem. Soc. Rev.*, 2022, **51**, 1415–1453.

120 B. T. Matsuo, P. H. R. Oliveira, E. F. Pissinati, K. B. Vega, I. S. de Jesus, J. T. M. Correia and M. Paixao, *Chem. Commun.*, 2022, **58**, 8322–8339.

121 G. Diaz-Muñoz, I. L. Miranda, S. K. Sartori, D. C. de Rezende and M. Alves Nogueira Diaz, *Chirality*, 2019, **31**, 776–812.

122 M. M. Heravi, V. Zadsirjan and B. Farajpour, *RSC Adv.*, 2016, **6**, 30498–30551.

123 J. M. Hawkins and T. J. N. Watson, *Angew. Chem. Int. Ed.*, 2004, **43**, 3224–3228.

124 Chang S, Halperin SD, Moore J and Britton R, *Stereoselective Synthesis of Drugs and Natural Products* , John Wiley & Sons, 2013.

125 J. Garcia-Martinez, *Angew. Chem. Int. Ed.*, 2021, **60**, 4956–4960.

126 T. Keijer, V. Bakker and J. C. Slootweg, *Nat. Chem.*, 2019, **11**, 190–195.

127 W.-P. Mai, G.-C. Sun, J.-T. Wang, G. Song, P. Mao, L.-R. Yang, J.-W. Yuan, Y.-M. Xiao and L.-B. Qu, *J. Org. Chem.*, 2014, **79**, 8094–8102.

128 S. Mandal, T. Bera, G. Dubey, J. Saha and J. K. Laha, *ACS Catal.*, 2018, **8**, 5085–5144.

129 J. Lee, U. von Gunten and J.-H. Kim, *Environ. Sci. Technol.*, 2020, **54**, 3064–3081.

130 C. Dai, F. Meschini, J. M. R. Narayanam and C. R. J. Stephenson, *J. Org. Chem.*, 2012, **77**, 4425–4431.

131 C. M. Mazodze and W. F. Petersen, *Org. Biomol. Chem.*, 2022, **20**, 3469–3474.

132 W. F. Petersen, R. J. K. Taylor and J. R. Donald, *Org. Lett.*, 2017, **19**, 874–877.

133 T. Matsuura, L. E. Overman and D. J. Poon, *J. Am. Chem. Soc.*, 1998, **120**, 6433–6634.

134 M. J. Oddy, D. A. Kusza and W. F. Petersen, *Org. Lett.*, 2021, **23**, 8963–8967.

135 B. Schmidt, F. Hölter, R. Berger and S. Jessel, *Adv. Synth. Catal.*, 2010, **352**, 2463–2473.

136 L. Zhang, L. Sonaglia, J. Stacey and M. Lautens, *Org. Lett.*, 2013, **15**, 2128–2131.

137 W. Sun, C. H. Ling, C. M. Au and W. Y. Yu, *Org. Lett.*, 2021, **23**, 3310–3314.

138 X. Yang, L. Wang, F. Hu, L. Xu, S. Li and S.-S. Li, *Org. Lett.*, 2021, **23**, 358–364.

139 Y. Yan, P. Zhou, D. P. Rotella, R. Feenstra, C. G. Kruse, J. H. Reinders, M. van der Neut, M. Lai, J. Zhang, D. M. Kowal, T. Carrick, K. L. Marquis, M. H. Pausch and A. J. Robichaud, *Bioorg. Med. Chem. Lett.*, 2010, **20**, 2983–2986.

140 Q. Hu, L. Yin and R. W. Hartmann, *J. Med. Chem.*, 2012, **55**, 7080–7089.

141 R. Uchida, R. Imasato, H. Tomoda and S. Omura, *J. Antibiot.*, 2006, **59**, 652–658.

142 K. Bernauer, G. Englert, W. Vetter and Ek. Weiss, *Helv. Chim. Acta.*, 1969, **52**, 1886–1905.

143 S. S. Ma, W. L. Mei, Z. K. Guo, S. B. Liu, Y. X. Zhao, D. L. Yang, Y. B. Zeng, B. Jiang and H. F. Dai, *Org. Lett.*, 2013, **15**, 1492–1495.

144 M. Cherest and X. Lusinchi, *Tetrahedron Lett.*, 1989, **30**, 715–718.

145 K. Li, L. N. Foresee and J. A. Tunge, *J. Org. Chem.*, 2005, **70**, 2881–2883.

146 H.-Z. Xiao, W.-S. Wang, Y.-S. Sun, H. Luo, B.-W. Li, X.-D. Wang, W.-L. Lin and F.-X. Luo, *Org. Lett.*, 2019, **21**, 1668–1671.

147 M. Guan, Y. Pang, J. Zhang and Y. Zhao, *Chem. Commun.*, 2016, **52**, 7043–7046.

148 J. X. Yan, H. Li, X. W. Liu, J. L. Shi, X. Wang and Z. J. Shi, *Angew. Chem. Int. Ed.*, 2014, **53**, 4945–4949.

149 M. Wasa and J. Q. Yu, *J. Am. Chem. Soc.*, 2008, **130**, 14058–14059.

150 H. Zhang, Z. Gu, Z. Li, C. Pan, W. Li, H. Hu and C. Zhu, *J. Org. Chem.*, 2016, **81**, 2122–2127.

151 Q. F. Bai, C. Jin, J. Y. He and G. Feng, *Org. Lett.*, 2018, **20**, 2172–2175.

152 W. P. Mai, G. C. Sun, J. T. Wang, G. Song, P. Mao, L. R. Yang, J. W. Yuan, Y. M. Xiao and L. B. Qu, *J. Org. Chem.*, 2014, **79**, 8094–8102.

153 S. L. Zhou, L. N. Guo, S. Wang and X. H. Duan, *Chem. Commun.*, 2014, **50**, 3589–3591.

154 X. Mi, C. Wang, M. Huang, J. Zhang, Y. Wu and Y. Wu, *Org. Lett.*, 2014, **16**, 3356–3359.

155 W. Yu, P. Hu, Y. Fan, C. Yu, X. Yan, X. Li and X. Xu, *Org. Biomol. Chem.*, 2015, **13**, 3308–3313.

156 Z. Kuang, B. Li and Q. Song, *Chem. Commun.*, 2017, **54**, 34–37.

157 A. Whyte, M. E. Olson and M. Lautens, *Org. Lett.*, 2018, **20**, 345–348.

158 B. Li, Y. Park and S. Chang, *J. Am. Chem. Soc.*, 2014, **136**, 1125–1131.

159 X. Yang, L. Wang, F. Hu, L. Xu, S. Li and S. S. Li, *Org. Lett.*, 2021, **23**, 358–364.

160 W. Sun, C. H. Ling, C. M. Au and W. Y. Yu, *Org. Lett.*, 2021, **23**, 3310–3314.

161 S. G. Modha, A. Pöthig, A. Dreuw and T. Bach, *J. Org. Chem.*, 2019, **84**, 1139–1153.

162 S. Yamada, M. Okuda and N. Yamamoto, *Tetrahedron Lett.*, 2015, **56**, 2098–2101.

163 A. J. L. Ayitou and J. Sivaguru, *J. Am. Chem. Soc.*, 2009, **131**, 5036–5037.

164 N. F. Nikitas, P. L. Gkizis and C. G. Kokotos, *Org. Biomol. Chem.*, 2021, 19, 5237–5253.

165 L. D. Elliott, S. Kayal, M. W. George and K. Booker-Milburn, *J. Am. Chem. Soc.* 2020, **142**, 14947-14956.

166 (i) A. Tröster, R. Alonso, A. Bauer and T. Bach, *J. Am. Chem. Soc.*, 2016, **138**, 7808–7811. (ii) X. Li, C. Jandl and T. Bach, *Org. Lett.*, 2020, **22**, 3618–3622.

167 T. Neveselý, C. G. Daniliuc and R. Gilmour, *Org. Lett.*, 2019, **21**, 9724–9728.

168 M. J. James, J. L. Schwarz, F. Strieth-Kalthoff, B. Wibbeling and F. Glorius, *J. Am. Chem. Soc.*, 2018, **140**, 8624–8628.

169 H. Cheng, T. L. Lam, Y. Liu, Z. Tang and C. M. Che, *Angew. Chem. Int. Ed.*, 2021, **60**, 1383–1389.

170 J. C. Dalton and F. C. Montgomery, *J. Am. Chem. Soc.*, 1974, **96**, 6230–6232.

171 S. Yamada, M. Okuda and N. Yamamoto, *Tetrahedron Lett.*, 2015, **56**, 2098–2101.

172 Z. Liu, S. Zhong, X. Ji, G. J. Deng and H. Huang, *Org. Lett.*, 2022, **24**, 349–353.

173 M. v. Popescu, A. Mekereeya, J. v. Alegre-Requena, R. S. Paton and M. D. Smith, *Angew. Chem. Int. Ed.*, 2020, **59**, 23020–23024.

174 https://www.sigmaaldrich.com/ZA/en/product/aldrich/342289.

175 B. S. Matada, R. Pattanashettar and N. G. Yernale, *Bioorg. Med. Chem.*, 2021, **32**, 115973.

176 M. Uchida, F. Tabusa, M. Komatsu, S. Morita, T. Kanbe and K. Nakagawa, *Chem. Pharm. Bull. (Tokyo)*, 1987, **35**, 853–856.

177 A. Ito, L. A. Shamon, B. Yu, E. Mata-Greenwood, S. K. Lee, R. B. van Breemen, R. G. Mehta, N. R. Farnsworth, H. H. S. Fong, J. M. Pezzuto and A. D. Kinghorn, *Antimutagenic Constituents of Casimiroa edulis with Potential Cancer Chemopreventive Activity*, 1998.

178 W. P. Hong, I. Shin and H. N. Lim, *Molecules*, 2020, 25.

179 A. v. Aksenov, A. N. Smirnov, N. A. Aksenov, I. v. Aksenova, J. P. Matheny and M. Rubin, *RSC Adv.*, 2015, **5**, 8647–8656.

180 W. Z. Zhang, S. Liu and X. B. Lu, *Beilstein J. Org. Chem.*, 2015, **11**, 906–912.

181 Z. Zhang, L.-L. Liao, S.-S. Yan, L. Wang, Y.-Q. He, J.-H. Ye, J. Li, Y.-G. Zhi and D.-G. Yu, *Angew. Chem.*, 2016, **128**, 7184–7188.

182 X. Yi, X. Yi, S. Lei, W. Liu, F. Che, C. Yu, X. Liu, Z. Wang, X. Zhou and Y. Zhang, *Org. Lett.*, 2020, **22**, 4583–4587.

183 M. J. Oddy, D. A. Kusza, R. G. Epton, J. M. Lynam, W. P. Unsworth and W. F. Petersen, *Angew. Chem. Int. Ed.*, 2022, **61**, .-.

184 M. Mora-Ochomogo and C. T. Lohans, *RSC Med. Chem.*, 2021, 12, 1623–1639.

185 D. J. Fu, Y. F. Zhang, A. Q. Chang and J. Li, *Eur. J. Med. Chem.*, 2020, 201, 112510.

186 K. Bush and P. A. Bradford, *Cold Spring Harb. Perspect. Med.*,

187 https://www.who.int/publications/i/item/who-report-on-surveillance-of-antibiotic-consumption.

188 D. J. Fu, L. Fu, Y. C. Liu, J. W. Wang, Y. Q. Wang, B. K. Han, X. R. Li, C. Zhang, F. Li, J. Song, B. Zhao, R. W. Mao, R. H. Zhao, S. Y. Zhang, L. Zhang, Y. B. Zhang and H. M. Liu, *Sci Rep*, 2017, **7**, 12788.

189 A. M. Malebari, D. Fayne, S. M. Nathwani, F. O'Connell, S. Noorani, B. Twamley, N. M. O'Boyle, J. O'Sullivan, D. M. Zisterer and M. J. Meegan, *Eur. J. Med. Chem.*, 2020, **189**, 112050.

190 G. Savarese, G. M. De Ferrari, G. M. C. Rosano and P. Perrone-Filardi, *Int. J. Cardiol.*, 2015, **201**, 247–252.

191 D. R. Parmar, J. Y. Soni, R. Guduru, R. H. Rayani, R. V. Kusurkar and A. G. Vala, *Arch. Pharm. (Weinheim)*, 2021, **354**, 2100062.

192 M. W. Holladay, J. T. Wasicak, N.-H. Lin, Y. He, K. B. Ryther, A. W. Bannon, M. J. Buckley, D. J. B. Kim, M. W. Decker, D. J. Anderson, J. E. Campbell, T. A. Kuntzweiler, D. L. Donnelly-Roberts, M. Piattoni-Kaplan, C. A. Briggs, M. Williams and S. P. Arneric, *Identification and Initial Structure-Activity Relationships of (R)-5-(2-Azetidinylmethoxy)-2-chloropyridine (ABT-594), a Potent, Orally Active, Non-Opiate Analgesic Agent Acting via Neuronal Nicotinic Acetylcholine Receptors*, 1998.

193 K. Oizumi, H. Nishino, H. Koike, T. Sada, M. Miyamoto and T. Kimura, *Jpn. J. Pharmacol.*, 1989, **51**, 57–64.

194 M. Maetani, N. Kato, V. A. P. Jabor, F. A. Calil, M. C. Nonato, C. A. Scherer and S. L. Schreiber, *ACS Med. Chem. Lett.*, 2017, **8**, 438–442.

195 S. Ernst, A. N. Volkov, M. Stark, L. Hölscher, K. Steinert, S. Fetzner, U. Hennecke and S. L. Drees, *J. Am. Chem. Soc.*, 2022, **144**, 7676–7685.

196 Z. Hong, A. Bolard, C. Giraud, S. Prévost, G. Genta-Jouve, C. Deregnaucourt, S. Häussler, K. Jeannot and Y. Li, *Angew. Chem.*, 2019, **131**, 3210–3214.

197 S. Hosseyni and A. Jarrahpour, *Org. Biomol. Chem.*, 2018, 16, 6840–6852.

198 C. R. Pitts and T. Lectka, *Chem. Rev.*, 2014, 114, 7930–7953.

199 M. Kinugasa and S. Hashimoto, *J. Chem. Soc. Chem. Commun*, 1972, 466.

200 A. Saura-Sanmartin and L. Andreu-Ardil, *Org. Biomol. Chem.*, 2023, **21**, 3296-3306

201 S. Calet, F. Urso and H. Alper, *J. Am. Chem. Soc.*, 1989, **111**, 931–934.

202 N. Piens, K. Van Hecke, D. Vogt and M. D'Hooghe, *Org. Biomol. Chem.*, 2017, **15**, 4816–4821.

203 M. Isoda, K. Sato, M. Funakoshi, K. Omura, A. Tarui, M. Omote and A. Ando, *J. Org. Chem.*, 2015, **80**, 8398–8405.

204 Z. Zhuang, S. Liu, J. T. Cheng, K. S. Yeung, J. X. Qiao, N. A. Meanwell and J. Q. Yu, *Angew. Chem. Int. Ed*, 2022, **61**, e202207354.

205 C. Li, K. Jiang, Q. Ouyang, T. Y. Liu and Y. C. Chen, *Org. Lett.*, 2016, **18**, 2738–2741.

206 M. P. Doyle, M. N. Protopopova, W. R. Winchester and K. L. Daniel, *Tetrahedron Lett.*, 1992, **33**, 7819–7822.

207 D. Solé, F. Pérez-Janer, M. L. Bennasar and I. Fernández, *European J. Org. Chem.*, 2018, **2018**, 4446–4455.

208 C. McMaster, R. N. Bream and R. S. Grainger, *Org. Biomol. Chem.*, 2012, **10**, 4752–4758.

209 J. L. Markley, T. L. Morse, N. P. Rath and T. A. Wencewicz, *Tetrahedron*, 2018, **74**, 2743–2753.

210 J. H. Ye, P. Bellotti, T. O. Paulisch, C. G. Daniliuc and F. Glorius, *Angew. Chem. Int. Ed.*, 2021, **60**, 13671–13676.

211 H. Yang, H. Li, G. Wei and Z. Jiang, *Angew. Chem. Int. Ed.*, 2021, **60**, 19696–19700.

212 C. Chen, *Org. Biomol. Chem.*, 2016, 14, 8641–8647.

213 S. Majhi, *Photochemical and Photobiological Sciences*, 2021, 20, 1357–1378.

214 H. Aoyama, T. Hasegawa, M. Watabe, H. Shiraishi and Y. Omote, *J. Org. Chem.*, 1978, **43**, 419–422.

215 H. Aoyama, T. Hasegawa and Y. Omote, *J. Am. Chem. Soc.*, 1979, **101**, 5343–5347.

216 H. Wehrli, *Helv. Chim. Acta.*, 1980, **63**, 1915–1919.

217 T. Hasegawa, M. Watabe, H. Aoyama and Y. Omote, *Tetrahedron*, 1977, **33**, 485–488.

218 A. J.-L. Ayitou, J. L. Jesuraj, N. Barooah, A. Ugrinov and J. Sivaguru, *J. Am. Chem. Soc.*, 2009, **131**, 11314–11315.

219 R. Wang, C. Chen, E. Duesler, P. S. Mariano and U. C. Yoon, *J. Org. Chem.*, 2004, **69**, 1215–1220.

220

220 J. L. Markley, T. L. Morse, N. P. Rath and T. A. Wencewicz, *Tetrahedron*, 2018, **74**, 2743–2753.

221 M. Sakamoto, H. Kawanishi, T. Mino and T. Fujita, *Chem. Commun.*, 2008, 2132.

222 M. Ruggeri, A. W. Dombrowski, S. W. Djuric and I. R. Baxendale, *ChemPhotoChem*, 2019, **3**, 1212–1218.

223 M. Singh, B. Gaskins, D. R. Johnson, C. G. Elles and Z. Boskovic, *J. Org. Chem.*, 2022, **87**, 15001–15010.

224 S. Kohmoto, T. Kreher, Y. Miyaji, M. Yamamoto and K. Yamada, *J. Org. Chem.*, 1992, **57**, 3490–3492.

225 S. Le Blanc, J.-P. Pete and O. Piva, *Tetrahedron Lett.*, 1992, **33**, 1993–1996.

226 Vallavoju, A. Sreenithya, A. J. -L. Ayitou, S. Jockusch, R. B. Sunoj and J. Sivaguru, *Chemistry – A European Journal*, 2016, **22**, 11339–11348.

227 J. B. Roque, Y. Kuroda, J. Jurczyk, L.-P. Xu, J. S. Ham, L. T. Göttemann, C. A. Roberts, D. Adpressa, J. Saurí, L. A. Joyce, D. G. Musaev, C. S. Yeung and R. Sarpong, *ACS Catal.*, 2020, **10**, 2929–2941.

228 T. Peez, V. Schmalz, K. Harms and U. Koert, *Org. Lett.*, 2019, **21**, 4365–4369.

229 M. Nechab, S. Mondal and M. P. Bertrand, *Chemistry - A European Journal*, 2014, 20, 16034–16059.

230 M. Milan, M. Salamone, M. Costas and M. Bietti, *Acc. Chem. Res.*, 2018, **51**, 1984–1995.

231 Y. Xiong, J. Großkopf, C. Jandl and T. Bach, *Angew. Chem. Int. Ed.*, 2022, **61**, e202200555.

232 S. Schunk and D. Enders, *J. Org. Chem.*, 2002, **67**, 8034–8042.

233 R. Pandey and S. Umapathy, *Chem. Phys.*, 2014, **428**, 175–180.

234 A. G. Griesbeck and H. Heckroth, *J. Am. Chem. Soc.*, 2002, **124**, 396–403.

235 J. Lambert, R. Bleicher, B. Soden, A. Edwards and A. Henderson, Energy: The Driver of Climate, https://www.ces.fau.edu/nasa/module-2/radiation-sun.php, (accessed 8 October 2023).

236 T. Wu, X. Mu and G. Liu, *Angew. Chem. Int. Ed.*, 2011, **50**, 12578–12581.

237 D. C. Fabry, M. Stodulski, S. Hoerner and T. Gulder, *Chemistry – A European Journal*, 2012, **18**, 10834–10838.

238 A. M. Schoevaars, W. Kruizinga, R. W. J. Zijlstra, N. Veldman, A. L. Spek and B. L. Feringa, *J. Org. Chem.*, 1997, **62**, 4943–4948.

239 Y. Cao, H. Zhao, D. Zhang-Negrerie, Y. Du and K. Zhao, *Adv. Synth. Catal.*, 2016, **358**, 3610–3615.

240 Y. Shi, H. Xing, T. Huang, X. Liu, J. Chen, X. Guo, G.-B. Li and Y. Wu, *Chem. Commun.*, 2020, **56**, 1585–1588.

241 S. Sun, J.-T. Yu, Y. Jiang and J. Cheng, *J. Org. Chem.*, 2015, **80**, 2855–2860.

242 H. Murakami, A. Yamada, K. Michigami and Y. Takemoto, *Asian J. Org. Chem.*, 2021, **10**, 1097–1101.

243 J. H. Reed, P. A. Donets, S. Miaskiewicz and N. Cramer, *Angew. Chem. Int. Ed.*, 2019, **58**, 8893–8897.

244 W. Luo, Y. Yang, B. Liu and B. Yin, *J. Org. Chem.*, 2020, **85**, 9396–9404.

245 A. V. Aksenov, A. N. Smirnov, N. A. Aksenov, I. V. Aksenova, L. V. Frolova, A. Kornienko, I. V. Magedov and M. Rubin, *Chem. Commum.*, 2013, **49**, 9305.

246 M. R. Nimlos, D. F. Kelley and E. R. Bernstein, *J. Phys. Chem.*, 1987, **91**, 6610–6614.

247 L. Liu, H. Lu, H. Wang, C. Yang, X. Zhang, D. Zhang-Negrerie, Y. Du and K. Zhao, *Org. Lett.*, 2013, **15**, 2906–2909.

248 Q.-L. Yang, Y.-K. Xing, X.-Y. Wang, H.-X. Ma, X.-J. Weng, X. Yang, H.-M. Guo and T.-S. Mei, *J. Am. Chem. Soc.*, 2019, **141**, 18970–18976.

249 X.-Y. Ye, Z.-Q. Liang, C. Jin, Q.-W. Lang, G.-Q. Chen and X. Zhang, *Chem. Commun.*, 2021, **57**, 195–198.

250 B. A. Sandoval, P. D. Clayman, D. G. Oblinsky, S. Oh, Y. Nakano, M. Bird, G. D. Scholes and T. K. Hyster, *J. Am. Chem. Soc.*, 2021, **143**, 1735–1739.

251 Z.-Y. Dai, Z.-S. Nong, S. Song and P.-S. Wang, *Org. Lett.*, 2021, **23**, 3157–3161.

252 S. Schunk and D. Enders, *J. Org. Chem*, 2002, **67**, 8034–8042.